CO_2 Hydrogenation to Methanol and DME over Ni-Ga Based Catalysts

Xiaowen Huang

Department of Chemical Engineering

Imperial College London

Thesis submitted for the degree of Doctor of Philosophy (PhD) to Imperial College London of Science, Technology and Medicine

August 2019

Abstract

Recently, climate change associated with the increasing level of atmospheric CO_2 provoked growing interest in the recycling of captured CO_2 to produce methanol and DME using renewable sources of hydrogen. For CO_2 hydrogenation, numerous catalysts have been investigated. Among them, bimetallic catalysts are promising due to their unique properties. In this work, the performance of Ni-Ga based catalysts for CO_2 hydrogenation to methanol and DME was investigated at elevated pressures. A passivation technique using N_2O was developed for the air-sensitive Ni-Ga catalysts to facilitate transfer to the reactor. The effect of Pd promotion on the reducibility and performance of a Ni-Ga catalyst was also studied. For the single-stage DME synthesis, Ni-Ga and Pd-Ga based catalysts were investigated as the methanol synthesis component with the zeolites ferrierite (FER) and ZSM-5 as the acid component.

Ni-Ga(5:3 and 1:1)/SiO_2 catalysts were found to have higher selectivity to methanol but lower activity compared to a commercial Cu/ZnO/Al_2O_3 catalyst at elevated pressures. Loss in activity and selectivity is attributed in part to the decomposition of the Ni-Ga intermetallic phase. The Ni-Ga catalyst was reversibly poisoned significantly in the presence of reaction products (especially CO). Addition of Pd to the Ni-Ga(5:3)/SiO_2 showed an enhanced methanol synthesis activity, possibly due to hydrogen spillover. Ferrierite and ZSM-5 worked well as the methanol dehydration component in single-stage DME synthesis with Ni-Ga or Pd-Ga catalysts under CO_2/H_2. FER based mixtures demonstrated good stability and selectivity due to the unidirectional channel structure that suppresses hydrocarbon formation, while the performance of ZSM-5 was greatly dependent on the water concentration. The effect of proximity between the two catalyst components in physical mixtures was found to be more pronounced in the Ni-Ga based mixtures due to metal transfer, which appeared to be facilitated by the relatively high re-activation temperature.

Keywords: intermetallic catalysts, CO_2 hydrogenation, methanol, single-stage DME synthesis, Ni-Ga

Declaration of Originality

I hereby declare that the work presented in this thesis comes from the result of my own work and any other ideas or quotations from the work by other people are appropriately referenced.

Xiaowen Huang

Imperial College London

August 2019

Copyright Declaration

The copyright of this thesis rests with the author and is made available under a Creative Commons Attribution Non-Commercial No Derivatives license. Researchers are free to copy, distribute or transmit the thesis on the condition that they attribute it, that they do not use it for commercial purposes and that they do not alter, transform or build upon it. For any reuse or distribution, researchers must make clear to others the license term of this work.

Acknowledgement

First and foremost, I would like to thank my supervisor, Professor David Chadwick for the opportunity to pursue this PhD and for his continuous guidance and advice throughout. For always being patient and supportive when I was confused or disappointed.

I deeply thank my mother, Chi Huang and father, Wenqing Huang for always encouraging me and loving me unconditionally. I would like to thank my husband, Dr Joseph Yao for his love, support and company in this journey. For always being there to listen to me, motivate me and believe in me.

I would like to thank the colleagues from David's group: Laurie and Jane for their help with some characterisation tests, as well as the good times we shared during our conference trips, Motaz for his expertise in XPS data analysis. I am also grateful to Ines and Diana for their help during their time in David's group.

I would like to thank Dr Mahmoud Ardakani for his help in TEM analysis; Patricia Carry for the training in the analytical lab; Richard and Tony for help with my equipment; Chin for help in electronics; Keith and Ben from the Chemical Engineering Store.

Abbreviations

BET – Brunauer–Emmett–Teller (method)

BJH – Barrett-Joyner-Halenda (method)

CCS – Carbon Capture and Storage

CCU – Carbon Capture and Utilisation

CSTR – Continuous Stirred Tank Reactor

DME – Dimethyl Ether

EDS – Energy Dispersive X-ray Spectroscopy

FER – Ferrierite (zeolite)

hr – Hour

ICP (ICP – OES) – Inductively Coupled Plasma Optical Emission Spectrometry

GHSV – Gas Hourly Space Velocity

MeOH – Methanol

MSC – Methanol Synthesis Catalyst

MTH/MTG/MTO – Methanol to Hydrocarbon/Gasoline/Olefins

PFR – Packed Bed Flow Reactor

rpm – Revolution per Minute

rWGS – Reverse Water Gas Shift

SEM - Scanning Electron Microscopy

STD – Syngas to Dimethyl ether

TEM - Transmission Electron Microscopy

TGA – Thermogravimetric Analysis

TPO – Temperature Programmed Oxidation

TPR – Temperature Programmed Reduction

TPRx – Temperature Programmed Reaction

XPS – X-ray Photoelectron Spectroscopy

XRD – X-ray Diffraction

Table of Contents

Abstract 2

Declaration of Originality 3

Copyright Declaration 4

Acknowledgement 5

Abbreviations 6

List of Figures 10

List of Tables 14

Chapter 1 Introduction 16

1.1 Research objectives 19

1.2 Thesis outline 20

Chapter 2 Literature Review 21

2.1 Methanol synthesis 21

2.1.1 Methanol economy 21

2.1.2 Sources of renewable CO_2/H_2 22

2.1.3 Methanol synthesis thermodynamic and kinetic considerations 25

2.1.4 Conventional $Cu/ZnO/Al_2O_3$ catalyst 34

2.1.5 Recent advances in CO_2 hydrogenation catalysts 38

2.2 DME synthesis 45

2.2.1 Single-stage process 45

2.2.2 γ-alumina and zeolites as the methanol dehydration components 47

2.2.3 Reaction mechanism 54

2.2.4 Challenges in single-stage DME synthesis 57

Chapter 3 Experimental Procedures 60

3.1 Reactor system setup 60

3.1.1 Fixed bed stirred tank reactor (CSTR) 61

3.1.2 Tubular flow reactor (PFR) 62

3.2 Catalyst preparation 62

3.2.1 Methanol synthesis catalysts (MSC) 62

3.2.2 Methanol dehydration catalysts 65

3.2.2 Mass transfer effects 66

3.2.3 Catalyst tests under elevated pressures 67

3.2.4 Product analysis 67

3.2.5 Calculation methods 68

3.3 Thermodynamic analysis of methanol synthesis process 70
3.4 Catalyst characterisation 72
3.4.1 X-ray powder diffraction (XRD) 72
3.4.2 Nitrogen physisorption 73
3.4.3 Thermogravimetric analysis (TGA) 73
3.4.4 Transmission electron microscopy (TEM) and energy dispersive spectroscopy (EDS) 73
3.4.5 X-ray photoelectron spectroscopy (XPS) 73
3.4.6 Inductive coupled plasma – optical emission spectrometry (ICP – OES) 74
3.4.7 Temperature programmed experiments 74
Chapter 4 CO_2 Hydrogenation to Methanol over Ni-Ga Based Catalyst at Elevated Pressures 76
4.1 Introduction 76
4.2 Preparation of Ni-Ga/SiO_2 catalysts 77
4.2.1 The need for a suitable passivation procedure 77
4.2.2 Development of passivation procedures 79
4.2.3 Methanol synthesis at elevated pressures in CSTR with CO_2/H_2 94
4.2.4 Effect of CO in the feed gas 108
4.3 Other support for the Ni-Ga based catalysts 116
4.3.1 NiGa(a) – LDH catalyst 116
4.4 Conclusions 121
Chapter 5 CO_2 Hydrogenation to Methanol over Pd-containing Intermetallic Catalysts 123
5.1 Introduction 123
5.2 Pd promoted NiGa(a)/SiO_2 124
5.2.1 Catalyst characterisation 124
5.2.2 Catalyst performance under CO_2/H_2 129
5.2.3 Catalyst performance under $CO/CO_2/H_2$ at 245 °C, 10 bar 135
5.2.4 Characterisation of spent Pd promoted NiGa(a)/SiO_2 catalyst 136
5.3 Pd-Ga/SiO_2 catalysts for CO_2 hydrogenation to methanol 138
5.3.1 Catalyst preparation and characterisation 139
5.3.2 Catalyst performance in the CSTR with CO_2/H_2 at 245 °C, 30 bar 141
5.3.3 Characterisation of spent catalysts from CO_2/H_2 runs 144
5.4 Conclusions 146
Chapter 6 Single-stage DME Synthesis over Intermetallic Catalysts and Solid Acids under CO_2/H_2 148
6.1 Introduction 148
6.2 Characterisation of γ-Al_2O_3 and zeolites 150

6.3 Performance of γ-Al_2O_3 and zeolites with intermetallic compounds for the combined methanol-DME synthesis in the CSTR under CO_2/H_2 151
6.3.1 Summary of catalyst tests 151
6.3.2 NiGa(a)/SiO_2 as the methanol synthesis component (MSC) 152
6.3.3 $PdGa_{0.5}/SiO_2$ as the methanol synthesis component for the single-stage DME synthesis from CO_2/H_2 171
6.4 Effect of CO in the PFR 177
6.4.1 Performance of γ-Al_2O_3 and zeolites with different MSCs 177
6.5 Conclusions 182
Chapter 7 Conclusions 184
7.1 Conclusions 184
7.2 Future work 187
References 189
Appendix A Experimental Procedures 213
Appendix B CO_2 Hydrogenation to Methanol over Ni-Ga Based Catalyst at Elevated Pressures..... 220
Appendix C Single-stage DME Synthesis over Intermetallic Catalysts and Solid Acids under CO_2/H_2 230

List of Figures

Figure 2.1, Equilibrium MeOH conversion as a function of temperature at 5 bar and 25 bar, feed compositions: CO_2/H_2 = 20/70, replotted from the work by Skrzypek et al. [9] 27
Figure 2.2, Different reaction pathways for methanol synthesis (figure adapted from Li et al. [10]..... 30
Figure 2.3, Schematic representation of the structures of bimetallic alloy nanoparticles (adapted from Li et al. [10]) 43
Figure 3.1, Rig setup 61
Figure 3.2, Equilibrium methanol conversion against temperature at different pressures ... 72
Figure 4.1, TPRx profiles of the catalytic performance of in situ reduced NiGa(a)/SiO_2 and air-oxidised NiGa(a)/SiO_2 (re-reduced at 350 °C) 78
Figure 4.2, TPR profiles for reduced NiGa(a)/SiO_2 81
Figure 4.3, TPRx profiles for NiGa(a)/SiO_2 re-activated at different temperatures 82
Figure 4.4, XRD of monometallic reference materials..... 86
Figure 4.5, XRD pattern of reduced-passivated NiGa(a)/SiO_2 (reference peaks: Ni_5Ga_3, NiGa and Ni_3Ga: Studt et al. [12], Ni/NiO: ICSD no. 011239 and 52265, γ-Ga_2O_3: ICSD no.0152085) 87
Figure 4.6, XRD pattern of reduced-passivated NiGa(b)/SiO_2 (reference peaks: Ni_5Ga_3, NiGa and Ni_3Ga: Studt et al. [12], Ni/NiO: ICSD no. 011239 and 52265, γ-Ga_2O_3: ICSD no.0152085) 89
Figure 4.7, XRD pattern of reduced-passivated NiGa(c)/SiO_2 (reference peaks: Ni_5Ga_3, NiGa and Ni_3Ga: Studt et al. [12], Ni/NiO: ICSD no. 011239 and 52265, γ-Ga_2O_3: ICSD no.0152085) 90
Figure 4.8, TEM images of reduced-passivated (a) NiGa(a)/SiO_2 (b) NiGa(b)/SiO_2 91
Figure 4.9, XPS spectra of passivated NiGa(a)/SiO_2 92
Figure 4.10, XPS spectra of passivated NiGa(b)/SiO_2 92
Figure 4.11, Catalytic performance of Ni-Ga/SiO_2 catalysts compared to Cu/ZnO/Al_2O_3 at 245 °C, 10 bar..... 95
Figure 4.12, Catalytic performance of Ni-Ga/SiO_2 catalysts compared to Cu/ZnO/Al_2O_3 at 245 °C, 30 bar..... 99
Figure 4.13, Normalised MeOH activity as a function of time at 10 bar and 30 bar..... 101
Figure 4.14, Catalytic performance of the fresh and regenerated NiGa(a)/SiO_2 catalyst at 245 °C, 30 bar..... 102
Figure 4.15, XRD of fresh (reduced-passivated) and spent catalysts 103
Figure 4.16, TPO profiles for spent catalysts..... 106

Figure 4.17, XPS spectra of spent Ni-Ga catalysts 107
Figure 4.18, Catalytic performance of NiGa(a)/SiO_2 at 245 °C, 10 bar under CO/CO_2/H_2 . 109
Figure 4.19, Catalytic performance of NiGa(a)/SiO_2 regenerated after CO/CO_2/H_2 run and fresh NiGa(a)/SiO_2 (reaction conditions: 245 °C, 10 bar, CO_2/H_2) 110
Figure 4.20, Catalytic performance of NiGa(b)/SiO_2 at 245 °C, 10 bar under CO/CO_2/H_2 . 111
Figure 4.21, Catalytic performance of NiGa(b)/SiO_2 regenerated after CO/CO_2/H_2 run and fresh NiGa(b)/SiO_2 (reaction conditions: 245 °C, 10 bar, CO_2/H_2) 112
Figure 4.22, Catalytic performance of the regenerated NiGa(b)/SiO_2 (after reaction under CO) and NiGa(a)/SiO_2 at 245 °C, 10 bar under CO_2/H_2 113
Figure 4.23, XRD of spent catalysts 115
Figure 4.24, TPO profiles of spent catalysts from CO/CO_2/H_2 run 116
Figure 4.25, XRD of NiZnGaAl-LDH precursor and reduced-passivated catalysts (reference peaks: ICSD no. 98-009-1553, 57450, 66559, 011239, 52265 and 15208) 118
Figure 4.26, Catalytic performance of NiZnGaAl-LDH at 260 °C, 10 bar 120
Figure 5.1, TPR profiles for the Pd promoted and unpromoted NiGa(a)/SiO_2 precursors (a) Over whole temperature range (b) enlarged low temperature section from the TPR of Pd promoted catalyst from (a) 125
Figure 5.2, XRD patterns of reduced-passivated Pd-NiGa(a)/SiO_2 (350 °C), NiGa(a)/SiO_2 (350 °C), NiGa(a)/SiO_2 (700 °C) (reference peaks: Pd_2Ga: ICSD no. 409939, PdO: JCPDS 85-0713, Pd: ICCD no. 087-0643, α-Ga_2O_3: ICSD no. 27431, Ni_3Ga: Studt et al. [12], Ni and NiO: ICSD no. 011239 and 52265) 128
Figure 5.3, Catalytic performance of Pd-NiGa(a)/SiO_2 (350 °C in situ), NiGa(a)/SiO_2 (700 °C ex situ) and NiGa(a)/SiO_2 (350 °C in situ) at 245 °C, 10 bar 132
Figure 5.4, Catalytic performance of Pd-NiGa(a)/SiO_2 (350 °C in situ) and NiGa(a)/SiO_2 (700 °C ex situ) at 245 °C, 30 bar 134
Figure 5.5, Catalytic performance of Pd-NiGa(a)/SiO_2 (350 °C in situ) and NiGa(a)/SiO_2 (700 °C ex situ) under CO/CO_2/H_2 at 245 °C, 10 bar 135
Figure 5.6, XRD of spent Pd-NiGa(a)/SiO_2 catalyst 136
Figure 5.7, TPO profiles of the spent Pd promoted catalysts 137
Figure 5.8, XRD patterns of reduced-passivated Pd-Ga/SiO_2 catalysts with reference materials (reference peaks: Pd_2Ga: ICSD no. 409939, PdO: JCPDS 85-0713, Pd: ICCD no. 087-0643, α-Ga_2O_3: ICSD no. 27431) 140
Figure 5.9, Catalytic performance of $PdGa_{0.5}$/SiO_2 and $PdGa_3SiO_2$ at 245 °C, 30 bar 142
Figure 5.10, XRD of spent Pd-Ga/SiO_2 catalysts with reference materials (refenrece peaks: Pd_2Ga: ICSD no. 409939, PdO: JCPDS 85-0713, Pd: ICCD no. 087-0643, α-Ga_2O_3: ICSD no. 27431) 144
Figure 5.11, TPO of spent Pd-Ga/SiO_2 catalysts 145

Figure 6.1, Diffraction patterns of fresh (calcined) FER (55) and ZSM-5 (50) and γ-Al_2O_3 150
Figure 6.2, Schematic of MSC and acid catalysts in separated beds in the CSTR 152
Figure 6.3, Total MeOH activity and selectivity at 245 °C, 10 bar (separated beds)..... 154
Figure 6.4, Total MeOH activity of NiGa(a)/SiO_2 with various solid acids at 270 °C, 30 bar 156
Figure 6.5, Product distribution of NiGa(a)/SiO_2 with FER and γ-Al_2O_3 at 270 °C, 30 bar.. 157
Figure 6.6, Product distribution over NiGa(a)/SiO_2 and ZSM-5 obtained from GC 158
Figure 6.7, Performance of Cu/ZnO/Al_2O_3 and ZSM-5 at 270 °C, 30 bar (separated beds) 159
Figure 6.8, XRD patterns of spent catalysts 160
Figure 6.9, TPO profiles for spent solid acid catalysts 162
Figure 6.10, Schematic of physical mixture of MSC with solid acids in the CSTR..... 164
Figure 6.11, Comparison of the total MeOH activity between MSC + solid acid in separated beds and physical mixtures 164
Figure 6.12, Comparison between the selectivity of NiGa(a)/SiO_2 + γ-Al_2O_3 in separated beds and physical mixture 166
Figure 6.13, Catalytic performance NiGa(a)/SiO_2 + ZSM-5 in physical mixture..... 167
Figure 6.14, TPO profiles for spent solid acids in physical mixture 170
Figure 6.15, Total MeOH production rate for $PdGa_{0.5}/SiO_2$ + FER/ZSM-5 at 270 °C, 30 bar (separated bed)..... 172
Figure 6.16, Product distribution for $PdGa_{0.5}/SiO_2$ + FER at 270 °C, 30 bar (separated bed) 173
Figure 6.17, Performance comparison between separated beds and physical mixture of $PdGa_{0.5}/SiO_2$ + FER 174
Figure 6.18, Performance comparison between separated beds and physical mixture of $PdGa_{0.5}/SiO_2$ + ZSM-5..... 175
Figure 6.19, TPO profiles of spent zeolites..... 176
Figure 6.20, Performance of NiGa(a)/SiO_2 based physical mixtures under $CO/CO_2/H_2$ 178
Figure 6.21, Product distribution (from GC data) over NiGa(a)/SiO_2 + ZSM-5 based physical mixtures under $CO/CO_2/H_2$..... 179
Figure 6.22, Performance of $PdGa_{0.5}/SiO_2$ based physical mixtures under $CO/CO_2/H_2$ 180
Figure 6.23, TPO profiles for spent solid acids from $CO/CO_2/H_2$ runs..... 181
Figure A.1, Damaged reactor vessel (inside) 214
Figure A.2, CH_4 concentration over time in a blank experiment (conditions: 245 °C, 10 bar, CO_2/H_2)..... 214
Figure A.3, MeOH production rate measured in the damaged reactor (conditions: 245 °C, 10 bar, CO_2/H_2)..... 215

Figure A.4, XRD pattern for catalysts reduced in different reactors 216
Figure B.1, Diffration patterns for the Ni-Ga catalysts using different passivation technique 220
Figure B.2, Diffraction pattern of reduced-passivated $Cu/ZnO/Al_2O_3$ catalyst 220
Figure B.3, Isotherms (a) SiO_2 (b) $NiGa(b)/SiO_2$ (c) $NiGa(a)/SiO_2$ 221
Figure B.4, XPS spectra of Ga 3d (a) $NiGa(a)/SiO_2$ (b) $NiGa(b)/SiO_2$ 222
Figure B.5, Catalytic performance (MeOH production rate) in pressure cycle experiment 223
Figure B.6, Selectivity for both catalysts in pressure cycle 224
Figure B.7, Catalytic performance (MeOH production rate) over $NiGa(a)/SiO_2$ in the PFR226
Figure B.8, Catalytic performance of $NiGa(a)/SiO_2$ at high conversion 228
Figure B.9, Normalised MeOH activity at high and low conversions 228
Figure B.10, XRD pattern of spent $Cu/ZnO/Al_2O_3$ 228
Figure B.11, TPO profile of catalyst exposed to CO_2/H_2 gas mixture without catalysis 229
Figure C.1, NH_3-TPD profiles of fresh zeolites. Adsorption at 110 °C, heating rate 10 °C/min. Figure taken from the work by R. Montesano [17] 230
Figure C.2, N_2 adsorption and desorption isotherm at 77 K 230
Figure C.3, SEM images of (a) ZSM-5 (b) FER (Figure taken from the work by R. Montesano [17]) 231
Figure C.4, GC trace from $Cu/ZnO/Al_2O_3$ + γ-Al_2O_3 experiment 231
Figure C.5, Product distribution over $NiGa(a)/SiO_2$ + γ-Al_2O_3 in separated beds at 245 °C, 10 bar 232
Figure C.6, Selectivity of $NiGa(a)/SiO_2$ + FER in physical mixtures and separated bed at 270 °C, 30 bar 233
Figure C.7, GC trace given by the reaction over $PdGa_{0.5}/SiO_2$ + ZSM-5 in separated bed at 270 °C, 30 bar 233

List of Tables

Table 2.1, K_a expressions for reactions 1 – 3 26
Table 2.2, Reactions at different acid sites (Y and ZSM-5 zeolites) and methanol dehydration mechanism 55
Table 2.3, Earlier rate equations for methanol dehydration, reproduced from [217] 56
Table 3.1, Effect of impeller speed on the methanol synthesis reaction rate* 66
Table 4.1, Methanol synthesis activity and selectivity of NiGa(a)/SiO_2 protected with cyclohexane 83
Table 4.2, Chemical composition of NiGa(a)/SiO_2, NiGa(c)/SiO_2 and NiGa(c)/SiO_2 84
Table 4.3, BET surface area and pore volume of Ni-Ga/SiO_2 catalysts 85
Table 4.4, Crystallite size of Ni-Ga/SiO_2 catalysts 91
Table 4.5, Ni:Ga ratio measured by different characterisation techniques 93
Table 4.6, Steady state catalytic performance of Ni-Ga/SiO_2 catalysts compared to Cu/ZnO/Al_2O_3 at 245 °C, 10 bar 95
Table 4.7, Catalytic performance obtained with different catalyst mass 98
Table 4.8, Steady state catalytic performance of Ni-Ga/SiO_2 catalysts compared to Cu/ZnO/Al_2O_3 at 245 °C, 30 bar 100
Table 4.9, Crystallite size of spent catalysts 104
Table 4.10, BET surface area and pore volume of spent Ni-Ga catalysts 105
Table 4.11, Coke content of spent catalysts 105
Table 4.12, Surface composition calculated from XPS data 108
Table 4.13, Effect of CO on the catalytic performance of NiGa(a)/SiO_2 109
Table 4.14, Effect of CO on the catalytic performance of NiGa(b)/SiO_2 111
Table 4.15, Coke content on the spent catalysts from CO/CO_2/H_2 run 116
Table 4.16, Comparison of catalytic performance 120
Table 5.1, H_2 consumption in low and high temperature regions for both Pd promoted and unpromoted catalysts 126
Table 5.2, Chemical composition of promoted and unpromoted catalysts 127
Table 5.3, Reduction and reaction conditions for various promoted and unpromoted catalysts 130
Table 5.4, Steady state activity and selectivity of Pd promoted and unpromoted NiGa(a)/SiO_2 catalysts at 245 °C, 10 bar 131
Table 5.5, Steady state activity and selectivity of Pd promoted and unpromoted NiGa(a)/SiO_2 catalysts at 245 °C, 30 bar 134
Table 5.6, Coke content and BET surface area of spent catalysts 137
Table 5.7, Chemical compositions and surface area for both Pd-Ga /SiO_2 catalysts 139

Table 5.8, Comparison of catalytic performance over NiGa(b)/SiO_2, Pd-Ga/SiO_2, commercial Cu/ZnO/Al_2O_3 catalysts 143
Table 5.9, BET surface area and coke content over spent Pd-Ga/SiO_2 catalysts..... 145
Table 6.1, Nominal composition, textural and chemical properties of γ-Al_2O_3, FER and ZSM-5 (data taken from Montesano's work [17]) 150
Table 6.2, Summary of catalyst tests 152
Table 6.3, Coke content on methanol synthesis and dehydration components 161
Table 6.4, Metal content on the recovered solid acids from NiGa(a)/SiO_2 based physical mixtures 168
Table 6.5, Comparison of coke content on different catalyst arrangements (NiGa(a)/SiO_2 as the MSC)..... 170
Table 6.6, Metal content on the recovered zeolites from $PdGa_{0.5}$/SiO_2 based physical mixtures 175
Table 6.7, Comparison of coke content on different catalyst arrangements 176
Table 6.8, Coke content on catalysts run under CO/CO_2/H_2 181
Table A.1, Catalytic performance of NiGa(a)/SiO_2 catalyst reduced in different reactors .. 216
Table A.2, Effect of particle size on the methanol synthesis and dehydration rates over physical mixtures of HiFuel R120 and γ-Al_2O_3 in an internal recycle Berty reactor* (results reproduced from R. Montesano's work [17])..... 217
Table A.3, Response factor for each substance detected in the GC 218
Table A.4, Values of $\Delta Hr, i \ominus$ and $\Delta Gi, 298K \circ$ used in the calculation are taken from the book by M. V. Twigg [53] 219
Table B.1, Chemical and textural properties of Cu/ZnO/Al_2O_3 catalyst..... 221

Chapter 1 Introduction

Currently, over 80% of global energy demand comes from fossil fuels. This has led to strain on global fossil fuel reserves and is exacerbated by the increasing population and rapidly improving living standards in developing countries. This situation is unlikely to change in the immediate future and the global energy demand is estimated to grow by 50% over the next 20 years. Although the proven gas and oil reserves have increased by 70% and 40% respectively [1], only a small fraction is accessible with current technology. Based on the expected demand growth rate, there is only enough supply to last for thirty years [2].

The risk of climate change associated with the use of fossil fuel makes the current situation even more difficult. The emission of greenhouse gas into the Earth's atmosphere, especially anthropogenically-produced carbon dioxide, is believed to be the cause of global temperature rises. As the concentration of CO_2 (and other greenhouse gas such as methane and CFCs) increases, the percentage of infrared radiation reflected back to the Earth increases, leading to an increased temperature of the Earth surface.

Extensive research is constantly being carried out to find solutions for both energy crisis and climate change. Carbon capture and storage (CCS) is one of the options that could help mitigate climate change. About 42% of the global CO_2 emissions from fuel combustions are owed to electricity and heat generation [3], hence, carbon emissions could be effectively reduced if CCS technologies were implemented at large point sources such as power plants. However, CCS is non-profitable and requires a lot of capital investment. On the other hand, carbon capture and utilisation (CCU), which refers to the technologies that turn waste CO_2 into valuable products such as fuels and various chemicals, is a promising way to achieve a profitable yet carbon neutral process. In particular, the hydrogenation of CO_2 using renewable hydrogen (from biomass or water splitting using renewable energy) to methanol, as suggested by the 'methanol economy' concept [4-6], has attracted a lot of attention in the research community since methanol is both a fuel and a key chemical reagent.

Methanol is a safer alternative to hydrogen and liquid natural gas, it can be directly integrated into existing fuel delivery system and infrastructure at a low cost [7]. Methanol is also an important building block for various hydrocarbons. The methanol synthesis process typically takes place over a $Cu/ZnO/Al_2O_3$ catalyst. Despite being the dominant catalyst, it is not most ideal for CO_2 hydrogenation owing to its tendency to catalyse the reverse water gas shift reaction and its accelerated deactivation under CO_2-rich conditions [8, 9]. Therefore, great efforts have been put into the development of more active, selective and stable catalysts for CO_2 hydrogenation to methanol. Among the catalyst innovations, bimetallic catalysts emerge as an important class of catalyst owing to the synergistic effect that could greatly enhance the specific chemical and physical properties of the catalysts compared to their constituent metals [10, 11]. Recently, Studt and co-workers [12] reported the discovery of Ni-Ga catalysts for CO_2 hydrogenation to methanol based on work carried out at atmospheric pressure. Ni_5Ga_3/SiO_2 was reported to have a methanol synthesis activity comparable to the conventional $Cu/ZnO/Al_2O_3$ catalysts but with significantly reduced CO production. However, the thermodynamic equilibrium for CO_2 to methanol is very low at atmospheric pressure (less than 0.02% conversion at 250 °C); for industrial applications Ni-Ga based catalysts would have to operate at elevated pressures. Despite the apparent promise of this catalyst system, due to the severe pre-reduction conditions (700 °C) involved in the preparation of these active Ni-Ga catalysts [13, 14], no high-pressure results have been reported.

In addition to green methanol synthesis, the dehydration of methanol to form dimethyl ether (DME) is also a subject of great interest. DME is a non-toxic, non-corrosive gas with a normal boiling point of -25 °C that can be easily liquefied at pressures above 5 bar at room temperature [15]. The physical properties of DME are similar to that of LPG (liquefied petroleum gas), making its integration into existing storage and distribution systems straightforward [16]. DME has also been identified as a clean alternative fuel for diesel engines due to its high cetane number and low NO_x, SO_x and particulate emissions. In addition to its

role as energy carrier, DME is also a key intermediate for production of many hydrocarbons and oxygenate products [16].

DME can be synthesised via two different routes, the direct and indirect synthesis. The indirect route involves two steps (1) traditional methanol synthesis from syngas over ternary $Cu/ZnO/Al_2O_3$ catalyst (2) methanol dehydration over solid acid catalysts. The direct route, as the name suggests, is a one-step process where syngas is converted to DME in the same reactor under reaction conditions similar to those for methanol synthesis. This requires two catalytic functions: a metallic function that catalyses the methanol synthesis via the hydrogenation of carbon oxides, and an acid function that catalyses the DME formation via methanol dehydration. This can be achieved by using either a physical mixture of methanol synthesis catalyst and solid acid catalyst for methanol dehydration, or a bi-functional catalyst. The direct route is a promising process not only because of the alleviated thermodynamic constraints associated with methanol synthesis by simultaneously forming DME, but also due to lower costs compared to the two-step process [15, 17]. In addition, the possibility of incorporating CO_2 into syngas for DME synthesis brings two main advantages: (1) utilisation of CO_2 [18] (2) hydrogenation of CO_2 to form methanol/DME is a safer way to store renewable H_2 as a fuel.

Unfortunately, the single-stage process has not yet been successfully demonstrated at large scale (demonstration plants) and the catalytic systems explored so far have been inadequate for industrial implementation [17]. Despite the potential of the intermetallic catalysts mentioned earlier, there is limited literature concerning their use as the methanol synthesis component for the single-stage DME synthesis. Furthermore, the potential of various solid acids as the methanol dehydration component as well as the compatibility between the two catalytic functions are still under extensive research [19]. Hence, investigation into the catalytic performance of intermetallic compound based catalysts with solid acid for the single-stage DME synthesis under CO_2-rich conditions is necessary.

1.1 Research objectives

Although intermetallic compound based catalysts (Ni-Ga/SiO_2) have been recognised as promising catalysts for methanol synthesis (refer to Chapter 2 for more detail), there are still many aspects that have not yet been investigated. Therefore, the aim of this thesis is to evaluate and discuss the performance of Ni-Ga based catalysts under elevated pressures as well as their use as the methanol synthesis catalyst in a dual-functional catalytic system with various solid acids for the single-stage DME synthesis under CO_2-rich conditions. To realise this aim, the air-sensitive nature of the Ni-Ga catalysts was overcome using a passivation procedure and the catalytic tests were conducted in a fixed bed stirred tank reactor (CSTR), which provides accurate rate information due to its gradientless nature (i.e. constant temperature, pressure and gas composition throughout the reactor). The research work presented here has the following objectives:

Methanol Synthesis

- To develop a passivation procedure for the Ni-Ga based to facilitate transfer to high-pressure reactors
- To evaluate the performance of Ni-Ga/SiO_2 catalysts under elevated pressures and compare to that of a commercial Cu/ZnO/Al_2O_3 catalyst under CO_2/H_2
- To study the effect of CO in the feed gas on the catalytic performance of the Ni-Ga based catalysts
- To investigate the effect of palladium addition to the Ni-Ga catalyst on the reducibility and performance of the catalyst
- To compare the catalytic performance of Ni-Ga/SiO_2 and Pd-Ga/SiO_2 catalysts

Single-stage DME Synthesis

- To examine the catalytic performance of Ni-Ga/SiO_2/Pd-Ga/SiO_2 + Zeolites system under CO_2/H_2. Ferrierite and ZSM-5 are to be investigated since they have been shown to be stable and selective under CO_2/H_2 [17, 20].

- To assess the influence of proximity between the intermetallic compound based catalysts and solid acid catalysts using physical mixtures
- To study the effect of CO on the catalytic performance of the Ni-Ga/Pd-Ga + zeolite catalysts

1.2 Thesis outline

Chapter 2 presents a literature review. Methanol synthesis via CO_2 hydrogenation is reviewed, with emphasis on the development of intermetallic based catalysts for CO_2 hydrogenation. The solid acid catalyst component for DME synthesis is discussed, followed by the catalytic challenges in the single-stage DME synthesis from CO_2.

Chapter 3 gives details of experiment set-ups and procedures used to test the catalysts. Relevant product analysis, calculation method and catalyst characterisation tests are also described.

Chapter 4 presents and discusses experimental work that examines the passivation approach for the Ni-Ga catalysts as well as the performance of these catalysts under elevated pressures in the CSTR. **Chapter 5** investigates Pd-promotion on the Ni-Ga catalyst and compares the Pd-Ga catalysts to the Ni-Ga catalysts.

Chapter 6 explores the suitability of using the Ni-Ga and Pd-Ga intermetallic based catalysts as the methanol synthesis component with zeolites for the single-stage DME synthesis. The influence of proximity between the catalytic functions is studied and discussed.

Chapter 7 summarises the conclusions and outlines potential future work.

Chapter 2 Literature Review

Climate change and fossil fuel depletion are provoking interest in alternative fuels that are commercially and environmentally friendly. Carbon capture and utilisation with renewable energy for the conversion of CO_2 to value-added products such as methanol and DME has been considered to be a viable option. In this chapter, the concept of methanol economy and aspects of methanol synthesis process (thermodynamics and reaction mechanisms) are addressed first. Next, the methanol synthesis catalysts are reviewed, with emphasis on the recent development in bimetallic catalysts for CO_2 hydrogenation. In the second part of this chapter, the single-stage DME synthesis process and various solid acid catalysts are discussed.

2.1 Methanol synthesis

2.1.1 Methanol economy

Methanol is an important liquid petrochemical in the chemical and energy industries. It is commonly used as solvent and starting material for other chemicals (e.g. formaldehyde, acetic acid and dimethyl terephthalate) and fuel additives (e.g. methyl tertiary butyl ether) [21]. Methanol is also an important feedstock for many other hydrocarbons, such as methanol-to-olefins. In addition, methanol is a liquid energy carrier for renewable hydrogen and it can be used as an alternative fuel or blended with gasoline [4].

Methanol is commercially synthesised from syngas, a mixture of carbon oxides and hydrogen. The mitigation of climate change requires effective utilisation of CO_2, great effort has been put on CO_2 conversion to methanol. Olah et al. [4] proposed the concept of methanol economy, where the production of methanol, dimethyl ether and various synthetic hydrocarbons from captured CO_2 and their uses as fuels and chemicals can free mankind from the dependence on non-renewable fossil fuels and mitigate global warming. Other advantages of methanol synthesis from chemical recycling of CO_2 include the avoidance of CO_2 collection and

sequestration (costly) and the possibility of unlimited sources of transportation fuels and energy [5]. With this approach, the nature of our current energy usage, storage and transportation infrastructure as well as usage of various hydrocarbons and products does not need to be altered drastically [5]. Due to the growing interest in CO_2 recycling, this topic has been subjected to a number of reviews [22-25] recently and novel CCU technologies have been reviewed and reported to the European Commission [26].

2.1.2 Sources of renewable CO_2/H_2

In 2011, Olah and co-workers [6] proposed that the methanol economy is based on the anthropogenic carbon cycle that combines carbon capture and storage with chemical recycling. Methanol is currently produced from fossil fuel-derived syngas, which is non-renewable and quickly diminishing. Therefore, the recycling of CO_2 should be coupled with hydrogen generated from water to offer long-term sustainable solution to meet our future energy demand.

Sources of CO_2

Today, 90% of the world's primary energy requirement is met by burning fossil fuel. Together with deforestation, this has led to a significant rise in the atmospheric CO_2 concentration from pre-industrial level of 280 ppm to the current level of 400 ppm. CO_2 being the most important greenhouse gas (GHG), is responsible for around 64% of the greenhouse effect, which is related to the global warming and climate change by absorption and reemission of the infrared radiation from the sun [27].

To prevent the CO_2 concentration reaching a predicted level of 570 ppm at the end of the century, assuming business as usual, it is necessary to curb CO_2 emission. This can be achieved by increasing the penetration of renewable energy systems, improving energy efficiency and deploying technologies such as carbon capture and storage (CCS) [22, 28]. Although the renewable energy systems can decarbonise electricity generation sector, they cannot reduce the CO_2 emissions from other industrial sectors. For these, CCS and CCU must be used. Currently, the individual components of CCS are well-established technologies but

there are several challenges in integrating them together for large-scale implementation. These barriers include high capital investment and the potential risk of CO_2 leakage [29]. On the other hand, the CCU process where the CO_2 is captured and reused has received increasing attention due to its economical benefits and the contribution to the sustainable energy and environmental sectors [22]. It is important to note that CCU is only a short term strategy as the CO_2 that is reused still needs to be stored at the end of its lifecycle.

The most significant source of CO_2 is from the flue gases emitted by power plants [30]. The three main techniques for the capture of these CO_2 are pre-combustion, post-combustion and oxy-fuel capture [31]. In the pre-combustion capture, CO_2 is removed by gasification of the fossil fuels before combustion. This produces a stream that is rich in CO_2, which makes the subsequent CO_2 removal easier. The post-combustion capture refers to the removal of CO_2 from the flue gas after the combustion is complete. Oxy-fuel capture is the process of using pure oxygen for combustion instead of air, this makes the separation more convenient as the combustion products are mainly water and CO_2.

Post-combustion capture is considered to be a more viable technology for existing power plants due to relatively easy retrofit. However, the major barrier of its implementation is the separation of CO_2 from flue gas stream with low CO_2 partial pressure. Many technologies have been investigated over the years, for example, chemical absorption, membrane separation, calcium-looping and cryogenic separation [32]. Among them, chemical absorption is a more suitable and mature technology. Amine solvents such as monoethanolamine (MEA), diethanolamine (DEA) and methyl diethanolamine (MDEA) are most widely used in the industries nowadays due to their good performance and low cost [33]. Ionic liquids have been reported to be a good replacement of amine-based solvents owing to the advantages of high CO_2 solubility, thermal stability and tuneable structures [34]. New materials such as solid sorbents (e.g. zeolites, layered double oxides, carbon-based adsorbents, etc.) are attracting more attention due to their promising adsorption capacity, selectivity and stability [35-37]. However, being more energy-intensive is usually associated with chemical absorption

processes. Recently, membrane-based separation is considered to become a promising option for CO_2 separation. The advantages of membrane technologies include simplicity, low environmental impact and less energy penalty [38]. In addition to CO_2 separation, impurities in CO_2 captured from combustion based power generation such as sulphur- or chlorine-containing substances are often an issue for the utilisation of captured CO_2, as these impurities can easily poison metal catalysts [8].

Sources of H_2

Currently, industrial manufacture of hydrogen is mainly carried out by coal gasification, steam reforming and partial oxidation of hydrocarbons. These technologies are based on fossil fuel processing, which has two main disadvantages, fossil fuel depletion and considerable CO_2 emission [39, 40]. Hydrogen can also be produced from renewable sources, for instance, water electrolysis with electricity from renewable energy [41]. Alkaline electrolysers (ALK) have been the most mature technology and they work by having two electrodes separated by a diaphragm in alkaline electrolyte solution, where the hydroxide ions (OH^-) are transported from the cathode to the anode. Recently, the state-of-the-art nickel based electrolyser demonstrated good corrosion resistance and high efficiency [42]. In addition to ALK, proton exchange membrane (PEM) electrolysers have been introduced as alternative that is more efficient and flexible.

Other than water electrolysis, photocatalytic water splitting is a promising technology to produce renewable hydrogen using solar energy. The decomposition of water under sunlight to produce hydrogen and oxygen takes place over semiconductor catalysts. Most of these catalysts are only active in the ultraviolet spectrum, therefore, numerous research has been conducted to develop active and stable catalysts for visible light applications [43]. TiO_2 is one of the most well-known photocatalyst because it is stable, cheap and environmental friendly [44]. However, the drawbacks of TiO_2 include the rapid recombination of photogenerated electron-hole pairs, backward reaction and poor activation by visible light [45]. To overcome these, modifications have been made to the TiO_2 catalysts, such as metal deposition (e.g.

Ag_2O/TiO_2 [46], deposition of Pt-group metals [47], hybridisation with carbon materials [48-50] and binary composites coupling (e.g. WO_3, SiO_2, Al_2O_3, CdS, etc. [48]).

Biomass derived CO_2/H_2

Biomass has the potential to be converted into renewable energy. Waste biomass can be sourced from various origins, which are not limited to agricultural crops, animal wastes and municipal solid wastes. The superficial water gasification (SWG) is an emerging process to convert biomass to synthesis gas, the advantages of SWG include higher conversion efficiency, drying not required, cost-effective and reduced pollutions [51]. Aqueous-phase reforming (APR) is also a promising process to produce CO_2/H_2 mixture. In APR, a wide range of biomass can be used as the feedstock and less CO is produced due to the facilitated reverse water gas shift reaction under typical APR operating temperature [52]. However, the products from the above processes need stoichiometric adjustment (addition of hydrogen or CO_2 removal) to give a higher H_2/CO_2 ratio (typically ≥ 3 is desirable) for methanol synthesis over most catalysts.

2.1.3 Methanol synthesis thermodynamic and kinetic considerations

In order to better understand the catalytic performance in CO_2 hydrogenation to methanol process, the thermodynamic and kinetic aspects of the methanol synthesis process should be addressed first. In this section, existing literature on the thermodynamics, reaction mechanisms and kinetic models are reviewed. It is noted that the mechanistic investigations on these areas are predominantly based on the most studied Cu-based catalytic systems.

2.1.3.1 Thermodynamic equilibrium

The main equations governing the methanol synthesis are as follows [53]:

$$CO + 2H_2 \rightleftharpoons CH_3OH \qquad \text{Reaction 1}$$

$$\Delta H = -91 kJ/mol\,;\ \Delta G = -25.34\, kJ/mol$$

$$CO_2 + 3H_2 \rightleftharpoons CH_3OH + H_2O \qquad \text{Reaction 2}$$

$$\Delta H = -49.5 kJ/mol\,;\ \Delta G = 3.30\, kJ/mol$$

$$CO + H_2O \rightleftharpoons CO_2 + H_2 \qquad \text{Reaction 3}$$

$$\Delta H = -41.2 kJ/mol\,;\ \Delta G = -28.60\, kJ/mol$$

Any two of reactions 1 – 3 can define the equilibrium compositions and describe the system thermodynamically. Hydrogenation of carbon monoxide (reaction 1) has always been the basic expression for methanol synthesis, however, others believe that methanol production over Cu-based catalysts is the result of carbon dioxide hydrogenation (reaction 2).

Both reactions 1 and 2 are reversible and exothermic, and both forward reactions undergo volume reduction. Therefore the maximum conversion can be achieved at low temperatures and high pressures. As a result, typical industrial methanol synthesis is performed at 250 °C and 50 bar.

Some of the expressions for the equilibrium constants (over Cu-containing catalysts) proposed by different authors are summarised in Table 2.1, where K_{a1}, K_{a2}, K_{a3} are the equilibrium constants for reaction 1, 2 and 3 respectively. Other expressions can be found in the book *Methanol Synthesis* [54].

Table 2.1, K_a expressions for reactions 1 – 3

Reaction	Author	Equilibrium constant
$\boldsymbol{CO + 2H_2 \rightleftharpoons CH_3OH}$	Kuznetzov et al. [55]	$lnK_{a1} = \frac{3748.7}{T} - 9.2833lnT + 3.1475 \times 10^{-3}T - 4.2613 \times 10^{-7}T^2 + 13.8144$
	Graaf et al. [56]	$log_{10}K_{a1} = \frac{5139}{T} - 12.621$
	LE Wade et al. [57]	$K_{a1} = 9.740 \times 10^{-5} \times \exp\left[21.225 + \left(\frac{9143.6}{T}\right) - (7.492lnT) + (4.076 \times 10^{-3})T - (7.161 \times 10^{-8})T^2\right]$
$\boldsymbol{CO_2 + 3H_2 \rightleftharpoons CH_3OH + H_2O}$	Kuznetzov et al. [55]	$lnK_{a2} = \frac{1581.7}{T} - 8.7639lnT + 2.1105 \times 10^{-3}T - 1.9303 \times 10^{-7}T^2 + 15.0921$

$\boldsymbol{CO_2 + H_2 \rightleftharpoons CO + H_2O}$	Kuznetzov et al. [55]	$lnK_{a3} = \frac{-2167}{T} + 0.5194lnT - 1.037 \times 10^{-3}T + 2.331 \times 10^{-7}T^2 + 1.2777$
	Graaf et al. [56]	$log_{10}K_{a3} = \frac{-2073}{T} + 2.029$
	L. Bissett [58]	$K_{a3} = \exp\left[-13.148 + \left(\frac{5639.5}{T}\right) + (1.077lnT) + (5.44 \times 10^{-4})T - (1.125 \times 10^{-7})T^2 - \left(\frac{49170}{T^2}\right)\right]$

Skrzypek et al. [9, 59] carried out comprehensive studies on the thermodynamics of methanol synthesis. The computational results were plotted as a function of temperature and pressure for a few feed gas compositions. Some of them (CO-free feed gas) are reproduced and shown in Figure 2.1.

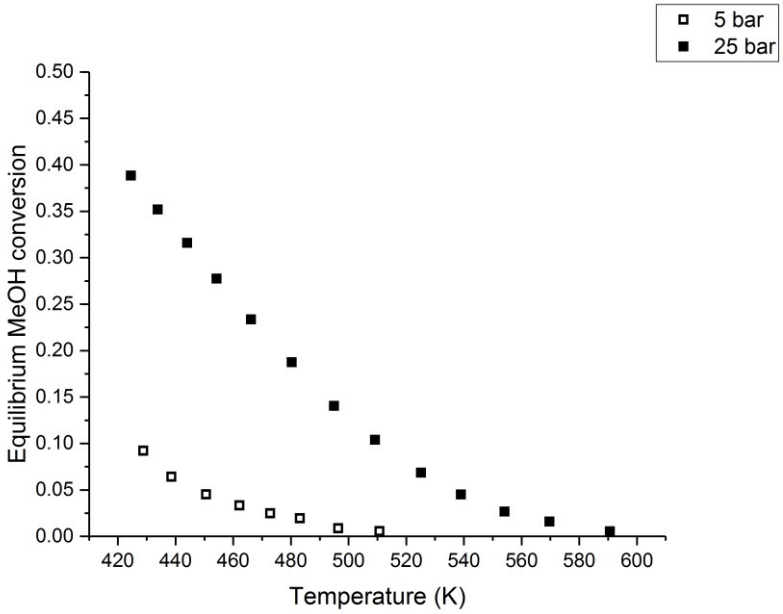


Figure 2.1, Equilibrium MeOH conversion as a function of temperature at 5 bar and 25 bar, feed compositions: CO_2/H_2 = 20/70, replotted from the work by Skrzypek et al. [9]

The CO_2 hydrogenation to methanol is not as thermodynamically favourable as CO hydrogenation. Arakawa et al. reported that the equilibrium methanol yield from CO_2 is about 40% while the yield from CO is 80% at 200 °C [60]. Under CO-free condition, the undesirable

reverse water gas shift reaction becomes important, which further decreases the methanol yield.

2.1.3.2 Reverse water-gas shift reaction

Reverse water-gas shift (rWGS) is the reaction between carbon dioxide and hydrogen to form carbon monoxide and water (reaction 3). rWGS is commonly involved in several industrial processes such as methanol synthesis and methanol steam reforming.

In catalytic CO_2 hydrogenation to methanol, a third of the H_2 is converted to water according to Reaction 2. This is significantly higher compared to commercial methanol synthesis from syngas [61]. In order to overcome the thermodynamic barrier associated with the unreactivity of CO_2, higher temperature is used to facilitate CO_2 activation. However, more undesirable CO and H_2O are produced as byproducts from the rWGS reaction. Consequently, it leads to higher H_2 consumption and reduced methanol synthesis [9]. Water formed from the rWGS is one of the major reasons for the suppression of catalytic activity. This is because water molecules compete with CO_2 for adsorption sites on the catalyst surface, preventing the adsorption of CO_2 for methanol formation [62]. In addition, water also causes rapid sintering in $Cu/ZnO/Al_2O_3$ catalyst, this will be discussed in the next section. Therefore, a catalyst with low rWGS activity should be developed for effective methanol synthesis from CO_2.

2.1.3.3 Reaction mechanism over Cu based catalysts

There had been a long debate whether methanol synthesis was CO hydrogenation or CO_2 hydrogenation. Klier and co-workers suggested that methanol was formed predominantly from CO since the maximum methanol production rate was observed at 2% CO_2 ($CO:CO_2:H_2$ = 28:2:70 and the rate decreased significantly as CO_2 concentration was increased [63]. This maximum was considered to be the result of the stabilising effect of CO_2 on the monovalent copper (Cu^+ or Cu_2O). Since CO_2 adsorbed more strongly on the catalyst, the methanol production dropped as CO_2 concentration increased. On the other hand, Rozovskii et al. [64] proposed an alternative mechanism, in which methanol synthesis was considered to proceed

via CO_2 hydrogenation instead of CO. In addition, they claimed that the net source of carbon is CO oxidised via WGS reaction. Following this work, Chinchen et al. [65] conducted isotope-labelling experiments in 1987, where ^{14}CO or $^{14}CO_2$ tracer was added to the syngas for methanol synthesis over a commercial Cu/ZnO catalyst. Strong evidence indicated that CO_2 was the major source of carbon under industrial conditions [66]. In addition, there was no common surface carbon intermediate for both methanol synthesis and WGS over Cu/ZnO catalyst. Methanol synthesis via direct CO hydrogenation only occurred when the CO_2 concentration was very low, or at high temperatures [67]. Other studies using isotope-labelled $C^{18}O_2$ showed that both CO_2 and CO hydrogenation were possible and the results were further complicated by the exchange of isotope-labelled oxygen atoms between the carbon oxides and catalyst oxides [68, 69]. Since Cu/ZnO catalyst is a good WGS catalyst which facilitates the interconversion of carbon oxides, the controversy about the source of methanol still exists, but it is now widely accepted that the main mechanism of methanol synthesis over copper-based catalyst is via CO_2 hydrogenation at the prevailing conditions used industrially.

Deduced from extensive observations from IR spectroscopy, X-ray photoelectron spectroscopy and scanning tunnelling microscopy, the most important intermediate involved in methanol synthesis is the formate species ($HCOO^*$). It arises due to direct CO_2 hydrogenation via an Eley – Rideal (E – R) mechanism [65, 70, 71], involving pre-adsorbed surface hydrogen on the catalyst surface. Hence, it is considered to be a step by step process where the formate species are converted to dioxymethylene ($H_2CO_2^*$), formaldehyde (H_2CO^*), methoxy (CH_3O^*) and finally methanol (CH_3OH) [71].

It was thought that when hydrogen molecules collided with cupper surface, dissociation of hydrogen occurred and hydrogen remained as adsorbed surface atoms [71]. On stepped/rough or flat surfaces such as Cu (775) and Cu (111), the co-adsorption of CO_2 led to the formation of carbonate and/or bicarbonate species, however, the initial release of an oxygen atom from CO_2 was essential. Thus CO_2 was converted to CO and surface oxygen (O*) and/or hydroxyl (HO*), which played an important role in methanol formation by promoting

the adsorption of CO_2 and its subsequent hydrogenation [67]. Although the source of formate remains unclear due to difficulties in measurement under harsh reaction conditions, the IRRAS (infrared reflection absorption spectroscopy) spectra provided evidence that the conversion of carbonate to formate had occurred [71].

However, other authors [72] claimed that on clean, single-crystal Cu (111), (110) and (100) surfaces, no reaction was observed upon adsorption of CO_2. DFT analysis showed that on Cu (111) surface, the formation of formate did not involve a carbonate intermediate and the hydrogenation of HCOO* resulted in HCOOH* instead of dioxymethylene. In this case, CO not only promoted the reaction, but CO* formed was also hydrogenated to HCO*, CH_2O*, CH_3O* and CH_3OH* [72]. In addition, kinetic studies demonstrated that formate formation was 100 times faster than the rate of methanol desorption [73]. Thus, methanol synthesis on copper could not be the result of direct hydrogenation from (bidentate) formate species by adsorbed hydrogen alone. A water-promoted mechanism involving carboxyl intermediate was also proposed by Yang and co-workers [74]. This hydrocarboxyl (COOH) mechanism was proposed to following the sequence COOH, HCOOH, HCO, HCOH, CH_2OH then CH_3OH (Figure 2.2), which was kinetically more favourable than the formate pathway for the CO_2 hydrogenation to methanol on Cu (111). Apart from formate and methoxy species, due to the unstable nature of other reaction intermediates, no spectroscopic observations have been obtained. Hence the route and reaction intermediates involved in methanol synthesis are still not fully understood.

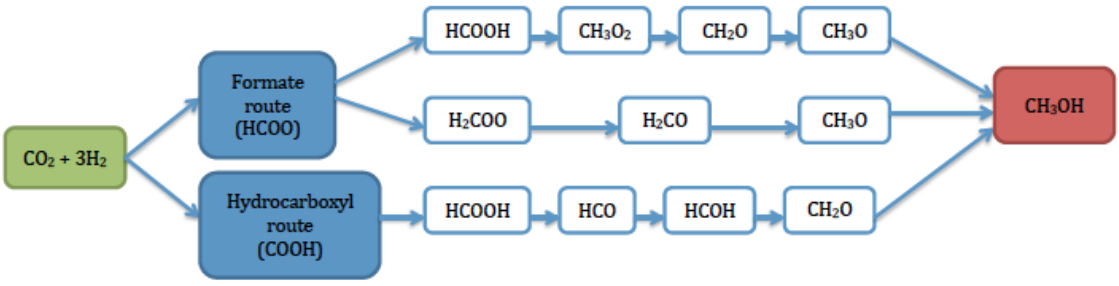


Figure 2.2, Different reaction pathways for methanol synthesis (figure adapted from Li et al. [10]

2.1.3.4 Kinetic models for methanol synthesis and WGS

Various kinetic equations haven been proposed in the last fifty years, however, development was slow due to the lack of clarity regarding the reaction mechanism. In this section, some of the important kinetic models will be presented. Leonov [75] proposed the first model for methanol synthesis over Cn/ZnO/Al_2O_3 catalysts, however, there was no CO_2-dependent term in the equation as it was assumed that CO was the only source of carbon for methanol formation. Klier and co-workers [76] carried out extensive experimental work on kinetics for methanol synthesis. They concluded that the reduced state of the catalyst was inactive while the intermediated oxidised state (Cu^+ dissolved in the ZnO lattice) was catalytically active. The ratio of the two states A_{ox}/A_{red} was controlled by the ratio of CO/CO_2 in the syngas through a redox-like mechanism (shown in the equation below) with an equilibrium constant K_{eq}.

$$CO_2 + A_{red} \rightleftharpoons CO + A_{ox}$$

Furthermore, it was assumed that CO_2 competed with CO and H_2 for active sites and the products CH_3OH and H_2O were weakly adsorbed. This led to the equation:

$$r_{CH_3OH} = const\frac{K_{redox}^3\left(\frac{p_{CO_2}}{p_{CO}}\right)^3(p_{CO}p_{H_2}^2 - \frac{p_{CH_3OH}}{K_1^*})}{[1+K_{redox}\left(\frac{p_{CO_2}}{p_{CO}}\right)]^3(F+K_{CO_2}p_{CO_2})^n} + k'(p_{CO_2} - \left(\frac{1}{K_2^*}\right)\left(\frac{p_{CH_3OH}p_{H_2O}}{p_{H_2}^3}\right))$$

Next, Villa came up with another set of equations, which assumed again only CO hydrogenation occurred but the WGS reaction must be considered [77]:

$$r_{CH_3OH} = \frac{f_{CO}f_{H_2}^2 - f_{CH_3OH}/K_1^*}{(C_1 + C_2f_{CO} + C_3f_{H_2} + C_4f_{CO_2} + C_5f_{CH_3OH})^3}$$

$$r_{rWGS} = \frac{f_{CO_2}f_{H_2} - f_{CO}f_{H_2O}K_3^*}{C_6(1 + C_7f_{CO} + C_8f_{CO_2} + C_9f_{H_2})^2}$$

where f is the fugacity in atm and C_i is a constant

Graaf presented kinetic expressions for three synthesis routes, taking into account both CO and CO_2 hydrogenation. A dual-site Langmuir-Hinshelwood mechanism was proposed where the formation of methanol occurred via successive hydrogenation steps while the WGS took place via a formate route [78]. The final set of equations is:

$$r_{CH_3OH1} = \frac{k'_{ps,1c}K_{CO}[f_{CO}f_{H_2}^{\frac{3}{2}} - \frac{f_{CH_3OH}}{f_{H_2}^{\frac{1}{2}}K_1^*}]}{(1 + K_{CO}f_{CO} + K_{CO_2}f_{CO_2})[f_{H_2}^{\frac{1}{2}} + \left(\frac{K_{H_2O}}{K_{H_2}^{\frac{1}{2}}}\right)f_{H_2O}]}$$

$$r_{CH_3OH2} = \frac{k'_{ps,2c}K_{CO_2}[f_{CO_2}f_{H_2}^{\frac{3}{2}} - \frac{f_{CH_3OH}f_{H_2O}}{f_{H_2}^{\frac{3}{2}}K_2^*}]}{(1 + K_{CO}f_{CO} + K_{CO_2}f_{CO_2})[f_{H_2}^{\frac{1}{2}} + \left(\frac{K_{H_2O}}{K_{H_2}^{\frac{1}{2}}}\right)f_{H_2O}]}$$

$$r_{rWGS} = \frac{k'_{ps,3b}K_{CO_2}(f_{CO_2}f_{H_2} - f_{H_2O}f_{CO}K_3^*)}{(1 + K_{CO}f_{CO} + K_{CO_2}f_{CO_2})[f_{H_2}^{\frac{1}{2}} + \left(\frac{K_{H_2O}}{K_{H_2}^{\frac{1}{2}}}\right)f_{H_2O}]}$$

However this model did not account for some intermediates that featured in two different reactions, hence it yields two different concentrations for the same intermediate such as the formyl and methoxy species [79].

Vanden Bussche and Froment [79] suggested another model for CO_2 hydrogenation, which took place on the oxidised copper surface via a carbonate, bicarbonate, Cu formate, formaldehyde, methoxy route, as shown below.

$H_2(g) + 2s \rightleftharpoons 2H.s$	K_{H_2}
$CO_2(g) + s \rightleftharpoons O.s + CO(g)$	k_1, K_1 (rds)
$CO_2(g) + O.s + s \rightleftharpoons CO_3.2s$	K_2

$$CO_3.2s + H.s \rightleftharpoons HCO_3.2s + s \qquad K_3$$

$$HCO_3.2s + s \rightleftharpoons HCO_2.2s + O.s \qquad K_4$$

$$HCO_2.2s + H.s \rightleftharpoons H_2CO_2.2s + s \qquad k_{5a} \text{ (rds)}$$

$$H_2CO_2.2s \rightleftharpoons H_2CO.s + O.s \qquad k_{5b}$$

$$H_2CO.s + H.s \rightleftharpoons H_3CO.s + s \qquad K_6$$

$$H_3CO.s + H.s \rightleftharpoons CH_3OH(g) + 2s \qquad K_7$$

$$O.s + H.s \rightleftharpoons OH.s + s \qquad K_8$$

$$OH.s + H.s \rightleftharpoons H_2O.s + s \qquad K_9$$

$$H_2O.s \rightleftharpoons H_2O(g) + s \qquad K_{H_2O}$$

The concentration of free active sites C_s was obtained from the balance over the total number of sites C_t, the concentrations of adsorbed intermediate species were neglected. The following expressions were proposed:

$$r_{CH_3OH} = k'_{5a}K'_2K_3K_4K_{H_2}p_{CO_2}p_{H_2}\left(1 - \frac{1}{K_2^*}\frac{p_{H_2O}p_{CH_3OH}}{p_{H_2}^3 p_{CO_2}}\right)\beta^3$$

$$r_{rWGS} = k'_1 p_{CO_2}\left(1 - K_3^*\frac{p_{H_2O}p_{CO}}{p_{CO_2}p_{H_2}}\right)\beta$$

$$\beta = \frac{C_s}{C_t} = \frac{-b+\sqrt{b^2+4a}}{2a}$$

where $a = K'_2K_3K_4\sqrt{K_{H_2}}p_{CO_2}\sqrt{p_{H_2}} + \frac{K'_2K_{H_2O}}{K_{H_2}K_8K_9}\frac{p_{H_2O}p_{CO_2}}{p_{H_2}}$

and $b = 1 + \frac{K_{H_2O}}{K_8K_9K_{H_2}}\frac{p_{H_2O}}{p_{H_2}} + \sqrt{K_{H_2}p_{H_2}} + K_{H_2O}p_{H_2O}$

in which $k'_{5a} = k_{5a}\cdot c_t^2$, $k'_1 = k_1\cdot C_t$, $K'_2 = K_2\cdot C_t$, p_i is the partial pressure for component i, k_i and K_i are the kinetic and equilibrium constants for the reaction steps proposed while K_2 and K_3 are the thermodynamic constants for the gas phase equilibrium for CO_2 hydrogenation and rWGS respectively.

Although Graaf and Froment models are widely used, they may have their limitations [80]. For

example, Bernardi and co-workers [81] demonstrated that the Graaf model yielded better results at low CO_2 inlet concentrations than the Froment model did, this observation was attributed to the fact that the Graaf model considered both direct CO and CO_2 hydrogenation while the Froment model only included the CO_2 hydrogenation step and the rWGS. Another example would be the assumption of a single type of surface active centres in both models, which was found to be inaccurate according to more recent studies [82-84]. Over the years, some of these limitations have been addressed in the literature and modifications were made to improve the models. For instance, Mignard et al. [80] modified the Froment model by adjusting the activation energies to make it more sensitive to temperature and Seidel et al. [85] proposed an extended model that takes into account different active centres and handles transient operating mode and a wide range of feed gas compositions.

2.1.4 Conventional $Cu/ZnO/Al_2O_3$ catalyst

In 1923, BASF was the first to commercialise the CO hydrogenation to methanol process, which operated at 300 bar and 350 – 400 °C over a $ZnO\text{-}Cr_2O_3$ catalyst [86]. Two years later, the Cu/ZnO based catalyst was reported to possess methanol synthesis activity [87]. However due to its poor lifetime in heavily sulphur and chlorine contaminated synthesis gas, it was not commercialised until the 1960s, when Imperial Chemical Industries (ICI) developed the low-pressure process [86]. Since then, the $Cu/ZnO/Al_2O_3$ based catalyst has been the main catalyst for industrial-scale methanol synthesis owing to its high activity and selectivity.

Despite extensive research on copper-based methanol synthesis catalyst, the nature of active sites is still not fully characterised. Klier suggested that monovalent Cu^+ sites were responsible for the catalytic activity [63], but other studies revealed that the catalytic activity was linearly proportional to the area of metallic copper. Thus, small Cu crystallites would result in higher catalytic activity. Particle size also has an influence on the proportions of low-index Cu (111) and (100) planes, corner and edge atoms. Surfaces with smaller particles tend to have more open planes and defect sites containing coordinately unsaturated atoms, which are generally more reactive [88]. Therefore, undistorted Cu surface was found to be catalytic inactive. The

presence of steps was required, which could be stabilised by bulk defects such as stacking faults and twin boundaries terminating at the surface [89]. It was reported by Fujitani and co-workers [90] that the turnover frequency (TOF) for Zn-free single-crystal Cu surfaces at 250 °C could be ranked as (110) > (311) > (100) > (111) [90]. This order was in agreement with the density function theory (DFT) study on the formate adsorption energy on Cu planes [91].

According to Chinchen, the turnover number (activity) of the catalyst remained the same regardless of type of metal oxide support used [92]. Spencer et al. [93] proposed that even though there was no synergetic effect between ZnO and copper, the basic ZnO was able to neutralise the surface acidity of alumina, retarding DME formation over alumina. On the contrary, other workers reported a synergetic effect between Cu and ZnO [94-98]. Burch et al. [99, 100] speculated that this effect involves the spillover of adsorbed species from ZnO to copper. Kanai et al. [96] thought that the synergy observed was related to the creation of active sites such as Cu^{+} stabilised by ZnO_x moieties on the Cu surface. Moreover, the authors also showed that the migrated ZnO_x species was partly dissolved into the Cu particles, forming Cu-Zn alloy. From DFT calculations, the beneficial role of Zn at the catalyst's surface was explained. By alloying Zn with copper, the adsorption strength of various surface intermediates (HCO, H_2CO and H_3CO) was improved [89]. Chinchen [65] measured the apparent copper surface area before and after methanol synthesis, it was found that the oxygen coverage varied between 25% and 40% depending on the syngas composition. Correlation was found between the catalytic activity and the surface oxygen coverage. Similar results were obtained for the positive relationship between catalytic activity and Zn coverage [101], hence further proved that ZnO species on the copper surface had a promotional effect on the catalytic activity. However, this is not true for all Cu surfaces. For instance, the Zn-deposited Cu (111) surface was 13 times more active compared to the same Cu surface without Zn; but for Cu (110), Zn acted as a poison [90].

The performance (activity, selectivity or stability) of the methanol synthesis catalyst can be improved by using a promoter. To this aim, Al_2O_3 is widely used as the promoter for the Cu-

based catalyst. In the presence of Al_2O_3, the highly dispersed Cu/ZnO structure is stabilised and the formation of zinc aluminate prevents the agglomeration of the active sites. Moreover, it accelerates the adsorption and activation of CO owing to its disorder and defect surface domain [102].

As also noted in the beginning of this section, although the copper based catalyst has been the most studied system for methanol synthesis, controversies still remain in areas concerning the active sites, roles of support and promoters as well as the reaction mechanism [102].

Catalyst deactivation

There are several factors that lead to the deactivation of Cu/ZnO based catalyst, including poisoning by trace impurities in the feed gas, coke deposition [103] and Cu sintering.

In industries, the low operating temperature thermodynamically favours the adsorption of poisons, and the lost in activity is mainly due to active sites being blocked by sulphur compounds [104]. In addition to sulphur compounds, chlorine compounds are known for their ability to deactivate methanol synthesis catalyst by blockage of active sites and/or modification of catalyst texture. The latter can lead to sintering of the catalyst due to the formation of volatile chloric compound of copper, which is then transported through the gaseous phase [54]. Other metal impurities (such as nickel and iron) in the system can catalyse side reactions, resulting in reduced methanol selectivity.

As mentioned earlier, the sintering of copper leads to the deactivation of the catalyst and it is the predominant deactivation mode for Cu/ZnO catalysts. For metals, the primary sintering mechanism in the bulk is the surface diffusion and fusion of atoms, supported by the presence of water [105]. In the 30s, Tammann introduced the Tammann temperature, which is defined as the temperature at which the solid phase becomes mobile. Baker further related the mobility temperature of various metals and the bulk melting temperature through the equation:

$$T_{mobile}\ (K) = 0.5 \times T_{bulk\ melting}$$

The mobility temperatures for Cu, ZnO and Al_2O_3 are 670K, 1160K and 1144K respectively. Another notation used is the Huttig temperature, at which the atoms at defects become mobile. It is defined as 1/3 of the melting point of metal. For Cu, the Huttig temperature (180 °C) is lower than the typical operating temperature, hence, at low-pressure operations only the sintering of copper is expected [54]. It was found that at temperatures above 227 °C, copper particles began to migrate and form larger agglomerates [106]. This phenomenon reduced the catalytic surface area and the interfacial contact with the oxide support, leading to a loss of catalytic activity. The addition of a spacer such as ZnO and Al_2O_3 to the catalytic system can significantly reduce the sintering of the copper particles [107]. Spacer is a chemically neutral refractory material, which mechanically isolates and stabilise the copper particles such that sintering of metallic particles is minimised. However, recent studies suggested that the deactivation was mainly driven by the change in ZnO moieties since ZnO is the most dynamic species in the catalyst system and no noticeable change was found on the Cu nanoparticles [108].

Even the reactants (syngas) can cause catalyst deactivation. Klier [63] discovered that the maximum catalyst activity was obtainable at an optimum surface oxidation state. The presence of CO_2 in syngas increases the oxidation of the catalyst surface, while CO and H_2 increase the reduction potential. Therefore, during prolonged heating of the catalyst under strongly reducing conditions, irreversible deactivation can occur due to the partial reduction of ZnO followed by the formation of α-brass [109-111]. However, CO_2-rich condition is also undesirable since it promotes the rWGS reaction, additional water produced accelerates the crystallisation of Cu and ZnO components and consequently the catalyst suffers more deactivation than under CO-rich condition [112]. Most recent work on the deactivation of $Cu/ZnO/Al_2O_3$ demonstrated that the combination of metallic Cu oxidation (to form Cu^{2+}) and agglomeration of ZnO caused the catalyst to deactivate during CO_2 hydrogenation to methanol [113].

2.1.5 Recent advances in CO_2 hydrogenation catalysts

With the current interest in climate change mitigation, the incorporation of CO_2 into syngas leads to great interests on catalysts for CO_2 hydrogenation. Extensive works have been done to modify the existing $Cu/ZnO/Al_2O_3$ catalyst. For example, Pd-promoted $Cu/ZnO/Al_2O_3$ was shown to improve the methanol production by hydrogen spillover without affecting the catalytic stability [114] and Pd also act as a reduction promoter [115]. As a metal oxide support for methanol synthesis catalyst, zirconia has attracted considerable attention due to its mechanical and thermal stability, the ability to form a high interfacial area through interaction with microcrystalline copper particles and a high stability under reducing/oxidising atmosphere [102]. Yang and co-workers doped Cu/ZnO with ZrO_2 and found that the copper dispersion was higher compared to Cu/ZnO alone. As a result, the ZrO_2-doped Cu/ZnO catalyst exhibited much higher activity and selectivity in CO_2 hydrogenation to methanol [116]. Many other ZrO_2 supported Cu/ZnO catalysts have been studied in the past years, usually with a different preparation method to modify catalytic properties [117-120]. Promoter such as Mn was also added to $Cu/ZnO/ZrO_2$, over which a higher methanol production rate was observed [117]. Multicomponent catalysts such as $Cu/ZnO/Al_2O_3/ZrO_2$ and $Cu/ZnO/Al_2O_3/Ga_2O_3$ were reported to be highly active for methanol synthesis from CO_2/H_2. The stability of these catalysts can be further improved by the addition of a small amount of colloidal SiO_2 [121].

Other than Cu/ZnO based catalysts, γ-Al_2O_3 supported catalysts such as $Cu/CeO_2/\gamma$-Al_2O_3 [122], $Cu\text{-}V/\gamma$-Al_2O_3 [123] were investigated and found to have good catalytic performance for CO_2 hydrogenation.

Besides Cu-containing catalysts, In_2O_3 supported on ZrO_2 was found to be a superior catalyst for methanol synthesis with excellent activity, selectivity and stability due to the creation and annihilation of oxygen vacancies as active sites [124]. Other than metal oxides, there are also catalysts such as metal carbides [125], $AB_{1-x}B_xO_3$ perovskite catalyst [126], Pd-based catalysts [127] and many more. Among them, bimetallic catalysts emerge as an important

class of catalysts for methanol synthesis from CO_2, some will be discussed in more detail in the next section.

2.1.5.1 Bimetallic catalysts for CO_2 hydrogenation to methanol

Bimetallic catalysts consist of two types of metals in various states, for example alloys, core-shell and metal oxide composites. Alloys can be either solid solution or intermetallic compounds. Solid solution usually contains metals that have similar atomic size, crystal structure and electronic properties. Intermetallic compounds are defined as solid phases that contain two or more metallic elements with defined stoichiometry and ordered crystal structure different from the constituent metals [13]. Since both 'alloy' and 'intermetallic compound' have been used interchangeably in the literature, both terms can appear when other people's work is quoted (depending on the original article). However, it should be noted that both Ni-Ga and Pd-Ga systems described in this thesis fall into the category of intermetallic compounds [11, 13], therefore the 'intermetallic' term has been used for the discussions concerning these catalysts. 'Alloying' and 'de-alloying' refer to the formation and decomposition of the intermetallic phase, respectively.

Bimetallic catalysts are attracting considerable attention due to their unique properties. Usually, there is a significant enhancement in the catalytic performance towards methanol synthesis due to a synergetic effect on the electronic or geometric properties of the two constituent metals [10]. In addition, the formation of alloy in the bimetallic catalysts gives rise to a higher resistance towards sintering owing to the covalent metal-metal bond [11]. For CO_2 hydrogenation to methanol, a number of bimetallic metals have been investigated. For example, Cu-Ni, Pd-Zn, Pd-Ga and Ni-Ga.

Ni-Ga based catalysts

Recently, Studt and co-workers [12] discovered a Ni-Ga catalyst for the methanol synthesis from carbon dioxide. A range of Ni-Ga catalysts with different Ni:Ga ratio supported on silica, were synthesised by incipient wetness impregnation and directly reduced under high

temperature [13]. Compared to Ni/SiO_2 catalyst, the addition of Ga and the subsequent formation of Ni-Ga intermetallic phase clearly enhanced the methanol synthesis activity of the catalyst.

These $Ni-Ga/SiO_2$ catalysts were tested for CO_2 hydrogenation at atmospheric pressure. Results indicated that Ni_5Ga_3/silica has a considerably higher methanol yield compared to $Cu/ZnO/Al_2O_3$ at temperatures above 220 °C [12]. This observation was explained by noting that both the activity and number of active sites influence the methanol synthesis rate. Although zinc promoted copper has near-optimal activity, active sites are relatively scarce as the copper particles are only active when zinc is present. On the other hand, active sites on intermetallic compounds are more abundant because a promoter is not needed.

Another difference between the Ni-Ga and Cu based catalysts is in the relation to activity for the reverse water-gas shift reaction (rWGS). The ratio between the rates of rWGS to methanol synthesis of Ni_5Ga_3/silica was found to be significantly lower than that of the conventional $Cu/ZnO/Al_2O_3$ [12]. The suppression of rWGS is highly desirable as CO produced has to be either recycled or burned and smaller amount of water can substantially shift the equilibrium towards methanol synthesis. Two catalytic sites are speculated to be present on the Ni-Ga based catalysts: nickel-rich sites that are responsible for methanation reaction and rWGS and gallium-rich sites that are responsible for methanol synthesis. The nickel-rich sites are eventually poisoned by CO and carbon thus reducing rWGS and methanation activity [12]. Since Cu based catalyst only has one type of surface site and CO does not have such poisoning effect, rWGS is more favourable unless high pressure is applied.

The Ni-Ga/silica catalysts also showed good stability for a period of over 60 h, after which the catalysts were able to recover their original activity by a 2-hour H_2 regeneration at 350 °C. 10% of the catalyst surface was found to be poisoned by carbon [12].

Although the Ni-Ga based catalysts are promising catalysts for CO_2 hydrogenation to methanol, a major technical barrier for its application is the high reduction temperature

required for the formation of active intermetallic phase. Since exposure to air during catalyst handling is usually unavoidable, it poses great risk to the intermetallic catalysts that have different standard enthalpies of oxide formation. Wencka et al. [128] studied the effect of surface oxidation on the Ga_3Ni_2 intermetallic catalyst for CO_2 hydrogenation to methanol. The XPS results revealed that the concentration of Ga on the oxidised surface is considerably higher compared to the bulk while Ni is depleted at the surface. This was thought to be due to high oxygen affinity of Ga pushing Ni into the subsurface region. Annealing the surface at 600 °C in ultra-high vacuum was only able to partially reconstruct the surface composition towards the energetically favourable bulk value. Hence, the instability and irreversibility of the oxidised Ni-Ga surface hinders the evaluation of catalytic performance under high pressures.

Pd-Ga based catalysts

Pd-based bimetallic catalysts (Pd-Ga, Pd-Zn and Pd-In) were first discovered by Iwasa et al. for the steam reforming of methanol [129]. It was found that the reduction of Pd-metal oxides led to the formation of alloy phase, which greatly increased the selectivity. Later on, Pd-Ga based catalyst was investigated for CO_2 hydrogenation to methanol. The bimetallic particles were revealed to be the active sites for methanol synthesis and the rWGS reaction was shown to be inhibited over the Pd-Ga sites, resulting in an active and selective catalyst [130].

The most extensively studied Pd-Ga based catalyst is the Ga_2O_3 supported Pd catalysts. Fujitani and co-workers found that an active Pd/ Ga_2O_3 could be prepared by co-precipitation as the Ga_xO_y stabilised an optimal amount of Pd^{n+} ($0 < n < 2$) on the surface of palladium. This catalyst was demonstrated to be more active than Cu/ZnO catalyst by a factor of two in yield and 20 in turnover over frequency [131]. More work has been done to investigate the types of Ga_2O_3 support used. Qu et al. showed that the strong interaction between Pd metal and plate-form Ga_2O_3 nanocrystals support gave a higher methanol yield from CO_2 hydrogenation. This is postulated to be due to the instability of the polar (002) surface of the plate-form Ga_2O_3 and the facilitated electron transfer that leads to higher metal dispersion and formation of Pd-Ga alloy [132]. The formation of Pd-Ga intermetallic compounds on porous polymorphs of α-, β-

and γ-Ga_2O_3 was reported by Li et al. [133]. Using α- and β-Ga_2O_3, Pd_2Ga intermetallic phase could be formed at lower temperature. As the reduction temperature increased further, Ga enrichment (formation of Pd_5Ga_3) was observed. No information on the metal particles on γ-Ga_2O_3 was obtained due to small particle size. Only Pd_2Ga/α-Ga_2O_3 reduced at 250 °C showed methanol synthesis selectivity under CO/H_2, although it quickly dropped to 0% due to the instability of the intermetallic surface in the presence of CO. For CO_2 hydrogenation, the same catalyst was found to be five times more active (activity normalised by active metal content) than Cu based catalyst, with stable selectivity.

A nanodispersed intermetallic $GaPd_2/SiO_2$ was successfully prepared using impregnation of nitrates, followed by drying, calcination and reduction. This catalyst also demonstrated higher activity and selectivity compared to commercial $Cu/ZnO/Al_2O_3$ catalyst under atmospheric pressure [134]. Intermetallic Pd_2Ga nanoparticles support on hydrotalcite-derived support has also been reported. This catalyst was synthesised by reductive decomposition of ternary hydrotalcite-like compounds obtained by co-precipitating aqueous solutions. Catalytic tests revealed that the presence of Ga improves the selectivity towards methanol synthesis from CO_2 when compared to the monometallic Pd counterpart [135].

2.1.5.2 Other bimetallic catalysts

In addition to Ni-Ga and Pd-Ga based catalysts, other bimetallic catalysts also exhibit good activity and selectivity to CO_2 hydrogenation to methanol. Pd-based catalysts are an important class. For example, PdZn alloy formation can be facilitated by the incorporation of multi-walled carbon nanotubes (MWCNTs) into Pd/ZnO catalyst. This is achieved by a step-wise incipient wetness method. The unique properties of the MWCNT support increase the surface concentration of active H-adspecies, resulting in increased surface hydrogenation reactions [136]. Apart from ZnO, the formation of PdZn bimetallic alloys are also investigated on TiO_2 and Al_2O_3 by using a chemical vapour impregnation method [137]. The Pd-Cu catalyst supported on amorphous silica showed significant synergistic promotion, that is, the methanol

production rate over Pd-Cu catalyst is more than the sum of the rates over the monometallic catalysts [138].

Besides supported Pd catalysts, many other bimetallic catalysts such as Ru-Co [139], PtW, PtCr [140] and Au/ZnO [141] have also been reported.

2.1.5.3 Synergistic promotion in bimetallic catalysts

As noted previously in section 2.1.5.1, the addition of particular metal onto existing metal system can sometimes modify the chemical properties of the original system in the desired ways depending on their electronic or geometric structures [10]. The mixing patterns and structures of bimetallic catalysts can be grouped into 3 main categories, mixed, core-shell or Janus alloys [142, 143], as illustrated in Figure 2.3. The d-band theory developed by Norskov and co-workers is often used to understand surface bond formation and catalytic behaviour of transition metals. It was proposed that the adsorption energy is related to the d-band valence of the surface metal atom [144, 145]. When alloy is formed, there are two ways that can drive a change in the structure of d-bands and filling [10]. The first one refers to the electronic ligand effect, where the heteroatomic bonds formation causes electronic interactions between two metals, thereby modifies the electronic configuration (hence chemical properties) of the primary metal [146, 147]. The second way is geometric irregularity (ensemble effect) induced by alloy formation of different-sized metal particles and the compression or expansion that often occurs in the core-shell type of alloy [10]. The surface bond lengths and bond angles, subsequently the chemical properties of primary metal, can be modified by these geometric differences [146-148].

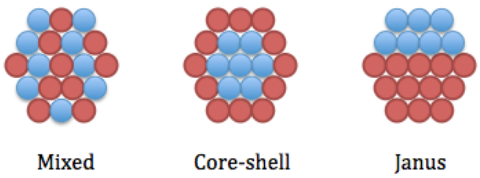


Figure 2.3, Schematic representation of the structures of bimetallic alloy nanoparticles (adapted from Li et al. [10])

In the Ni-Ga system proposed by Studt et al. [12], the adsorption strength of the Ni surface was modified upon alloying with Ga, hence methanol synthesis was enhanced. Ni alone binds oxygen too strongly, which causes surface poisoning by formate or the surface primarily catalyses methanation reaction. The type of secondary metal can also affect the adsorption properties, for example, rhodium-based catalysts are active for CO_2 hydrogenation to CO or CH_4, however, the Fe-Rh catalysts have considerable selectivity to ethanol [149] while alloying Co and Rh promotes methanol synthesis [139]. This was attributed to the modification of the electronic state of Rh by the added metals. In Pd-Zn systems, the change in adsorptivity of the active surfaces was also observed. Liao and co-workers found that the Pd core Zn shell alloy increases the adsorption strength of the bidentate formate species, which is the key intermediate to methanol [150]. Similarly in Pd-Ga based catalysts, the alloyed surface was speculated to be able to stabilise the methanol synthesis intermediates such as formate and methoxy species [151].

In the above-mentioned works, the mechanisms derived from the copper based catalysts were used to speculate the reaction pathways and intermediates in bimetallic catalysts. It should be stressed that the underlying reaction mechanisms of CO_2 hydrogenation to methanol over bimetallic catalysts remain largely unknown [10].

2.1.5.4 Deactivation in bimetallic catalysts

Although the bimetallic catalysts have been shown to be better than conventional catalysts in a number of applications [152], many of them still suffer loss of activity over time. The most common mode of deactivation observed in the bimetallic catalysts is the decomposition of the intermetallic phase. Despite their intrinsic stability towards sintering [11], they can be susceptible to de-alloying [153] or the alteration of surface compositions under reaction conditions [133, 154, 155]. This deactivation is especially common in bimetallic catalysts with constituent metals having very different oxygen affinity [128]. For example, the Pd-Ga catalyst was reported to lose activity due to the decomposition of the active phase and re-oxidation of gallium [154, 156]. In addition to the decomposition of the active phase, coke deposition has

also been reported as another cause of deactivation for the intermetallic based catalysts [133, 157].

2.2 DME synthesis

2.2.1 Single-stage process

Catalysts do not affect the equilibrium position, therefore methanol synthesis is always limited by chemical equilibrium. One way to alleviate the limitation is by in situ dehydration of methanol to DME according to reaction 4.

$$2CH_3OH \rightleftharpoons CH_3OCH_3 + H_2O \qquad \text{Reaction 4}$$

$$\Delta H = -21\,kJ/mol\,;\Delta G = -50.63\,kJ/mol$$

DME is a non-toxic ether that has a boiling point of -25 °C. It can be easily liquefied at 0.5 MPa at room temperature [158] and its properties are similar to liquid petroleum gas (LPG). DME is a very promising ultra-clean fuel for both transportation and power generation due to its high cetane number (around 55-60). It can be used directly in diesel engines to obtain comparable performance as diesel-fuelled engines, with a significantly lower emission of NO_x, SO_x and particulates [159]. DME is also gaining popularity as a propellant in aerosol formulations, replacing the ozone-destroying chlorofluorocarbons (CFCs). Moreover, DME is a useful intermediate or starting material for many important chemicals such as methyl sulphate, gasoline-range hydrocarbons, light olefins and other oxygenates.

DME can be produced either by the indirect or direct route. In the conventional indirect process, methanol produced from syngas (obtained from natural gas or coal) is dehydrated to DME over solid acids. In the direct DME synthesis, methanol synthesis and dehydration are combined. The single-stage DME synthesis from syngas requires the catalytic system to have two functions: methanol synthesis from the hydrogenation of carbon oxides and methanol dehydration. This can be achieved by using either a dual catalyst, which consists of a physical mixture of methanol synthesis catalyst and methanol dehydration catalyst, or a hybrid catalyst

that has both catalytic functions. In comparison to the indirect synthesis, the dual catalytic mode of operation has three main advantages:

- The thermodynamic constraints associated with methanol synthesis from syngas can be alleviated by the synergy effect of the combine catalytic functions. This is because the production of water drives the WGS to produce more H_2, which then enhances methanol yield (reaction 2) by shifting the equilibrium towards methanol production. In addition, the consumption of H_2 is reduced [160]

- Cost associated with methanol purification can be eliminated as methanol is converted to DME simultaneously

- Higher conversions achieved allows recycling of CO_2 by using CO_2-rich syngas to be used as feed gas

2.2.1.1 Catalysts for the single-stage process

As discussed in the previous sections, $Cu/ZnO/Al_2O_3$ is a well-established catalyst for methanol synthesis while other catalysts have been shown to be active and selective towards methanol synthesis. For methanol dehydration, several solid acid catalysts have been identified as good candidates for the catalytic conversion of methanol to DME. These include γ-alumina and zeolites, they operate in a temperature range of 250 – 400 °C. Studies found that alumina-based catalysts were more selective while zeolites showed better activity and long-term stability [161]. However, most of these catalysts have the tendency to produce hydrocarbons and coke due to the presence of strong acid sites at high dehydration temperature. Moreover, the solid acids, as well as the classic methanol catalyst, are prone to deactivation in the presence of water [162]. This is particularly problematic if the syngas is CO_2-rich since high concentration of CO_2 drives rWGS to produce more water. Water is believed to block the access of methanol to the active sites on catalyst surface. Hence extensive research is still being carried out to identify suitable catalysts that have high

selectivity towards DME formation with less undesirable side products [163], as well as good stability under high partial pressure of water.

Besides γ-alumina and zeolites, there are other types of acid catalysts for methanol dehydration. Heteropolyacids (HPAs) are materials with the formula $H_{8-n}[X_n^+M_{12}O_{40}]$, where 'X' can be P^{5+}, Si^{4+} andl Al^{3+}, etc., 'n' is the oxidation state and 'M' is the metal ions [19]. Owing to their high Brønsted acidity, HPAs generally have better performance than zeolites. For example, Alharbi and co-workers showed that the tungsten Keggin HPA has a TOF value of 53 h^{-1} versus a value of 1 h^{-1} over ZSM-5 [164]. Ion exchange resins (IERs) are another type of acid catalysts capable of methanol dehydration. Nafion resin, Nafion/silica composites and Amberlyst 35/36 are recently found to be suitable for methanol dehydration to DME [165, 166]. They are especially active at low temperature (< 150 °C), however, their application as the acid component in dual-function catalyst system for CO_2 hydrogenation to DME is restricted by their low thermal stability under typical STD operating conditions.

2.2.2 γ-alumina and zeolites as the methanol dehydration components

Dehydration of methanol takes place over solid acid catalysts. Two acid sites, namely Brønsted acid and Lewis acid, can be found in common solid acids. According to Brønsted – Lowry theory, an acid is the species that donates a proton (H^+) to form conjugate base, while the base is the species that accepts the proton to form conjugate acid. In Lewis acids and bases, the acid reacted with base by accepting the lone pair of electrons donated by the Lewis base.

The reaction mechanisms involved in γ-alumina and zeolites are different. For alumina-based solid acid catalysts, the dehydration mechanism involves the interactions between Lewis acid (electron-deficient aluminium cation) and Lewis base (electron-rich oxygen anion) pairs. However in zeolites, the reaction is associated with the Brønsted acid (for hydrogen transfer) and Lewis base (stabilise carbonium ions or regenerate acidic site) pairs [167].

2.2.2.1 Alumina-based catalysts

Transition aluminas (Al_2O_3) are the high-surface materials obtained from alumina precursors (such as aluminium hydroxides) by thermal treatment (below 800 °C). Among various transition aluminas, γ-alumina is probably the most important catalyst and catalyst support owing to its properties such as surface area, pore size distribution and acid/base characteristics. The amorphous γ-alumina is considered to have a cubic defective spinel structure with oxygen atoms in a cubic close packing and Al atoms in octahedral and tetrahedral sites. The defective structure is formed as Mg^{2+} ions in the ideal spinel $MgAl_2O_4$ are replaced by Al^{3+}, and some vacancies (33%) remain to satisfy the stoichiometry [168].

Alumina is a typical Lewis acid catalyst with no Brønsted acid site [169]. Similar to other metal oxides, γ-alumina surface is covered by hydroxyl layers, which are formed by chemisorption of water. Upon heat treatment, dehydroxylation of the surface hydroxyl groups creates coordinatively unsaturated *cus* cation (aluminium) and oxide anions that behave as Lewis acid – base pairs. Hence, the removal of surface hydroxyl groups (as water) is essential for the catalytic activity of aluminas. Evidence suggested that γ-alumina preferentially exposed the (100) plane of spinel, according to Peri's model on the dehydration of the ideal (100) plane, the maximum removal of OH groups was 67% if the local order was preserved. 90.4% removal was possible by removing the local order restriction and creating various types of defects. It was believed that the remaining 10% of the isolated hydroxyls were catalytically active, where five different types of OH groups differing in nearest neighbour configuration were identified. To remove the last hydroxyl ions, the mobility of surface ions was required [170].

However, Peri's model overestimated the number of active sites for some reaction, and it oversimplified the spinel structure by assuming that the (100) plane was the only possible termination of aluminas [171, 172]. Later in 1978, Knözinger and Ratnasamy provided a more completed model for the complex OH system on aluminas. In addition to the (100) plane in Peri's model, the termination of aluminas also occurred along other low-index crystal planes

(111) and (110). It was also assumed that the uppermost layer of the exposed crystal planes was able to reproduce the typical anion and cation array without reconstruction or ion migration, even at a dehydration temperature as high as 1100K. By determining the net charge at the OH group, the coordination number of both the OH groups and Al cations, Knözinger found five different OH configurations [173]. The net charge changes the acidity of the hydroxyl groups: the more positive the net charge is, the more acidic is the proton. The proton acidity and ease of OH group removal both governs the dehydroxylation process. For instance, at (111) plane, dehydroxylation occurs between more basic type Ia OH group and the hydrogen from the more acidic IIa OH group to produce water molecule. As mentioned earlier, this process creates anion vacancy (Lewis acid site), which exposes a *cus* 3-coordinate-Al^{3+} cation in a tetrahedral interstice with a *cus* oxygen (Lewis base site) [173]. However the experimentally found number of active sites was at least one magnitude lower than the number of Lewis acid and base sites produced from regular dehydroxylation. Knözinger suggested that sometimes less favourable combination of the hydroxyl groups (between identical OH groups) might occur, leading to irregular configuration, and only such defect sites, low in concentration, were considered to be catalytically active. Knözinger's model is still an idealised model, as (1) it does not consider the crystallographically defective configurations that are frequently present in mesoporous materials (2) it does not consider the effects of reconstruction at high dehydration temperature (3) it does not consider the effect of the cation vacancies imposed to the spinel structure by the stoichiometry of Al_2O_3 [174].

Deactivation of γ-alumina

γ-Al_2O_3 is the most widely used and investigated solid acid for methanol dehydration due to its low cost, high surface area and good thermal and mechanical stability. It has high selectivity to DME even at high temperatures due to the relatively weak Lewis acid sites that do not promote side reactions [19]. Despite of these advantages, γ-Al_2O_3 is not considered to be a reliable acid catalyst for CO_2 hydrogenation to DME. This is mainly because relatively high water content prevails under CO free condition and water strongly adsorbs on

γ-Al_2O_3, inhibiting catalytically active sites [19, 175]. It was shown that the presence of 20% (by weight) water increases the deactivation of γ-Al_2O_3 by 12.5 folds [176]. In addition to this, deactivation of the γ-Al_2O_3 catalyst can also be the irreversible formation of boehmite at high partial pressure of steam [177] according to the following reaction:

$$\gamma - Al_2O_3 + H_2O \rightleftharpoons 2\gamma - AlO(OH)$$

This is particularly relevant for CO_2 hydrogenation to DME, Boon and co-workers demonstrated that at 250 °C and above 14 bar steam, the conversion of γ-Al_2O_3 to γ-AlO(OH) reduces the catalytic activity [178]. However, there is currently very limited literature on this deactivation route.

Over the years, research has been conducted to modify the activity and stability of the γ-Al_2O_3 catalyst. For instance, Nb_2O_5 addition to γ-Al_2O_3 has been found to reduce the acid strength but increase the number of acid sites, leading to an enhanced reactivity and stability [179]. Similarly, the modification of γ-Al_2O_3 surface has also been carried out with silica, aluminium-phosphate and other species [179-183].

2.2.2.2 Zeolites

Zeolites are aluminosilicates made from tetrahedral alumina (AlO_4) and SiO_4, interlinked by the shared oxygen atoms. When some of the silicon atoms are substituted by aluminium, negative charge generated on the shared O atoms needs to be balanced by a nearby cation. In the case of the cation being a proton, a bridged hydroxyl group Si – OH – Al is formed, which acts as a Brønsted acid site[184]. Zeolites typically have Brønsted acid sites, but some Lewis sites can be formed during calcination. Zeolites have shown better efficiency than γ-Al_2O_3 due to good stability in the presence of water [175] and the possibility to modulate acidity for direct DME synthesis from CO_2/H_2 [19].

The rate of zeolite-catalysed reaction was found to be in linear correlation [185] with the concentration of Brønsted acid sites. The catalytic activity of zeolites depends on the acid

strength of the hydroxyl proton, which is influenced by the nature of the substituting metal atoms (Si – OH – T where T = Al, Ga, Fe, etc.) and the Si – O – T bond angle. As the bond angle increases, the deprotonation energy decreases resulting in stronger acid strength. For instance, zeolite ZSM-5 (137° – 177°) and mordenite (143° – 180°) have stronger acidity compared to zeolite Y (138° – 147°) [186]. The acid strength of Si – OH – Al group is also affected by the aluminium site distribution. Aluminium atoms have lower electronegativity compared to the silicon atoms, therefore the acid strength is higher with lower number of framework aluminium atoms (higher number of silicon atoms). Finally, the interaction between the Brønsted and Lewis sites can significantly increase the acidity of the Brønsted acid sites. It was believed that the partially hydrolysed framework aluminium atoms acted as Lewis acids, or in other words, strong electron acceptor for the neighbouring bridging OH groups, thus weakened the OH bond [186].

Zeolite properties and product distribution

Zeolites are well known for their shape-selectivity properties, i.e. the ability to discriminate between different reactants, transition states and products based on their size and shape. This is because zeolites have well defined pore structure with pore openings 3 – 8 Å in size, making them effective molecular sieves that offer a number of advantages as potential methanol dehydration catalysts. These advantages include: (1) higher stability in the presence of water (2) good conversion and selectivity due to highly active and uniform strong acid sites [187] (3) possibility to improve catalytic performance by manipulating catalyst properties such as acidity, surface area, crystal size and channel topology [188-190].

Both the acidity and pore structure (topology) of zeolites are important factors that affect the catalytic activity and selectivity, especially under typical operating temperature of syngas to DME process. In the temperature range of 260 – 300 °C, zeolites may start converting methanol to various hydrocarbons (methanol to hydrocarbon, MTH) and the channel size of zeolites significantly influences the product distribution. This is also influenced by the acidity of the zeolites. The reaction products are more likely to undergo further reactions if the zeolite

has high density of acid sites or high acid strength. For zeolites with smaller pore structures, light olefins are selectively produced since only small molecules are able to escape through the narrow pores. For example, Montesano et al. reported a stable performance of ferrierite (FER) and theta-1 under CO/H_2 [20]. FER has high methanol dehydration activity [191], it was also found to be very selective towards DME synthesis even though it has 20% more Brønsted sites (and higher acid strength) compared to theta-1. The reason for this was thought to be due to its unique pore structure (orthorhombic pore structure with 10-ring channels perpendicularly intersected with 8-ring channels) that limits hydrocarbon and coke formation by providing preferential diffusion path for smaller product molecules such as methanol and DME [20]. This also shifted the chemical equilibrium of reactions 1, 2 and 4 towards right [192], further increasing the CO conversion.

On the other hand, zeolites such as ZSM-5 that possess medium pores and interconnected structures (3D pore system with straight 10-ring channels connected by sinusoidal channels) and medium to strong acidity, the formation of bigger alkylaromatics compounds is promoted. Therefore, the typical dehydration products over ZSM-5 usually include olefins, aromatics and paraffins [193]. Montesano and co-workers [20] found that the performance of ZSM-5 based physical mixture for CO hydrogenation to DME was strongly dependent on the reaction temperature and time on stream. The DME selectivity was high initially (at lower temperature), but gradually decreased due to the formation of entrained hydrocarbon species that has built up in the zeolite voids from reactions involving methanol and DME [20]. Although ZSM-5 exhibits high methanol conversion under CO/H_2, it is prone to fast deactivation and loss of DME selectivity. However, recent work suggested that ZSM-5 has a stable and DME-selective performance under CO free condition [17]. This was speculated to be due to relatively higher partial pressure of water under CO_2/H_2 from the rWGS activity of the methanol synthesis catalyst ($Cu/ZnO/Al_2O_3$), as water is known to reduce the acidity of zeolites.

Deactivation of zeolites

Under typical DME synthesis temperature (260 – 280 °C), the combination of hydrocarbon formation, acid sites and high temperature facilitate coke formation. Methanol dehydration to DME (MTD) is often the first step in many methanol to hydrocarbon (MTH) processes such as methanol to olefins (MTO) and methanol to gasoline (MTG) [194]. As noted earlier, the catalyst structure (such as the channel size and configuration) and acidity are the main factors affecting the product distribution. In these processes, zeolites with large cages of 3D channels are more likely to trap aromatic compounds such as poly-methylbenzenes [195], methanol and DME are then attracted to form alkenes and water in a closed cycle through a 'hydrocarbon pool' mechanisms. Poly-methylbenzenes are often the precursors of coke in MTO processes, but they are also found in methanol to DME synthesis despite the lower operating temperature of MTD process. It is widely known that pore or active sites blockage by coke deposition is the main cause of deactivation of zeolites [196]. The preferential location of coke deposition is still under debate, some demonstrated that the carbonaceous deposits are found inside the zeolite structure [197] but others proposed that coke is favourably located outside the pores on the crystal surface because the channels and size of the zeolite channels restrict the internal deposition of solids [198]. In the latter case, coke precursors are thought to be able to diffuse from micropores to the external surfaces, particularly when the external surface area is large with short diffusion path lengths [199].

Many studies have demonstrated that FER has high DME selectivity, resistance to coke deposition and deactivation due to its unique 8-10 rings, 2D small pore channel structure [190, 200-202]. However, Catizzone et al. found more Lewis sites on aluminium-rich FER, these sites are more active towards methanol conversion but they also promote by-product formation (mainly methane) and coke deposition [202]. As a result, the stability and selectivity of FER can be further improved by carefully varying the Si/Al ratio.

On the other hand, modifications of ZSM-5 are investigated to reduce coke formation. For example, having both microporous and mesoporous size distribution in the ZSM-5 can

increase the activity as well as the stability by limiting coke formation [203, 204]. Reducing the acid site strength or total acidity is another way to improve the performance of ZSM-5. This can been done by impregnating ZSM-5 with γ-Al_2O_3 [205], impregnating with metal (Na, Mg, Zn or Zr [206, 207]) loadings or increasing Si/Al ratio of the zeolite [208, 209].

2.2.3 Reaction mechanism

The kinetics of DME synthesis over solid acid catalysts have been studied extensively. It is widely accepted that the reaction proceeds via a bimolecular mechanism, however two different mechanisms have been reported. The Langmuir – Hinshelwood (L – H) mechanism involves the reaction of two surface species, an acid site and a conjugate base site are required. Over certain zeolite (H-Mordenite), Bandiera and Nacchache [210] proposed that the L – H mechanism started with an initial reaction of a methanol molecule at the Brønsted acid site (H^+). At the same time another methanol molecule reacted at the adjacent base site (O^{2-}). Two surface species were formed, $[CH_3{\cdot}OH_2]^+$ and $[CH_3O]^-$, which then gave DME and water upon condensation. These steps [211] are given as:

$$CH_3 - OH + H^+ \rightleftharpoons [CH_3 \cdot OH_2]^+$$

$$CH_3O - H + O^{2-} \rightleftharpoons [CH_3O]^- + [OH]^-$$

$[CH_3{\cdot}OH_2]^+$ undergoes a fast reaction:

$$[CH_3 \cdot OH_2]^+ \rightleftharpoons [CH_3]^+ + H_2O$$

which is followed by a rate-determining step:

$$[CH_3]^+ + [CH_3O]^- \rightleftharpoons CH_3OCH_3$$

The acid and base sites are regenerated via fast reactions:

$$[H_3O]^+ \rightleftharpoons H^+ + H_2O$$

$$H_2O + [OH]^- \rightleftharpoons [H_3O]^+ + O^{2-}$$

On the other hand, the Eley – Rideal (E – R) mechanism involves the reaction between a surface species and a gaseous methanol molecule, in this case only an acid site is needed to

attack the nucleophilic oxygen of the methanol molecule [211]. According to Kubelkova et al. [212], the FTIR spectra suggested that a methanol molecule was protonated at the active site to methyloxonium ion ($CH_3OH_2^+$), which underwent dehydration to give methyl group that remained attached to the catalytic surface. DME was formed when another methanol molecule approached and reacted with the methyl group via nucleophilic attack. The reactions taking place at different acid sites on certain zeolites are shown below.

Table 2.2, Reactions at different acid sites (Y and ZSM-5 zeolites) and methanol dehydration mechanism

Type of acid site	Reaction at acid site	Methanol dehydration
Brønsted	$CH_3OH \cdots H\text{–}Si\text{–}O\text{–}Al \rightleftharpoons CH_3OH^+ \quad Si\text{–}O^-\text{–}Al^-$	$Si\text{–}O\text{–}Al(CH_3) + CH_3OH \rightleftharpoons Si\text{–}O\text{–}Al(H) + CH_3OCH_3$
Lewis	$Al \cdots OH + Si\text{–}O\text{–}Al(CH_3) \rightleftharpoons Al\text{–}OCH_3 + Si\text{–}O\text{–}Al(H)$	$Al\text{–}OCH_3 + CH_3OH \rightleftharpoons CH_3OCH_3 + Al + H_2O$

However, the primary mechanism for methanol dehydration is still not fully understood. Using a cluster model of the active sites to analyse the calculated energy diagrams, Blaszkowski and co-workers suggested that the L – H model was preferable to the E – R model due to the lower activation energy involved in the L – H pathway [213]. However, there was evidence that surface methoxy was an important intermediate in the initial C – C bond formation [214, 215]. Furthermore, Ono and Mori exposed H-ZSM-5 to CD_3OH and evacuated at 437 K, bands at 2220 cm^{-1} and 2070 cm^{-1} were observed in IR spectra, which corresponded to the anti-symmetric and symmetric vibrational modes of C – D bonds in CD_3, indicating the replacement of surface OH group by OCD_3. These bands disappeared at 512 K as DME and other hydrocarbons were formed [216].

For both reaction mechanisms, various rate equations were derived from experiments under laboratory conditions. A summary of the published rate equations can be found in Table 2.3.

Most of the rates of reaction are proportional to the square root of the methanol concentration, suggesting dissociative adsorption of methanol on the catalyst surface during dehydration.

Table 2.3, Earlier rate equations for methanol dehydration, reproduced from [217]

Author	Rate equation	Catalyst used
Klusacek and Schneider, 1982	$-r_M = \frac{kK_M C_M}{(1+2(K_M C_M)^{\frac{1}{2}}+(K_W C_W))^2}$	Acidic ion exchange resin
	$-r_M = \frac{kK_M {C_M}^2}{(1+2(K_M C_M)^{\frac{1}{2}}+(K_W C_W))^3}$	
	$-r_M = \frac{kK_M {C_M}^2}{(1+2(K_M C_M)^{\frac{1}{2}}+(K_W C_W))^4}$	
Kallo and Knozinger, 1967	$-r_M = \frac{{C_M}^{1/2}}{{C_M}^{\frac{1}{2}}+k_2 C_W}$	Alumina/silica alumina
Sinicyna et al., 1986; Gates and Johanson, 1971 [218]	$-r_M = \frac{k{K_M}^2 {C_M}^2}{(1+K_M C_M+K_W C_W)^2}$	Ion exchange resin
Figueras et al., 1971	$-r_M = \frac{kK_M {C_M}^{1/2}}{1+K_M {C_M}^{1/2}+K_W C_W}$	Alumina/silica alumina
Than et al., 1972	$-r_M = \frac{kK_M C_M}{(1+K_M C_M)^2}$	Acidic ion exchange resin
Schmitz, 1978	$-r_M = k_1 + k_2 C_M$	Alumina/silica alumina

Bercic and Levec proposed the following rate equation based on the L – H model by assuming that the surface reaction was rate-determining [217]. In this model, the adsorption term for DME in the denominator was neglected as the adsorption constant was negligible in comparison to that of methanol and water [218].

$$-r_M = \frac{k_s {K_M}^2 ({C_M}^2 - \frac{C_W C_E}{K})}{(1 + 2(K_M C_M)^{\frac{1}{2}} + (K_W C_W))^4}$$

It has been demonstrated that this model fits well with experimental results over a range of CO_2 feed concentrations [81, 219].

2.2.4 Challenges in single-stage DME synthesis

As mentioned earlier, the singe-stage DME synthesis from syngas is both scientifically and commercially beneficial due to higher once-through conversion and cost savings from smaller equipment. However, as the reaction products contain CO_2 and DME, the downstream separation for the one step process can be costly due to their high volatility. To tackle this problem, DME and methanol can be scrubbed out of the reactor effluent while CO_2 is recycled back to the reactor. However this solution is not ideal as CO_2 build-up in the reactor significantly decreases the reactor productivity. It was considered to be more cost-effective to remove CO_2 together with DME and methanol from the reactor effluent, and to develop an optimised downstream separation scheme [220].

Compatibility between methanol synthesis and dehydration catalytic functions

The single-stage DME synthesis requires two catalytic functions, one that catalyses methanol synthesis from syngas while the other catalyses methanol dehydration. For the direct CO_2 hydrogenation to DME, the combined catalyst should have good methanol synthesis and dehydration activities with a low CO and hydrocarbon yield [19]. The overall efficiency of the one-step process largely depends on the properties of the dehydration catalyst [221, 222], which is still being researched to achieve optimisation. The acid catalyst should be stable when water is present with well-distributed and not too strong acid sites to prevent excessive hydrocarbon formation [19]. The main challenges from catalytic perspective are the identification of suitable solid acid and methanol synthesis catalyst (MSC) components for CO_2 hydrogenation and the compatibility between the two catalytic components.

Various studies revealed that when a dual catalyst system is used, both catalysts suffer rapid and simultaneous deactivation from the interaction between the catalysts. Naik et al. [223]

carried out a comparison between the activity of MSC + γ-Al_2O_3 and MSC + ZSM-5 and found that the zeolite based physical mixture have superior performance in terms of CO_2 conversion (30%), DME selectivity (75%) and stability. In a different study involving slurry-phase DME synthesis, the Cu/ZnO/Al_2O_3 + γ-Al_2O_3 physical mixture deactivated rapidly, which led to the conclusion that the detrimental interaction between the two catalysts was the main cause of loss in catalytic activity [224]. It was further speculated that the interaction was likely due to the migration of Cu- and Zn-containing species from the MSC to the γ-alumina. This phenomena has also been reported for zeolite based catalyst, for example, it was suggested that the migration of Cu and Zn species from the methanol synthesis catalyst to the zeolites deactivates the catalyst by reducing the concentration of Brønsted acid sites (due to ion exchange between copper and zeolite hydroxyl groups [225]. In other studies, Cu/ZnO/Al_2O_3 component in the hybrid catalyst was prone to deactivation as the migration of aluminium species caused undesirable interaction with metallic copper, reducing its activity [226] There are different views on the efficiency of physical mixture compared to the bifunctional catalysts (composites). Bifunctional catalysts can be prepared by various methods, including impregnation, co-precipitation [227-231] and sol-gel [232, 233] and it is anticipated that the mixing methods of the bifunctional catalysts influence the stability of the catalysts [234]. For the bifunctional catalysts, it was claimed that the generation of metal oxide and acid sites in a single system could improve the CO_2 conversion by enhancing methanol synthesis and dehydration on the neighbouring sites [19]. Among various bifunctional catalysts with different acid components studied, Cu/ZnO/Al_2O_3 + ferrierite was found to be superior to others. The better conversion and high selectivity were attributed to the facile reducibility of metallic copper, suitable topology and acidity [235]. Taking another example of ZrO_2-doped Cu/ZnO/Al_2O_3 + ZSM-5 bifunctional catalyst, the conversion obtained was higher due to the close contact between the two catalytic functions, which enabled the formation of DME directly from the adsorbed methoxy species without intermediate synthesis of methanol [236, 237]. Indeed, Ge and co-workers concluded that both active sites of MSC and solid acids should be in close contact to achieve the synergistic effect but the coverage of both sites during the reaction must

be avoided to reduce loss of active surface area [233]. The latter statement is supported by a study that demonstrated the hybrid catalyst has much lower efficiency due to significant pore blockage (decreased active surface area) [238] and inter-cation exchange of Cu^{2+} (possibly also Zn^{2+}) species. The author also stressed that other kinds of interaction between catalysts cannot be ruled out.

The hybrid catalysts developed so far are generally prone to deactivation by metal sintering, coke deposition or blockage of active sites [237, 239]. There is currently very limited literature on the deactivation mechanism for the dual-function catalytic system since the focus has been put on the methanol synthesis components. Deeper understanding of the underlying interactions and deactivation mechanism in both physical mixture and bifunctional catalyst is required, in addition to the individual catalyst performance and process design, for the success of the single-stage DME synthesis from CO_2 [19].

Chapter 3 Experimental Procedures

3.1 Reactor system setup

Catalyst tests were carried out in a continuous flow reactor system consisted of a fixed bed stirred tank reactor (CSTR) and a packed bed flow reactor (PFR) as illustrated in Figure 3.1. To maintain safe operation, flammable gas cylinders (BOC, CP grade) were stored outside the laboratory in a ventilated cabinet with gas detector. The cylinders were connected to the reactor rig with stainless steel tubing. The reactor rig and online product analysis equipment were contained in a well-ventilated and monitored enclosure. A gas detector was used with a control unit to shut off supply gas from the cylinders if a leak was detected. The control unit also monitored temperature and pressure in the reactor system. Three high-pressure Brooks 5850E mass flow controllers were used to control the flowrate of the feed. The feed gas (except H_2/N_2 used for catalyst reduction) first passed through an activated-carbon trap at room temperature before entering the reactors. The operating pressure in the system was regulated and controlled by a Tescom backpressure regulator. The regulator and exit lines from the reactors were traced-heated to prevent condensation of products such as water and methanol. The online product analysis was conducted in a gas chromatograph (GC2014) with automatic sampling valves. At reactor exits before the backpressure regulator, 3 mL/min of the reactor effluent was directed (using three consecutive need valves) to an H-Plot/Q column (30 m × 0.32 mm × 20 μm) where hydrocarbons and oxygenates were separated and then detected with a flame ionisation detector (FID). After the backpressure regulator, approximately 10 mL/min of the reactor effluent was directed to a carbon molecular sieve (80 – 100 mesh) column where permanent gases were separated and then analysed by a thermal conductivity detector (TCD).

Blank experiment was run to ensure that the whole system was inert and there was no background CO_2 conversion.

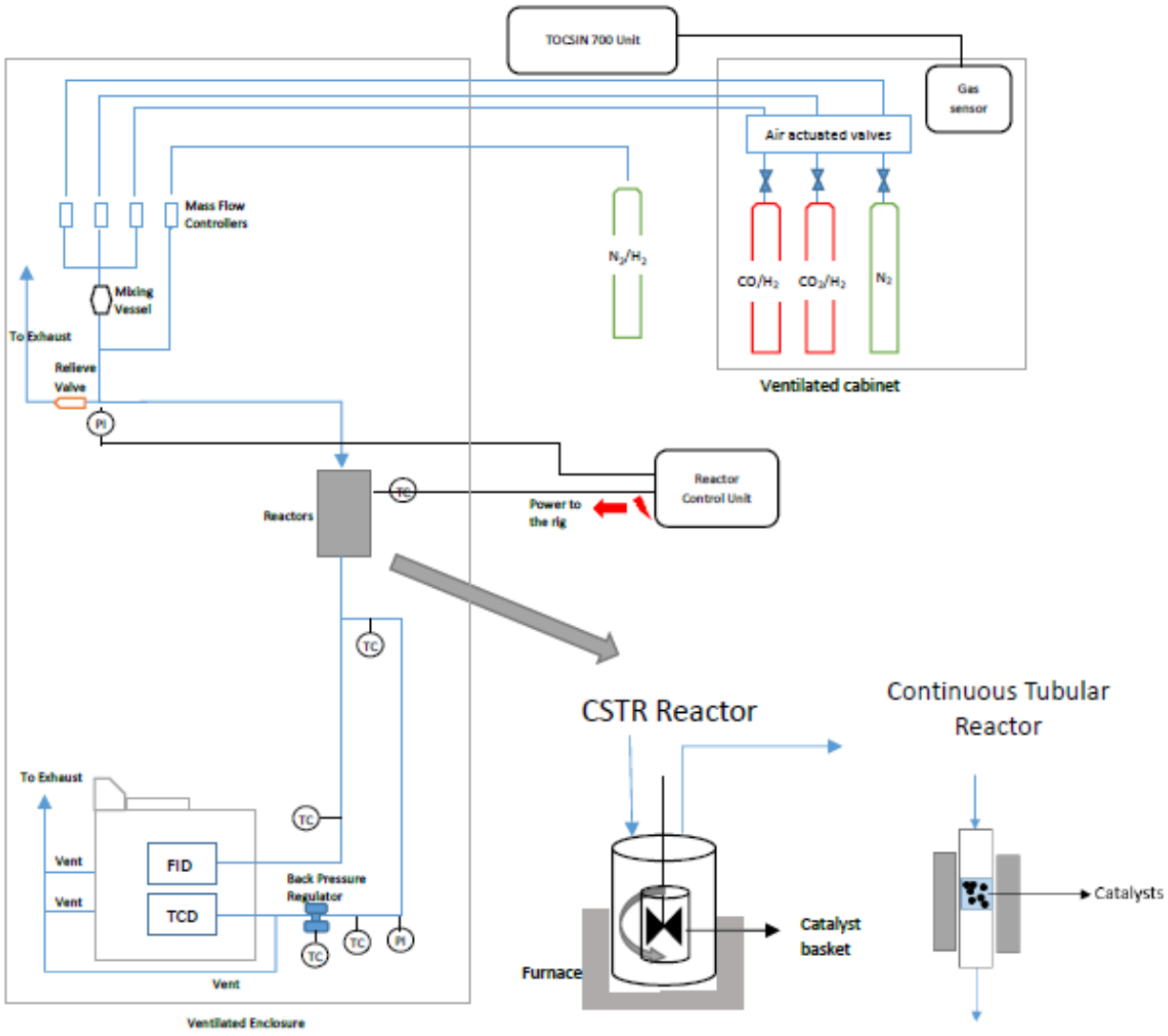


Figure 3.1, Rig setup

3.1.1 Fixed bed stirred tank reactor (CSTR)

The CSTR is a bench-top Parr stirred pressure vessel with a volume of 300 mL. It was fitted with a high-speed impeller and a stationary catalyst basket. Heating was provided by a mantle. Typical stirring speed was 1000 rpm. The reactor temperature and impeller speed were both regulated by a Parr 4848B reactor controller. The catalyst (106 – 250 μm) was placed in stainless steel mesh (70 μm) inside the catalyst basket. To compare the performance of the Parr reactor to an ideal CSTR, the fluid dynamics of the catalyst bed were evaluated (details given in Appendix A). The pressure drop through the catalyst bed was 3 Pa and the superficial

velocity was 0.6 m/s under typical operation conditions (245 °C, 110 mL/min STP and 30 bar). This is equivalent to a recycle ratio of 130, which greatly exceeds the critical value of 20, above which the reactor is considered to operate as a perfectly mixed CSTR [17].

During CSTR operation, issues with the impeller design developed over time, causing damages on the internal surface of the reactor vessel. This further led to strong background production of methane and the rapid deterioration of catalyst performance. The observations and remedial actions are described in Appendix A.

3.1.2 Tubular flow reactor (PFR)

To use the rig with the flow reactor, the lines into and out of the CSTR were closed. The flow reactor was a stainless tube with an internal diameter of 9.5 mm and a length of 30 cm. The reactor was heated by a cartridge heater block. Temperature inside the reactor was measured by a thermocouple fitted through the top of the reactor. Catalyst (106 – 250 μm) was diluted with inert SiC (Fisher Scientific, 24 Grit) in a 1:2 volume ratio and packed in the middle of the reactor. The particle size was chosen to achieve low pressure drop and prevent wall effects (d_t/d_p = 38, which exceeds 12 to avoid deviation from plug flow regime) [17]. The rest of the reactor was packed with SiC to ensure good heat distribution. This reactor was used in Chapter 5 for the study of Pd promoted Ni-Ga catalysts as well as in Chapter 6 for the investigation of effect CO on the single-stage DME synthesis, no comparison has been made between the results obtained in the CSTR and PFR.

3.2 Catalyst preparation

3.2.1 Methanol synthesis catalysts (MSC)

3.2.1.1 Ni-Ga based catalysts supported on silica

Influence of preparation conditions

Sharafutdinov et al. [14] extensively studied the effects of metal loading and preparation conditions on the Ni-Ga based catalyst supported on SiO_2. The authors prepared the catalyst

by incipient wetness impregnation with a mixed aqueous solution of nickel and gallium nitrates. It was found that calcination of the catalyst precursor had detrimental effect on the particle size, and consequently the catalytic activity. Therefore the dried catalyst precursors were directly reduced in flowing H_2. In situ XRD was carried out on the reduction of Ni-Ga catalysts to demonstrate that a reduction temperature of 700 °C is required for the complete formation of stoichiometric Ni-Ga intermetallic compounds, especially in the case of the most complex δ-Ni_5Ga_3 phase [13]. This particular composition was also revealed to have the highest methanol turnover frequency. Therefore in the present study, the same catalyst preparation method will be used to prepare SiO_2 supported Ni-Ga catalysts with three different nominal Ni:Ga ratio, i.e. 0.6 (designated as NiGa(a)/SiO_2), 1.0 (NiGa(b)/SiO_2) and 0.33 (NiGa(c)/SiO_2), whose activities at atmospheric pressure have been previously reported in the literature.

In addition to above, it was found that the material of the reactor in which the catalyst was reduced played crucial role in the formation of correct Ni-Ga intermetallic phase. The Ni-Ga catalysts reduced in steel reactor had poor methanol synthesis performance, it was speculated that the presence of foreign metal resulted in undesirable interactions with Ni and Ga in the catalyst. The details of this investigation is given in Appendix A. Hence, all the reduction of the Ni-Ga based catalysts was carried out in a quartz tube.

Summary of catalyst preparation details

Ni-Ga at a weight loading of 17% was supported on a commercial EP10 silica (106 – 250 μm) by incipient wetness co-impregnation with an aqueous mixture of nickel and gallium nitrates (both from Sigma Aldrich). Three different Ni:Ga ratios were prepared, 5:3, 1:1 and 3:1. The catalyst precursor was dried in N_2 and directly ex situ reduced in a quartz tube with a flow of 5% H_2/N_2 (BOC) for 2 hours at 700 °C. The reduced catalyst was cooled down to 25 °C and a flow of 10% N_2O in N_2 was used to passivate the catalyst for 30 min. The sample was kept under flowing N_2 before transfer to the high-pressure reactor. Prior to catalysis, the catalysts

were re-activated in situ at 340 °C for 3 hours under flowing 5% H_2/N_2. The development of this passivation and re-activation procedure will be discussed in Chapter 4 section 4.2.2.

3.2.1.2 NiGa(a) based hydrotalcites (LDH)

NiZnGaAl-LDH with a Ni:Ga molar ratio of 5:3 was synthesised on a γ-alumina support, following the procedures given by Ning et al. [240]. Spherical γ-Al_2O_3 pellets (Sasol) were crushed and sieved to 250 – 500 µm. 0.2616 g of $Ni(NO_3)_2{\cdot}6H_2O$, 0.2678 g of $Zn(NO_3)_2{\cdot}6H_2O$, 0.0345 g of $Ga(NO_3)_3{\cdot}xH_2O$ and 0.1035 g of urea (all chemicals from Sigma Aldrich) were dissolved in 1.5 mL of DI water before transfer to an autoclave. 1 g of γ-Al_2O_3 was added, which acted as the source of Al and the support. The solid suspension was sealed in the autoclave to allowing aging at 100 °C for 12 hours. The resulting solid was filtered with a 0.2 µm nylon membrane and washed thoroughly with DI water. Subsequently, the solid was dried overnight in a recirculating oven at 100 °C. The reduction of the catalyst was performed in a quartz tube at 700 °C with 70 mL/min 5% H_2/N_2 for 2 hours. Passivation of this catalyst was done at 25 °C with 10% N_2O/N_2 for 30 min. Prior to catalyst test, it was re-activated in situ at 340 °C for 3 hours under flowing 5% H_2/N_2.

3.2.1.3 Palladium promoted NiGa(a)/SiO_2

Pd promoted NiGa(a)/SiO_2 was prepared by a two-stage incipient wetness co-impregnation method. First, Pd was impregnated onto a commercial EP10 silica (106 – 250 µm) by incipient wetness impregnation using dissolved palladium acetate in toluene (both from Sigma Aldrich). The amount of Pd promotion was 0.04 mol Pd to 1 mol Ni+Ga [241]. The precursor was dried at room temperature overnight before second incipient wetness impregnation was carried out, this time with an aqueous solution of nickel and gallium nitrates (Sigma Aldrich). The weight loading of Ni+Ga on SiO_2 was kept at 17% and Ni:Ga ratio was 5:3. The resulting catalyst was directly reduced in situ at 350 °C for 4 hours with 5% H_2/N_2. The development of this reduction condition is given in Chapter 5 section 5.2.1.

3.2.1.4 Pd-Ga based catalysts supported on silica

The preparation method of Pd-Ga based catalysts was modified from the work by Chiavassa et al. [242]. 2 wt% palladium was impregnated onto a commercial EP10 silica (106 – 250 µm) by incipient wetness impregnation using dissolved palladium acetate in toluene (both from Sigma Aldrich). The precursor was dried and then calcined in air (200 mL/min STP) at 150 °C for 2 hours. Gallium was then impregnated using an aqueous solution of gallium nitrates (Sigma Aldrich). Pd_2Ga and $PdGa_3$ were prepared. Final calcination was carried out in air (200 mL/min STP) at 400 °C for 2 hours. The calcined catalysts were ex situ pre-reduced at 460 °C for 2 hours under flowing 5% H_2/N_2, cooled down and passivated with 10% N_2O/N_2. Before activity measurements, the passivated catalysts were reduced in situ at 250 °C with 5% H_2/N_2.

3.2.1.5 Cu/ZnO/Al_2O_3

The commercial $Cu/ZnO/Al_2O_3$ (Johnson Matthey) was crushed and sieved to pellets with a particle size of 106 – 250 µm. This catalyst was reduced in situ at 225 °C for 2 hours under flowing 5% H_2/N_2.

3.2.2 Methanol dehydration catalysts

3.2.2.1 γ-alumina (γ-Al_2O_3)

γ-Al_2O_3 pellets from Sasol were crushed and sieved to obtain the desired particle size 106 – 250 µm. The catalyst was ex situ calcined in air at 400 °C for 4 hours.

3.2.2.2 Zeolites

Ferrierite (FER, CP914) and ZSM-5 (CBV5524G) were used. Powdered zeolites from Zeolyst were pressed into disc form by applying a load of 10 ton. The discs were crushed and sieved to pellets (106 – 250 µm). To obtain the required H-form, both zeolites were calcined ex situ at 550 °C for 6 hours under flowing air.

3.2.2 Mass transfer effects

Although kinetic modeling is not the research objective of this work, it is still necessary to carry out catalyst tests without significant external or internal mass transfer limitations in order to study the deactivation behaviour the catalysts.

The external mass transfer effect is dependent on the fluid dynamics in the reactor. In the CSTR, the existence of external gradient was assessed by varying the impeller speed. The reaction rates at different impeller speed are summarised in Table 3.1.

Table 3.1, Effect of impeller speed on the methanol synthesis reaction rate*

Impeller speed (rpm)	**800**	**1000**	**1300**
MeOH production rate (mol [MeOH]/mol [Ni+Ga]*hr	0.54	0.54	0.53

*conditions: 0.3 g NiGa(a)/SiO_2, particle size: 106 – 250 μm, 245 °C, 10 bar, 5%Ar/24%CO_2/H_2, flow rate: 110 mL/min (GHSV: 6640 h^{-1})

The conversions (0.6%) obtained are far from equilibrium. No significant difference in the reaction rates was observed at all three impeller speeds, indicating the absence of external gradients. Therefore the impeller speed was set to 1000 rpm for all the experiments conducted in the CSTR.

The internal mass transfer is controlled by the pore size and pore volume of the catalysts. Typically, the particle size of the catalyst is reduced until no further increase in reaction rates is observed. R. Montesano conducted an investigation on the effect of particle size on the reaction rates in the single-stage DME synthesis [17]. It was found that practically the same reaction rates were obtained using particles with size range of 106 – 250 μm and 250 – 500 μm and the Weisz-Prater numbers for these size ranges were well below 0.3 (two orders of magnitude lower) [243]. The reproduced results are shown in Appendix A Table A.2. Since this study was carried out in a similar setup as the present one and the catalysts (HiFuel R120

and Sasol γ-alumina) tested were used in the present study, therefore it is safe to assume a size range of 106 – 250 μm would be adequate to prevent significant intraparticle diffusion limitation.

3.2.3 Catalyst tests under elevated pressures

After the catalysts were loaded into the reactor, the system was pressurised with N_2 at the operating pressure to test for leaks. When no leak was present, the pressure was released and a flow of 100 mL/min STP 5% H_2/N_2 was introduced and the reactor was heated to the desired re-activation temperature. After the catalyst re-activation was complete, the reactor was cooled down to below 100 °C under flowing N_2 before the desired reaction temperature was set. Once the reaction temperature was reached (either 245 °C in methanol synthesis or 270 °C in DME synthesis), the backpressure regulator was set to the desired operating pressure and the reactants were gradually fed into the system. The reactor effluent was analysed by the GC instrument every 20 minutes. After the experiment was complete, the pressure was released and the system was flushed with N_2 while cooling down to room temperature.

3.2.4 Product analysis

Two injection loops of 500 μL maintained at 250 °C were used to carry out sample injections. During each analysis, the columns were maintained at 50 °C for 2 minutes and then heated to 150 °C at a rate of 10 °C/min. The final temperature was maintained for 2 minutes. The FID was maintained at 250 °C for the analysis of methane, methanol, DME and other hydrocarbons. The TCD was kept at 150 °C and was used to detect CO, CO_2 and Ar (internal standard).

For both detectors, the retention times of the substances were identified by analysing a flow of calibration mixtures (BOC, 1% DME, 5% Ar, 5% CH_4 in He and 5% CO, 5% Ar, 5% CO_2, 5% CH_4 in He). The TCD was also calibrated with certified reactant mixture (BOC, 5% Ar, 24% CO_2 in H_2 and 5 %Ar, 4% CO, 20% CO_2 in H_2). From the calibration results, the response

factor of substance i, RF_i, was calculated from the ratio between the area under the GC peak and the molar concentration $y_{i,CM}$ in the calibration mixture (Equation 3.1). Volume of each injection was assumed to be constant. The RF_i values for common reaction products are summarised in Appendix A Table A.3. From the response factor, the amount of each product $y_{i,out}$ in the effluent was quantified using Equation 3.2.

$$RF_i = \frac{Peak\ area\ in\ chromatogram}{y_{i,CM}} \qquad \text{Equation 3.1}$$

$$y_{i,out} = \frac{Peak\ area\ given\ by\ GC}{RF_i} \qquad \text{Equation 3.2}$$

For methanol, it was impossible to obtain a gaseous calibration standard due to its low boiling point. Hence, its response factor was calculated from that of methane using the ratio between the factors of these two substances given by R. Montesano [17], assuming that the ratio remain constant.

3.2.5 Calculation methods

3.2.5.1 Conversion and production rate

The reaction progress was quantified by the conversion and production rate of methanol. The reactions involved and the extents of reaction are presented below:

$$CO + 2H_2 \rightarrow CH_3OH \qquad \xi_1$$

$$CO_2 + H_2 \rightarrow CO + H_2O \qquad \xi_2$$

$$CO + 3H_2 \rightarrow CH_4 + H_2O \qquad \xi_3$$

$$2CH_3OH \rightarrow CH_3OCH_3 + H_2O \qquad \xi_4$$

The extent of reaction $\dot{\xi}_j$ (mole per hour) of reaction j is defined as

$$\dot{\xi}_j = \frac{\dot{n}_i - \dot{n}_i^0}{v_i} \qquad \text{Equation 3.3}$$

where $\dot{n}_i^0$ and $\dot{n}_i$ are the molar flowrates of substance i, in the feed and outlet respectively. v_i is the stoichiometric ratio of i in reaction j.

The molar concentration y_i of substance i in the reactor effluent obtained from FID and TCD measurements can be expressed as:

$$y_{MeOH} = \frac{\dot{\xi}_1 - \dot{\xi}_4}{\dot{n}_T^0 - 2\dot{\xi}_1 - 2\dot{\xi}_3} \quad \text{Equation 3.4}$$

$$y_{DME} = \frac{\dot{\xi}_4}{\dot{n}_T^0 - 2\dot{\xi}_1 - 2\dot{\xi}_3} \quad \text{Equation 3.5}$$

$$y_{CO} = \frac{\dot{n}_{CO}^0 - \dot{\xi}_2 - \dot{\xi}_1 - \dot{\xi}_3}{\dot{n}_T^0 - 2\dot{\xi}_1 - 2\dot{\xi}_3} \quad \text{Equation 3.6}$$

$$y_{CO_2} = \frac{\dot{n}_{CO_2}^0 - \dot{\xi}_2}{\dot{n}_T^0 - 2\dot{\xi}_1 - 2\dot{\xi}_3} \quad \text{Equation 3.7}$$

$$y_{CH_4} = \frac{\dot{\xi}_3}{\dot{n}_T^0 - 2\dot{\xi}_1 - 2\dot{\xi}_3} \quad \text{Equation 3.8}$$

From the extents of reaction, the methanol conversions and hence the rate of methanol production were calculated from FID measurements as

Methanol synthesis

$$X_{MeOH} = \frac{\dot{\xi}_1}{\dot{n}_{CO_2}^0} \quad \text{Equation 3.9}$$

$$R_{MeOH} = \frac{X_{MeOH} \times \dot{n}_{CO_2}^0}{n_{cat}} \quad \text{Equation 3.10}$$

DME synthesis

$$X_{MeOH} = \frac{\dot{\xi}_1 + 2 \times \dot{\xi}_4}{\dot{n}_{CO_2}^0} \quad \text{Equation 3.11}$$

$$R_{MeOH} = \frac{X_{MeOH} \times \dot{n}_{CO_2}^0}{n_{cat}} \quad \text{Equation 3.12}$$

where X_{MeOH} is the MeOH conversion, R_{MeOH} is the rate of methanol production, $\dot{n}_{CO_2}^0$ is the inlet molar flowrate of CO_2 in mole per hour and n_{cat} is the amount of active metal (Ni+Ga or Pd+Ga or Cu) in moles.

Due to the very low conversion achieved in all the experiments, error associated with the TCD measurement (CO_2 signal) was large. Therefore it was not possible to balance the conversion obtained in the FID and TCD.

3.2.5.2 Selectivity

The selectivity of products were calculated as the molar percentage of each product, as shown in Equation 3.13 below.

$$S_i = \frac{y_i}{\sum y_i} \qquad \text{Equation 3.13}$$

where S_i is the selectivity of product i and y_i is the molar concentration of product i (MeOH, DME, CH_4 and CO) in the reactor effluent.

In some cases, the selectivity was also calculated as the ratio between MeOH and CO or CH_4.

$$\text{MeOH/CO} = \frac{y_{MeOH}}{y_{CO}} \qquad \text{Equation 3.14}$$

$$\text{MeOH/CH}_4 = \frac{y_{MeOH}}{y_{CH_4}} \qquad \text{Equation 3.15}$$

where MeOH/CO stands for the ratio between MeOH and CO, y_{MeOH} and y_{CO} are the molar fractions of MeOH and CO.

The errors in conversion, methanol production rate and selectivity were estimated using the standard deviation in the GC response for each substance and uncertainty in sample weight. Example of calculation is given in Appendix A.

3.3 Thermodynamic analysis of methanol synthesis process

The experiments conducted in this study were atmospheric pressure, 10 bar and 30 bar. To ensure that the catalytic performance observed was not limited by the equilibrium at these pressures, the thermodynamic equilibrium analysis of the methanol synthesis process was carried out.

$$CO + 2H_2 \rightarrow CH_3OH \qquad \text{Reaction 1}$$

$$CO_2 + 3H_2 \rightarrow CH_3OH + H_2O \qquad \text{Reaction 2}$$

$$CO + H_2O \rightarrow CO_2 + H_2 \qquad \text{Reaction 3}$$

The equilibrium constant for each reaction at a given total pressure can be written as follows (assuming the fugacity coefficient is unity):

$$K_{p1} = \frac{P_{CH_3OH}}{P_{CO} \times {P_{H_2}}^2} \qquad \text{Equation 3.16}$$

$$K_{p2} = \frac{P_{CH_3OH} \times P_{H_2O}}{P_{CO_2} \times {P_{H_2}}^3} \qquad \text{Equation 3.17}$$

$$K_{p3} = \frac{P_{CO_2} \times P_{H_2}}{P_{CO} \times P_{H_2O}} \qquad \text{Equation 3.18}$$

where K_{pi} is the equilibrium constant for reaction i, P_j is the partial pressure of substance j.

On the other hand, the equilibrium constants dependent on temperature only can also be calculated from the Van't Hoff equation.

$$ln\frac{K_i}{K_{i,298K}} = \frac{-\Delta H^{\ominus}_{r,i}}{R}\left(\frac{1}{T} - \frac{1}{T_{298K}}\right) \qquad \text{Equation 3.19}$$

where $K_{i,298K}$ is the equilibrium constant at temperature 298K, K_i is the equilibrium constant of reaction i at T (reaction temperature), $\Delta H^{\ominus}_{r,i}$ is the standard heat of reaction i, R is the universal gas constant.

$K_{i,298K}$ is further defined as:

$$K_{i,298K} = \exp\left(\frac{-\Delta G^{\circ}_{298K}}{RT}\right) \qquad \text{Equation 3.20}$$

where $\Delta G^{\circ}_{i,298K}$ is the Gibbs energy change at 298K. The values of $\Delta H^{\ominus}_{r,i}$ and $\Delta G^{\circ}_{i,298K}$ used are given in Appendix A Table A.4.

Equating both equilibrium constants for each reaction [244] and solve the three reactions as a whole system, the partial pressure of each substance (consequently the molar concentration) can be calculated. The MeOH conversion achieved at each temperature was subsequently determined using Equation 3.9. The process was repeated for different pressures. The results for the equilibrium MeOH conversion as a function of temperature are presented in Figure 3.2.

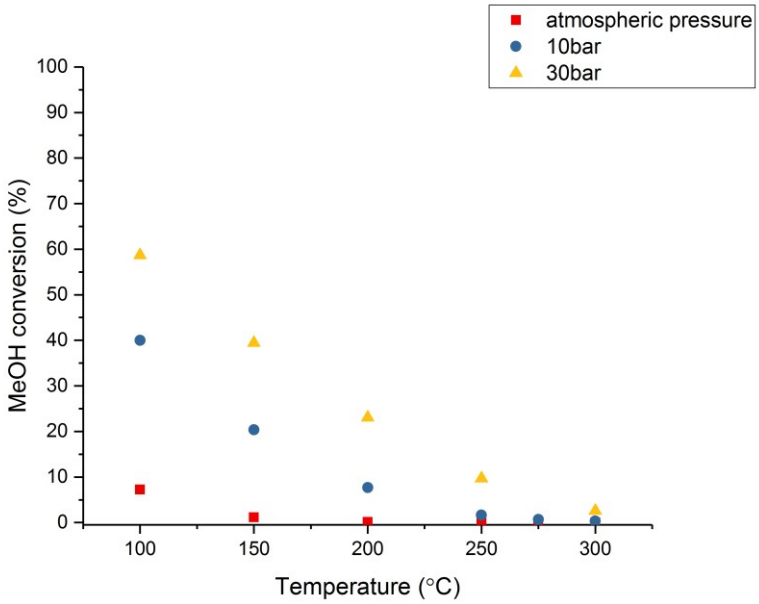


Figure 3.2, Equilibrium methanol conversion against temperature at different pressures

3.4 Catalyst characterisation

3.4.1 X-ray powder diffraction (XRD)

The diffraction patterns of powdered catalysts were obtained in a PANalytical X'pert Pro multipurpose diffractometer by exposing them to Cu - K_α radiation. X-ray was generated with 40 kV and 20 mA. The data was collected over a range of 6 – 80° (2θ) at room temperature. The particle sizes of the Ni-Ga and Cu catalysts were determined using the Scherrer equation. The full width at half maximum was taken from the main diffraction peak.

3.4.2 Nitrogen physisorption

The surface area and porosity measurements were obtained by conducting nitrogen physisorption at 77 K in Micrometrics Tristar 3000. Samples were degassed overnight under N_2 flow at 120 °C. The specific surface area was calculated using the BET method. The pore volume and pore size for SiO_2 supported catalysts were calculated by the BJH method.

3.4.3 Thermogravimetric analysis (TGA)

A Netzsch thermogravimetric analysis instrument coupled with online mass spectrometry (MS) was used to determine the coke content on the spent catalysts (temperature programmed oxidation, TPO). 20 mg of spent material was loaded in a TGA pan. Air was used, the sample was heated from room temperature to 120 °C and stayed at this temperature for half an hour to oxidise the catalyst. It was then heated to 800 °C at a rate of 20 °C/min. CO_2 evolution was monitored by the online MS at signal m/z 44. The CO_2 signal was quantified by calibrating the detector with TPO of known amount of $MnCO_3$ (Sigma Aldrich).

3.4.4 Transmission electron microscopy (TEM) and energy dispersive spectroscopy (EDS)

TEM images were obtained with a JEOL2010 Transmission Electron Microscope, operated at 200 kV. A small amount of fine catalyst powders were dispersed in ethanol and a drop was added to a copper grid coated with holey carbon film (300 mesh, Agar Scientific) to dry. EDS spectrum was also obtained to determine the elemental composition of the sample.

3.4.5 X-ray photoelectron spectroscopy (XPS)

Prior to analysis, the samples were dried (and de-gassed) under flowing N_2 at 100 °C overnight.

A Thermo K-Alpha Spectrometer equipped with Al K_α source gun was used to obtain XPS data. An X-ray spot size of 400 μm and pass energy of 20 eV were used. Samples were mounted on double-sided adhesive tape and the spectra were collected with 0.1 eV

increments. The binding energies (BE) were referenced to the C 1s peak of adventitious carbon at 284.8 eV. Data analysis was performed using Avantage software from Thermo Scientific.

3.4.6 Inductive coupled plasma – optical emission spectrometry (ICP – OES)

The chemical composition of the catalysts were determined by ICP – OES analysis (Perkin Elmer Optima 2000DV). Catalysts (about 10 mg) were digested overnight in 10mL aqua regia, which consisted of 3:1 (volume) hydrochloric and nitric acids. Before analysis, the concentrated acid solution was diluted with DI water (10% acid solution in final diluted mixture). Calibration was done using standard solutions (Fluka, Sigma Aldrich).

Samples containing SiO_2 were analysed by Medac Ltd using HF digestion.

3.4.7 Temperature programmed experiments

Temperature programmed experiments were conducted in an in-house-built reactor system, which consisted of a quartz tube microreactor, electric furnace and a gas chromatograph (FID or TCD, depending on the experiments).

3.4.7.1 Temperature programmed reduction (TPR)

Temperature programmed reduction experiments were conducted in a quartz tube microreactor with a thermal conductivity detector (TCD). The quart reactor has an internal diameter of 6 mm, thickness 1 mm and length 27 cm. The electric furnace had wires coiled around a quartz cylinder (diameter 2 cm), which was heavily insulated. Two thermocouples were placed inside the cylinder, one to control the heating rate and another to act as a thermal cutoff. A third thermocouple was attached to the quartz reactor and connected to EasyLog temperature logger for temperature recording. 5% H_2/N_2 (BOC) was fed at a flowrate of 40 mL/min, which was controlled by the gas chromatograph (GC14B). The reactor effluent was passed through a moisture trap before entering the GC. The TCD measured the difference in the hydrogen concentration in the reactor effluent and on the reference side (fresh feed).

During experiments, the reactor was heated from room temperature to 800 °C at a rate of 10 °C/min. Hydrogen consumption was quantified by calibrating the detector with known amount of pure CuO (Sigma Aldrich).

3.4.7.2 Passivation study of NiGa(a)/SiO_2

During passivation study of NiGa(a)/SiO_2 catalysts, the catalyst was reduced in situ in the quartz tube with 5% H_2/N_2 (70 mL/min) at 700 °C for 2 hours. It was then cooled down to the desired passivation temperature and 10% N_2O/N_2 (BOC) was fed for 30 minutes. After passivation, the catalyst was cooled down to room temperature and exposed to air for 30 min to simulate transfer to reactor. TPR was subsequently carried out to find the optimum re-activation temperature.

3.4.7.3 Temperature programmed reaction (TPRx)

Temperature programmed reactions were carried out to screen different catalysts. The same quartz tube (with the same electric furnace) was used. 5%Ar/24%CO_2/H_2 (BOC) feed flowrate was controlled by Brooks 5850E mass flow controllers, the rates were set to be around 100 mL/min STP. Product analysis was done with both FID and TCD from GC2014 instrument, as described in section 3.2.4. The catalyst precursor was reduced with 5% H_2/N_2 in situ at the desired temperature, after cooling down (and passivated with 10% N_2O and then re-activated with 5% H_2 during passivation studies), reactant mixture was fed and the reactor was heated from room temperature to the target reaction temperature. Product analysis was carried out at each desired temperature.

Chapter 4 CO_2 Hydrogenation to Methanol over Ni-Ga Based Catalyst at Elevated Pressures

4.1 Introduction

In this chapter, the performance of Ni-Ga based catalysts in CO_2 hydrogenation to methanol are investigated.

Over conventional Cu-based methanol catalysts, a CO_2-rich feed promotes the production of unwanted CO through the reverse water-gas shift reaction (rWGS), increasing H_2 consumption while reducing methanol production. The additional water produced can accelerate deactivation of the catalyst through sintering [245]. Hence, considerable research has been directed to development of new catalysts for CO_2 hydrogenation. Among them, the intermetallic compounds have gained increasing popularity as methanol-forming catalysts due to their structural stability and the modified electronic structure of the active metal [11]. As discussed in Chapter 2, Studt and co-workers [12] reported the discovery of Ni-Ga catalysts for CO_2 hydrogenation to methanol at atmospheric pressure. Ni_5Ga_3 supported on silica was reported to have a methanol synthesis activity comparable to conventional $Cu/ZnO/Al_2O_3$ catalysts but with significantly reduced CO production. However, despite the apparent promise of this catalyst system, the thermodynamic equilibrium for CO_2 to methanol is very low at atmospheric pressure (less than 0.02% conversion at 250 °C); for industrial applications Ni-Ga based catalysts would have to operate at elevated pressures. Recently, Wencka et al. [128] in a surface science study have shown that the catalytic activity of Ni-Ga intermetallic compound is strongly affected by exposure to air and that the effect cannot be fully reversed even at 600 °C. Thus, due to the severe pre-reduction conditions (700 °C) involved in the preparation of these active Ni-Ga catalysts [7, 8], the performance and stability of $Ni-Ga/SiO_2$ catalysts at elevated pressures remain largely unknown.

Firstly, the identification and evaluation of a suitable passivation and in situ re-activation procedure is presented, which is essential to overcome the challenge of preserving the active Ni-Ga catalyst that was reduced at 700 °C. The characterisation of the passivated catalysts is given. The performance and stability NiGa(a)/SiO_2 (5:3), NiGa(b)/SiO_2 (1:1) and NiGa(c)/SiO_2 (3:1) catalysts at elevated pressures have been investigated and compared to that of a commercial Cu/ZnO/Al_2O_3 catalyst in a fixed bed stirred reactor (CSTR), which provides accurate kinetic information due to its gradientless nature (constant temperature, pressure and composition throughout the reactor). The impact of low levels of CO was investigated by addition of CO to the feed gas.

Hydrotalcites (double layered hydroxide, LDH) have been found to be versatile precursors as there is flexibility to incorporate different metal cations into the structure and the uniform dispersion and interaction of metal cations in the structure are beneficial for alloy formation [135]. Recently, a CoGa based catalyst was reported to convert syngas to ethanol and higher alcohols efficiently [240]. This was achieved by trapping the uniformly dispersed CoGa particles on the ZnAl layered double oxide (LDHs). Moreover, higher stability was achieved due to the unique structure of the catalyst. This approach is applied to a Ni-Ga based catalyst briefly towards the end of the chapter.

4.2 Preparation of Ni-Ga/SiO_2 catalysts

4.2.1 The need for a suitable passivation procedure

From the Ni-Ga catalysts, NiGa(a)/SiO_2 was selected for preliminary study as the Ni-Ga catalyst with a Ni:Ga ratio of 5:3 was reported to be the most active [12]. The detailed catalyst preparation procedures and source of chemicals used can be found in Chapter 3 section 3.2.1.1.

The preliminary studies of NiGa(a)/SiO_2 were conducted in a TPRx system with online mass spectrometry for product analysis to allow quick screening of the catalyst. NiGa(a)/SiO_2 was

reduced in situ at 700 °C direct from the impregnated nitrates. A TPRx experiment with CO_2/H_2 was then carried out to confirm the activity of the catalyst prepared. The maximum methanol production rate at atmospheric pressure at 245 °C was found to be 0.06 mol [MeOH]/mol [active metal]*hr, which is comparable to the literature value reported (0.07) [12]. This suggests that an active intermetallic Ni-Ga based catalyst was successfully prepared.

To measure the catalytic performance of these Ni-Ga based catalysts in high-pressure reactor, which has a temperature limit of 350 °C, in situ reduction of the NiGa(a)/SiO_2 catalyst precursor would be very difficult. Therefore, the catalyst precursor must be reduced ex situ and subsequently transferred to the high-pressure reactor. The catalyst tests conducted by Sharafutdinov et al. [13, 14] at atmospheric pressure were always in the same reactor, where reduction of the catalyst took place to avoid contact with air. More recently, Wencka and co-workers [128] found that the catalytic activity of noble metal free intermetallic catalysts, such as Ni-Ga based catalysts, was strongly influenced by exposure to air due to the instability of active surface. Hence, it was expected that the Ni-Ga based catalysts would suffer a significant loss in activity upon exposure to air. Hence, another TPRx experiment was carried out with a reduced and air-oxidised NiGa(a)/SiO_2 catalyst to investigate the effect of air on the reduced catalyst. Prior to the reaction, the oxidised catalyst was re-activated in situ using the regeneration conditions suggested by Studt et al. (350 °C for 2 hours under flowing 5% H_2/N_2). The comparison of the activities is shown in Figure 4.1.

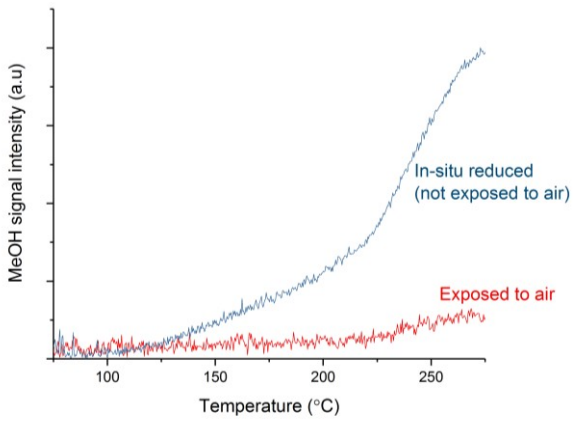


Figure 4.1, TPRx profiles of the catalytic performance of in situ reduced NiGa(a)/SiO_2 and air-oxidised NiGa(a)/SiO_2 (re-reduced at 350 °C)

Clearly, direct exposure to air of the reduced catalyst had detrimental effect on the activity of the catalyst. As suggested by Wencka et al. [128] that once the Ni-Ga based catalyst was oxidised by air, reducing at temperatures as high as 600 °C can only restore the active surface composition partially. Therefore, a suitable passivation method to preserve the activity of the catalyst for transport under air is of paramount importance if these catalysts are to be used under industrial conditions.

4.2.2 Development of passivation procedures

4.2.2.1 Passivation with N_2O

Methodology for the development of passivation procedure

As noted above, a convenient and effective passivation technique should be developed in order that the Ni-Ga based catalysts can be used under high pressures.

Low concentrations of oxygen or nitrous oxide (N_2O) can be used as passivating agents. Nitrous oxide surface oxidation is a well-established technique for surface area determination and passivation of Cu-based methanol catalysts owing to the ease of N_2O handling, control over extent of oxidation and simple oxidation products (N_2O decomposes to O(s) and N_2 at 60 °C on Cu) [246-248], it was selected for Ni-Ga catalyst passivation. The passivation and subsequent re-activation temperatures for Ni-Ga/SiO_2 were varied to find the optimum combination.

The active Ni-Ga catalyst was obtained by reducing the catalyst precursor in situ at 700 °C for 2 hours under a flow of 5% H_2/N_2, as described in section 3.2.1.1. Subsequently, the catalyst was cooled down to the desired passivation temperature (25 °C, 50 °C, 80 °C and 120 °C) before feeding 10% N_2O/N_2 for 30 minutes. To simulate air exposure during transfer to high-pressure reactors, once the passivated catalyst was cooled down to room temperature, it was left in air for 30 minutes. In situ TPR with 5% H_2/N_2 was carried out over the passivated catalyst to investigate its reducibility. Next, TPRx with a CO_2/H_2 mixture at atmospheric pressure were

conducted over the passivated and re-activated catalyst to assess the effectiveness of the passivation procedure.

Effect of passivation temperature

The TPR profiles for different passivation temperatures (for NiGa(a)/SiO_2) are presented in Figure 4.2. The size of the signal measured by the TC detector during the TPRs clearly indicates that the peaks observed mainly originated from H_2 consumption and not N_2O desorption, since the thermal conductivity of N_2O is very similar to that of N_2 (carrier gas). The sample passivated at 25 °C have well-defined hydrogen consumption peaks at a lower temperature (80 – 100 °C). This suggests that samples passivated at lower temperatures are easier to re-reduce, hence under these conditions N_2O mainly oxidised the surface. At 25 °C, the amount of hydrogen consumption was found to be 0.455 mmol/g (NiGa(a)/SiO_2). This value is equivalent to 15 mol% of active metal (Ni+Ga) being reduced, indicating that the catalyst had been passivated successfully via surface oxidation.

On the other hand, the hydrogen consumption peaks became broader and more irregular when the passivation temperature was increased to 120 °C. The trend is similar to that of unpassivated sample that was exposed to air. This observation implies that high passivation temperature can cause deep (bulk) oxidation of the catalysts, which is undesirable but expected. Hence, a passivation temperature of 25 °C was considered to be the most convenient and effective, it was used in all the subsequent experiments.

In order to study the long-term stability of the passivated catalyst under air, a sample of reduced NiGa(a)/SiO_2 was passivated at 25 °C and stored in air for one month. TPR experiment was performed over this catalyst. As can be seen from Figure 4.2 (b), passivated sample that was stored under air for long period of time has a TPR profile similar to an unpassivated sample. Hence, the air exposure time after passivation (during catalyst handling and transportation) should be kept as short as possible to prevent further oxidation.

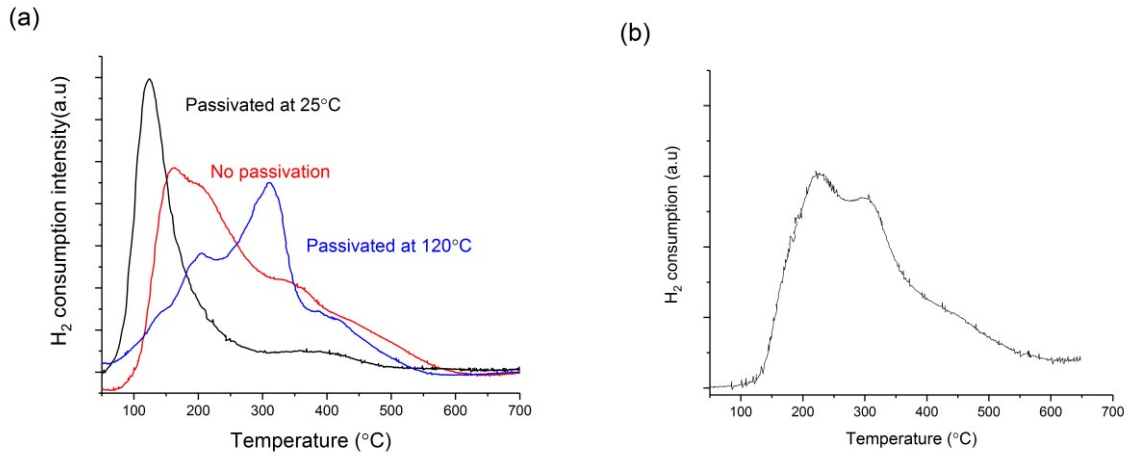


Figure 4.2, TPR profiles for reduced NiGa(a)/SiO_2
(a) Passivated at different temperatures (b) Passivation at 25 °C and exposed to air for long period of time

Effect of re-activation temperature

Taking a closer look at Figure 4.2 (a), although the majority of reduction of the passivated (at 25 °C) catalyst is completed below 200 °C, there is a small H_2 consumption peak at 300 – 450 °C. This indicates that there are oxidised species that can only be re-reduced above 300 °C.

To confirm whether re-activation above 300 °C was required, re-activation temperatures of 270 °C (below 300 °C) and 340 °C (above 300 °C) were investigated. 340 °C was chosen because it is close to the reactor temperature limit. The re-activation was carried out with 5% H_2/N_2 and the time was preliminarily chosen to be 3 hours, which is slightly longer than the reduction time used by Wencka et al. [128] to ensure that the re-activation is completed. The catalytic activity of the passivated catalysts re-activated at 270 °C and 340 °C were measured separately by TPRx of CO_2/H_2 at atmospheric pressure. The TPRx profiles are given in Figure 4.3, the result for an in situ reduced catalyst at 700 °C (without passivation) is also shown for comparison.

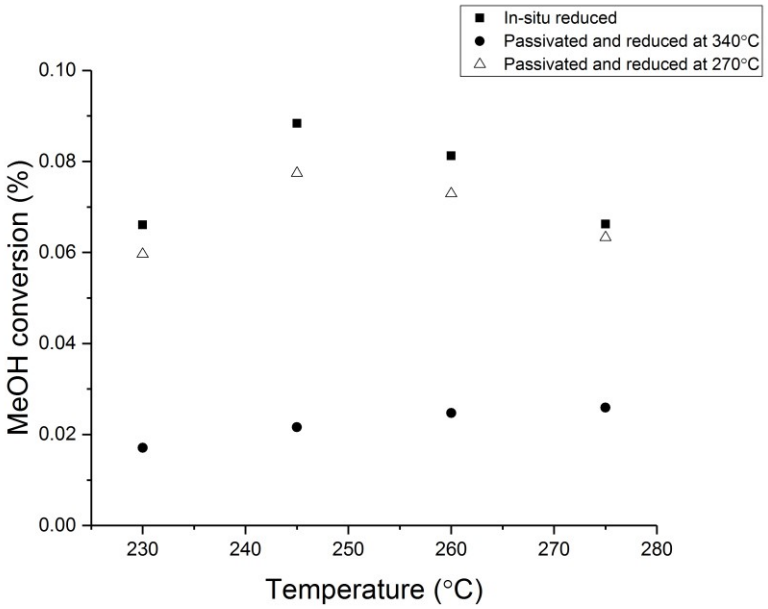


Figure 4.3, TPRx profiles for NiGa(a)/SiO_2 re-activated at different temperatures

The passivated sample re-reduced at 270 °C only recovered half of the maximum activity compared to the in situ reduced catalyst, this implies that these hard-to-reactivate species play crucial role in CO_2 hydrogenation to methanol. Therefore, a higher re-activation temperature is required in order to re-reduce oxidised species produced by passivation.

It can be clearly seen that the sample re-activated at 340 °C achieved similar performance as the in situ reduced sample. The performance of the passivated and re-activated sample was still slightly lower than that of the high temperature (700 °C) in situ reduced sample. This shows that surface composition was not 100% restored to the state prior to the passivation. Wencka et al. [128] found that a reduction temperature of 300 °C was insufficient in cleaning the surface oxides of the Ni-Ga intermetallic compound that was directly exposed to air, higher temperature (600 °C) was required to partially reconstruct the surface composition to the energetically more favourable bulk value. This suggests that by passivating with nitrous oxide, most of the active sites can be restored easily at a lower temperature. Since the reactors have a temperature limit of 350 °C, the re-activation temperature of 340 °C was deemed the best choice within the desired range. This passivation procedure was able to preserve the active catalyst for quick transport under air. Hence for all the catalyst tests in the high pressure

reactor, Ni-Ga based catalysts were first reduced ex situ at 700 °C for 2 hours with 5% H_2/N_2 and then passivated at 25 °C with 10% N_2O/N_2 before transfer to the reactor, where the catalysts underwent re-activation at 340 °C for 3 hours in 5% H_2/N_2.

4.2.2.2 Protection by liquid

Another approach was also tested: the use of liquid protection. This is done by quickly immersing the ex situ reduced catalyst in excess oil, liquids or polymeric solvent [249, 250] to protect air-sensitive catalysts. The liquid protecting agent is then removed in situ by evaporation prior to catalyst use.

Cyclohexane was selected as the protecting liquid because it is fairly unreactive and it has a relatively low boiling point [251]. Once the catalyst precursor was reduced, cyclohexane was injected into the reduction reactor. The protected sample was left in open air for 30 minutes to simulate transport in air, after which it was dried in situ with flowing N_2 at 120 °C for 1 hour to ensure that all the cyclohexane was evaporated. TPRx was conducted to evaluate the success of this technique. The activity and selectivity of the catalyst were given in Table 4.1.

Table 4.1, Methanol synthesis activity and selectivity of NiGa(a)/SiO_2 protected with cyclohexane

Methanol conversion (%)	**Selectivity to CO (%)**	**Selectivity to CH_4 (%)**
0	84	16

Clearly, the liquid protection method was unsuccessful in preserving the active catalyst since no methanol synthesis activity was detected and mainly CO and CH_4 were produced. No other products or cyclohexane were detected. The XRD pattern (Appendix B, Figure B.1) for the protected catalyst did not give any evidence of a difference in the morphology compared to the N_2O-passivated sample. Hence, cyclohexane might be incompatible with the active metal surface, perhaps by blocking the active sites for methanol synthesis by some cracking. Due

to the unsuccessful protection and the difficulties associated with the handling/loading of catalyst immersed in excessive liquid, protection with liquid was not pursued further.

4.2.2.3 Characterisation of passivated catalysts

The reduced-passivated NiGa(a)/SiO_2, NiGa(c)/SiO_2 and NiGa(c)/SiO_2 catalysts were characterised by a range of techniques.

Chemical composition

The chemical compositions of both dried precursor and reduced-passivated catalysts were analysed for all three catalysts, NiGa(a)/SiO_2, NiGa(c)/SiO_2 and NiGa(c)/SiO_2, results are summarised in Table 4.2.

Table 4.2, Chemical composition of NiGa(a)/SiO_2, NiGa(c)/SiO_2 and NiGa(c)/SiO_2

		NiGa(a)/SiO_2		**NiGa(b)/SiO_2**		**NiGa(c)/SiO_2**	
		Dried precursor	Reduced - Passivated	Dried precursor	Reduced - Passivated	Dried precursor	Reduced - Passivated
Wt% Ni	nominal	6.3	9.9	4.9	7.8	7.5	12.2
	actual	7.5 ± 0.3	10.1 ± 0.5	4.9 ± 0.2	7.9 ± 0.3	6.8 ± 0.3	12.1 ± 0.6
Wt% Ga	nominal	4.5	7.1	5.8	9.2	3.0	4.8
	actual	4.4 ± 0.3	5.1 ± 0.4	4.6 ± 0.3	6.2 ± 0.3	2.3 ± 0.2	3.5 ± 0.2
Ni:Ga (ICP)		2.4	2.3	1.2	1.5	3.5	4.2
Ni:Ga (EDS)		-	2.0	-	1.6	-	-

The prepared catalysts have consistently low Ga content, especially the passivated catalysts. This could be due to inaccurate determination of water content of metal nitrates ($Ga(NO_3)_3 \cdot xH_2O$) used during incipient wetness impregnation. However, the significant decrease in Ga content after passivation implies that Ga has been lost during the preparation

process, most likely during the high temperature reduction where Ga_2O_3 may sublimate. It was found that the outlet line of the reduction reactor had a build-up of white solid after two years of frequent usage. This confirms the suspicion that the high temperature reduction of catalyst precursor caused the observed loss of Ga.

BET surface area and porosity of catalysts

Some of the following measurements were carried out with the help of Yiming Zhang.

Table 4.3, BET surface area and pore volume of Ni-Ga/SiO_2 catalysts

Catalyst	BET surface area (± 1 m^2/g)	BJH pore volume (cm^3/g)	BJH pore size (nm)
SiO_2	279	1.78	17.5
NiGa(a)/SiO_2	250	1.41	16.8
NiGa(b)/SiO_2	244	1.22	15.9
NiGa(c)/SiO_2	Not measured		

The isotherms of these catalysts can be found in Appendix B Figure B.3. Compared to the porous SiO_2 support, the BET surface area for both Ni-Ga catalysts decreased by a similar small amount as is usual for impregnated catalysts.

XRD of monometallic (Ni and Ga) reference materials

The SiO_2 supported monometallic Ni and Ga were prepared using the same synthesis method as the Ni-Ga intermetallic catalysts, nickel nitrate impregnated on SiO_2 (denoted Ni/SiO_2) and gallium nitrate impregnated on SiO_2 (denoted Ga/SiO_2), in order to differentiate the diffraction peaks of the intermetallic catalysts from their monometallic counterparts. These monometallic precursors (dried) were reduced at 700 °C for 2 hours under 5% H_2/N_2, cooled down and passivated at 25 °C with N_2O/N_2 before analysis with XRD.

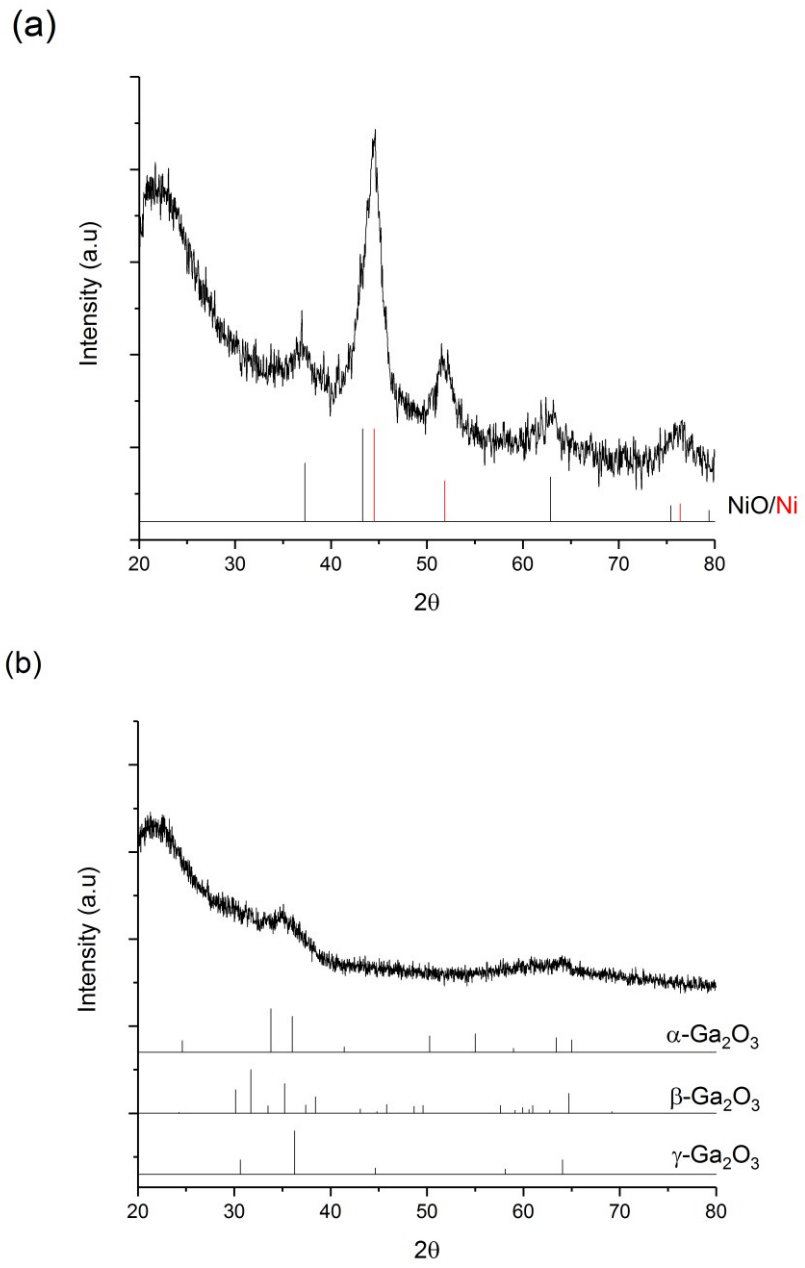


Figure 4.4, XRD of monometallic reference materials
(a) Ni/SiO_2 (reference peaks: ICSD no. 011239 and 52265) (b) Ga/SiO_2 (refence peaks: ICSD no. 27431, 83645, and 152085)

Diffraction pattern of Ni/SiO_2 (Figure 4.4 (a)) clearly shows that the sample is a mixture of metallic nickel and nickel oxide. Distinctive peaks of NiO were found at 37.3° (111) and 62.9° (220) and metallic Ni at 51.9° (200), all of which match well with reference data (ICSD no. 011239 and 52265). The peaks at around 43° – 45° and 76° can be attributed to the combined reflections of Ni ((200) reflection at 43.3° and (311) at 75.4°) and NiO ((111) at 44.5° and (220) at 76.4°).

In the case of Ga/SiO_2 (Figure 4.4 (b)), peaks found at 2θ = 35°, 43° – 46° (merged low-intensity peaks) and 65° can be attributed to different polymorphs of Ga_2O_3 (α- and β-Ga_2O_3) due to their similar diffraction peak positions. Since the characteristic peak of α-Ga_2O_3 at 55° was not detected, it is likely that crystalline α-Ga_2O_3 was not present or only in very low quantity. The diffraction pattern in Figure 4.4 (b) resembles that of the more amorphous-like γ-Ga_2O_3 [133] and characteristic (311) reflection of β-Ga_2O_3 at 38.4° appears to be missing (or masked). Hence the crystalline structure of this sample probably primarily consists of γ-Ga_2O_3 phase.

XRD of reduced-passivated NiGa(a)/SiO_2

The XRD pattern of a reduced-passivated NiGa(a)/SiO_2 catalyst is shown in Figure 4.5.

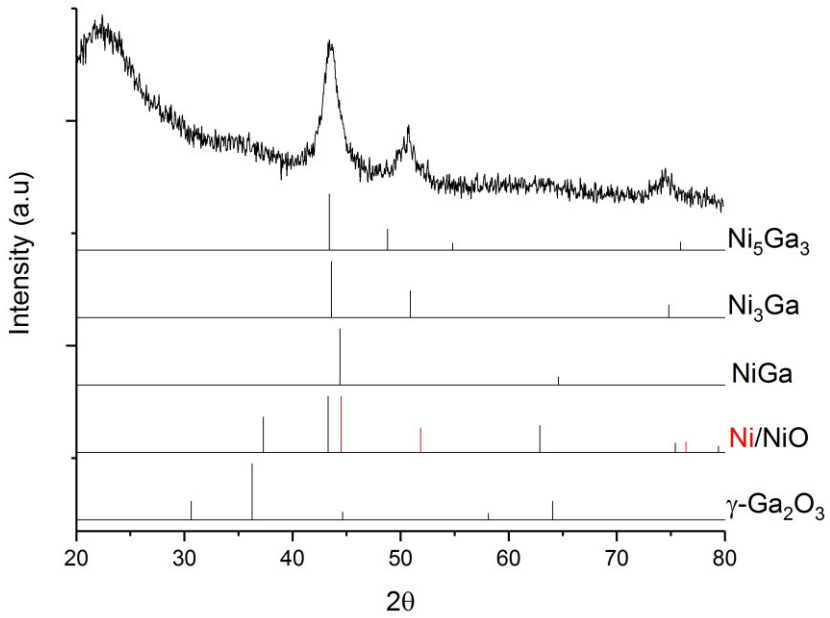


Figure 4.5, XRD pattern of reduced-passivated NiGa(a)/SiO_2 (reference peaks: Ni_5Ga_3, NiGa and Ni_3Ga: Studt et al. [12], Ni/NiO: ICSD no. 011239 and 52265, γ-Ga_2O_3: ICSD no.0152085)

With the addition of Ga, the characteristic NiO peak at 62.9° can no longer be detected and characteristic Ni peak at 44.5° has clearly been shifted towards lower 2θ value, which corresponds to the intermetallic Ni-Ga phases. This suggests that crystalline NiO or Ni are not

present in the sample due to the formation of Ni-Ga intermetallic phase. However, the presence of minor amount of Ni or NiO species cannot be entirely ruled out. NiGa peak at around 64° as well as the characteristic Ni_5Ga_3 peak at 48.8° ((131) reflection) were not observed, indicating that the NiGa and Ni_5Ga_3 intermetallic phases are not present. The major peak at 43.6° and the small peaks at 50.9° and 74.8° correspond to the (111) and (220) reflections of Ni_3Ga phase. These observations imply that the sample contains mainly Ni_3Ga intermetallic phase, which is expected since the actual Ni to Ga ratio (2.34) is closer to 3:1 than to the nominal 5:3 value. However, a Ni_3Ga catalyst would be expected to produce methane from CO_2/H_2 as the catalyst was reported to function as metallic nickel catalyst [252-254]. The TPRx results clearly show that the catalyst is active and selective for methanol synthesis with no detectable methane formation. In fact, Sharafutdinov et al. [13] tested several Ni-Ga catalysts with varying Ni content and found that the catalyst with 67.5 wt% of Ni content is the most active and selective towards methanol synthesis under atmospheric pressure. The NiGa(a)/SiO_2 prepared in this study has an actual Ni content of 66.4 wt%, which is very close to the optimal composition determined by Sharafutdinov et al. Therefore the NiGa(a)/SiO_2 catalyst cannot be solely Ni_3Ga crystallites during the reaction even though only a Ni_3Ga phase was detected in ex situ XRD of the passivated material.

A possibility is that there was further Ga-depletion of the intermetallic phase to Ni_3Ga during passivation or storage under air for XRD analysis, where the Ni-Ga particles were oxidised and possibly gallium de-alloyed from the intermetallic phase to form oxide due to its high oxygen affinity [128]. Peaks at around 36° and 64° that correspond to the reflections of Ga_2O_3 can be observed in Figure 4.5, indicating the presence of gallium oxide. However based on the ex situ XRD result, it is not possible to know whether this gallium oxide was formed from the decomposition of nitrate and was not incorporated into Ni-Ga intermetallic phase during catalyst reduction, or during/after passivation due to de-alloying of Ga from the intermetallic phase. Although decomposition of Ga-based intermetallic phases has been reported in the literature [13, 133, 154], this phenomenon was only observed for catalysts exposed to

catalysis for a long period of time. Therefore, it is not possible at this stage to conclude that the de-alloying of gallium is the main reason for the Ni_3Ga phase being observed in the XRD pattern. Resolution of this issue would require in situ study by XRD or EXAFS which were not available during the study.

XRD of reduced-passivated NiGa(b)/SiO_2

NiGa(b)/SiO_2 was expected to give a XRD pattern closer to Ni_5Ga_3 than to the NiGa phase since the actual Ni:Ga ratio proved to be 1.5. This speculation is confirmed in Figure 4.6.

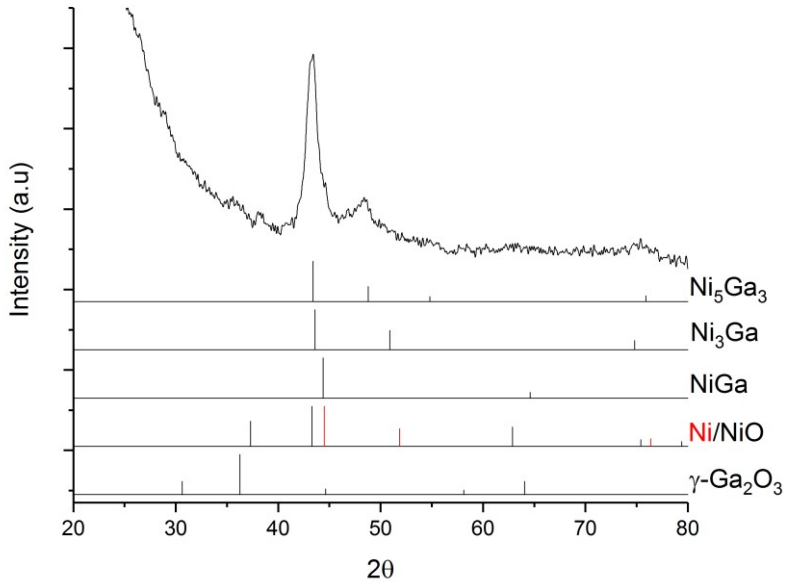


Figure 4.6, XRD pattern of reduced-passivated NiGa(b)/SiO_2 (reference peaks: Ni_5Ga_3, NiGa and Ni_3Ga: Studt et al. [12], Ni/NiO: ICSD no. 011239 and 52265, γ-Ga_2O_3: ICSD no.0152085)

Here, the characteristic peak for (131) reflection of Ni_5Ga_3 at 48.8° is clearly present and the major peak at 43.4° matches well with reference Ni_5Ga_3 phase. Reflections of Ga_2O_3 were found at 36° and 64°. These peaks indicate that Ga_2O_3 was also present in this sample. Again, due to significant overlap between the Ni/NiO and Ni-Ga diffraction peaks, the presence of Ni and NiO cannot be excluded even though there was no significant evidence of Ni or NiO in the XRD pattern.

XRD of reduced-passivated NiGa(c)/SiO_2

The XRD pattern for NiGa(c)/SiO_2 is shown in Figure 4.7. This sample appears to be a rather phase-pure Ni_3Ga/SiO_2 catalyst as all the characteristic Ni_3Ga peaks at 2θ = 43.6°, 50.9° and 74.8° were observed with no evidence of Ga_2O_3, nickel oxide, nickel metal or any other Ni-Ga phases.

Since this catalyst is Ga-depleted, formation of either un-incorporated or de-alloyed Ga_2O_3 is less likely, which is consistent with the absence of Ga_2O_3 in the diffraction pattern. Ni/NiO was not observed (at 63°) even though the catalyst has excess Ni content compared to the nominal value. This could be due to a number of effects including any very small or amorphous species or reaction with the support.

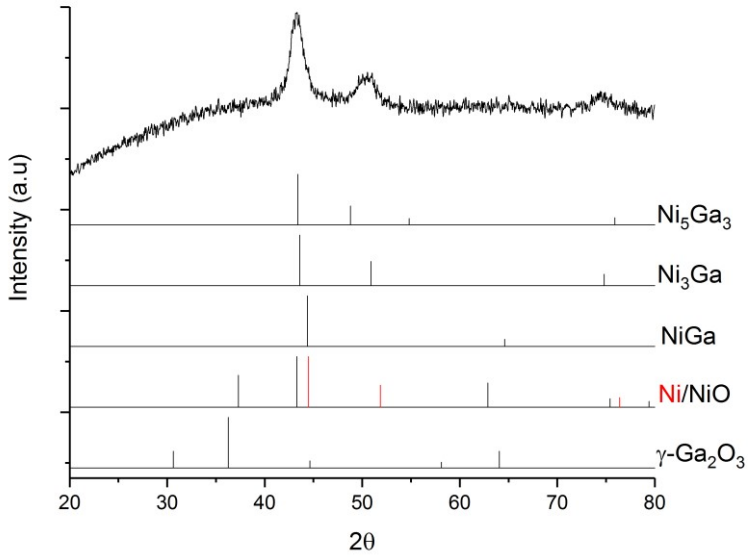


Figure 4.7, XRD pattern of reduced-passivated NiGa(c)/SiO_2 (reference peaks: Ni_5Ga_3, NiGa and Ni_3Ga: Studt et al. [12], Ni/NiO: ICSD no. 011239 and 52265, γ-Ga_2O_3: ICSD no.0152085)

Since the Cu/ZnO/Al_2O_3 catalyst is a commercially available and extensively studied material, its XRD pattern and chemical composition are not given here (Appendix B). Some of its properties such as crystallite size are presented together with that of Ni-Ga/SiO_2 in the following sections.

TEM and particle size of catalysts

The TEM images were obtained with the help of Dr Mahmoud Ardakani. The TEM for the passivated NiGa(a)/SiO_2 and NiGa(b)/SiO_2 catalysts are presented in Figure 4.8 (a) and (b) respectively.

The TEM images showed that there was crystallinity in the Ni-Ga particles. The crystallite size estimated from TEM image is slightly below 10 nm, which is similar to the crystallite size calculated from XRD (Table 4.4).

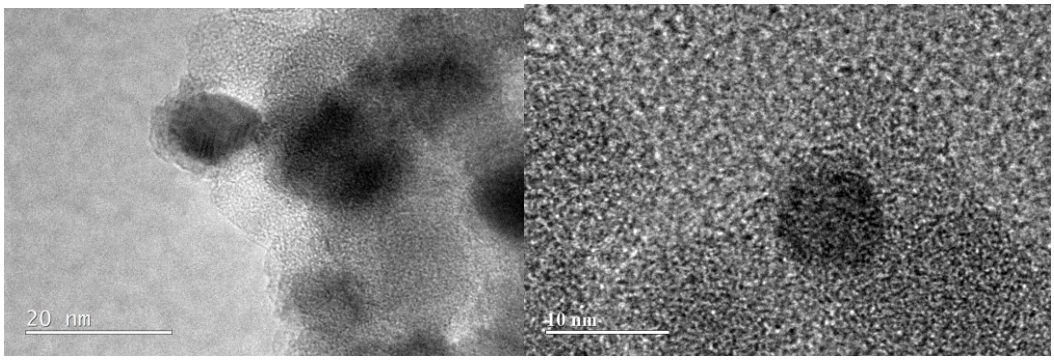


Figure 4.8, TEM images of reduced-passivated (a) NiGa(a)/SiO_2 (b) NiGa(b)/SiO_2

The Ni-Ga based catalysts have roughly identical crystallite sizes, which are comparable to literature values [12]. TEM crystallite size was measured from single particles therefore it is not completely representative.

Table 4.4, Crystallite size of Ni-Ga/SiO_2 catalysts

Catalyst	XRD crystallite size (nm)	TEM crystallite size (nm)
NiGa(a)/SiO_2	5.6 ± 0.6	8.6
NiGa(b)/SiO_2	5.6 ± 0.6	8.1
NiGa(c)/SiO_2	5.6 ± 0.6	-
Cu/ZnO/Al_2O_3	6.5 ± 0.6	-

XPS of passivated NiGa(a)/SiO_2 and NiGa(b)/SiO_2 catalysts

The XPS measurements and analysis were carried out with the help of Rui Zhang and Motaz Khawaji.

The XPS spectra of passivated NiGa(a)/SiO_2 and passivated NiGa(b)/SiO_2 catalysts are presented in Figure 4.9 and Figure 4.10 respectively.

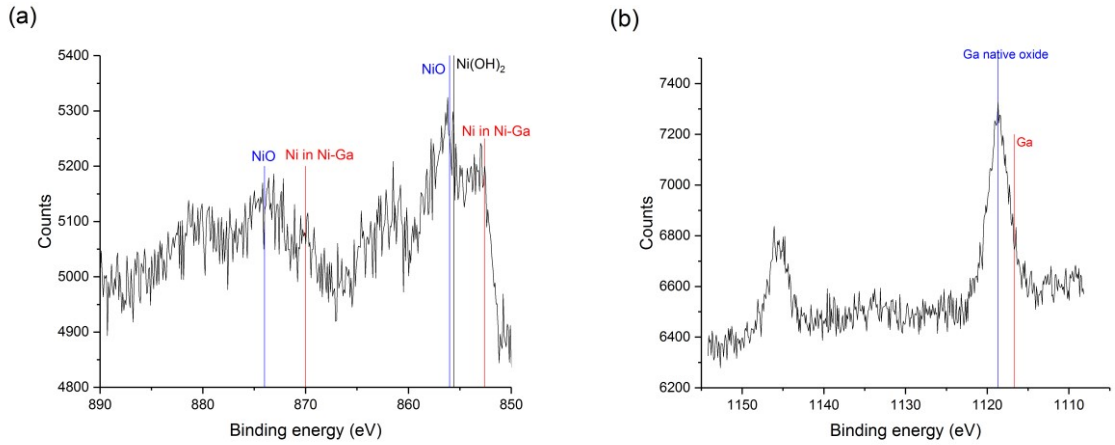


Figure 4.9, XPS spectra of passivated NiGa(a)/SiO_2
(a) Ni 2p (b) Ga 2p

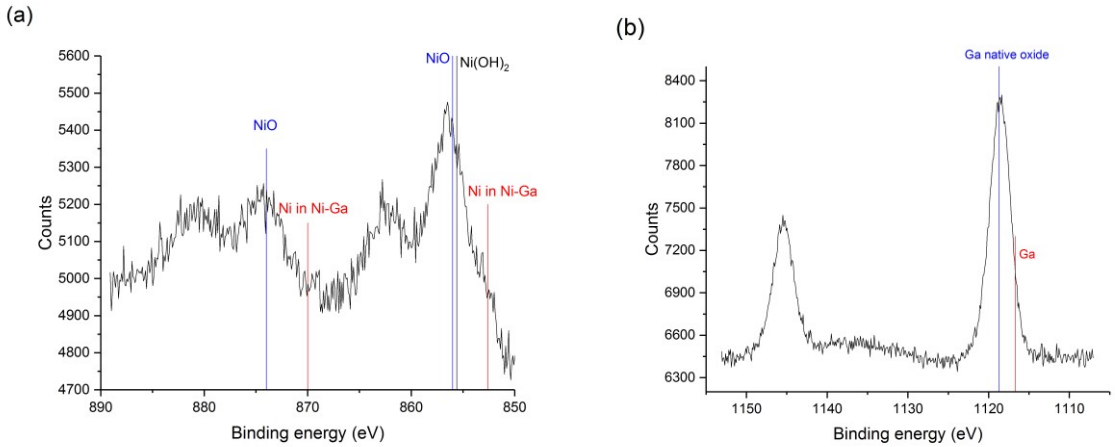


Figure 4.10, XPS spectra of passivated NiGa(b)/SiO_2
(a) Ni 2p (b) Ga 2p

For both catalysts, the XPS spectra of Ni 2p shows two states of Ni. The peaks at 856 eV and 874 eV correspond to nickel oxide, which was formed during passivation of the catalyst, drying at 100 °C and transfer to the XPS instrument. Nickel hydroxide may also be present (binding

energy at 856 eV and 874 eV, overlapping with peaks from NiO). The peaks at 853 eV and 870 eV correspond to a Ni metallic state, which is consistent with a Ni-Ga alloy, as suggested by Torelli et al. [255]. Metallic Ni is more pronounced in NiGa(a)/SiO_2 as this catalyst is Ni-rich.

In contrary, metal-like gallium was not detected in the Gallium 2p XPS specra for both catalysts. Peaks were only found at 1119 eV, which indicate that the gallium mainly exists as native oxide on the surface. This is expected because gallium is readily oxidised upon contact with air due to its high oxygen affinity. Study of the deeper sampling Ga 3d was attempted for both catalysts (Appendix B Figure B.4) in the hope that it would reveal the presence of underlying metallic Ga in its alloy form. However, the results did not show any significant evidence of alloyed Ga.

The surface chemical composition calculated from the XPS result are compared to the values obtained from ICP and EDS (in Table 4.5).

Table 4.5, Ni:Ga ratio measured by different characterisation techniques

	Ni:Ga ratio	
	NiGa(a)/SiO_2	NiGa(b)/SiO_2
Nominal	1.67	1.00
ICP	2.34	1.50
EDS	2.05	1.60
XPS	1.09	0.67

The ICP and EDS ratios are measured from the bulk catalyst. As discussed previously, the prepared catalyst has a higher Ni:Ga ratio than desired. The ratio measured by XPS for both Ni-Ga catalysts is significantly lower than the bulk value, suggesting that the surface is enriched in gallium oxide. As Wenca et al. [128] pointed out in their work on the surface

oxidation of Ni-Ga compounds, gallium oxide has 4.5 times more negative enthalpy of formation than nickel oxide. Upon contact with air, gallium rapidly forms oxide on the surface while driving nickel deeper into the subsurface layer. This explains why the surface composition found by XPS is significantly richer in Ga.

4.2.3 Methanol synthesis at elevated pressures in CSTR with CO_2/H_2

4.2.3.1 Choice of conversion level

For preliminary catalyst tests, low conversions and moderate temperatures are usually used to prevent serious mass and heat transfer effects. Although kinetic modeling is not the focus of this work, low conversion level should be used to make sure that the effects of interphase and intraparticle gradients are negligible and the conversion is not close to the thermodynamic equilibrium. However, high conversion should also be tested to study the impacts of increasing product concentration. A few attempts were made to increase the conversion, which will be discussed later in section 4.2.3.2.

4.2.3.2 Performance of Ni-Ga based catalysts at 10 bar (CSTR)

The catalytic performance of the Ni-Ga/SiO_2 catalysts reported by Studt et al. was measured at atmospheric pressure [12], where the thermodynamic equilibrium is very low. To evaluate the performance of these catalysts at elevated pressure, a pressure of 10 bar was chosen for the initial investigation. Previously, the TPRx results in section 4.2.2.1 demonstrated that the highest methanol synthesis activity was found at 245 °C. Therefore, the performance of NiGa(a)/SiO_2, NiGa(b)/SiO_2 and NiGa(c)/SiO_2 catalysts were first studied at 10 bar in the CSTR reactor at 245 °C as a function of time and compared to that of a commercial Cu/ZnO/Al_2O_3 catalyst under the same conditions. A stoichiometric feed (CO_2:H_2 = 1:3) was used and the flowrate was 110 mL/min STP (GHSV: 6640 h^{-1} based on catalyst volume). The methanol synthesis rate and the selectivity are presented in Figure 4.11.

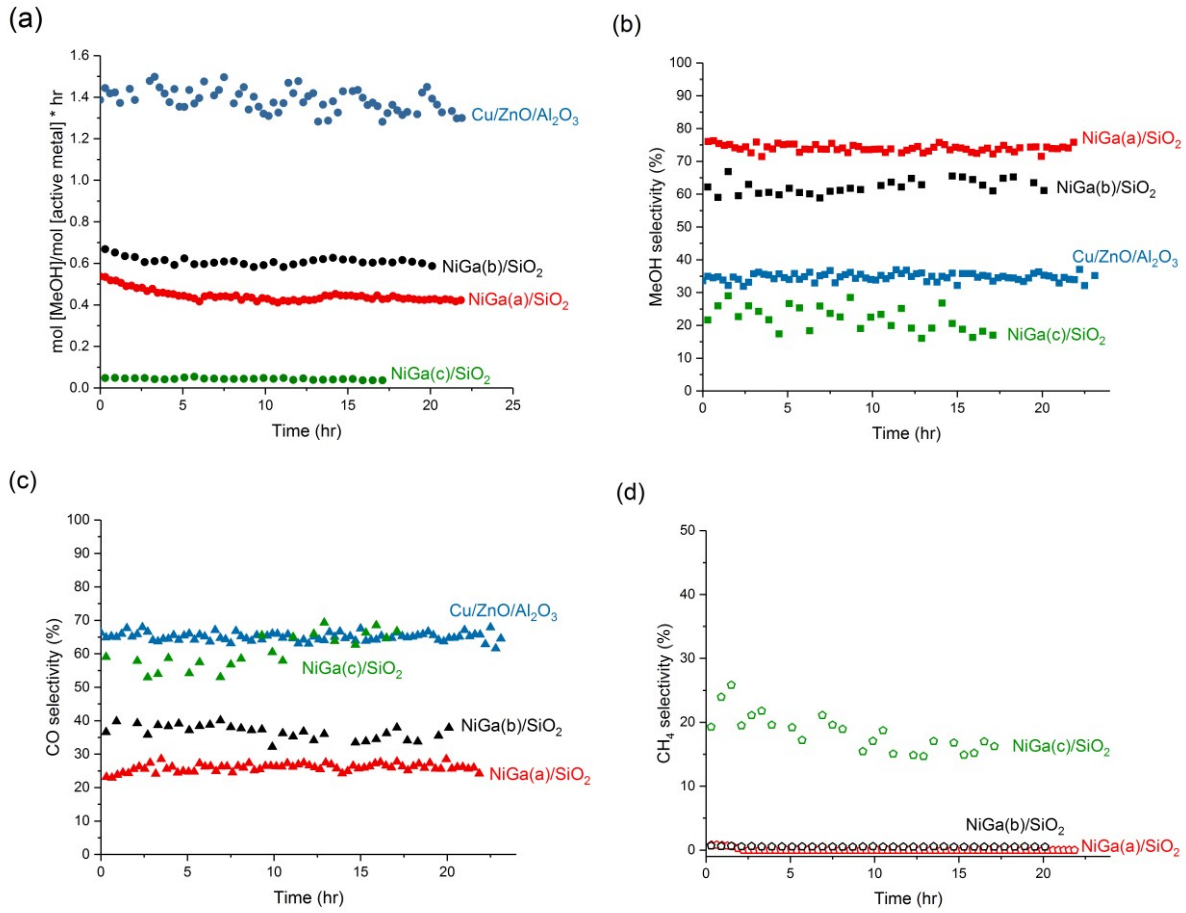


Figure 4.11, Catalytic performance of Ni-Ga/SiO_2 catalysts compared to Cu/ZnO/Al_2O_3 at 245 °C, 10 bar

(a) MeOH production rate (b) MeOH selectivity (c) CO selectivity (d) CH_4 selectivity

Table 4.6, Steady state catalytic performance of Ni-Ga/SiO_2 catalysts compared to Cu/ZnO/Al_2O_3 at 245 °C, 10 bar

Catalyst	**Steady state conversion (%)**	**Steady state MeOH production rate**		**Product distribution (%)**		
		mol [MeOH]/mol [active metal]*hr	mol [MeOH]/g cat*hr × 10^{-3}	MeOH	CO	CH_4
NiGa(a)/SiO_2	0.50 ± 0.03	0.43 ± 0.02	1.04 ± 0.05	74 ± 1	26.0 ± 0.5	0
NiGa(b)/SiO_2	0.71 ± 0.04	0.61 ± 0.03	1.50 ± 0.08	63 ± 1	36.2 ± 0.8	0.50 ± 0.01

NiGa(c)/SiO_2	0.040 ± 0.002	0.042 ± 0.002	0.104 ± 0.005	17.0 ± 0.3	67 ± 1	16.2 ± 0.3
Cu/ZnO/Al_2O_3	1.65 ± 0.08	1.35 ± 0.07	8.5 ± 0.4	34.8 ± 0.6	65 ± 1	trace

Activity and stability of Ni-Ga based catalysts compared to Cu/ZnO/Al_2O_3

The maximum MeOH conversion achieved by NiGa(a)/SiO_2 was approximately 0.65% at 10 bar, which is equivalent to an hourly methanol production rate of 0.53 mol per mole of active metal (Ni+Ga). About 20% of the initial activity dropped gradually in the first 10 hours on stream, but eventually reached a steady value of 0.43 mol MeOH/mol [Ni+Ga]*hr. As expected from the charactersation, NiGa(b)/SiO_2 showed a higher activity since it has the structure that is closest to the most active Ni_5Ga_3 phase [12].

The activity of the Cu catalyst is higher comparing to the Ni-Ga based catalysts. This conversion is closer to the thermodynamic equilibrium (1.9% at 245 °C) since the Cu based catalyst is more active. The level of deactivation was found to be similar to that of NiGa(b)/SiO_2 catalyst (8% drop in activity) during the 20-hour period. In contrast with Ni-Ga based catalyst, the deactivation of copper based catalyst took place throughout the run without significant initial deactivation. This suggests that the deactivation mechanisms in the Ni-Ga based catalysts and the commercial Cu based catalyst are different. The deactivation of Cu based methanol synthesis catalyst has been widely studied and the main reasons relevant to this study include accelerated sintering in the presence of water and coke formation, both of which could lead to the gradual loss of activity observed. On the other hand, the deactivation of Ni-Ga based catalysts is mostly rapid initial deactivation. This could indicate that the deactivation is associated with the buildup of products, possible surface composition changes and formation of surface carbon that quickly reduce the number of active sites available [127, 133].

As expected, NiGa(c)/SiO_2 is not an active methanol catalyst, in contrast to NiGa(a)/SiO_2 and NiGa(b)/SiO_2 (Table 4.6). The majority products are methane and CO. This result is in

agreement with the available literature, where Ni_3Ga based catalyst was thought to behave like metallic nickel due to the intermetallic phase being rich in nickel. Due to its poor performance, this catalyst was not investigated further.

Selectivity of Ni-Ga based catalysts

Main products over NiGa(a)/SiO_2 catalyst include methanol (74%), CO (26%) and trace level of methane and DME. No other hydrocarbons were detected. Initially, DME and CH_4 were produced with a selectivity of 0.8% (each), but after a few hours their production gradually decreased to zero. This is accompanied by an increase in methanol selectivity. This change in methane selectivity agrees with literature, which suggested that the nickel-rich sites on the Ni-Ga based catalysts facilitate the methanation reaction, but they are easily poisoned by adsorbed CO [12]. Low level of DME suggests that some gallium oxide was present on the catalyst, which is known to have methanol dehydration activity due to its moderate acidity [175, 256].

It appears that NiGa(b)/SiO_2 is slightly less selective to MeOH at this pressure and has higher CO production. As this catalyst contains less Ni, it might be expected to be more selective towards methanol. Hence, there is no clear link between the selectivity observed and the catalyst structure as determined by XRD. Again, it might be resolved by an in situ XRD study. For both NiGa(a)/SiO_2 and NiGa(b)/SiO_2 catalysts, the selectivity after the initial period remained stable in the time frame of this particular experiment, implying that the catalyst structure was maintained (no deactivation by de-alloying) at this low level of conversion. The considerable drop in activity is not accompanied by a significant change in selectivity, implying that the deactivation observed in the Ni-Ga based catalysts should be due to a decrease in the number of active sites available to the reactants (as speculated earlier), rather than a change of active phase itself [133].

Although the commercial Cu based catalyst has higher activity, it is not as selective to MeOH as the Ni-Ga based catalysts, Table 4.6, due to its tendency to catalyse the reverse water gas shift (rWGS) reaction under CO free condition at lower pressures [257, 258].

Effect of catalyst mass

Due to the very low conversion achieved by the Ni-Ga based catalysts, the mass of catalyst was increased in the attempt to increase the conversion. Previously, 0.3 gram of catalyst was used (GHSV: 6640 h^{-1}). Hence for this investigation, 0.6 gram of NiGa(a)/SiO_2 (GHSV: 3320 h^{-1}) was used. Table 4.7 shows the conversion obtained for different catalyst masses, the reaction conditions were kept same. Since the conversion obtained with 0.3 g catalyst is much lower than the thermodynamic equilibrium, it was expected that doubling the mass would increase the conversion. However, the conversion achieved by 0.6 g catalyst is only slightly higher compared to that achieved by just half the catalyst. This could be due to instantaneous deactivation of the catalyst (even before the first activity measurement was taken) by the products as their concentration was higher (e.g. CO concentration was 50% higher) when using 0.6 g catalyst. Comparing the activity after 2 hours on stream, it can be seen that activity of 0.6 g catalyst deteriorated more quickly. This indicates that the catalyst strongly deactivates in the presence of products, therefore increasing the amount of catalyst further does not lead to a significant increase of activity. This catalyst works better at low conversion levels. Therefore, for all subsequent catalyst test, the mass of Ni-Ga based catalysts was kept at 0.3 g. Another attempt to increase the conversion with lower GHSV (1280 h^{-1}) was carried out in the tubular flow reactor, where a similar conclusion was reached. The results are included in Appendix B Figure B.8 and B.9.

Table 4.7, Catalytic performance obtained with different catalyst mass

Catalyst mass (g)	**0.3**	**0.6**
Initial MeOH rate (mol [MeOH]/mol [Ni+Ga]*hr)	0.55 ± 0.03	0.71 ± 0.04

MeOH rate (mol [MeOH]/mol [Ni+Ga]*hr) after 2 hours	0.50 ± 0.03	0.55 ± 0.03
Selectivity to MeOH (%)	74 ± 1	66 ± 1

4.2.3.3 Performance of Ni-Ga based catalysts at 30 bar (CSTR)

Following the preliminary investigation at 10 bar, a study was conducted at the higher pressure of 30 bar, which is closer to a typical industrial methanol process. Since NiGa(c)/SiO_2 was not active for methanol synthesis, only NiGa(a)/SiO_2 and NiGa(b)/SiO_2 catalysts were studied at higher pressure and compared to the commercial Cu based catalyst. The results were plotted in Figure 4.12.

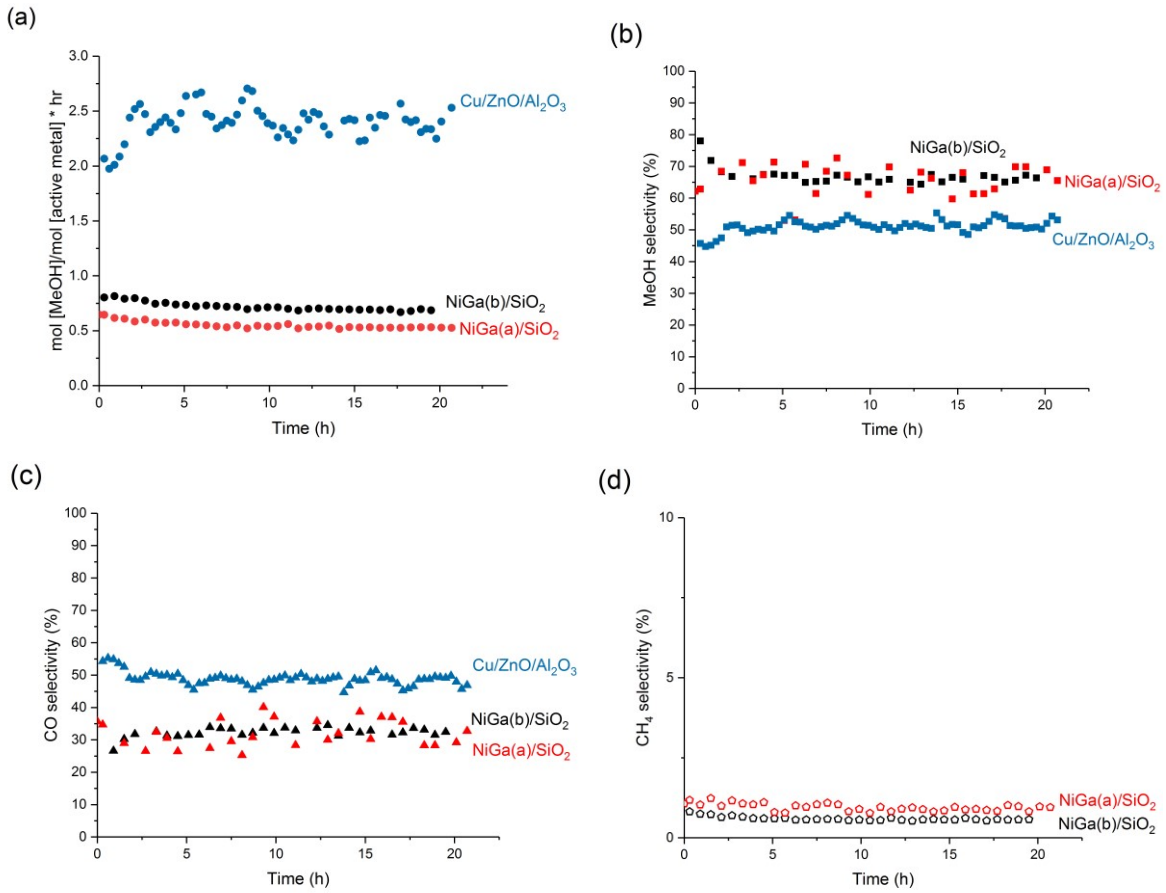


Figure 4.12, Catalytic performance of Ni-Ga/SiO_2 catalysts compared to Cu/ZnO/Al_2O_3 at 245 °C, 30 bar

(a) MeOH production rate (b) MeOH selectivity (c) CO selectivity (d) CH_4 selectivity

Table 4.8, Steady state catalytic performance of Ni-Ga/SiO_2 catalysts compared to Cu/ZnO/Al_2O_3 at 245 °C, 30 bar

Catalyst	Steady state conversion (%)	Steady state MeOH production rate		% increase from 10 bar	Product distribution (%)		
		mol [MeOH]/mol [active metal]*hr	mol [MeOH]/g cat*hr × 10^{-3}		MeOH	CO	CH_4
NiGa(a)/SiO_2	0.64 ± 0.03	0.54 ± 0.03	1.08 ± 0.05	22 ± 2	68 ± 1	30.8 ± 0.6	0.89 ± 0.01
NiGa(b)/SiO_2	0.81 ± 0.04	0.72 ± 0.04	1.76 ± 0.09	22 ± 3	67 ± 1	32 ± 0.7	0.57 ± 0.01
Cu/ZnO/Al_2O_3	3.0 ± 0.2	2.5 ± 0.1	15.5 ± 0.8	80 ± 10	52.0 ± 0.9	48 ± 1	trace

For both NiGa(a)/SiO_2 and NiGa(b)/SiO_2 catalysts, increasing the pressure to 30 bar only increased the activity by 22%. This is expected since it was shown previously that increasing catalyst mass only brought a small increase in activity due to the deleterious effect of the products.

Methanol synthesis reaction produces less number of moles of products than reactants, higher pressure shifts the reaction towards the side with lower number of moles according to the Le Chatellier's principle. Hence, methanol synthesis is favoured at higher pressures. Only the NiGa(b)/SiO_2 catalyst improved selectivity to MeOH at higher pressure (see Figure 4.12). In fact the two Ni-Ga catalysts gave very similar selectivity at 30 bar, which might suggest surface compositions adjust to the gas mixture.

In the case of the Cu based catalyst, significantly higher MeOH synthesis activity (2.5 mol MeOH/mol [Ni+Ga]*hr) and MeOH selectivity were obtained at 30 bar, although selectivity is still lower than the Ni-Ga based catalysts.

Effect of pressure on the deactivation behaviour of Ni-Ga catalysts

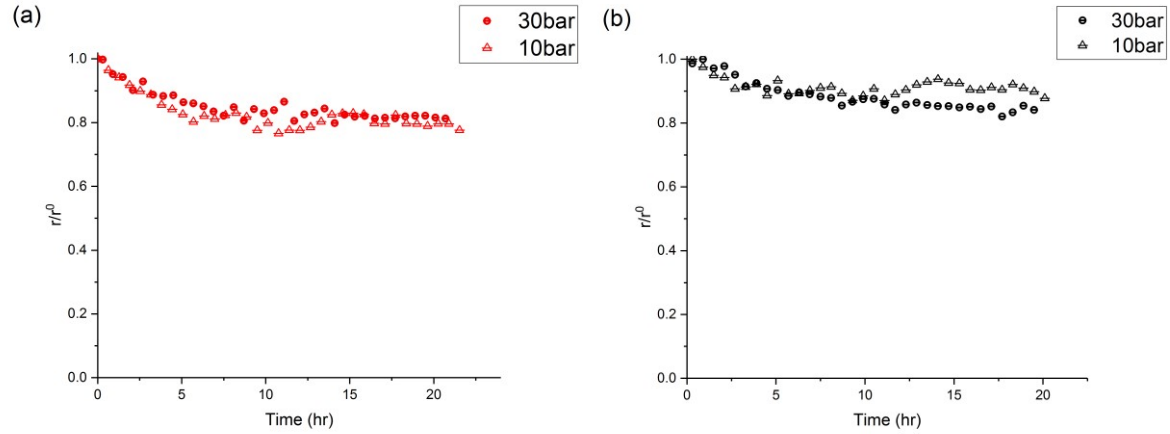


Figure 4.13, Normalised MeOH activity as a function of time at 10 bar and 30 bar (a) NiGa(a)/SiO_2 (b) NiGa(b)/SiO_2

Initial deactivation was observed again at this pressure for both Ni-Ga based catalysts. For both catalysts, the rate of deactivation (20% in 10 hours) was similar to that obtained at 10 bar.

Catalyst regeneration

In the Ni-Ga work by Studt et al. [12], it was shown that the catalytic performance of Ni-Ga catalysts at atmospheric pressure can be completely recovered by reduction at 350 °C for 2 hours. To study the reversibility of the catalyst deactivation observed at elevated pressure, in situ regeneration was carried out after the reaction at 30 bar. Subsequently, the regenerated catalyst was subjected to catalysis under the same conditions (245 °C, 30 bar). NiGa(a)/SiO_2 was chosen for this study as it showed more deactivation at both pressures studied earlier. The results are presented in Figure 4.14.

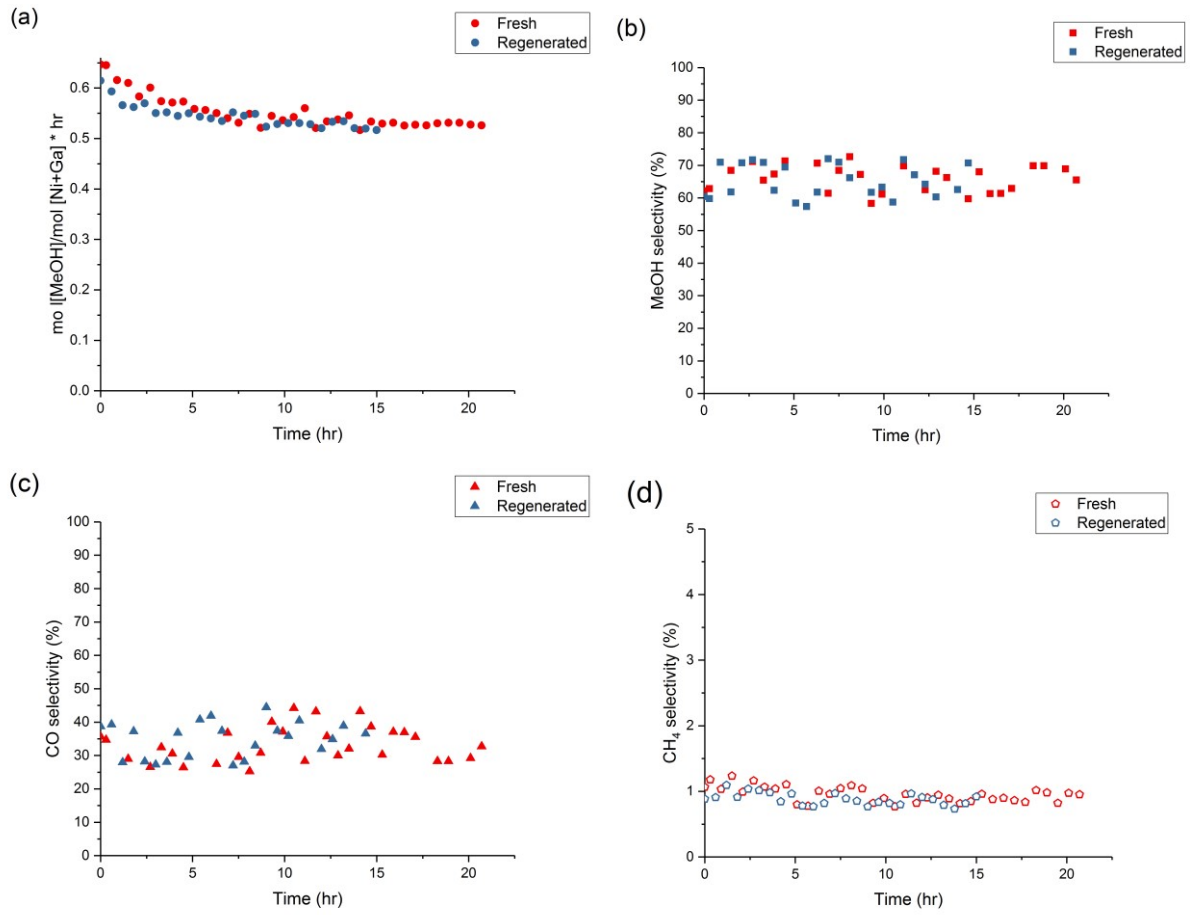


Figure 4.14, Catalytic performance of the fresh and regenerated NiGa(a)/SiO_2 catalyst at 245 °C, 30 bar

(a) MeOH production rate (b) MeOH selectivity (c) CO selectivity (d) CH_4 selectivity

Clearly, the regenerated catalyst achieved a similar methanol production rate as the fresh catalyst. Again, same extent of initial deactivation was observed in the regenerated catalyst. Moreover, the selectivity of the regenerated catalyst is unchanged compared to the fresh catalyst. These observations suggest that the deactivation in a 20-hour run at 30 bar is reversible and the catalyst does not suffer permanent structural change during reaction. For intermetallic compound based catalysts such as Pd-Ga catalysts, products such as CO and water have been reported to cause instability of the intermetallic phase and coking was also found to cause certain extent of catalyst deactivation [12, 127, 133]. Because of the low conversion, coking is less likely to be the main cause of deactivation observed (although it cannot be entirely disregarded). Therefore, the initial drop of activity in the Ni-Ga catalysts is likely due to the adsorption of products such as CO on the catalytic sites, reducing the amount

of active sites for methanol synthesis until a saturation surface equilibrium is reached [133]. Within the timeframe (20 hours) studied so far, such impact of products (and coke deposition) is fully reversible by reducing the catalyst at 350 °C for 2 hours.

4.2.3.4 Characterisation of spent catalysts from CO_2/H_2 runs

To elucidate the causes of deactivation for the catalysts from CO_2/H_2 runs, the spent catalysts were characterised by XRD, nitrogen physisorption, XPS and temperature-programmed oxidation. The spent catalysts from 30 bar runs were used as their extents of deactivation would be greater.

XRD of spent catalysts

The XRD patterns for both spent Ni-Ga catalysts are shown in Figure 4.15. XRD for $Cu/ZnO/Al_2O_3$ can be found in Appendix B Figure B.10.

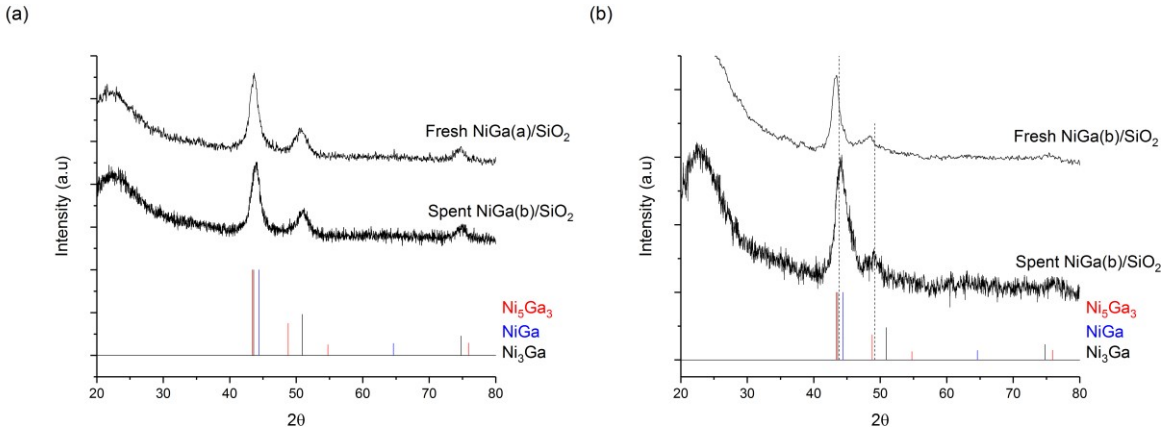


Figure 4.15, XRD of fresh (reduced-passivated) and spent catalysts (a) $NiGa(a)/SiO_2$ (b) $NiGa(b)/SiO_2$ (reference peaks: Studt et al. [12])

For all catalysts, there are no significant change in the position of diffraction peaks and no additional peak. This could suggest that the crystalline structures remained the same during the reaction, which is in agreement with the speculation regarding constant selectivity. Therefore, the initial deactivation observed in both Ni-Ga catalysts was more likely the result of reduced accessibility of active sites, not structural change of such sites.

The crystallite size of fresh (reduced-passivated) and spent catalysts for all catalysts were calculated from the XRD using the Scherrer equation and the results are summarised in Table 4.9 below.

Table 4.9, Crystallite size of spent catalysts

Catalyst	Crystallite size of spent catalyst (nm)	% increase in size
NiGa(a)/SiO_2	5.6 ± 0.6	0
NiGa(b)/SiO_2	5.6 ± 0.6	0
Cu/ZnO/Al_2O_3	8.4 ± 0.8	30

Both Ni-Ga based catalysts did not show any particle growth after the reaction, indicating higher stability against sintering. Sharafutdinov and co-workers [14] revealed that gallium in the Ni-Ga intermetallic phase reduced sintering. The high sintering resistance was speculated to be a consequence of high melting point (also the Tamman temperature) of the intermetallic compounds due to strong covalent metal-metal bond [11].

In contrast, the particle size of Cu based catalyst increased significantly. Increase in particle size leads to a decrease in surface area and hence a decrease in the number of active sites. Under CO-free conditions, rWGS activity over Cu based catalyst is significant. High water partial pressure is known to cause deactivation of the Cu catalyst due to particle growth via thermal sintering [8]. Therefore, particle size growth is the main cause of deactivation for the commercial Cu based catalyst, but it was not the cause of deactivation for the Ni-Ga catalysts.

BET surface area and porosity

Table 4.10, BET surface area and pore volume of spent Ni-Ga catalysts

Catalyst	BET surface area (± 1 m^2/g)		BJH pore volume (cm^3/g)		BJH pore size (nm)	
	Fresh	Spent	Fresh	Spent	Fresh	Spent
NiGa(a)/SiO_2	250	239	1.41	1.03	16.8	14.5
NiGa(b)/SiO_2	244	238	1.22	1.32	15.9	16.5

After the reaction, the BET surface area of both catalysts showed similar amount of reduction. The changes in porosity are negligible, suggesting that no blockage of pores took place.

Coke deposition measured by TPO

Table 4.11, Coke content of spent catalysts

Catalyst	Coke content (µmol/g active metal)	CO_2 evolution temperature (°C)
NiGa(a)/SiO_2	6.41 ± 0.06	365 and 590
NiGa(b)/SiO_2	7.03 ± 0.07	300 and 500
Cu/ZnO/Al_2O_3	77.4 ± 0.8	410

The amount of coke deposition on the spent catalyst was determined by temperature-programmed oxidation (TPO). The change in CO_2 concentration during TPO measured by the mass spectrometry are shown in Figure 4.16.

As can be clearly seen from the CO_2 evolution temperature, different types of carbonaceous compounds were present on both Ni-Ga catalysts. The peak below 300 °C observed in the Ni-Ga catalysts is attributed to the desorption of CO_2, as confirmed by the TPO of a control sample that was exposed to the reaction gas mixture without catalysis (details in Appendix B

Figure B.11). Therefore only the peaks above 300 °C are considered as coke oxidation. Even though different types of coke were found, the amount of coke in both catalysts are very low. The CO_2 evolved from the spent Ni-Ga catalyst is equivalent to approximately 0.7% catalyst surface area being poisoned by coke, which is significantly lower than the amount of coke poisoning reported in the literature (10%) for Ni-Ga catalysts used under atmospheric pressure [12]. This was due to the low conversion and high selectivity towards methanol at elevated pressures. Therefore it is unlikely that coke was the main cause of deactivation observed over NiGa(a)/SiO_2 and NiGa(b)/SiO_2.

On the other hand, coke deposition on Cu based catalyst is significantly higher since the catalyst is more active. Moreover, the Boudouard reaction in the presence of CO can also lead to loss of activity by coke deposition [8]. Therefore besides significant particle agglomeration, the buildup of carbonaceous species on the catalyst is also a reason for the gradual deactivation of the Cu catalyst.

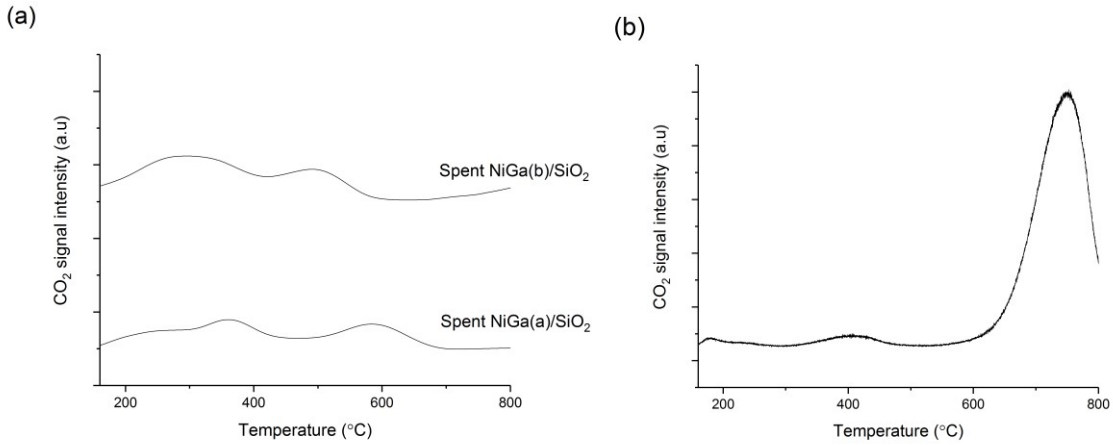


Figure 4.16, TPO profiles for spent catalysts
(a) NiGa(b)/SiO_2 and NiGa(a)/SiO_2 (b) Cu/ZnO/Al_2O_3

For Cu based catalyst, the huge peak observed above 600 °C is due to the oxidation of the graphite in the catalyst, hence it was not included in the calculation as well as the interpretation of coke type. Only one CO_2 evolution peak corresponding to oxidation of coke was found over the Cu/ZnO/Al_2O_3 catalyst, which is at 410 °C. This suggests that heavier type of coke is more likely to form on the Ni-Ga catalysts (even though only in small quantity).

XPS of spent Ni-Ga catalysts

No significant change in the state of Ni and Ga was observed for both spent Ni-Ga catalysts. Metallic Ni peaks became more pronounced after catalysis, which could be due to the fact that the catalysts have been subjected to re-activation, long reaction time as well as some segregation of Ga.

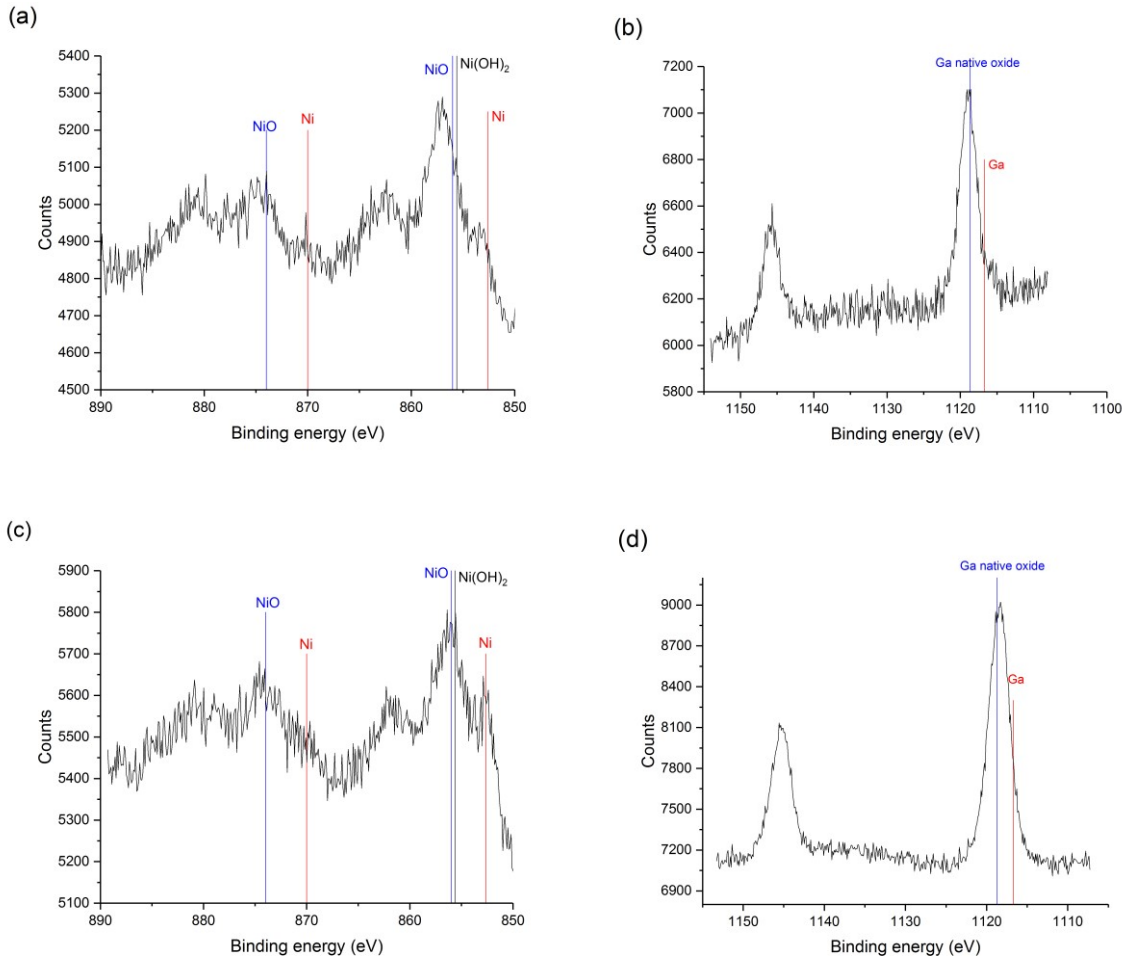


Figure 4.17, XPS spectra of spent Ni-Ga catalysts
(a) Ni 2p of NiGa(a)/SiO_2 (b) Ga 2p of NiGa(a)/SiO_2 (c) Ni 2p of 2p of NiGa(b)/SiO_2 (d) Ga 2p of 2p of NiGa(b)/SiO_2

Table 4.12, Surface composition calculated from XPS data

Catalyst	Ni:Ga ratio	
	Fresh	Spent
NiGa(a)/SiO_2	1.09	1.18
NiGa(b)/SiO_2	0.67	0.50

A reduction in Ni:Ga ratio was observed in the case of NiGa(b)/SiO_2 catalyst. This indicates that more Ga has migrated to the surface during the reaction, possibly in a de-alloyed form due to gallium segregation.

4.2.4 Effect of CO in the feed gas

4.2.4.1 Catalytic performance of Ni-Ga catalysts under $CO/CO_2/H_2$

For intermetallic compounds such as Pd-Ga based catalysts, their instability in CO-rich environment has been reported [133, 154-156]. To investigate the effect of CO on the NiGa(a)/SiO_2 and NiGa(b)/SiO_2 catalysts, a $CO/CO_2/H_2$ feed was used to measure the catalytic performance. In a preliminary study, the reaction pressure was kept at 10 bar. The CO composition of the feed was chosen to be 4%, which is significantly higher than the highest CO concentration ever measured in the reactor (0.1% at 30 bar) in earlier CO_2/H_2 runs above. The carbon oxides to hydrogen ratio was kept constant. Due to the high CO concentration in the feed, it was very difficult to quantify the change in CO concentration in the GC, therefore the catalyst selectivity in the experiments with CO-containing feed is shown as a ratio between methanol and methane.

NiGa(a)/SiO_2 catalyst under the effect of CO

The catalytic performance of NiGa(a)/SiO_2 in $CO/CO_2/H_2$ is shown in Figure 4.18.

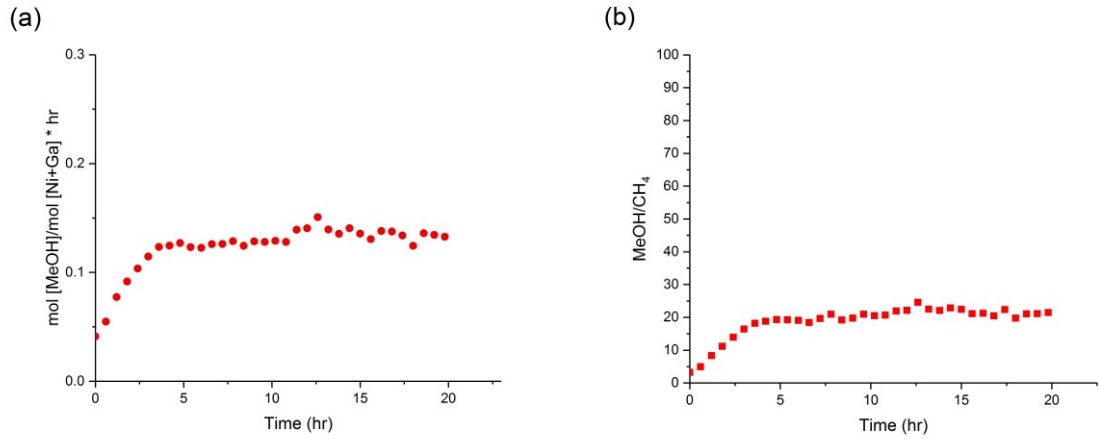


Figure 4.18, Catalytic performance of NiGa(a)/SiO_2 at 245 °C, 10 bar under CO/CO_2/H_2 (a) MeOH production rate (b) MeOH/CH_4 ratio

Table 4.13, Effect of CO on the catalytic performance of NiGa(a)/SiO_2

Feed	Steady state MeOH rate (mol [MeOH]/mol [Ni+Ga]*hr)	MeOH/CH_4 ratio
CO_2/H_2	0.43 ± 0.02	100 ± 4
CO/CO_2/H_2	0.26 ± 0.01	21.6 ± 0.7

When carbon monoxide is present in the feed, the methanol synthesis activity was very low in the beginning because the catalyst was producing large amount of methane. This suggests that when the catalyst was first exposed to high level of CO, an instant change (at least partially) of the catalytic surface occurred. In Pd_2Ga based catalysts, exposure to CO has been shown to cause the breakup of the intermetallic compound into surface regions rich in Ga-depleted metallic Pd species [133, 155]. It is very likely that the Ni-Ga intermetallic surface responded to CO in similar way since high methane production suggests that the catalyst surface becomes so Ni-rich that it behaves like metallic Ni, which is widely known as a good methanation catalyst [252-254]. Because of the poisoning effect of CO on the Ni-rich sites as suggested by Studt et al. [12], the methane production eventually dropped to similar level obtained under CO free condition.

After the Ni-rich sites became poisoned, the methanol conversion gradually increased to 0.35% (0.26 mol MeOH/mol [Ni+Ga]*hr) and the activity remained stable after 5 hours on stream. Compared to the reaction without CO, the stabilised activity in the presence of CO was much lower (30% of the steady state activity obtained under CO free condition).

To determine if the strong poisoning effect of CO is reversible, in situ regeneration was carried out after the reaction under $CO/CO_2/H_2$ and reaction was carried out with CO_2/H_2 at 10 bar. The comparison with the performance of a fresh catalyst is shown in Figure 4.19.

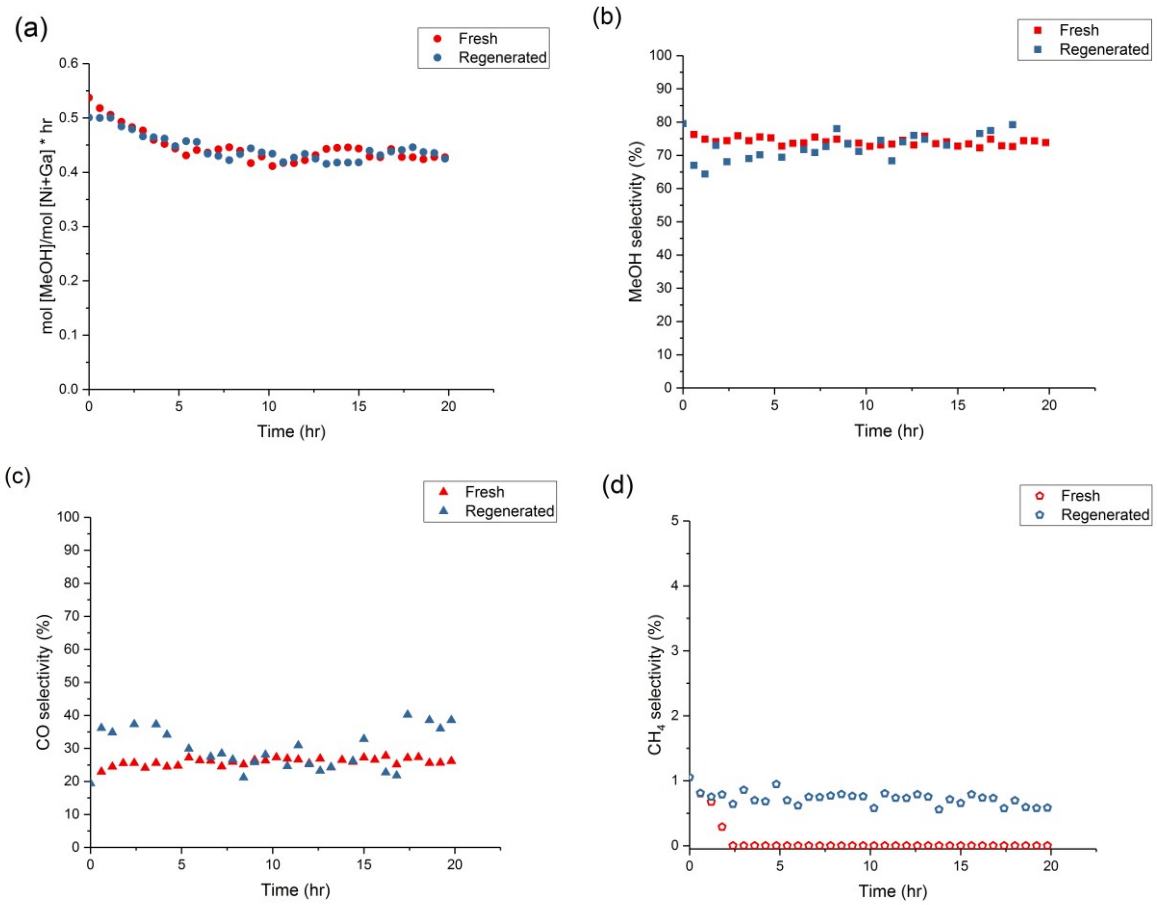


Figure 4.19, Catalytic performance of NiGa(a)/SiO_2 regenerated after $CO/CO_2/H_2$ run and fresh NiGa(a)/SiO_2 (reaction conditions: 245 °C, 10 bar, CO_2/H_2)
(a) MeOH production rate (b) MeOH selectivity (c) CO selectivity (d) CH_4 selectivity

It can be seen that both the selectivity and activity were completely restored. The small difference in CH_4 selectivity (< 1%) may be due to slight variation in the catalysts used (CH_4 production was found to vary between 0 – 1% between different batches). This implies that

the poisoning effect of CO on the catalyst is reversible in the timeframe studied, i.e. the surface composition can be restored to the original state by reducing the catalyst in dilute hydrogen.

NiGa(b)/SiO_2 catalyst under the effect of CO

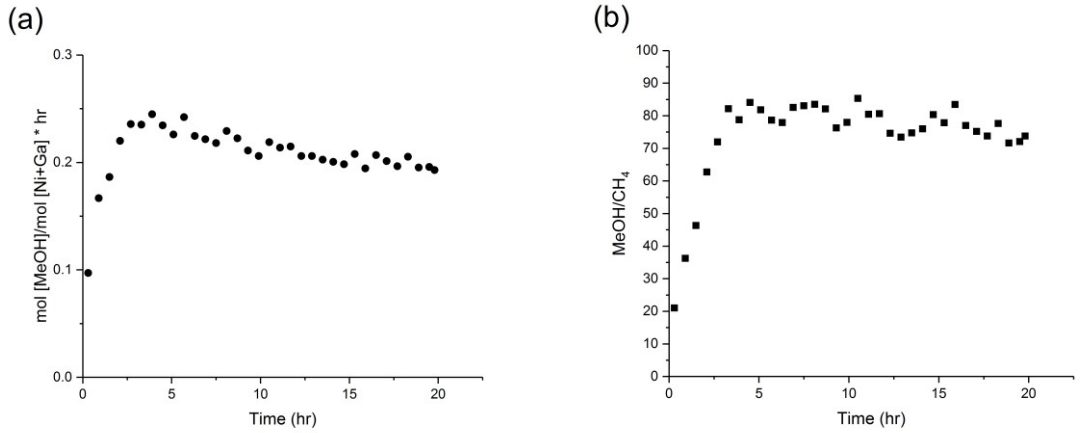


Figure 4.20, Catalytic performance of NiGa(b)/SiO_2 at 245 °C, 10 bar under $CO/CO_2/H_2$ (a) MeOH production rate (b) MeOH/CH_4 ratio

Table 4.14, Effect of CO on the catalytic performance of NiGa(b)/SiO_2

Feed gas	Steady state MeOH rate (mol [MeOH]/mol [Ni+Ga]*hr)	MeOH/CH_4 ratio
CO_2/H_2	0.61 ± 0.03	124 ± 5
$CO/CO_2/H_2$	0.20 ± 0.01	73 ± 3

Over NiGa(b)/SiO_2 catalyst, a similar trend in catalytic performance was obtained, that is, the activity was very low in the beginning but gradually increased. For NiGa(b)/SiO_2 catalyst, the methanol synthesis activity was always higher compared to NiGa(a)/SiO_2 and the methanol selectivity is significantly. But its activity did not become stable after it reached a maximum value, instead it gradually declined throughout the rest of the run. The activity at the end of the 20 hours is about 30% of the stabilised activity obtained under CO free condition. Similarly, the MeOH selectivity increased to a maximum value in 5 hours but gradually decreased afterwards due to declining methanol production. This suggests that in addition to the initial reconstruction of catalytic surface to Ni-rich regions, continuous partial decomposition of the

Ni_5Ga_3 intermetallic compounds into Ni-rich intermetallic phase and re-oxidised gallium could be the reason for the continuous deactivation of the catalyst. Because NiGa(b)/SiO_2 contains more Ga, it is more likely to suffer intermetallic phase decomposition due to the high oxophilicity of gallium [155].

The catalyst was subjected to the same regeneration process and another run with CO_2/H_2 at 10 bar was carried out to find out if the effect of CO is reversible in this case. Clearly, the regenerated NiGa(b)/SiO_2 catalyst has a lower activity compared to a fresh catalyst. In other words, the catalyst only recovered about 90% of the initial activity after it has been run under CO for 20 hours and then regenerated, and the activity continued to decrease by another 22% in 16 hours. It appears that the high CO level caused irreversible deactivation in NiGa(b)/SiO_2. The MeOH selectivity after the regeneration is similar to the selectivity over a fresh catalyst.

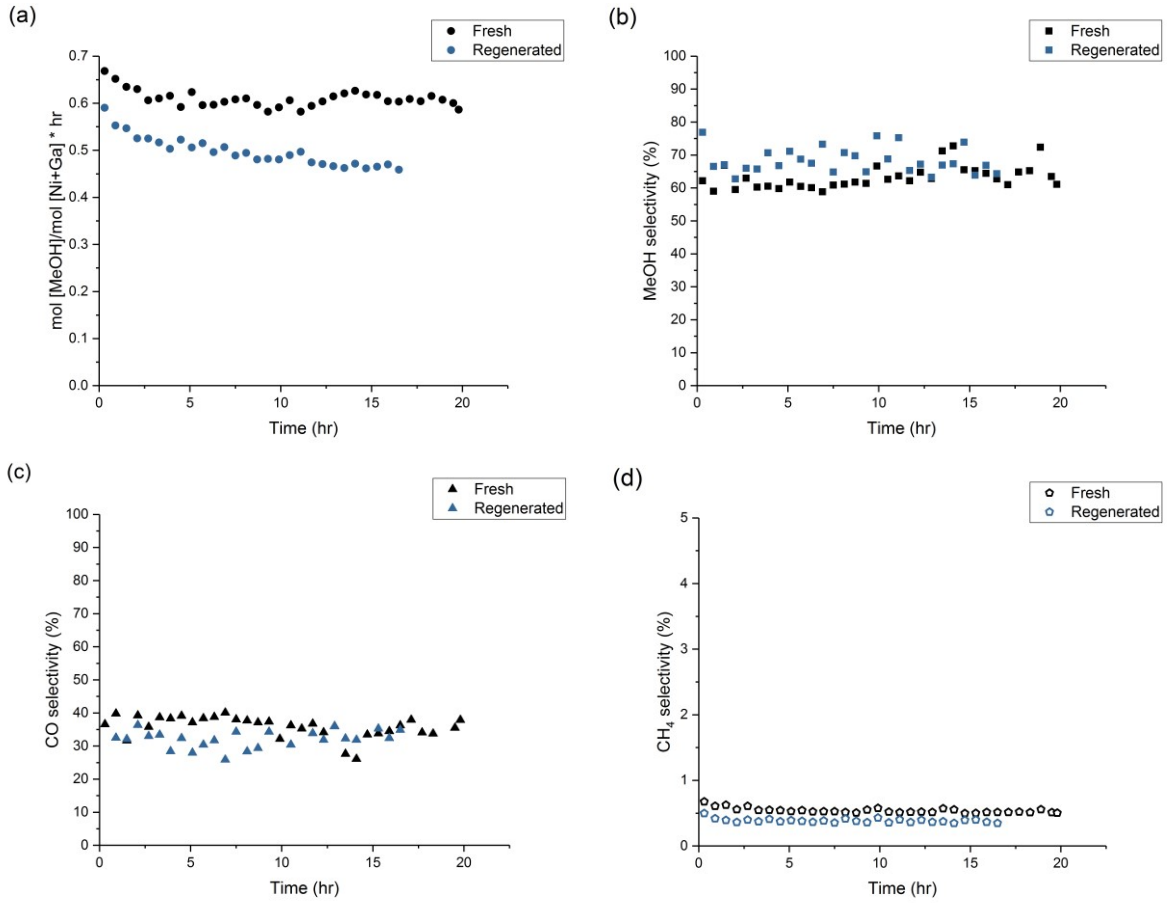


Figure 4.21, Catalytic performance of NiGa(b)/SiO_2 regenerated after CO/CO_2/H_2 run and fresh NiGa(b)/SiO_2 (reaction conditions: 245 °C, 10 bar, CO_2/H_2)
(a) MeOH production rate (b) MeOH selectivity (c) CO selectivity (d) CH_4 selectivity

Comparison between regenerated NiGa(a)/SiO_2 and NiGa(b)/SiO_2

The change in catalyst activity and the irreversibility of the deactivation suggest that the NiGa(b)/SiO_2 catalyst underwent a structural change during the reaction under high CO concentration, that even the regeneration procedure was unable to fully reverse the change.

If the activity of the regenerated NiGa(b)/SiO_2 and NiGa(a)/SiO_2 catalysts are plotted on the same graph (Figure 4.22), it can be observed that both regenerated catalysts have similar performance in terms of activity and selectivity, implying similar surface structure.

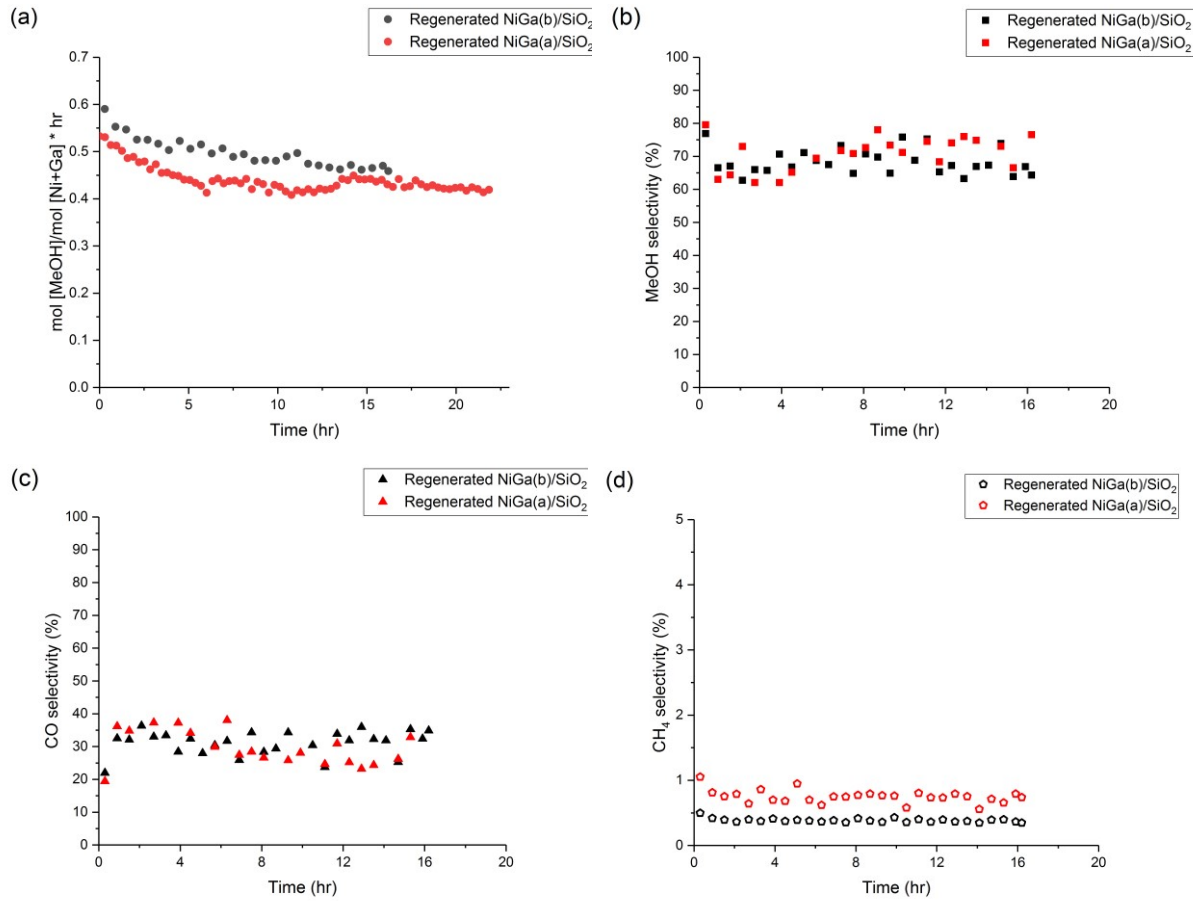


Figure 4.22, Catalytic performance of the regenerated NiGa(b)/SiO_2 (after reaction under CO) and NiGa(a)/SiO_2 at 245 °C, 10 bar under CO_2/H_2
(a) MeOH production rate (b) MeOH selectivity (c) CO selectivity (d) CH_4 selectivity

The result points to the possibility that the effect of CO causes some of the active phase (Ni_5Ga_3 as found in XRD) in NiGa(b)/SiO_2 catalyst to become closer to that of NiGa(a)/SiO_2 by the de-alloying of Ga from the intermetallic phase, as discussed previously. This phenomenon is not uncommon, especially in Ga-containing intermetallic compounds. Sharafutdinov et al.

[13] also reported that a certain amount of gallium was released from the Ni_5Ga_3 intermetallic phase as soon as the temperature reached 200 °C under oxidative environments such as CO_2/H_2. This loss of gallium is accelerated in the presence of water from rWGS activity and CO dissociation, leading to the formation of a Ni-rich phase, for instance, Ni_3Ga. The de-alloying process proceeds according to the equation proposed by Sharafutdinov et al. [13].

$$3Ni_5Ga_3 \rightarrow 5Ni_3Ga + 4Ga$$

Given that the activity and selectivity of the regenerated NiGa(b)/SiO_2 catalyst approaches that of the NiGa(a)/SiO_2 catalyst, the Ni_5Ga_3 phase appears to be partially decomposed to an active phase similar to that present on the NiGa(a)/SiO_2 catalyst (Ni_xGa, 1.6 < x < 3) and not to a Ni_3Ga phase, which would be expected to behave as a methanation catalyst.

This de-alloying of the Ni-Ga intermetallic is also expected to be difficult to reverse as the formation of pure Ni_5Ga_3 phase from Ni_3Ga phase requires a reduction temperature of at least 700 °C [14]. Therefore the reduction at 350 °C was not able to convert the active phase back to the Ni_5Ga_3 composition, hence the irreversibility observed.

Since the detrimental effects of CO on the Ni-Ga catalysts are already significant at 10 bar, therefore the same experiments were not carried out at a higher pressure.

4.2.4.2 Characterisation of spent catalysts from CO/CO_2/H_2 runs

The diffraction patterns of the spent catalysts run under CO/CO_2/H_2 are presented in Figure 4.23.

Figure 4.23 (a) shows that no significant change of diffraction peaks has occurred on the NiGa(a)/SiO_2 catalyst after the reaction. Since the catalyst was found to regenerate fully, no permanent structural change was expected. The unexpected peak at 35.7° does not belong to Ni- or Ga-species or the SiO_2 support, suggesting it may come from contamination during catalyst handling.

The peaks in the spent NiGa(b)/SiO_2 catalyst are slightly shifted towards higher 2θ values. The characteristic Ni_5Ga_3 reflection at 48.8° becomes broader with a weak shoulder at 50.9° that corresponds to (110) reflection of Ni_3Ga phase. This suggests that the spent catalyst now contains a higher fraction of Ni_3Ga phase (or Ni-rich phase) comparing to the fresh catalyst. This result provides evidence to support the speculation above that the lower activity of the regenerated NiGa(b)/SiO_2 catalyst is due to the de-alloying of Ni_5Ga_3 phase to a more Ni-rich phase (Ni_xGa, $1.6 < x < 3$).

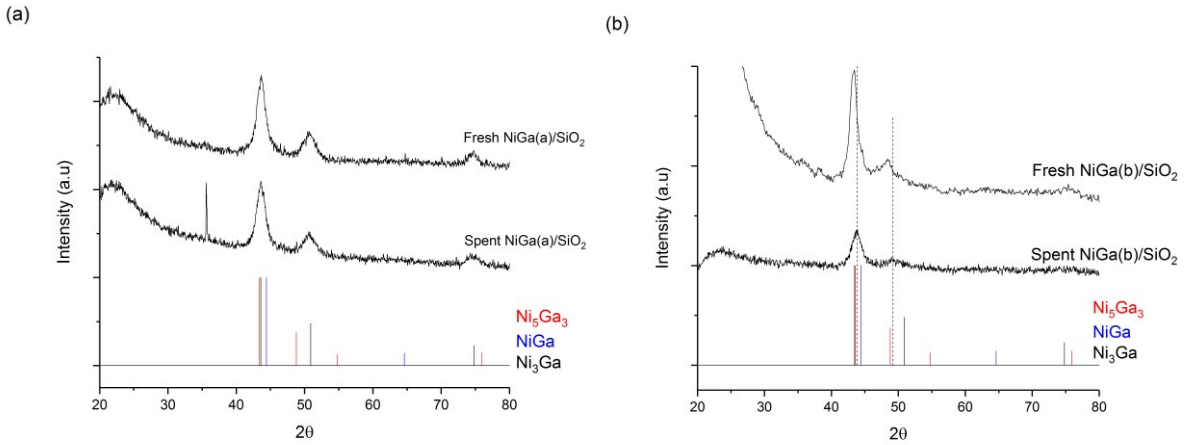


Figure 4.23, XRD of spent catalysts
(a) NiGa(a)/SiO_2 (b) NiGa(b)/SiO_2 (reference peaks: Studt et al. [12])

TPO was also carried out for the spent catalysts (after regeneration and CO_2/H_2 run). In Figure 4.24, a large CO_2 desorption peak was found over each spent catalyst, especially NiGa(b)/SiO_2. These were not included in the calculation for coke deposition. Both the coke oxidation temperature and amount of coke (slightly lower) are comparable to that obtained over the spent catalyst from CO_2/H_2 run. It appears that heavy type of coke observed in CO_2/H_2 reaction is reduced when feed contains high level of CO. This suggests that the extent of soft coke formation is independent of reaction conditions but heavy type of coke is suppressed after the catalyst has been exposed to a more reducing environment.

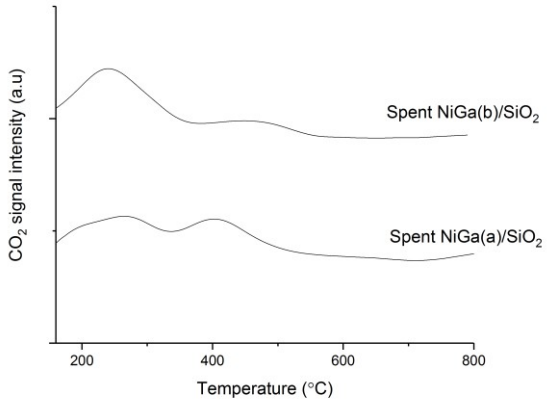


Figure 4.24, TPO profiles of spent catalysts from $CO/CO_2/H_2$ run

Table 4.15, Coke content on the spent catalysts from $CO/CO_2/H_2$ run

Catalyst	Coke content (µmol/g active metal)	CO_2 evolution temperature (°C)
NiGa(a)/SiO_2	4.74 ± 0.05	280 and 410
NiGa(b)/SiO_2	5.34 ± 0.05	240 and 460

4.3 Other support for the Ni-Ga based catalysts

4.3.1 NiGa(a) – LDH catalyst

4.3.1.1 Background

Recently, a CoGa based catalyst was reported to convert syngas to ethanol and higher alcohols efficiently [240]. By forming CoGa particles, Ga promotes the CO insertion and improves the chain growth probability. This was achieved by trapping the uniformly dispersed CoGa (molar ratio 5:3) particles on the ZnAl layered double oxide (LDHs). During the reduction, LDHs are transformed into LDOs and metal particles, which consist of Zn and Al oxides and CoGa particles respectively. It was shown that all four elements were distributed evenly in the highly ordered LDH layers and the performance of the catalyst greatly depends on the particle size and contiguous distribution of Co and Ga. It was found that the CoGa

particles trapped by the ZnAl-LDO prevented the aggregation of active particles, therefore this catalyst remained stable even after a long reaction time.

Although syngas conversion to ethanol and higher alcohols is not the focus of this work, the idea of the CoGa alloy is similar to the Ni-Ga based catalysts. Previously and also in the literature, it was demonstrated that Ni-Ga intermetallic compounds are active towards methanol synthesis but the intermetallic phase has a tendency to decompose under oxidative environment or under the influence of CO [13]. Owing to the unique structure of the LDHs, they are effective catalyst supports and precursors that accommodates well-dispersed and high-density active sites. It was postulated that if Co in the CoGaZnAl-LDHs was replaced with Ni, the Ni_5Ga_3 methanol synthesis catalyst might benefit additionally from the trapping effects of ZnAl-LDOs, thus improving its stability.

4.3.1.2 Catalyst characterisation

In the XRD pattern (Figure 4.25) for NiZnGaAl-LDH precursor, peak positions at 37.4°, 39.2°, 45.9° and 66.9° came from the reflections of the γ-Al_2O_3 support (ICSD no. 66559). Peaks at 2θ = 11.7°, 23.5° and 61.2° are observed, which correspond to (003), (006) and (113) reflections of hydrotalcite-like structure [240]. However the rest of the characteristic reflections at (009) 35.4° and (110) 60.3° were not detected, possibly masked by other peaks. The diffraction pattern clearly shows that a precursor with hydrotalcite-type of structure was successfully prepared.

After the reduction of the NiZnGaAl-LDH, residue was found around the outlet of the quartz tube. The residue is white, which suggest that it may be from the desublimation of Ga, Zn and/or Al during reduction where the temperature difference between the middle (700 °C) and outlet (< 200 °C, non-insulated sitting at room temperature) of reactor is big. The Ni:Ga ratio measured by ICP is 4.0, clearly indicating that Ga has been lost during the catalyst preparation process, either it is not incorporated into the LDH structure or it sublimated during high temperature reduction.

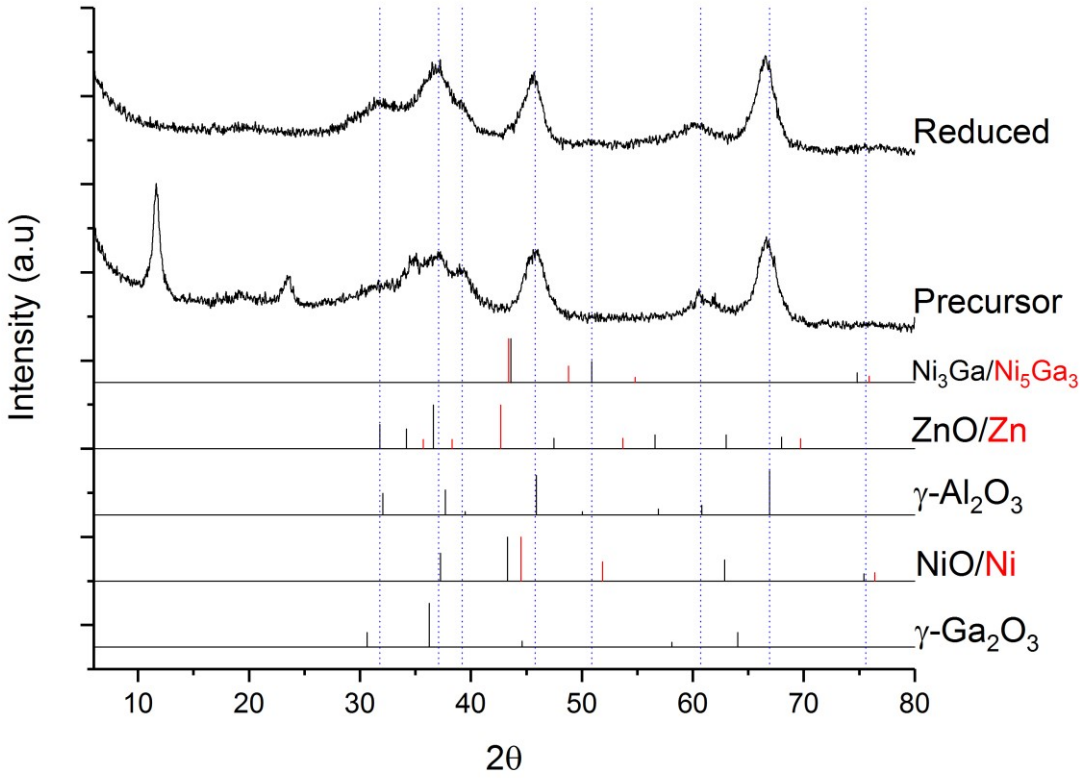


Figure 4.25, XRD of NiZnGaAl-LDH precursor and reduced-passivated catalysts (reference peaks: ICSD no. 98-009-1553, 57450, 66559, 011239, 52265 and 15208)

In the diffraction pattern of reduced catalyst, no Ni_5Ga_3 intermetallic phase is observed. It is expected since the Ni to Ga ratio is far from the nominal value of 5 to 3. Weak presence of Ni_3Ga phase was found at 50.9°. As reported by Sharafutdinov et al. [13], using metal oxide supports such as Al_2O_3 drastically reduces the methanol synthesis activity of Ni-Ga based catalyst due to incomplete alloying between Ni and Ga (if reduction time is kept constant at 2 hours) and poor dispersion. Moreover, as discussed previously in Chapter 3 section 3.2.1.1, the presence of other metals could also hinder the formation of Ni-Ga alloy. In the case of NiGaZnAl, Zn and Al are present that might have interacted with Ni and Ga, resulting in poor intermetallic phase formation.

The peaks of hydrotalcite-like structure at 2θ = 11.7° and 23.5° have disappeared after reduction. This could be due to the loss of Zn and Al due to high temperature sublimation,

causing the LDH structure to collapse. This phenomenon was not observed in the literature possibly because the reduction was performed in relatively stagnant reducing gas. Compared to the precursor, the reduced sample has more well defined peaks in the region 2θ = 30° – 40°. The new peak at 31.7° can be an indication of ZnO, both are likely to be present in the sample. ZnAl is likely to be present as suggested by Ning et al. [240]. However its characteristic peaks at 32.2° and 37.5° are difficult to differentiate from peaks of other species such as NiO, γ-Al_2O_3. The presence of Ga_2O_3, Ni or NiO is difficult to differentiate as some of their characteristic peaks overlap with that of other materials.

4.3.1.3 Catalyst performance under CO_2/H_2

Prior to catalysis, the catalyst was ex situ reduced, passivated and re-activated in situ, following the same procedures as the Ni-Ga/SiO_2 catalysts. A TPRx with CO_2/H_2 at atmospheric pressure was carried out.

Despite the hope that Ni-Ga based LDH would be active towards methanol synthesis, TPRx results revealed the opposite. At atmospheric pressure and 250 °C, no methanol was produced. CO was found to be the only product. This suggests that the catalyst functions as an rWGS catalyst at atmospheric pressure.

To evaluate the catalytic performance at elevated pressure, CO_2/H_2 reaction was conducted at 10 bar, 260 °C (temperature used by Ning et al. [240]).The results are presented in Figure 4.26 and Table 4.16 below.

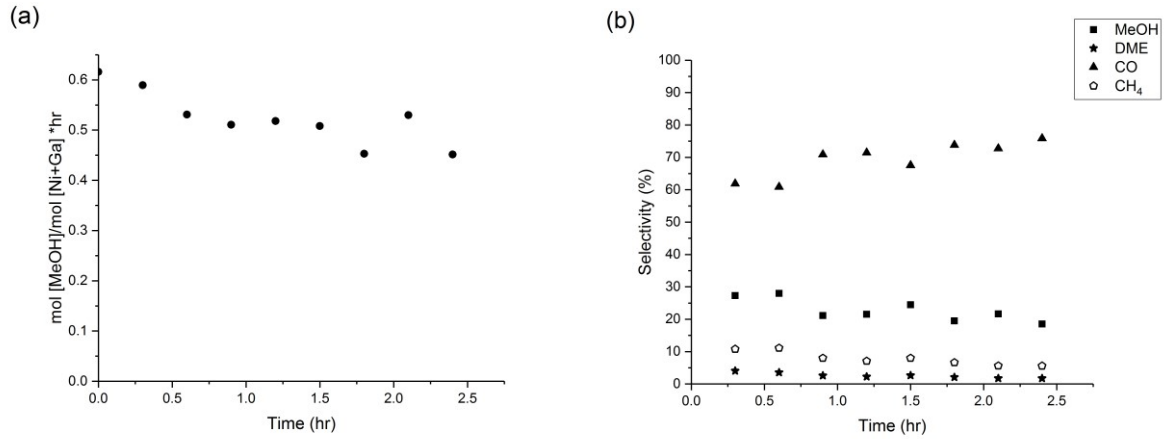


Figure 4.26, Catalytic performance of NiZnGaAl-LDH at 260 °C, 10 bar
(a) MeOH production rate (b) Product distribution

Table 4.16, Comparison of catalytic performance

Catalyst	Steady state conversion (%)	Steady state MeOH rate (mol [MeOH]/g cat*hr) × 10^{-3}	Product distribution (%)		
			MeOH	CO	CH_4
NiGa(b)/SiO_2	0.71 ± 0.04	1.50 ± 0.08	63 ± 1	36.2 ± 0.8	0.50 ± 0.01
NiZnGaAl-LDH	0.181 ± 0.009	0.30 ± 0.02	22.8 ± 0.4	69 ± 1	7.8 ± 0.1

Methanol production rate is 0.0003 mol/g cat * hr, which is much lower than the activity of NiGa(b)/SiO_2 catalyst under similar reaction conditions. This catalyst is clearly not promising for methanol synthesis, consistent with the absence of active Ni-Ga intermetallic phase. Therefore, the catalyst preparation method reported for the CoGa based catalyst is clearly not suitable for the Ni-Ga based catalyst and this study was not pursued further.

4.4 Conclusions

The performance of Ni-Ga based catalysts supported on silica was reported for CO_2 hydrogenation under elevated temperature. All three catalysts (NiGa(a)/SiO_2, NiGa(b)/SiO_2 and NiGa(c)/SiO_2) prepared had consistently higher Ni to Ga ratio than nominal values due to loss of gallium during high temperature reduction. As a result the NiGa(a)/SiO_2 catalyst contains active phase that is close to Ni_3Ga and NiGa(b)/SiO_2 catalyst contains Ni_5Ga_3.

Due to the instability of the active intermetallic phase under air, a passivation technique was developed to allow the Ni-Ga based catalysts to be evaluated under industrial conditions. It was shown that the ex situ reduced Ni-Ga catalysts can be successfully passivated at 25 °C with 10% N_2O/N_2 and later re-activated in situ at 340 °C. The re-activated catalyst has similar activity as the in situ reduced catalyst, demonstrating the effectiveness of the passivation procedures.

Under elevated pressures, it was found that NiGa(a)/SiO_2 has lower activity compared to NiGa(b)/SiO_2 due to the latter having the more active Ni_5Ga_3 structure, the steady state hourly methanol production rates range from 0.54 to 0.72 mol/mol (active metals) at 30 bar. Both catalysts have significantly lower activity compared to the commercial Cu/ZnO/Al_2O_3 catalyst, but they are both more selective towards methanol (> 70%). As expected, the NiGa(c)/SiO_2 catalyst has very poor methanol synthesis activity and selectivity due to its Ni-rich nature.

Regardless of pressure, initial deactivation (about 20%) of the Ni-Ga based catalysts was always observed. Despite the significant deactivation, the selectivity of Ni-Ga catalysts is stable throughout the run. The initial deactivation was speculated to be due to the impact of reaction products that reduces the number of accessible active sites. The catalysts have stable activity afterwards. The characterisation of the spent catalysts confirmed that no structural changes occurred.

Subjecting the Ni-Ga catalysts to a feed gas containing 4% CO revealed that the Ni-Ga intermetallic phase was susceptible to the poisoning effect of CO, possibly due to a reconstruction of surface composition towards Ni-rich. This deactivation by CO was found to be reversible in the case of NiGa(a)/SiO_2. However, as NiGa(b)/SiO_2 catalyst is more Ga-rich, its intermetallic phase is less stable against decomposition of intermetallic phase and Ga re-oxidation. Hence, this catalyst showed continuous deactivation both under CO and after regeneration.

Using a LDH based support for Ni-Ga did not result in an active methanol synthesis catalyst.

Chapter 5 CO_2 Hydrogenation to Methanol over Pd-containing Intermetallic Catalysts

5.1 Introduction

In the previous chapter, it was shown that a passivation technique is necessary to preserve the activity of intermetallic Ni-Ga based catalyst for high-pressure applications due to its instability upon contacting with air [128]. Although the passivation procedure was developed successfully, the Ni-Ga catalysts still have to be reduced at 700 °C for the formation of the active intermetallic phase [14]. This high temperature preparation is not desirable for industrial applications since it is costly and involves more catalyst handling. Therefore it would be advantageous if an active catalyst with similar performance can be prepared at a lower temperature. This can be achieved by adding a 'reduction promoter' to the existing catalyst. This approach has been widely demonstrated in the literature [259-261]. Regarding the choice of reduction promoter, palladium appears to be a suitable candidate as it has been shown by Sahibzada and co-workers [259] that Pd addition to the $Cu/ZnO/Al_2O_3$ catalyst reduced the reduction temperature. Moreover, Fujimoto and Yu found that palladium promoted Cu based catalyst has enhanced methanol synthesis activity from CO_2 through hydrogen spillover as well as increased stability in the presence of water [262]. Another motivation for the use of a Pd promoter is the superior performance of Pd-Ga based catalysts such as Pd/Ga_2O_3 and Pd/SiO_2 promoted by Ga_2O_3 [127, 130, 133, 263]. As discussed in Chapter 2 section 2.1.5.1, these Pd-Ga intermetallic compounds can be fully activated at lower temperatures and they exhibit superior activity and selectivity towards CO_2 hydrogenation to methanol. It was speculated that by promoting the Ni-Ga based catalyst with Pd, the high temperature ex situ reduction can be avoided. Enhancement in the methanol synthesis activity is also possible due to H_2 spillover from Pd and/or the formation of a Pd-Ni-Ga alloy.

In the first section of this chapter, a palladium promoted NiGa(a)/SiO_2 catalyst was synthesised and characterised. Its reducibility and performance were investigated and compared to the unpromoted catalyst.

The performance of Pd-Ga based intermetallic catalysts have been previously studied [127, 133, 134, 263, 264]. However, in this study the catalysts were synthesised by a modified method. Furthermore, Pd-Ga catalysts have not been examined in combination with zeolites for DME synthesis as will be done in Chapter 6. Therefore in the final section of this chapter, $PdGa_{0.5}/SiO_2$ and $PdGa_3/SiO_2$ catalysts were prepared and tested for CO_2 hydrogenation to methanol in the CSTR to establish the performance in direct comparison with Ni-Ga.

5.2 Pd promoted NiGa(a)/SiO_2

5.2.1 Catalyst characterisation

5.2.1.1 Temperature programmed reduction

In the published work on Pd promoted Cu/ZnO/Al_2O_3 catalysts, Pd/Cu molar ratios of 0.04 and 0.09 were used to impregnate the Cu based catalysts [259]. The authors found that the introduction of Pd shifted the reduction temperature of CuO from 255 °C to approximately 180 °C (0.04 Pd/Cu/Zn/Al). The higher Pd loading (0.09 Pd/Cu/Zn/Al) only led to a small further decrease of reduction temperature to 175 °C. Moreover, it was demonstrated that the enhancement in the methanol production was independent of Pd loading. Therefore, a Pd to active metal (Ni+Ga) ratio of 0.04 was chosen as the starting point for the promotion of NiGa(a)/SiO_2 (nominal Ni:Ga ratio is 1.67). The palladium promoted NiGa(a)/SiO_2 catalyst precursor was prepared using the method described in Chapter 3 section 3.2.1.3.

Temperature programmed reduction of the Pd promoted NiGa(a)/SiO_2 precursor was conducted to find the reducibility of the promoted catalyst. The TPR results for both Pd promoted and unpromoted catalyst precursor are given in Figure 5.1 (a).

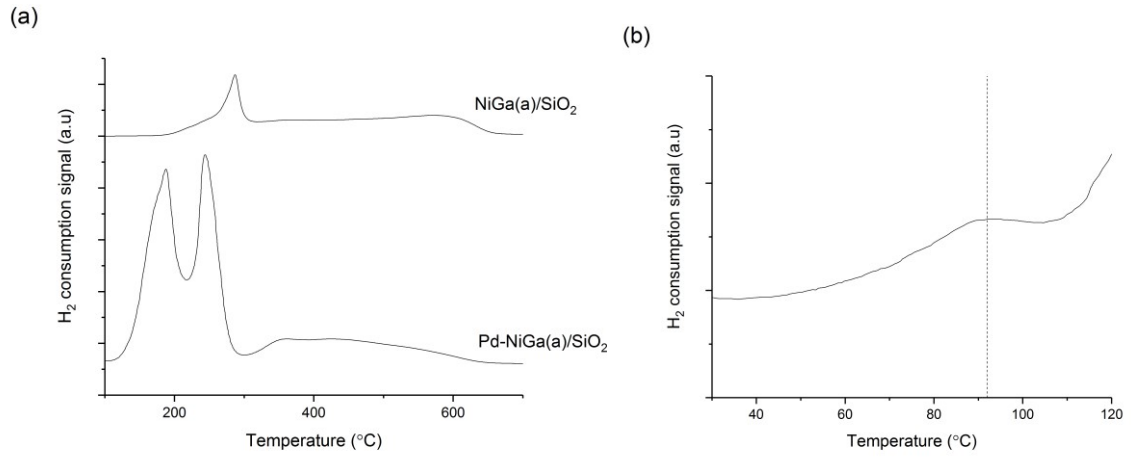


Figure 5.1, TPR profiles for the Pd promoted and unpromoted NiGa(a)/SiO_2 precursors (a) Over whole temperature range (b) enlarged low temperature section from the TPR of Pd promoted catalyst from (a)

The NiGa(a)/SiO_2 precursor (unpromoted) has a sharp reduction peak at around 290 °C followed by a broad hydrogen consumption peak that spans from 300 °C to 670 °C. According to the in situ XRD study of Ni-Ga catalysts by Sharafutdinov et al. [13, 14], the sharp peak below 300 °C corresponds to the decomposition of nitrates to oxides. Above 400 °C, NiO and Ga_2O_3 start to alloy and the Ni-rich Ni_3Ga phase was the first to form. At this point, the catalyst is a mixture of Ni_3Ga and NiO with the latter being the dominant species. Ga_2O_3 was not detected due to its amorphous nature, however its existence was confirmed by XAS study. As temperature increases further, Ni-Ga alloy continues to shift towards the composition in the initial impregnated precursor. In this region, the gallium enrichment of the intermetallic phase becomes a gradual process with continuous hydrogen consumption. Therefore a reduction temperature of 700 °C is needed for the complete formation of Ni-Ga alloy, which was shown by Sharafutdinov et al. [14] to be crucial to obtain an active and selective methanol synthesis catalyst.

The promoted catalyst (Pd-NiGa(a)/SiO_2) showed a clear shift of reduction peaks towards the low temperature side. A small hydrogen consumption peak can be seen at around 90 °C (Figure 5.1 (b)), which could be due to the formation of metallic Pd. Relatively easy formation of metallic Pd is known to be beneficial for the reduction of Pd-impregnated materials owing

to the hydrogen spillover effect [265]. For example, in Pd-Ga nanoparticles it was found that the presence of already-reduced Pd nanoclusters facilitates Ga_2O_3 reduction [133, 266, 267]. Two major reduction peaks were observed at 190 °C and 250 °C. These peaks correspond to the reduction of nitrates to oxide, hydride species, large PdO crystallites and maybe even the formation of Ni-Ga or Pd-Ga intermetallic phase [14, 265, 267, 268]. The subsequent peak at 370 °C and even higher temperatures may be due to the reduction of smaller PdO particles as they have stronger interaction with the support [268] and/or the formation of Ni-Ga intermetallic phase [14].

The hydrogen consumptions for both catalysts are presented in Table 5.1. For the Pd promoted catalyst, the fraction of hydrogen consumed at temperatures lower than 300 °C was significantly higher, while for the unpromoted catalyst, the majority of the reduction occurs at temperatures above 300 °C. Clearly, the addition of Pd enhanced the reducibility of the NiGa(a)/SiO_2 catalyst by spillover of activated hydrogen from metallic Pd to NiO and Ga_2O_3 sites at lower temperatures.

Table 5.1, H_2 consumption in low and high temperature regions for both Pd promoted and unpromoted catalysts

Catalyst	**H_2 consumption (mmol/g)**		
	Total	Below 300 °C	Above 300 °C
NiGa(a)/SiO_2	2.4 ± 0.2	0.79 ± 0.08	1.6 ± 0.2
	% of total consumption	34%	66%
Pd-NiGa(a)/SiO_2	10 ± 1	7.7 ± 0.8	2.4 ± 0.2
	% of total consumption	77%	23%

Another interesting result is that the total H_2 consumption for the promoted catalyst is significantly higher compared to the unpromoted catalyst. Clearly, the addition of Pd not only shifted the reduction process to lower temperatures, but also changed the way the catalyst precursor reduces. Moreover, the extra H_2 consumption was found to be much higher than the requirement for stoichiometric Pd acetate reduction (0.11 mmol/g) [269]. Metallic Pd can form palladium hydride and also transfer hydrogen to the support by spillover, both of which could result in higher hydrogen consumption than stoichiometric reduction of Pd^{2+} [135].

The majority of the reduction is seen to be complete below 350 °C and this temperature is the reactor limit for in situ reduction, therefore the reduction condition determined for the Pd promoted catalyst precursor is therefore at 350 °C for 4 hours.

5.2.1.2 Chemical composition and XRD pattern of reduced-passivated catalyst

The reduced catalyst was passivated with 10% N_2O/N_2 at room temperature before characterisation tests were carried out. The chemical composition of the reduced and passivated Pd promoted NiGa(a)/SiO_2 catalyst was measured by ICP – OES.

Table 5.2, Chemical composition of promoted and unpromoted catalysts

Catalyst	Molar ratio	Nominal	Actual
Pd-NiGa(a)/SiO_2	Pd/(Ni+Ga)	0.04	0.03
	Ni/Ga	1.67	2.34
NiGa(a)/SiO_2	Ni/Ga	1.67	2.34

The catalyst prepared has slightly lower Pd loading than intended. This is possibly due to low solubility of palladium acetate in toluene, causing the impregnating solution to have lower concentration of Pd. The Ni to Ga ratio obtained is identical to that of unpromoted catalyst (ex situ reduced at 700 °C). As observed in the previous chapter, some Ga appears to have been lost during reduction of the Ni-Ga catalyst. This phenomenon was observed again for the Pd

promoted catalyst that was reduced at a lower temperature (350 °C), suggesting that the loss of Ga from the catalyst occurs ≤ 350 °C and increasing temperature further to 700 °C does not cause further change in chemical composition.

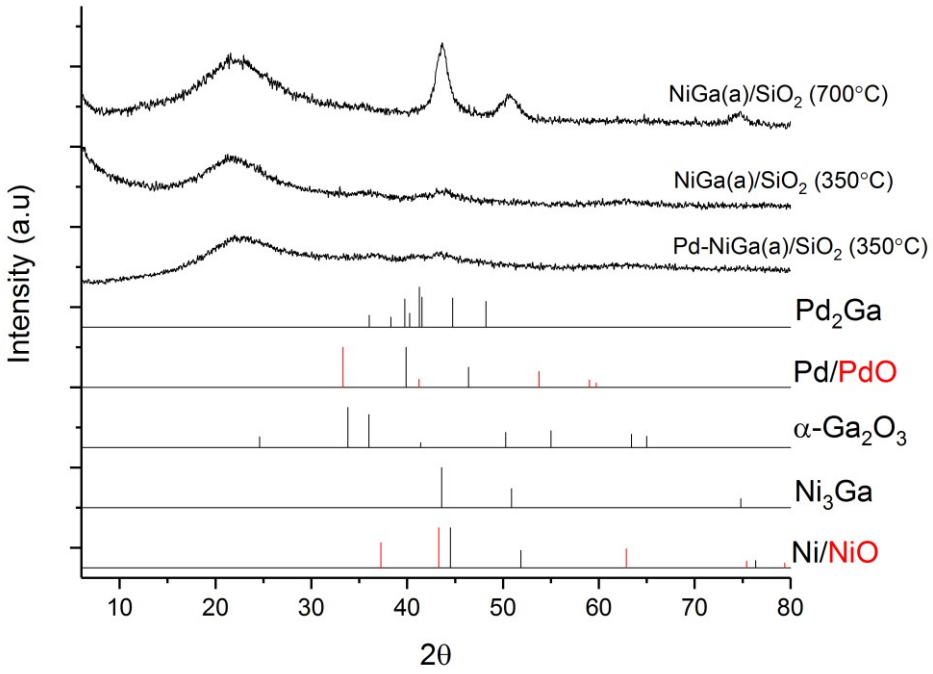


Figure 5.2, XRD patterns of reduced-passivated Pd-NiGa(a)/SiO_2 (350 °C), NiGa(a)/SiO_2 (350 °C), NiGa(a)/SiO_2 (700 °C) (reference peaks: Pd_2Ga: ICSD no. 409939, PdO: JCPDS 85-0713, Pd: ICCD no. 087-0643, α-Ga_2O_3: ICSD no. 27431, Ni_3Ga: Studt et al. [12], Ni and NiO: ICSD no. 011239 and 52265)

The XRD pattern of the reduced-passivated catalyst is shown in Figure 5.2. For easy comparison, the XRD data for two NiGa(a)/SiO_2 catalysts (ex situ reduced at 700 °C and another in situ reduced at 350 °C, both passivated) are also included. Both Pd promoted and unpromoted catalyst reduced under the same conditions (350 °C) have similar diffraction patterns. In the Pd promoted catalyst, peaks at 36° and 41.2° may be attributed to the (110) and (113) reflections of α-Ga_2O_3 [133, 270], indicating the possible presence of α-Ga_2O_3 in the sample. However, the peak at 41.2° can also correspond to the (1 1 0) reflection of PdO (JCPDS no. 85-0713) and Pd_2Ga (ICDD 65-1511) and it is only observed in the Pd promoted catalyst, therefore it is more likely that this peak comes from Pd-containing species (not α-

Ga_2O_3). However, no other peaks from PdO or Pd_2Ga were detected, which may be due to the low Pd loading and small particle size [133]. The peak at around 2θ = 43.5° is most likely due to the (200) reflection of NiO because another characteristic peak of NiO at 63° is also present. As discussed in the previous chapter, the NiGa(a)/SiO_2 catalyst has a structure that resembles Ni_3Ga intermetallic phase. Since the Pd promoted sample has the same Ni to Ga ratio (Table 5.2) as the NiGa(a)/SiO_2 catalyst characterised in Chapter 4, similar Ni-Ga structure is expected for the Pd promoted catalyst. Hence, the peak at 43.5° could also be attributed to the (111) reflection of Ni_3Ga. However, no other peaks from Ni-Ga intermetallic phase (in particular, the peak at 50.9° from Ni_3Ga) were observed over both promoted and unpromoted (350 °C) catalyst. Phase identification of Ni-Ga and Pd-Ga intermetallic compounds is difficult by XRD alone due to the overlap of diffractions from different oxides and overall low intensities of reflections. Based on the result, it can be said that the reduction temperature of 350 °C was too low to allow a complete formation of Ni-Ga intermetallic phase since the ex situ reduced (700 °C) and passivated unpromoted catalyst has a much more intense and pure intermetallic phase. The Pd promoted catalyst may be a mixture of oxides with some intermetallic species. Hence, Pd promotion indeed lowered the reduction temperature of certain species in the NiGa(a)/SiO_2, but it did not successfully promote the complete formation of Ni-Ga intermetallic compounds at 350 °C.

5.2.2 Catalyst performance under CO_2/H_2

Even though there is limited evidence of Pd-Ni-Ga intermetallic compounds from the XRD, their existence cannot be entirely disregarded and the catalyst may still benefit from the promotional effect of Pd addition (via hydrogen spillover). Therefore the catalytic performance of the Pd promoted catalyst was investigated.

In the PFR reactor, the detrimental effect of reaction products on the Ni-Ga based catalyst can be minimised since the catalysts are always exposed to an atmosphere with compositions close to the feed, this allows the effect of Pd promotion to be seen more clearly. Therefore,

the Pd promoted catalyst was reduced in situ using the conditions determined in the previous section (350 °C under flowing 5% H_2/N_2 for 4 hours) and its performance was measured in the PFR under essentially CO-free condition. Previously the unpromoted Ni-Ga catalyst was studied first at 245 °C, 10 bar (Chapter 4 section 4.2.3.2). Hence for the preliminary evaluation of the success of Pd promotion, the experiments were first carried out 245 °C, 10 bar. The performances of two unpromoted catalysts were also measured: one reduced under the same conditions (350 °C for 4 hours) and the other ex situ reduced at 700 °C, passivated and re-activated in situ (340 °C for 3 hours). All the reduction/re-activation was done using 5% H_2/N_2. The details of each catalyst test are given in Table 5.3.

Table 5.3, Reduction and reaction conditions for various promoted and unpromoted catalysts

Catalyst tested	Reduction conditions	Any passivation procedure	Reaction conditions tested	
			10 bar	30 bar
NiGa(a)/SiO_2 (700 °C ex situ)	Ex situ 700 °C (2 h)	✓	✓	✓
NiGa(a)/SiO_2 (350 °C)	In situ 350 °C (4 h)	×	✓	×
Pd-NiGa(a)/SiO_2	In situ 350 °C (4 h)	×	✓	✓

Catalytic performance at 245 °C, 10 bar

The catalytic performance of Pd promoted catalyst and two unpromoted catalysts reduced under different conditions are shown in Figure 5.3 and steady state values of activity and selectivity are summarised in Table 5.4. Since the Ni-Ga intermetallic phase of the Pd promoted catalyst was shown to be incomplete by the XRD results, it was anticipated that the promoted catalyst would have low methanol synthesis activity. As can be seen from Figure 5.3, the methanol production rate of the promoted catalyst is indeed lower than NiGa(a)/SiO_2 (700 °C ex situ). At 10 bar and 245 °C, main products from the Pd-promoted catalyst were

methanol (48%) and CO (51%). CH_4 selectivity was low (1.5%) and no other higher hydrocarbons were detected by the GC. Compared to the unpromoted catalyst (700 °C ex situ), the catalyst was less selective towards methanol synthesis as it produced more CO and methane, possibly due to the presence of free Ni and/or Pd. However, it should be noted that these two catalysts have different preparation procedures. The promoted catalyst was reduced in situ at 350 °C, while the unpromoted catalyst was reduced ex situ at 700 °C and passivated before in situ re-activation. Therefore, the discussion above involves a comparison of the Pd promoted catalyst to the unpromoted catalyst prepared using the best procedure.

Table 5.4, Steady state activity and selectivity of Pd promoted and unpromoted NiGa(a)/SiO_2 catalysts at 245 °C, 10 bar

Catalyst	**Steady state MeOH conversion (%)**	**Steady state MeOH rate (mol [MeOH]/mol [active metal]*hr)**	**Selectivity (%)**		
			MeOH	CO	CH_4
Pd-NiGa(a)/SiO_2 (350 °C)	0.60 ± 0.03	0.49 ± 0.02	48.1 ± 0.9	50 ± 1	1.33 ± 0.03
NiGa(a)/SiO_2 (350 °C)	0.41 ± 0.02	0.35 ± 0.02	32.1 ± 0.6	61 ± 1	6.9 ± 0.1
NiGa(a)/SiO_2 (700 °C ex situ)	0.78 ± 0.04	0.66 ± 0.03	60 ± 1	39.2 ± 0.8	0.483 ± 0.007

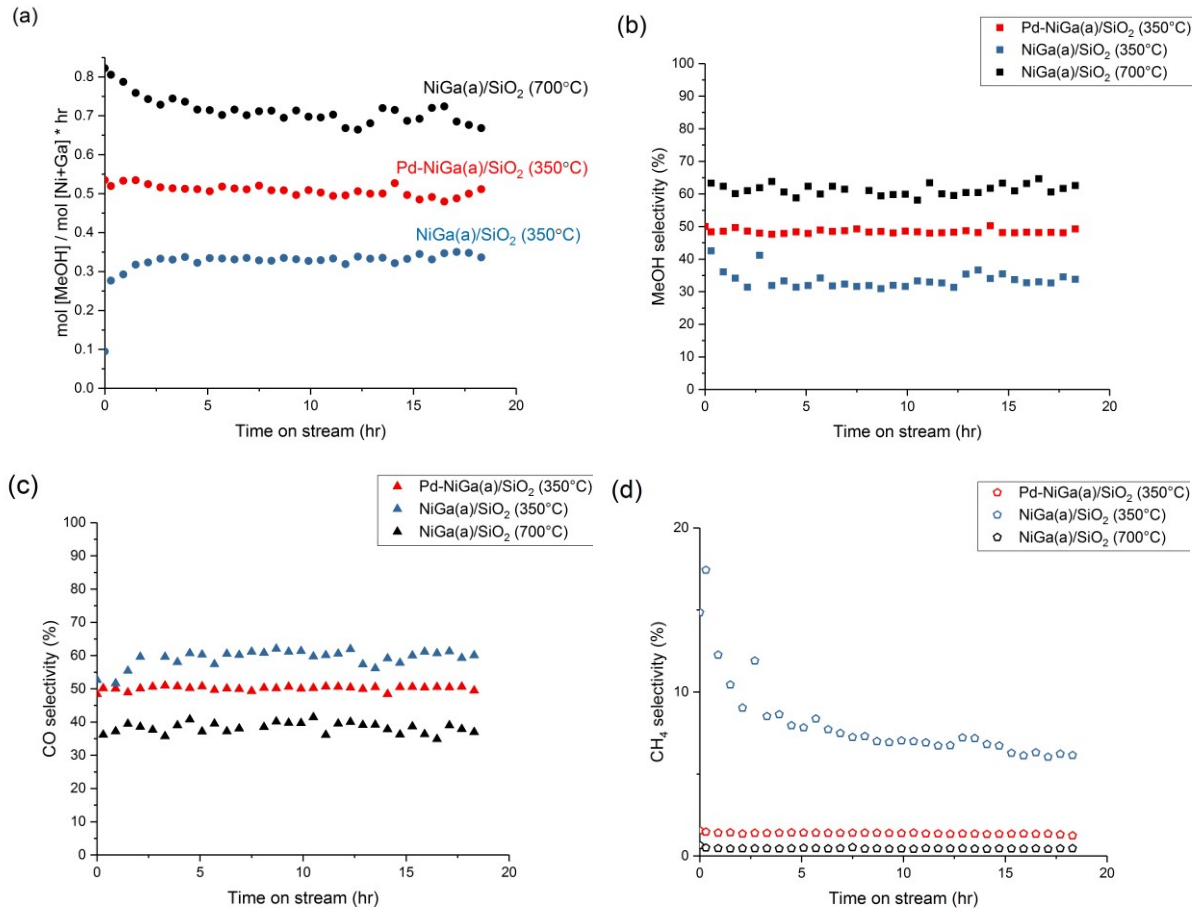


Figure 5.3, Catalytic performance of Pd-NiGa(a)/SiO_2 (350 °C in situ), NiGa(a)/SiO_2 (700 °C ex situ) and NiGa(a)/SiO_2 (350 °C in situ) at 245 °C, 10 bar
(a) MeOH production rates (b) MeOH selectivity (c) CO selectivity (d) CH_4 selectivity

Now comparing to NiGa(a)/SiO_2 (350 °C) that was reduced under the same condition, the CO_2 conversion to methanol activity was significantly enhanced (approximately 47%) by the addition of Pd. The selectivity to MeOH (48%) is also much better over Pd-NiGa(a)/SiO_2 catalyst as NiGa(a)/SiO_2 (350 °C in situ) produces even more CO (60%) and methane (7%) (Figure 5.3). It is likely that hydrogen spillover from Pd crystallites to the Ga sites was responsible for the enhancement in the methanol synthesis activity [263], compensating for the incomplete formation of active Ni-Ga phase [127, 271, 272]. The suppressed methanation reaction in the case Pd promoted catalyst may be linked to the presence of Ga_2O_3 found in the XRD, since it was speculated by Sharafutdinov et al. [13] that surface Ga_2O_3 was able to reduce the methanation activity of the Ni-Ga catalysts by blocking the Ni-rich sites.

The deactivation behaviour of the Pd promoted catalyst is also different. Unlike NiGa(a)/SiO_2 reduced at 700 °C (ex situ), it did not suffer an initial deactivation, its activity remained stable throughout the whole run. From the results in Chapter 4, the initial deactivation observed in the unpromoted catalyst was thought to be the result of competitive adsorption of products as they build up in concentration and consequently block the intermetallic active sites for methanol synthesis. This behaviour has been seen in both Ni-Ga and Pd-Ga based intermetallic compounds [12, 127]. Since the unpromoted catalyst reduced at 350 °C does not possess the same intermetallic structure, it was not surprising that the initial deactivation period was not observed in this case. Similarly for the Pd promoted catalyst, it was stable from the beginning due to the lack of completely formed intermetallic phase.

Catalytic performance at 245 °C, 30 bar

Preliminary study on the Pd promotions clearly shows an enhancement in the catalytic performance. To further evaluate the performance of the Pd promoted catalyst under industrial conditions, the experiment was repeated at 30 bar and 245 °C. The best performance achieved by an unpromoted catalyst is also included in Figure 5.4 and Table 5.5. As shown in Chapter 4, the performance of NiGa(a)/SiO_2 is not very dependent on reaction pressure, therefore increasing the pressure to 30 bar did not significantly increase the methanol production rate. On the other hand, the methanol synthesis rate of the Pd promoted catalyst showed a significant increase at higher pressure. Moreover, the MeOH selectivity of the Pd promoted catalyst is improved at higher pressure with low level production of CO and CH_4. The activity at 30 bar is found to be approximately 1.6 times the activity at 10 bar. This again shows the enhancement of activity by Pd promotion is probably due to hydrogen spillover, which is known to have square root pressure dependence [273, 274].

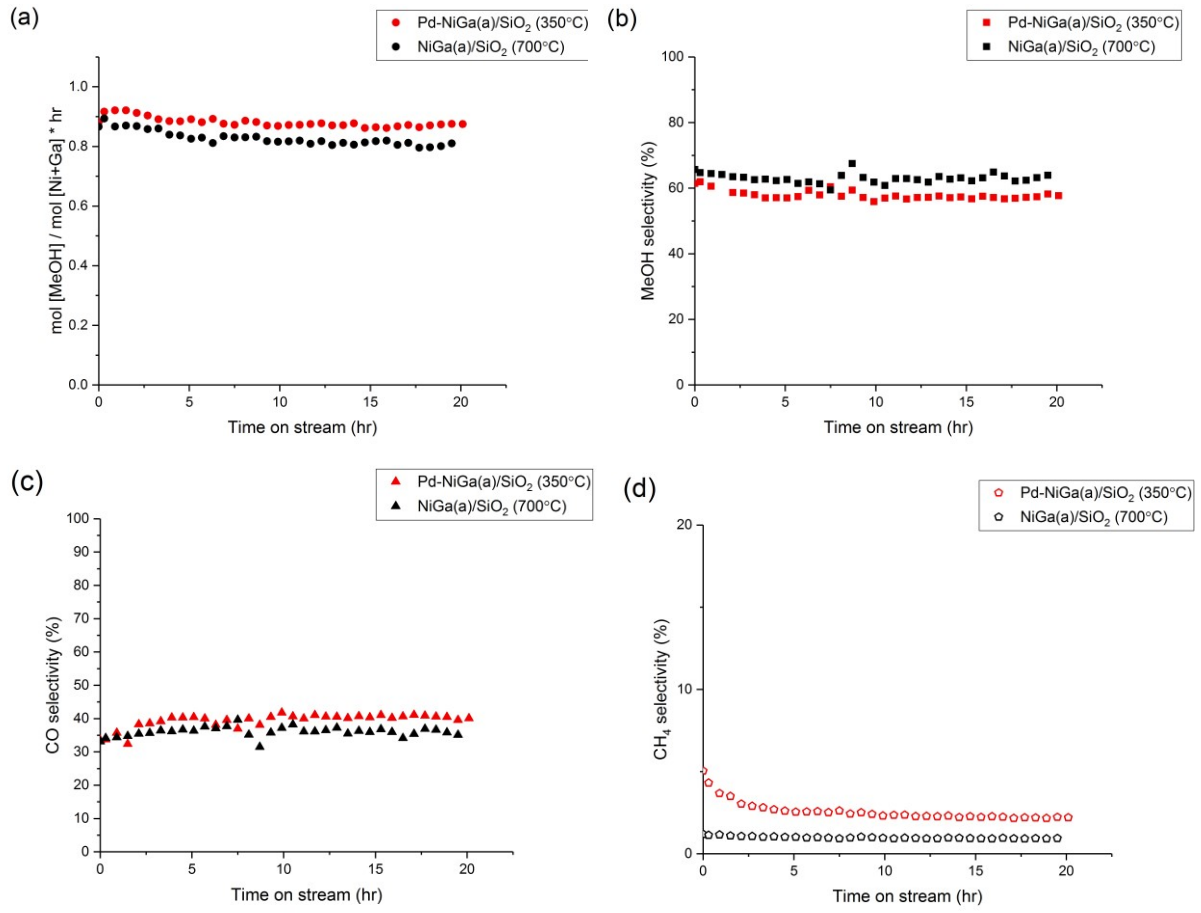


Figure 5.4, Catalytic performance of Pd-NiGa(a)/SiO_2 (350 °C in situ) and NiGa(a)/SiO_2 (700 °C ex situ) at 245 °C, 30 bar

(a) MeOH production rate (b) MeOH selectivity (c) CO selectivity (d) CH_4 selectivity

Table 5.5, Steady state activity and selectivity of Pd promoted and unpromoted NiGa(a)/SiO_2 catalysts at 245 °C, 30 bar

Catalyst	**Steady state MeOH conversion (%)**	**Steady state MeOH rate (mol [MeOH]/mol [active metal]*hr)**	**Selectivity (%)**		
			MeOH	CO	CH_4
Pd-NiGa(a)/SiO_2 (350 °C)	1.05 ± 0.05	0.87 ± 0.04	57 ± 1	40.5 ± 0.8	2.21 ± 0.04
NiGa(a)/SiO_2 (700 °C ex situ)	0.98 ± 0.05	0.80 ± 0.04	63 ± 1	35.9 ± 0.7	0.92 ± 0.01

5.2.3 Catalyst performance under $CO/CO_2/H_2$ at 245 °C, 10 bar

Over the Pd promoted catalyst, the absence of the initial deactivation period may suggest that it is more stable towards the presence of reaction products. Therefore, the Pd promoted catalyst was subjected to catalysis under $CO/CO_2/H_2$. Since the unpromoted catalyst (700 °C ex situ) had been previously tested under 245 °C and 10 bar (Chapter 4 section 4.2.4.1), the effect of CO in the feed on the Pd promoted catalyst was also carried out under the same conditions (still in the PFR).

Changing the CO-free feed to $CO/CO_2/H_2$ revealed that CO could cause serious deactivation in the Pd promoted catalyst, as seen in Figure 5.5.

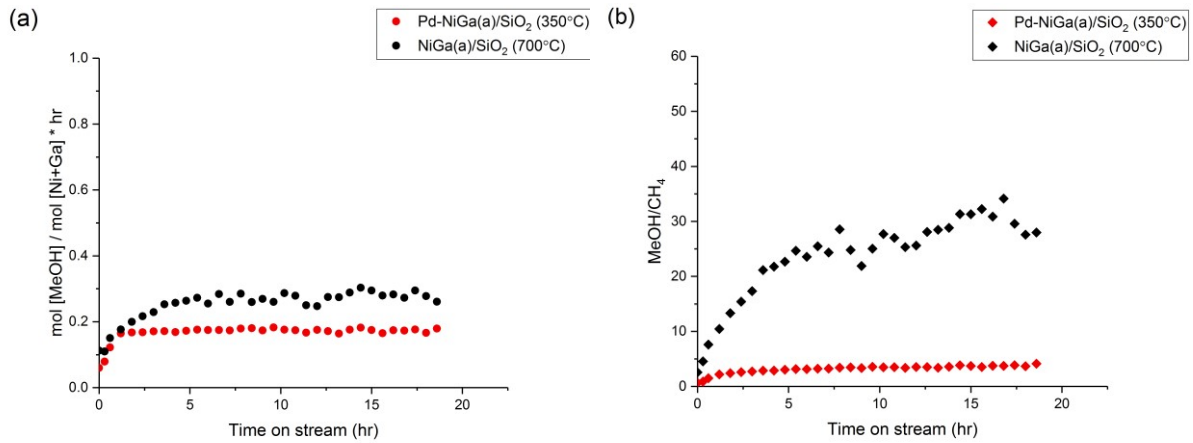


Figure 5.5, Catalytic performance of Pd-NiGa(a)/SiO_2 (350 °C in situ) and NiGa(a)/SiO_2 (700 °C ex situ) under $CO/CO_2/H_2$ at 245 °C, 10 bar
(a) MeOH production rate (b) $MeOH/CH_4$ ratio

Figure 5.5 shows the activity of the promoted catalyst in reactions with $CO/CO_2/H_2$. The performance of the ex situ reduced (700 °C ex situ), passivated and re-activated catalyst under the same conditions is also included. The promoted catalyst exhibited low activity and selectivity in the presence of CO due to significant formation of CH_4. Chiavassa and co-workers in their Pd-Ga work concluded that CO chemisorbed strongly on Pd crystallites hence reduced MeOH activity through a decrease in H_2 dissociation by the metal [127]. As the presence of PdO and NiO cannot be ruled out from the XRD diffraction pattern of the Pd promoted catalyst, it is possible that the oxides were reduced to metallic Pd and/or Ni, or the

surface composition became Pd- and/or Ni-rich under high level of CO in the feed gas [275]. Therefore, the catalyst behaved like Pd and Ni metals under the effect of CO [12]. Consequently, the Pd promoted NiGa(a)/SiO_2 is not suitable for use under high level of CO (for example in a CSTR where product concentration is relatively high) as its performance can be severely affected.

5.2.4 Characterisation of spent Pd promoted NiGa(a)/SiO_2 catalyst

The spent Pd promoted NiGa(a)/SiO_2 catalyst (after catalysis under CO_2/H_2, 245 °C, 30 bar) was characterised by N_2 physisorption, XRD (Figure 5.6) and TPO (Table 5.6 and Figure 5.7).

No change in the diffraction pattern was observed, indicating that the catalyst maintained its crystalline structure during the reaction. Indeed, the catalyst did not show any significant change in selectivity during the reactions as noted in the previous section.

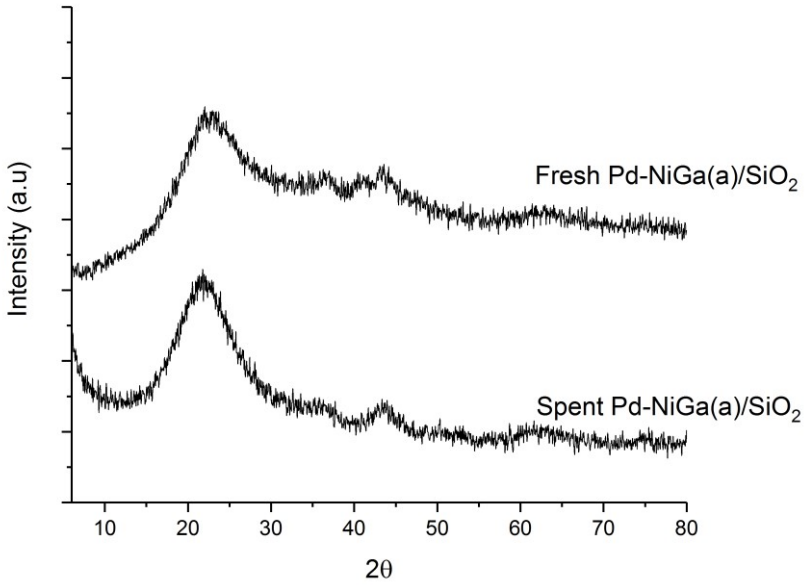


Figure 5.6, XRD of spent Pd-NiGa(a)/SiO_2 catalyst

The coke content and the TPO profiles for the Pd promoted catalysts exposed to different feed gas is presented in Table 5.6 and Figure 5.7 respectively.

Table 5.6, Coke content and BET surface area of spent catalysts

Spent catalyst	Feed gas used	BET surface area (± 1 m^2/g)	Coke content (µmol/g active metals)	CO_2 evolution temperature (°C)
Pd-NiGa(a)/SiO_2 (350 °C)	CO_2/H_2	258	5.98 ± 0.06	250, 480, 640
	$CO/CO_2/H_2$	-	2.35 ± 0.02	250, 450
NiGa(a)/SiO_2 (700 °C ex situ)	CO_2/H_2	239	6.37 ± 0.06	360, 600

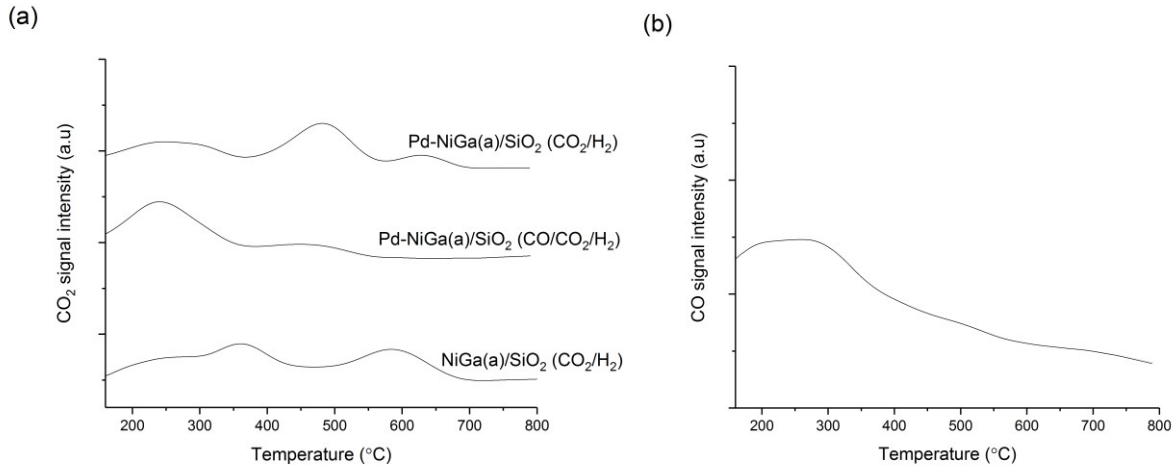


Figure 5.7, TPO profiles of the spent Pd promoted catalysts
(a) CO_2 evolution (b) CO evolution from $CO/CO_2/H_2$ run

The coke content calculated for the Pd promoted catalyst does not include the broad peak observed at around 250 °C. This is because at such low temperature, this peak may not come from the oxidation of carbonaceous materials. Firstly, this peak is not present in the unpromoted catalyst, indicating its association with the Pd species in the promoted catalysts. Secondly, this peak is more significant in the Pd promoted catalyst that was exposed to high level of CO in the feed gas. In fact, a weak CO evolution peak was also seen at the same time (Figure 5.7 (a)). According to Zhu et al. [275], there are different ways CO_2 can be produced when Pd based catalyst is exposed to high CO level. For example, interaction of CO with surface hydroxyl groups on the catalyst, reduction of reducible species such as PdO,

decomposition of carbonated species and disproportionation of CO [275]. Therefore it is possible that the CO_2 evolution peak at 250 °C comes from the CO adsorbed on the Pd species.

For CO-free reaction, the coke deposition on the spent catalyst was found to be 5.98 μmol/g (Ni+Ga), which is similar to the coke content (6.37 μmol/g (Ni+Ga)) of unpromoted catalyst (700 °C ex situ reduced). The type of coke found on the Pd promoted catalyst appears to be different from that on the unpromoted catalyst. For the promoted catalyst, the majority of coke oxidation occurs at a temperature of 480 °C while for the unpromoted catalyst, two distinctive coke oxidation peaks were observed at both 360 °C and 600 °C. This suggests that the type of coke formed over the promoted catalyst could be different due to a different catalyst structure/morphology with Pd promotion [276, 277] and different reduction/passivation procedures.

With CO in the feed, the coke deposition was found to be lower than that obtained under CO_2/H_2 and one coke oxidation peak was found (at 450 °C). This suggests that the additional CO in the feed and the methane produced did not result in an increase in coke deposition by either CO disproportionation or CH_4 decomposition [278, 279].

5.3 Pd-Ga/SiO_2 catalysts for CO_2 hydrogenation to methanol

Pd-Ga intermetallic compound based catalysts have been reported to be promising catalysts for CO_2 hydrogenation to methanol [137, 156, 242, 263, 264]. Due to the similarity between Pd-Ga and Ni-Ga based catalysts, it was speculated that Pd-Ga based catalyst would also be suitable as the methanol synthesis component for the single-stage DME synthesis. A direct comparison between the two catalysts may yield a better understanding of the catalytic properties of intermetallic compounds for CO_2 hydrogenation to methanol. Therefore, Pd-Ga/SiO_2 catalysts were prepared by a two-stage incipient wetness impregnation method and their catalytic performance was measured and compared to that of Ni-Ga/SiO_2.

5.3.1 Catalyst preparation and characterisation

Two Pd-Ga/SiO_2 catalysts with different Pd:Ga ratios were prepared. Pd-Ga/SiO_2 catalyst with a Pd:Ga ratio of 2 (stoichiometric composition of the active Pd_2Ga intermetallic phase) at the time of preparation will be designated as $PdGa_{0.5}/SiO_2$ and the one with Pd:Ga ratio of 1:3 (ratio used in published work [127, 242]) will be $PdGa_3/SiO_2$. To make these catalysts more comparable to the Ni-Ga based catalysts, both catalysts were prepared following the procedures given in Chapter 3 section 3.2.1.4, which are modified from the method reported by Chiavassa et al. [127]. Calcined samples were reduced and passivated before characterising with XRD (Figure 5.8), ICP – OES (Table 5.7) and N_2 physisorption.

Table 5.7, Chemical compositions and surface area for both Pd-Ga /SiO_2 catalysts

	Pd:Ga ratio		**Pd wt%**		**BET surface area (± 1 m^2/g)**
	Nominal	Actual	Nominal	Actual	
$PdGa_{0.5}/SiO_2$	2	1.87	2	1.34	281
$PdGa_3/SiO_2$	0.33	0.34	2	1.49	271

The Pd loading (wt%) is consistently lower than the desired value. The fact that Pd to Ga ratios obtained for both Pd-Ga/SiO_2 catalysts are close to the nominal ratios despite low Pd loadings indicates that the actual Ga content is also lower than desired, possibly due to loss of Ga during reduction as observed previously in all Ga-containing samples. The SiO_2 support (EP10) has a BET surface area of 279 m^2/g, therefore the addition of Pd and Ga did not result in significant decrease of surface area. $PdGa_{0.5}/SiO_2$ has very similar BET surface area (281 m^2/g) compared to the $PdGa_3/SiO_2$ (271 m^2/g).

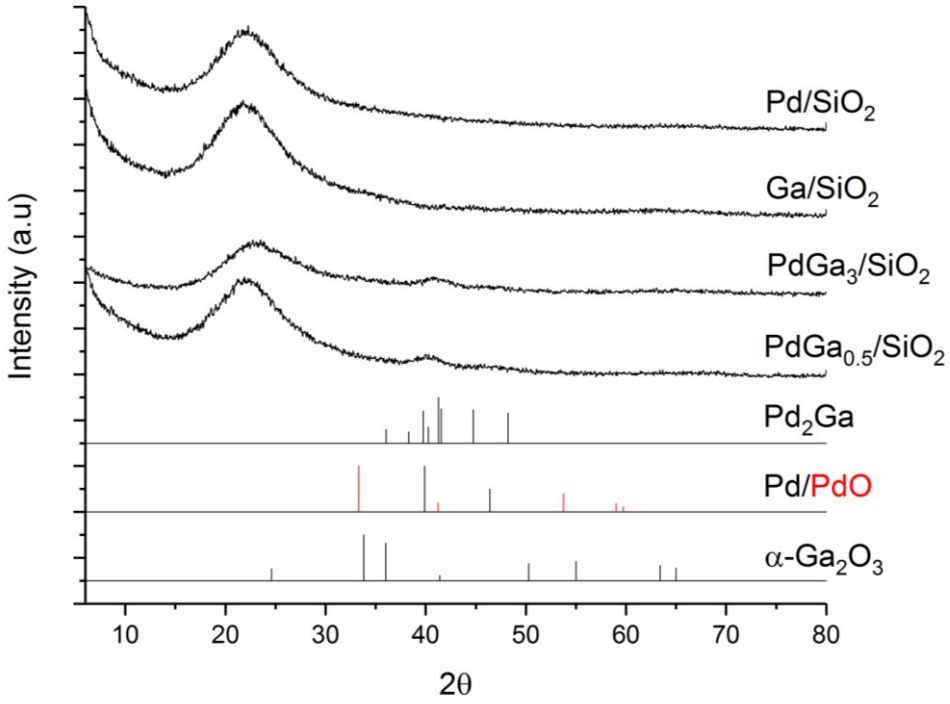


Figure 5.8, XRD patterns of reduced-passivated Pd-Ga/SiO_2 catalysts with reference materials (reference peaks: Pd_2Ga: ICSD no. 409939, PdO: JCPDS 85-0713, Pd: ICCD no. 087-0643, α-Ga_2O_3: ICSD no. 27431)

The XRD patterns for 2 wt% Pd/SiO_2 and Ga/SiO_2 (monometallic reference samples synthesised in the same way as the Pd-Ga based catalysts) were also obtained for comparison. As can be seen from Figure 5.8, very weak peaks at 2θ = 33.8° and 65° can be attributed to the presence of α-Ga_2O_3 [133, 270]. No crystalline Pd species can be seen clearly on the single-metal reference material, however the presence of minor amount of Pd particles cannot be ruled out. Therefore the new peaks around 41° that appear in the bimetallic catalysts are likely due to the formation of Pd_2Ga intermetallic phase (even though the (110) reflection of PdO can also be found at this 2θ value [280]). The weak and broad peak starting from 2θ = 45° to 48° can also be attributed to the characteristic peaks of the Pd_2Ga intermetallic phase at 44.9° and 48.2° being merged due to low intensity [156]. No evidence of other Pd-rich intermetallic compounds can be found here but their existence cannot be completely excluded.

The two Pd-Ga/SiO_2 catalysts with different Pd:Ga ratios have very similar peak positions as well as peak intensity. This suggests similar intermetallic compound was formed even when

gallium is in large excess. Indeed, it has been reported by a few studies that the Pd_2Ga intermetallic phase is always formed regardless of Pd:Ga ratio used [156, 281]. The authors speculated that the preferential formation of Pd_2Ga phase is due to its higher stability and the ability of this compound to reduce the concentration of Ga^{3+} in the vicinity by forming highly reactive hydrides [156, 281]. Besides the Ga_2O_3 phase identified earlier on both Pd-Ga catalysts, no other Ga-containing crystalline phases or higher Ga_2O_3 intensity were found on the $PdGa_3/SiO_2$ catalyst. The excess gallium that did not alloy as Pd_2Ga phase must have been present as amorphous Ga_2O_3, as also observed by García-Trenco et al. [156].

5.3.2 Catalyst performance in the CSTR with CO_2/H_2 at 245 °C, 30 bar

The catalytic performance of the Pd-Ga catalyst supported on SiO_2 was measured in the CSTR at 245 °C and 30 bar to allow comparison with previous measurements on the Ni-Ga based catalyst as well as literature values for Pd-Ga. The results are shown in Figure 5.9, which clearly show that active Pd_2Ga intermetallic based methanol synthesis catalysts were successfully prepared (using procedures modified based on Ni-Ga catalysts (Chapter 4) and Ga_2O_3-Pd/SiO_2 (Chiavassa et al. [127]). The conversion level obtained for both catalysts ranges from 0.9 to 1.9%. The initial methanol conversion of $PdGa_3/SiO_2$ is higher than that of $PdGa_{0.5}/SiO_2$, however it dropped to the same level as the $PdGa_{0.5}/SiO_2$ after 6 hours on stream and the activity of the two catalysts remained similar in the next 10 hours. In terms of methanol production rate, it is obvious that $PdGa_{0.5}/SiO_2$ would have much higher rate as it contains less active metals. Indeed, the methanol production rate is about 2 times the rate of $PdGa_3/SiO_2$ catalyst. The methanol production rate obtained over $PdGa_3/SiO_2$ (85×10^{-8} mol MeOH g_{cat}^{-1} s^{-1}) is lower than that reported over the same catalyst under similar reaction conditions (140.7×10^{-8} mol MeOH g_{cat}^{-1} s^{-1}) [242] in the literature. This could be due to a combination of slightly lower reaction temperature used, a different catalyst preparation method and silica resulting in small variation of catalyst structure, composition and morphology. The reaction with CO_2/H_2 produced only methanol (70%) and CO (30%). The

selectivity to methanol of both catalysts was found to be better than values reported in the literature (55% MeOH, 44% CO [127]).

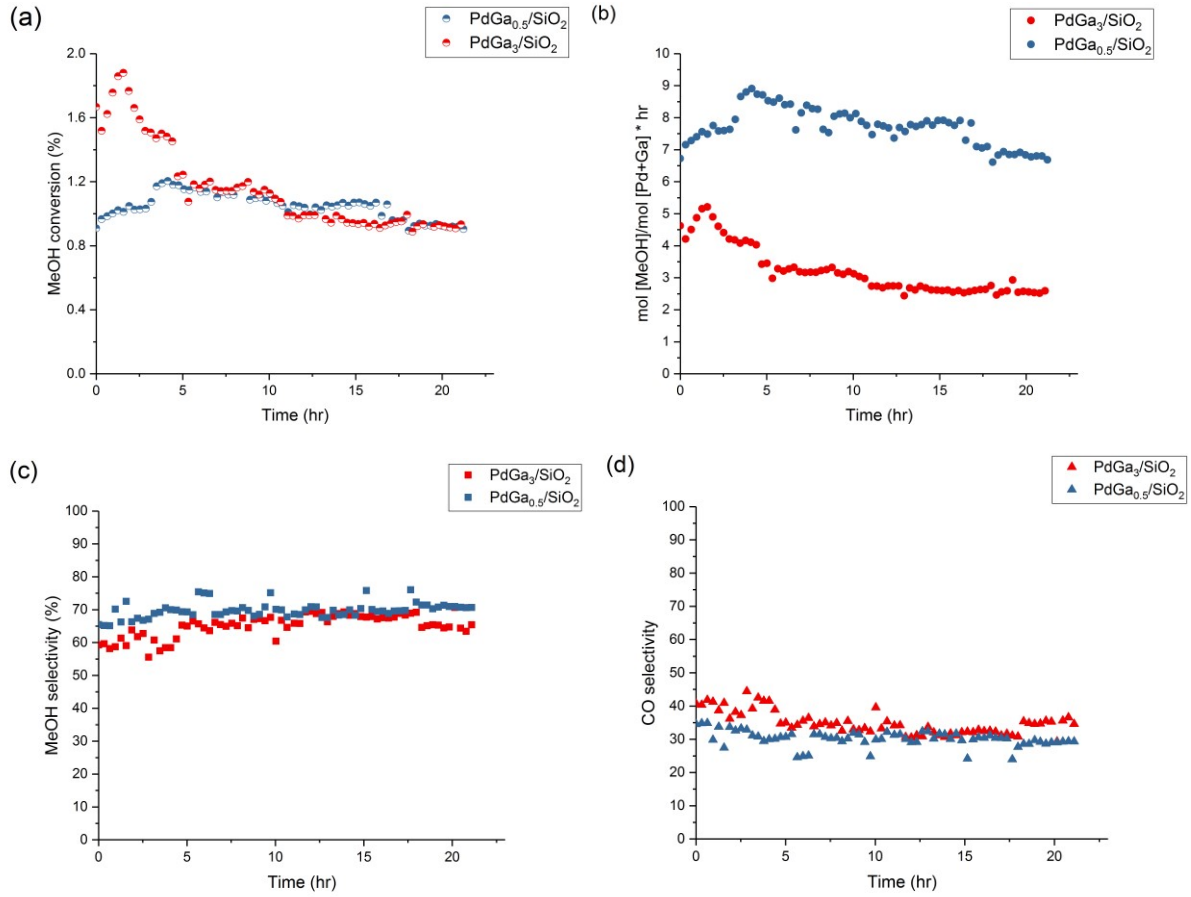


Figure 5.9, Catalytic performance of $PdGa_{0.5}/SiO_2$ and $PdGa_3SiO_2$ at 245 °C, 30 bar (a) MeOH conversion (b) Normalised MeOH production rate (c) MeOH selectivity (d) CO selectivity

The selectivity of both catalysts appears to be the same throughout the run, indicating that the initial deactivation where $PdGa_3/SiO_2$ lost nearly half of the initial activity was due to rapid reduction in the number of accessible active sites and not a change in the nature of active sites [133]. In addition, this observation also shows that Ga-rich sites are the catalytically active species since the excess gallium in the $PdGa_3/SiO_2$ catalyst is linked to a high initial overall conversion. However these sites are also prone to deactivation, possibly by adsorption of products that reduces the availability of these active sites [127, 133]. It was shown by Chiavassa and co-workers [127] that the chemisorption of CO on Pd crystallites causes the most significant deactivation by reducing the amount of dissociated hydrogen transferred to

the gallia sites, while water was also found to impact the activity of Pd-Ga based catalysts by limiting the availability of *cus* on Ga_2O_3. Therefore it is not surprising that the catalyst with higher initial activity ($PdGa_3/SiO_2$) suffered a greater extent of initial deactivation.

Table 5.8, Comparison of catalytic performance over NiGa(b)/SiO_2, Pd-Ga/SiO_2, commercial Cu/ZnO/Al_2O_3 catalysts

Catalyst	Steady state MeOH conversion (%)	Steady state MeOH rate (mol [MeOH]/mol [active metal]*hr)	Selectivity (%)		
			MeOH	CO	CH_4
NiGa(b)/SiO_2	0.81 ± 0.04	0.69 ± 0.03	67 ± 1	32.3 ± 0.7	0.6 ± 0.01
$PdGa_{0.5}/SiO_2$	0.92 ± 0.05	6.8 ± 0.3	71 ± 1	29.2 ± 0.6	trace
$PdGa_3/SiO_2$	0.93 ± 0.05	2.5 ± 0.1	66 ± 1	33.6 ± 0.7	trace
Cu/ZnO/Al_2O_3	3.0 ± 0.2	2.5 ± 0.1	52.0 ± 0.9	48 ± 1	trace

Comparing to the Ni-Ga/SiO_2 catalyst (the most active NiGa(b)/SiO_2 was chosen for comparison), $PdGa_{0.5}/SiO_2$ is the most active among the four catalysts due to its intermediate conversion level achieved by a low active metal loading. Selectivity of both Ni-Ga and Pd-Ga catalysts are similar and better compared to the conventional Cu based catalyst. The impacts of reaction products on the Pd-Ga/SiO_2 catalysts are strikingly similar to the Ni-Ga/SiO_2 based catalysts. For Pd-Ga based catalysts about 24% of the maximum activity was gradually lost throughout 20 hours. In the case of Ni-Ga based catalyst, about 20% of the activity was lost (Chapter 4 section 4.2.3.3). Another similarity between the deactivation behaviour of these two types of catalyst is the higher extent of deactivation (and higher initial conversion) observed in the Ga-rich catalyst, i.e. NiGa(b)/SiO_2 and $PdGa_3/SiO_2$. Moreover, the selectivity of both intermetallic based catalysts remained stable despite of the significant drop in conversion. All these observations suggest that it is possible that both Ga-based intermetallic catalysts deactivates via similar mechanism described above.

5.3.3 Characterisation of spent catalysts from CO_2/H_2 runs

The diffraction pattern for the spent $PdGa_{0.5}/SiO_2$ and $PdGa_3/SiO_2$ are presented in Figure 5.10. No obvious change in peak intensity and position were observed over $PdGa_{0.5}/SiO_2$. For $PdGa_3/SiO_2$, the peak originally at 41° has shifted slightly to lower 2θ value of 40°, which corresponds to the (111) reflection of Pd [156, 282]. This could be due to the result of de-alloying of gallium from a Ga rich intermetallic phase to form monometallic Pd and oxidised gallia patches [154]. The fact that only $PdGa_3/SiO_2$ shows a change in peak position towards Pd-rich phase is consistent with the results obtained over Ni-Ga catalyst from Chapter 4 as well as the literature, that the Ga-rich catalyst is more sensitive to decomposition (de-alloy) and re-oxidation of Ga-species [133].

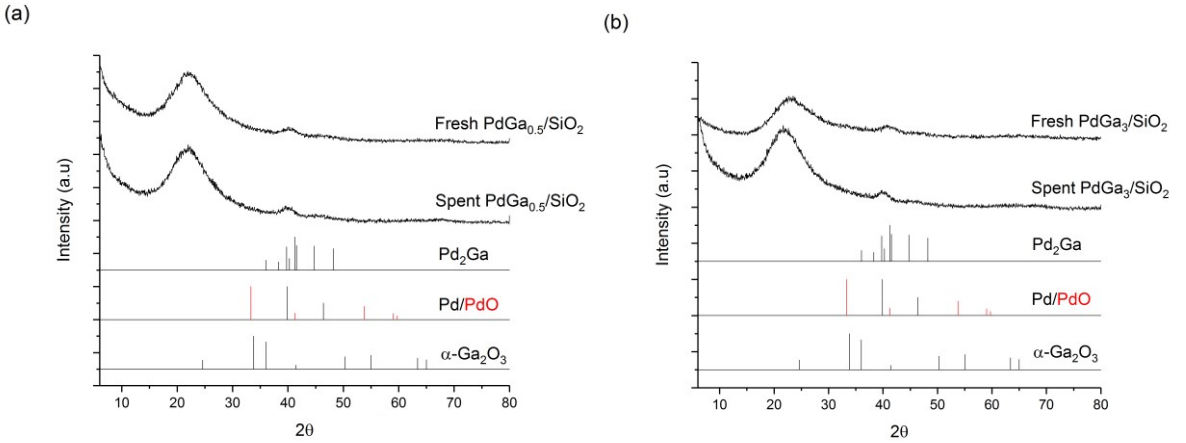


Figure 5.10, XRD of spent Pd-Ga/SiO_2 catalysts with reference materials (refenrece peaks: Pd_2Ga: ICSD no. 409939, PdO: JCPDS 85-0713, Pd: ICCD no. 087-0643, α-Ga_2O_3: ICSD no. 27431)
(a) $PdGa_{0.5}/SiO_2$ (b) $PdGa_3/SiO_2$

The BET surface measured by N_2 physisorption and the coke content for both spent catalysts are given in Table 5.9.

Table 5.9, BET surface area and coke content over spent Pd-Ga/SiO_2 catalysts

Spent catalyst	BET surface area (± 1 m^2/g)	% decrease in surface area (%)	Coke deposition (mmol/g Pd+Ga)	Coke deposition (mmol/g cat)
$PdGa_{0.5}/SiO_2$	271	3.6	5.44 ± 0.05	0.163 ± 0.001
$PdGa_3/SiO_2$	262	3.3	1.63 ± 0.01	0.0816 ± 0.0008

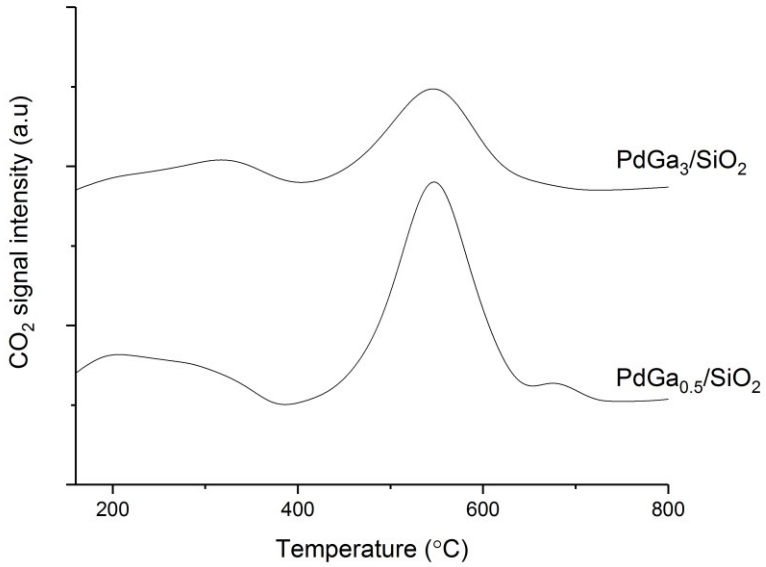


Figure 5.11, TPO of spent Pd-Ga/SiO_2 catalysts

Both catalysts lost similarly small amount of surface area after catalysis, hence it is unlikely that loss of surface area is the main cause of initial deactivation observed in $PdGa_3/SiO_2$ catalyst or even the gradual deactivation observed in both catalysts.

The carbonaceous species found on the Pd-Ga catalysts appear to be heavier compared to those on Ni-Ga catalysts, as the CO_2 evolution temperature of the major coke oxidation was found at 550 °C and another minor one at 680 °C in the case of $PdGa_{0.5}/SiO_2$. The amount of coke deposited on the Pd-Ga catalysts is nearly 3 orders of magnitude higher than that found on Ni-Ga/SiO_2 based catalyst (0.0064 mmol/g active metal). It is well known that the deposition of coke (often with low H/C ratio) on the palladium surface (and catalyst pores) causes slow

deactivation of the Pd-based catalysts over time [133, 157, 283]. Coking over Pd-based catalysts can be affected by various factors such as surface area, presence of certain metals, interactions with the support, etc. [157, 276]. For example, the lower coke content observed in the $PdGa_3/SiO_2$ might be due to the excess gallium (in the form of Ga_2O_3) on the $PdGa_3/SiO_2$ surface, which restricts the accessibility of Pd sites that are responsible for the transformation of carbon to aromatic/graphitic coke [276]. Therefore, in addition to the impacts of reaction products, the buildup of carbonaceous materials on the Pd-Ga based catalysts can also be a cause of the deactivation observed [133].

5.4 Conclusions

Pd promoted $NiGa(a)/SiO_2$ was investigated to improve the reducibility and catalytic performance of the Ni-Ga catalyst. The $Pd\text{-}NiGa(a)/SiO_2$ catalyst was successfully synthesised and was active and selective towards methanol synthesis from CO_2. It was found that the addition of Pd did not reduce the formation temperature of Ni-Ga intermetallic phase. However, there is clear enhancement of methanol synthesis activity, which is likely due to H_2 spillover from Pd. When CO is present in the feed gas, the Pd promoted catalyst lost more methanol synthesis activity due to high methane production, this is possibly due to the presence of free Pd and Ni. Palladium promotion of the Ni-Ga based catalysts shows promise but further experiments are needed to optimise the performance of the Pd promoted catalyst.

Active Pd-Ga based catalysts supported on SiO_2 can be successfully prepared. Despite the large excess of Ga in $PdGa_3/SiO_2$ catalyst, a Pd_2Ga intermetallic phase was preferentially formed. The resulting catalysts have activities similar to values reported in the literature and slightly better selectivity towards methanol synthesis. Both $Pd\text{-}Ga/SiO_2$ and $Ni\text{-}Ga/SiO_2$ based catalysts show similar trend of deactivation, which led to the conclusion that the decreasing accessibility of these active intermetallic compounds due to the competing adsorption of reaction products is the main cause of deactivation for these intermetallic base catalysts.

Moreover, the gallium content in the intermetallic catalysts influences both the initial activity and rate of deactivation. In Pd-Ga based catalysts, the deposition of carbonaceous species is also found to be significant. Overall, the good performance of the Pd-Ga/SiO_2 catalyst makes it a suitable candidate for the single-stage DME synthesis.

Chapter 6 Single-stage DME Synthesis over Intermetallic Catalysts and Solid Acids under CO_2/H_2

6.1 Introduction

The single-stage DME synthesis from syngas requires the combination of methanol synthesis and dehydration catalytic functions. For the methanol synthesis component, $Cu/ZnO/Al_2O_3$ catalyst has been studied extensively for both methanol-only synthesis and the one-step syngas to DME (STD) process. Although copper based catalyst has high methanol synthesis activity, it suffers deactivation by thermal sintering in the presence of water, especially under CO_2/H_2 [8, 112]. Moreover, many studies have demonstrated that the close proximity of Cu catalyst with solid acid catalysts (both γ-Al_2O_3 and zeolites) can cause rapid deactivation of both catalysts [224-226, 233, 238]. It was revealed that the detrimental interaction between Cu/ZnO and solid acid catalysts involves the surface transfer of active species [224, 238]. In the previous chapters, both Ni-Ga and Pd-Ga based intermetallic catalysts have shown good activity and selectivity towards methanol synthesis under CO_2/H_2. In addition, their intermetallic nature leads to the speculation that they might be more stable against contact-induced deactivation in the combined methanol and DME synthesis.

Various acidic catalysts can be used for the methanol dehydration reaction. Among them, γ-alumina (γ-Al_2O_3) is most investigated because of its low cost, good activity and selectivity towards DME synthesis [19]. However, as γ-alumina deactivates by strong adsorption of water [175, 179, 256], it was not considered to be a reliable methanol dehydration component for direct DME synthesis from CO_2 [19]. On the other hand, zeolites have received increasing attention due to their high stability in the presence of water, good methanol dehydration activity and tunable properties [19]. However, they can have poor stability when used as the

dehydration component for STD process due to various mechanisms, i.e. coke formation [196], de-alumination [284] and solid-state copper exchange [238].

As discussed in Chapter 2, it has been shown that the topology of zeolites greatly influences the selectivity of zeolites in MTH and STD processes [20, 284]. Many investigations has been focused on ZSM-5 since its medium to strong acid sites offer high methanol dehydration activity [19] and the medium pores prevent extensive coking without hindering the diffusion of the reactants and products in DME synthesis [222, 238, 285, 286]. Besides ZSM-5, ferrierite was shown to be very stable and selective towards DME synthesis for both methanol dehydration and single-stage DME synthesis owing to its unique topology [20, 200-202].

So far, there is very limited study on the performance and compatibility of the combined intermetallic compounds and solid acid catalysts. In this chapter, the catalytic performance and stability during the single-stage DME synthesis from CO_2/H_2 has been studied using intermetallic compounds (Ni-Ga and Pd-Ga based catalysts) as the methanol synthesis component and zeolites (ZSM-5 and FER) as the dehydration catalyst. These two particular zeolites were chosen because they have similar acidity, 10-membered ring structure but different topology [20]. γ-Al_2O_3 is also used to serve as a reference material. The main focus is on the use of ferrierite and ZSM-5 to allow direct comparison with work on Cu/ZnO based catalytic mixtures. First, the characterisations of calcined γ-Al_2O_3 and zeolites are given. The performance and stability of different dehydration catalysts with NiGa(a)/SiO_2 or $PdGa_{0.5}/SiO_2$ in separated beds (to eliminate possible effect of close proximity) was investigated in the continuous stirred tank reactor (CSTR) under CO_2/H_2. Next, the effect of proximity between the methanol synthesis and dehydration catalysts was studied using physical mixtures in the same gradientless reactor, where all particles were exposed to the same gas composition regardless of their positions in the reactor. The use of physical mixtures allows the individual component to be recovered and characterised easily to investigate the causes of any deactivation. In the last section, the impact of CO in the feed on the catalytic activity, selectivity and stability is investigated for all physical mixtures in a tubular flow reactor.

6.2 Characterisation of γ-Al_2O_3 and zeolites

γ-Al_2O_3 (Sasol), FER (55) (Zeolyst CP914) and ZSM-5 (50) (Zeolyst CBV5524G) were used as the solid acid catalysts. The XRD patterns for the fresh γ-Al_2O_3, FER (55) and ZSM-5 (50) are given in Figure 6.1. They are consistent with known patterns [20].

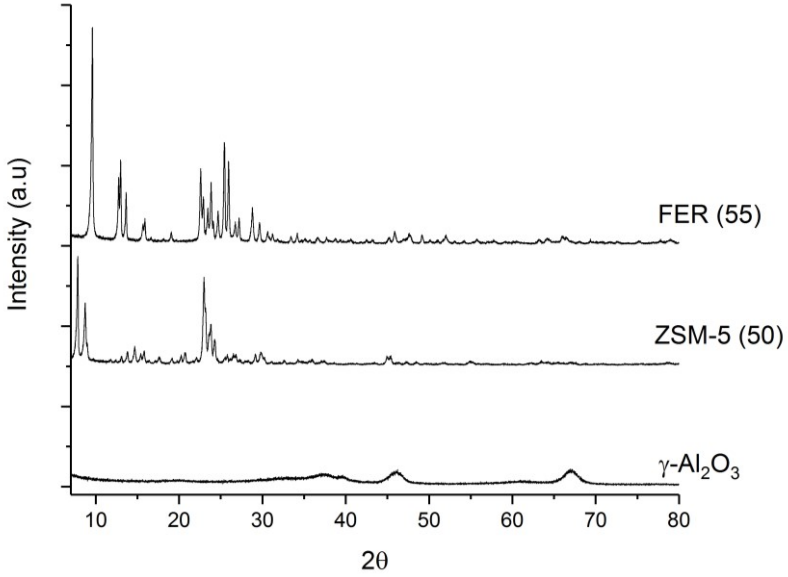


Figure 6.1, Diffraction patterns of fresh (calcined) FER (55) and ZSM-5 (50) and γ-Al_2O_3

The textural and chemical properties of these commercial solid acid catalysts have been studied extensively in the literature. Therefore data was directly taken from the work by R. Montesano [17, 287].

Table 6.1, Nominal composition, textural and chemical properties of γ-Al_2O_3, FER and ZSM-5 (data taken from Montesano's work [17])

	S_{BET} (m^2/g)	Pore volume (m^3/g)	SiO_2/Al_2O_3 (mol/mol)	LT NH_3 desorption (mmol/g)	HT NH_3 desorption (mmol/g)	Framework site conc.* (mmol/g)
γ-Al_2O_3	202	0.51	-	0.016		-
FER (CP914)	308	0.124	55	0.41	0.60	0.59
ZSM-5 (CBV5524G)	404	0.173	50	0.32	0.52	0.64

* calculated from nominal SiO_2/Al_2O_3 ratios

Ammonia temperature programmed desorption (NH_3-TPD) of zeolites in their protonated forms are adapted from Montesano [20] and given in Appendix C, which shows a low temperature (LT) and a high temperature (HT) desorption peak. These correspond to the desorption of weakly bonded ammonia and desorption of NH_3 from strong acid sites [288, 289] respectively. From the temperature of HT peak and by disregarding the possible effect of channel structure on the diffusion of NH_3, the order of acid strength was determined as FER (55) > ZSM-5 (50).

As microporous materials, both zeolites show significant adsorption at very low relative pressure (p/p°) in the nitrogen physisorption isotherm at 77 K (Appendix C Figure C.2). For ZSM-5, the isotherm corresponds to a monolayer overlapping with multilayer adsorption and a broad hysteresis in the mesoporous region due to inter-crystallite voids was observed. FER exhibits monolayer adsorption and hysteresis was only found near $p/p^\circ = 0.8$. This was considered to come from inter-crystallite voids due to small particle size and shape, as confirmed by SEM image (< 0.8 μm, plates) (Appendix C Figure C.3).

Prior to the catalyst tests, the acid catalysts were crushed to obtain desired particle size (106 – 250 μm) and calcined in air to obtain the required H-form. The details of catalyst preparation can be found in Chapter 3 section 3.2.2.

6.3 Performance of γ-Al_2O_3 and zeolites with intermetallic compounds for the combined methanol-DME synthesis in the CSTR under CO_2/H_2

6.3.1 Summary of catalyst tests

The experiments for various combination of MSC with solid acids and catalyst arrangement in the reactor are summarised in Table 6.2. Details of each experiment will be discussed in the following sections.

Table 6.2, Summary of catalyst tests

Methanol synthesis component	Methanol dehydration component	Separated beds		Physical mixture
		245 °C, 10 bar	270 °C, 30 bar	270 °C, 30 bar
$NiGa(a)/SiO_2$	-	✓	✓	
	γ-Al_2O_3	✓	✓	✓
	FER	✓	✓	✓
	ZSM-5		✓	✓
$Cu/ZnO/Al_2O_3$	-	✓		
	γ-Al_2O_3	✓		
	FER	✓		
	ZSM-5		✓	
$PdGa_{0.5}/SiO_2$	FER		✓	✓
	ZSM-5		✓	✓

6.3.2 $NiGa(a)/SiO_2$ as the methanol synthesis component (MSC)

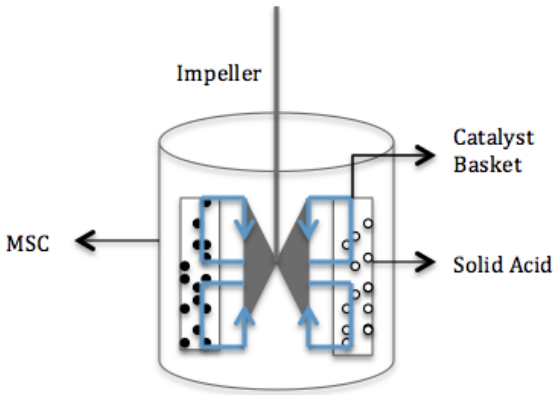


Figure 6.2, Schematic of MSC and acid catalysts in separated beds in the CSTR

The suitability of using NiGa(a)/SiO_2 as the MSC is investigated first using γ-Al_2O_3, FER and ZSM-5 as the dehydration component. To ensure that the intimate contact between catalyst components does not affect the measured performance, in this section, measurements were taken by packing catalysts in separated beds within the catalyst basket in the CSTR, as shown in Figure 6.2. In this arrangement, both catalytic components are exposed to the same gaseous composition, temperature and pressure.

6.3.2.1 Comparison between γ-Al_2O_3 and zeolites at 245 °C, 10 bar (separated beds)

The performance of NiGa(a)/SiO_2 and commercial Cu/ZnO/Al_2O_3 as the methanol synthesis component (MSC) in combination with solid acids are studied first at 245 °C and 10 bar (CO_2/H_2), the same conditions used in the study of methanol-only synthesis in Chapter 4 to allow direct comparison. However, since typical syngas to DME operate at higher temperature (260 – 280 °C) [19], these experiments will also be repeated at higher temperature (270 °C) and pressure (30 bar). The results are discussed in next section (6.3.2.2).

The conversion levels (around 0.6 – 1%, defined as the total carbon conversion to methanol and DME) are low because in the CSTR under CO_2-rich conditions, the reverse water-gas shift reaction maintains relatively high concentration of CO and water in the reactor, which deactivate the intermetallic NiGa(a)/SiO_2 catalyst according to the results in Chapter 4 section 4.2.3. Under these reaction conditions (245 °C, 10 bar), the total methanol production rates (defined as total amount of methanol and the methanol converted to DME, according to Equation 3.11 and Equation 3.12 in Chapter 3) of the combined methanol-DME synthesis for γ-Al_2O_3 or FER are similar to the methanol-only synthesis. This is because no thermodynamic synergy is obtained, since the methanol synthesis reaction is far from the equilibrium [290]. Moreover, it has been shown by various researchers that negligible synergy effect is observed under CO_2-rich condition due to favourable rWGS reaction producing a large amount of water [219, 291].

The results for NiGa(a)/SiO_2 and Cu/ZnO/Al_2O_3 are presented in Figure 6.3 (a) – (d) respectively. Since FER and γ-Al_2O_3 gave a similar product distribution, only the results for FER are given in Figure 6.3 (b) and (d) (γ-Al_2O_3 selectivity result is given in Appendix C Figure C.5).

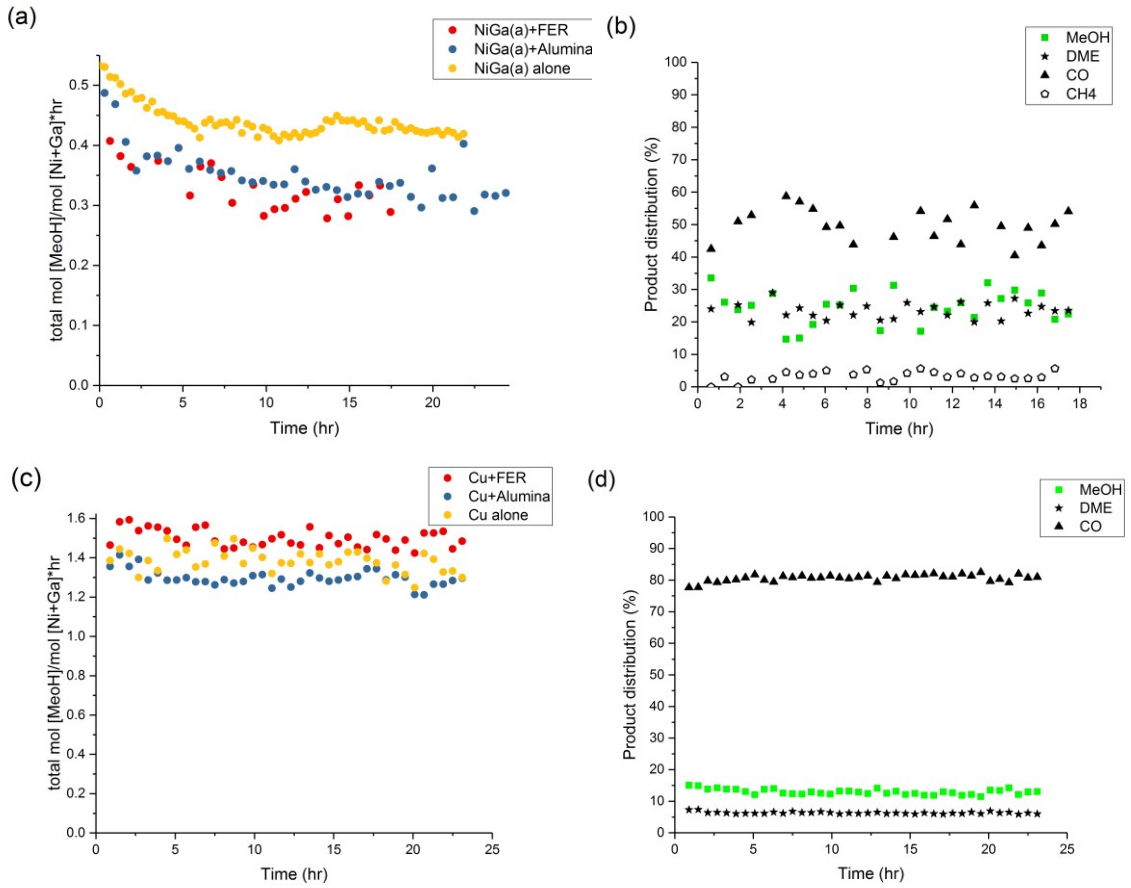


Figure 6.3, Total MeOH activity and selectivity at 245 °C, 10 bar (separated beds)
(a) NiGa(a)/SiO_2 as the MSC (b) Selectivity over NiGa(a)/SiO_2+FER
(c) Cu/ZnO/Al_2O_2 as the MSC (d) Selectivity over Cu/ZnO/Al_2O_2+FER

The slightly higher activity observed for the methanol-only synthesis is due to the relatively lower water concentration in the reactor in the absence of a methanol dehydration catalyst. In Chapter 4 section 4.2.3.2, it was proposed that products such as CO and water caused deactivation of the NiGa(a)/SiO_2 catalyst. Apart from the difference in activity level, the deactivation behaviour of the combined methanol-DME synthesis was the same as methanol-only synthesis for both γ-alumina and FER. That is, approximately 20% of the initial activity

gradually declined throughout 20 hours. This suggests that the deactivation behaviour of the separated bed catalysts is governed by the deactivation of the MSC.

In the reactions with solid acids, CH_4, methanol, DME and CO were detected (Figure 6.3 (b)). Methane selectivity (3% over NiGa(a)/SiO_2 + FER) is higher compared to methanol-only synthesis (< 0.8%) but CO production is similar. The additional CH_4 could have been produced from the surface methoxy species on the acid catalyst, as proposed by Hutchings et al. [292].

In the case of commercial Cu based catalyst systems, the activity of methanol-only synthesis is similar to the combined methanol-DME synthesis using either γ-alumina or FER. This is due to the relatively good stability of Cu catalyst at low conversion level, as discussed in Chapter 4 section 4.2.3.2.

6.3.2.2 Comparison between γ-Al_2O_3 and zeolites at 270 °C, 30 bar (separated beds)

Syngas-to-DME (STD) process usually takes place at a slightly higher temperature than methanol synthesis since the catalytic performance is greatly dependent on the reaction temperature. It has been previously demonstrated in the literature that a temperature range of 250 – 300 °C gives the highest concentration of oxygenates (MeOH and DME) [293] and the solid acid catalysts tend to be more active at above 250 °C [16]. However, a temperature above 300 °C is undesirable as Cu based MSC starts to sinter at high temperature [8, 294]. In addition, hydrocracking reactions over acid catalysts becomes more favourable and thermodynamic restricts the exothermic reactions at high temperatures [293]. Since the CO_2 hydrogenation to DME results in decreased number of moles, the conversion and DME yield of this process are both favoured at high pressure (typically ≥ 30 bar) [19]. Therefore, the performance of the NiGa(a)/SiO_2 + γ-alumina/FER/ZSM-5 system (separated beds) was studied at higher temperature and pressure (270 °C, 30 bar) to investigate the catalytic performance and stability of the catalysts.

The comparison between NiGa(a)/SiO_2 alone and with γ-Al_2O_3, ferrierite and ZSM-5 at 270 °C, 30 bar are presented in Figure 6.4. The conversion level achieved under these conditions ranges from 0.7 – 0 .9% (excluding ZSM-5).

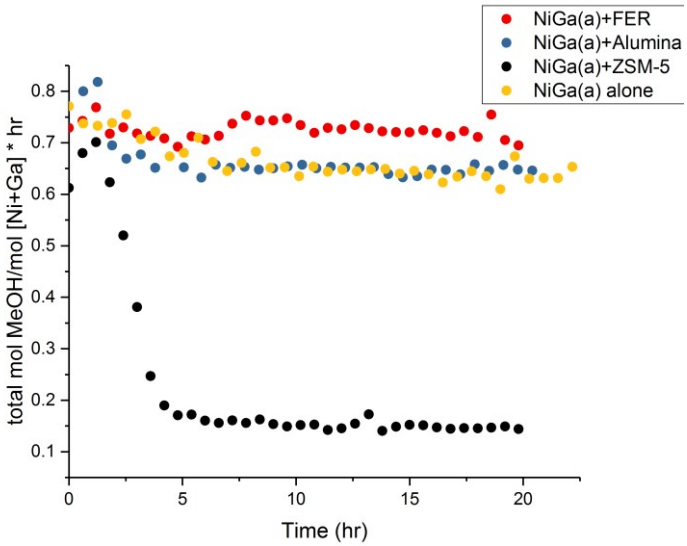


Figure 6.4, Total MeOH activity of NiGa(a)/SiO_2 with various solid acids at 270 °C, 30 bar

NiGa(a)/SiO_2 appears to work well as the methanol forming catalyst with FER and γ-Al_2O_3 at higher temperature since the activity profiles are similar to that of NiGa(a)/SiO_2 alone, suggesting that the deactivation behaviour of the separated catalysts at higher temperature and pressure is still governed by the deactivation of the MSC. The additional production of water and DME from the dehydration reaction does not seem to have significant adverse effect on the NiGa(a)/SiO_2 catalyst.

When FER was used as the dehydration catalyst, the methanol synthesis and dehydration activity is slightly higher. γ-Al_2O_3 appears to have a higher activity initially, but soon it declines by 20% to values lower than that of FER. This is likely due to the competitive adsorption of water on γ-Al_2O_3, which is known to reduce number of acid sites available for methanol dehydration [175, 179, 256]. At this temperature and pressure, the CH_4 yield when a dehydration catalyst is present is similar to MSC alone, implying that CH_4 is produced mainly from NiGa(a)/SiO_2.

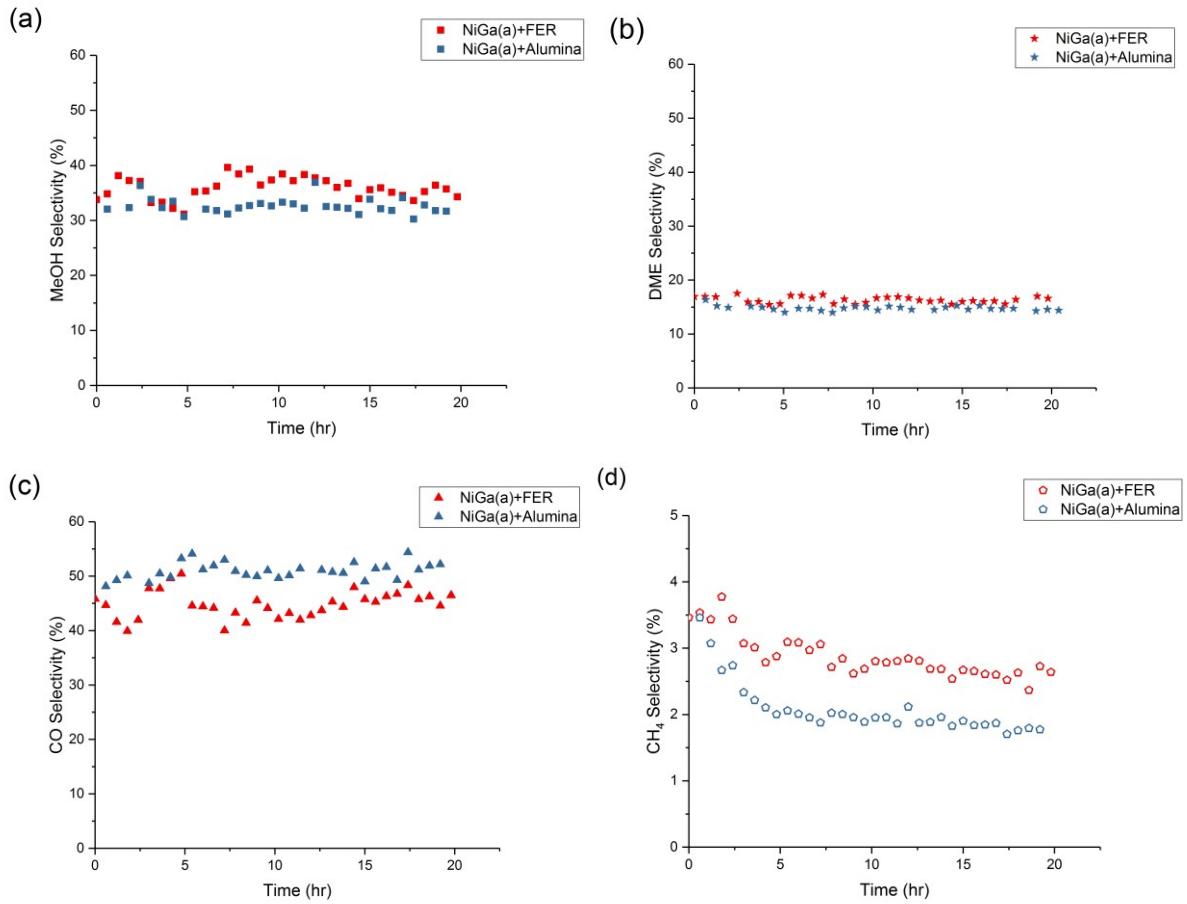


Figure 6.5, Product distribution of NiGa(a)/SiO_2 with FER and γ-Al_2O_3 at 270 °C, 30 bar (a) MeOH (b) DME (c) CO (d) CH_4

Instability in ZSM-5 based catalysts

ZSM-5 gave a completely different trend in catalytic performance, Figure 6.4. Initially in the first 2 hours on stream, a similar activity to FER or γ-Al_2O_3 was achieved. In the next 2 hours, the methanol synthesis and dehydration activity rapidly dropped to about 21% of the initial value and stayed fairly constant at this low value throughout the remainder of the run. Initially, DME and methanol are the main carbon products besides CO and CH_4. The drop in methanol and DME synthesis activity is accompanied by the formation of various hydrocarbons. This phenomenon is well-known in methanol-to-hydrocarbon processes, where a kinetic induction period is often observed due to the establishment of a carbon pool within zeolites that are active for MTO process (such as ZSM-5). The GC profile of the product distribution at 20th hour can be found in Figure 6.6. Since the hydrocarbons produced over ZSM-5 have been widely reported in the literature, the hydrocarbons produced in this experiment were not

calibrated. The formation of these hydrocarbons, which are mainly paraffins and olefins, over ZSM-5 based DME synthesis catalyst under CO/H_2 has been previously reported by Montesano [20]. In contrast to the fast deactivation observed, ZSM-5 in separated beds with $Cu/ZnO/Al_2O_3$ was reported to give stable performance under CO_2/H_2 [17] in an internal recycle Berty reactor. The reason for the good stability was considered to be a consequence of high water partial pressure under CO free condition, which reduces the acidity of the zeolite. Although the type of reactor used is different from literature in this study, the more important difference is that $NiGa(a)/SiO_2$ has significantly lower total CO_2 conversion (to DME and CO) compared to the Cu based catalyst used in literature. Consequently, the water content in the reactor is relatively low, which is insufficient for adequate reduction of acidity on the ZSM-5. At the same time, MeOH triggers ZSM-5 to produce hydrocarbons since the intersections of medium-size channels in the ZSM-5 provide enough space for formation and diffusion of entrained hydrocarbon species [20]. Therefore, the $MeOH/H_2O$ ratio is an important factor that influences the DME selectivity and stability of the ZSM-5 catalyst.

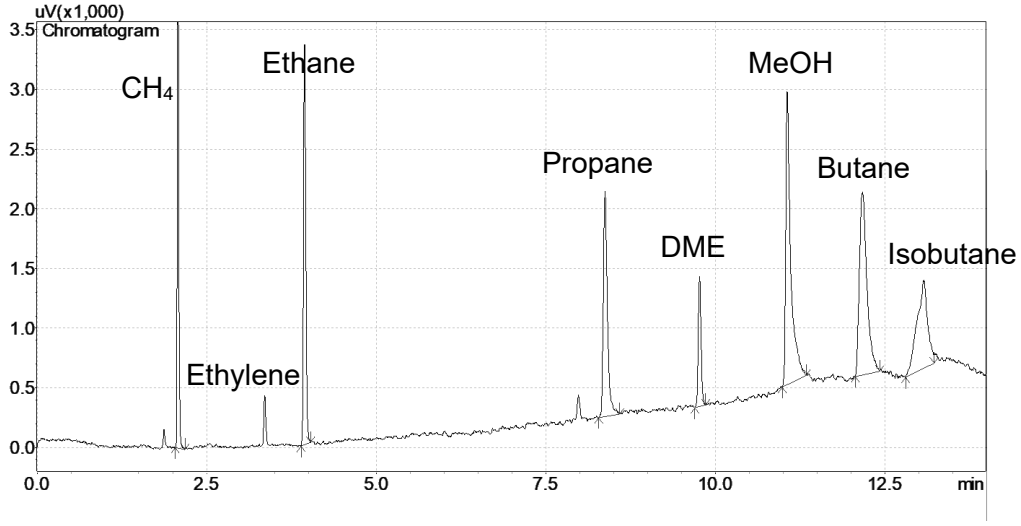


Figure 6.6, Product distribution over $NiGa(a)/SiO_2$ and ZSM-5 obtained from GC

To confirm the difference in stability of ZSM-5 between current study and literature is mainly due to a difference in the total CO_2 conversion, the same experiment was carried out with $Cu/ZnO/Al_2O_3$ + ZSM-5 (separated beds) in the CSTR. The performance over this catalytic system is shown in Figure 6.7 (a) and (b).

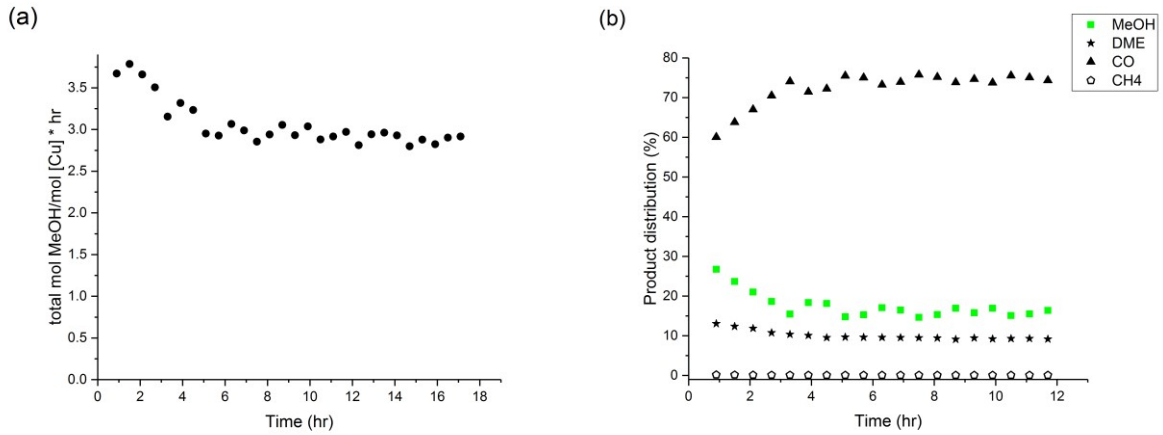


Figure 6.7, Performance of $Cu/ZnO/Al_2O_3$ and ZSM-5 at 270 °C, 30 bar (separated beds) (a) Total MeOH production rate (b) Product distribution

Indeed, the performance of the separated Cu based catalyst and ZSM-5 is rather stable throughout the run. MeOH accounts for 15% of total products, DME 10%, only trace level of CH_4, ethane were found. No other hydrocarbon was detected. This supports the speculation that the instability of ZSM-5 towards methanol and DME synthesis observed in the $NiGa(a)/SiO_2$ system is related to the MeOH to water ratio. In fact, when $Cu/ZnO/Al_2O_3$ was used, 1.7 v/v% water prevails in the reactor due to high overall conversion whereas only 0.14 v/v% water is present when $NiGa(a)/SiO_2$ was used as the MSC. Water has the ability to reduce the acidity of ZSM-5, therefore hydrocarbon formation is limited if the reaction environment is water-rich [17].

6.3.2.3 Characterisation of spent catalysts from CO_2/H_2 runs

To investigate how the $NiGa(a)/SiO_2$ and acid catalysts deactivate, the individual catalysts were characterised by XRD, TPO and in some cases, N_2 physisorption.

The XRD diffraction patterns for both fresh (calcined) and spent γ-Al_2O_3 or zeolites are presented in Figure 6.8.

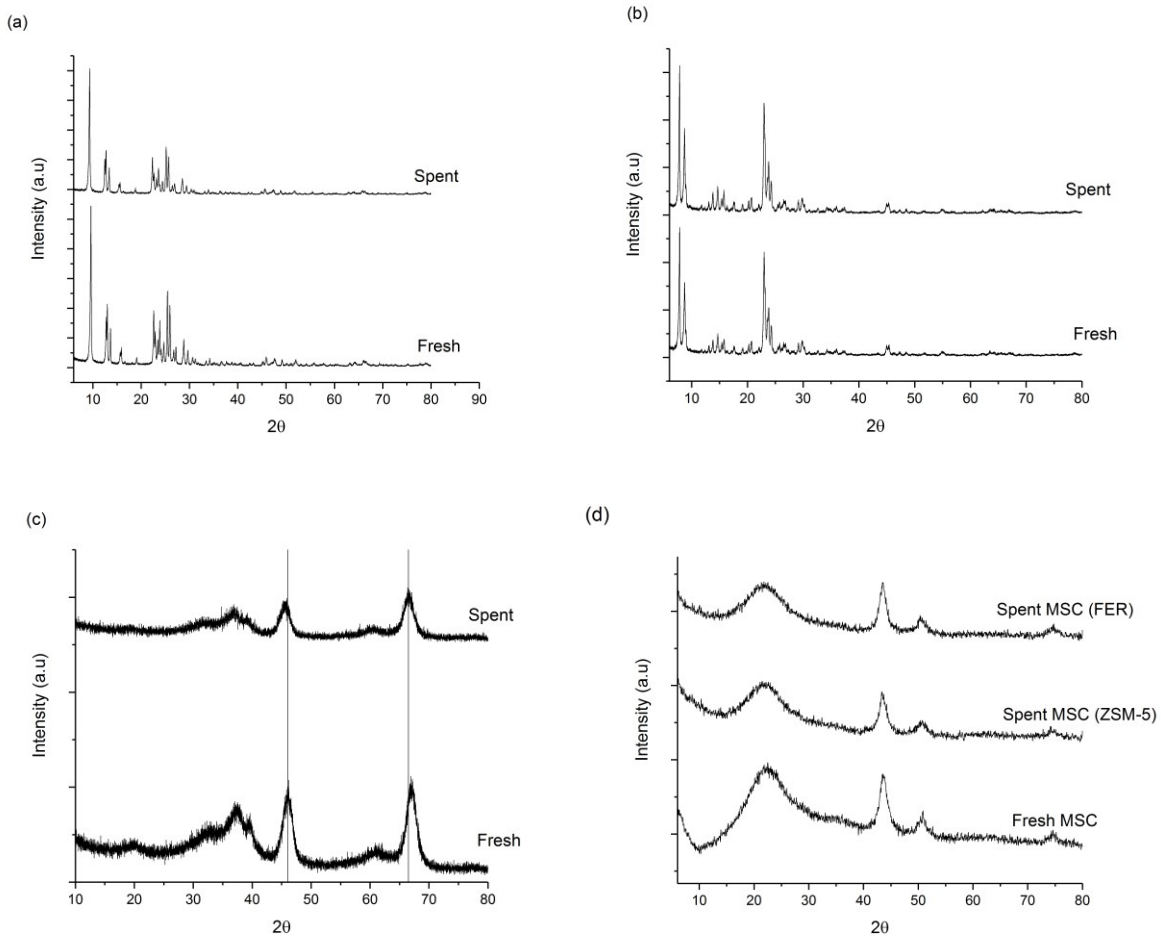


Figure 6.8, XRD patterns of spent catalysts
(a) FER (b) ZSM-5 (c) γ-Al_2O_3 (d) Spent NiGa(a)/SiO_2 with different zeolites

For the zeolites, no obvious change in peak positions was observed. However, the intensity of all the peaks is significantly lower compared to the fresh zeolites. This could be caused by the deposition of carbonaceous materials in the pores within zeolites [17].

For γ-Al_2O_3, all peaks appear to have shifted towards lower 2θ values and the major peaks became broader. This corresponds to a particle size increase of around 10%. In addition to the prevailing deactivation by the adsorption of water on the surface of γ-Al_2O_3, an irreversible deactivation mechanism has also been reported [178]. This involves the formation of surface boehmite (aluminium oxide hydroxide, γ-AlO(OH)) under high partial pressures of steam. However, there is no evidence that γ-AlO(OH) has been formed on the spent γ-Al_2O_3 since the characteristic diffraction peaks of boehmite at 2θ = 14.55° and 28.25° are not observed in Figure 6.8 (c). This is expected since the water partial pressure that the γ-Al_2O_3 catalyst

exposed to in the present experiments is far from the pressure (14 bar) used in the literature where boehmite was observed after a long exposure time [178].

For the spent MSC component, negligible changes in peak position suggest that the intermetallic phase was maintained throughout the run. However, the peak at 2θ = 43.6° is broader in the spent NiGa(a)/SiO_2. This translates to a particle size increase of 24% and 33% when FER and ZSM-5 are used as the solid acid. Compared to a negligible particle size increase in methanol-only synthesis (Chapter 4 Table 4.9), it is obvious that the additional water in MeOH-DME synthesis accelerates particle size growth [8].

Table 6.3, Coke content on methanol synthesis and dehydration components

Coke content	Methanol synthesis component (μmol/g)	Methanol dehydration component (μmol/g)	Coke selectivity* (mg C/g_{MeOH})
NiGa(a)/SiO_2 + FER	5.48 ± 0.05	4.59 ± 0.05	0.173 ± 0.009
NiGa(a)/SiO_2 + ZSM-5	23.8 ± 0.2	48.9 ± 0.5	1.22 ± 0.06
NiGa(a)/SiO_2 + γ-Al_2O_3	8.47 ± 0.08	10.3 ± 0.1	0.41 ± 0.02

*coke selectivity is defined as total mass of coke per mass of MeOH converted (to DME, hydrocarbons and coke) [17]

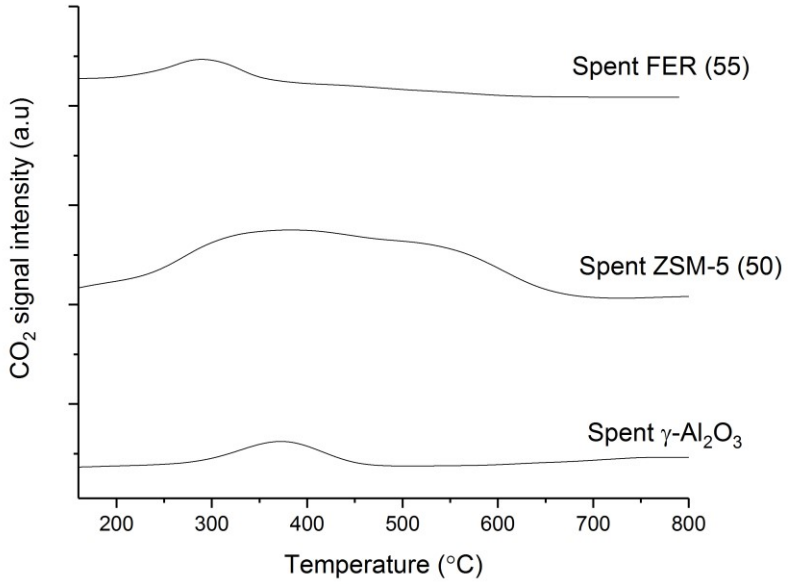


Figure 6.9, TPO profiles for spent solid acid catalysts

Coke deposition is recognised as one of the main causes of deactivation in the single-stage DME synthesis, especially over zeolites [196]. Due to the nature of reaction under CO free condition, the conversion level is low and selectivity to methanol and DME is high in most cases. Therefore, coke content and coke selectivity on all catalysts are low with the exception of NiGa(a)/SiO_2 and ZSM-5 in separated beds (Table 6.3). Since significant formation of hydrocarbons was observed over separated NiGa(a)/SiO_2 and ZSM-5, it is not surprising that coke deposition is most severe on these catalysts and ZSM-5 has high selectivity to coke. In particular, over the spent ZSM-5 catalyst the oxidation of carbonaceous species occurs continuously from 310 °C to 560 °C [20]. This suggests that coke ranging from lighter, more hydrogenated (or oxygenated) species to bulkier aromatics was formed due to the strong acidity of the ZSM-5 catalyst [17]. The deposition of these carbonaceous materials significantly reduces the active sites on both catalysts and hinders the transport of reactants and products, leading to the steep drop of activity [196, 238, 295].

For the spent FER, the amount of coke on the dehydration component is comparable to that formed on the methanol synthesis component and coke oxidation was found at around 300 °C (light coke). Over the spent γ-Al_2O_3, the amount of coke was slightly higher compared to

the spent FER and the coke oxidised at a slightly higher temperature (380 °C). Evidently, very bulky carbonaceous species were not formed over these two solid acids. Therefore, it is unlikely that coke formation is responsible for the deactivation in most catalytic systems but for ZSM-5 separated from NiGa(a)/SiO_2, it is certainly a factor that contributes to the instability of the catalytic performance. The BET surface area of the spent NiGa(a)/SiO_2 in separated ZSM-5 was measured to be 239 m^2/g, which is only slightly lower compared to a fresh sample (250 m^2/g).

6.3.2.4 Study of NiGa(a)/SiO_2 with solid acids in physical mixtures – effect of proximity

The detrimental interactions between the methanol synthesis and dehydration functions that cause significant deactivation have been widely reported for physical mixtures and composite catalysts [224-226]. As discussed in Chapter 2 section 2.2.4, there are different opinions regarding the efficiency of admixed systems compared to the hybrid catalysts [19]. In both cases, it has been shown that the interactions between the two catalysts cause deactivation [224, 226, 238]. García-Trenco et al. suggested that the extent of interaction due to close proximity is lower in physical mixtures [238]. However, a major advantage of using physical mixture is the ease of separation and characterisation of individual catalyst components post reactions, which allows the cause of deactivation to be determined more reliably. Therefore, to determine the effect of close contact between NiGa(a)/SiO_2 and solid acid catalysts and find out the cause of any deactivation, physical mixtures are used in the following section. The schematic of the catalyst set-up is shown in Figure 6.10. The NiGa(a)/SiO_2 catalyst was ex situ reduced and passivated using the technique described in Chapter 4. It was then mixed with the dehydration catalyst in a weight ratio of 1:1 [20] before loading into the reactor. The resulting physical mixture was re-activated in situ under the conditions (340 °C, 5% H_2/N_2 for 3 hours) for the passivated MSC to recover its activity.

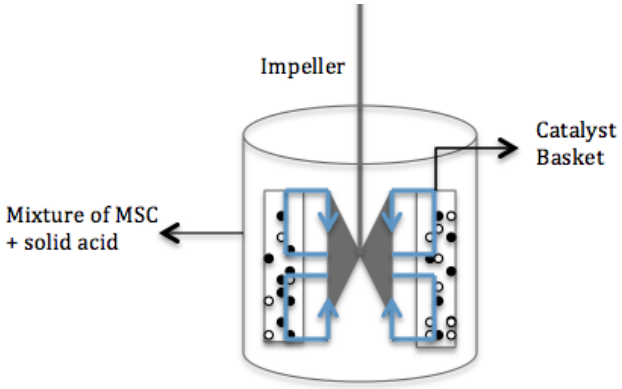


Figure 6.10, Schematic of physical mixture of MSC with solid acids in the CSTR

The performance of the physical mixture of NiGa(a)/SiO_2 and various acid components was investigated at 270 °C, 30 bar, the same conditions as those used for the study of separated beds. The total methanol production rate for each solid acid in with different proximity is presented in Figure 6.11 (a) – (c). The selectivity will be discussed later.

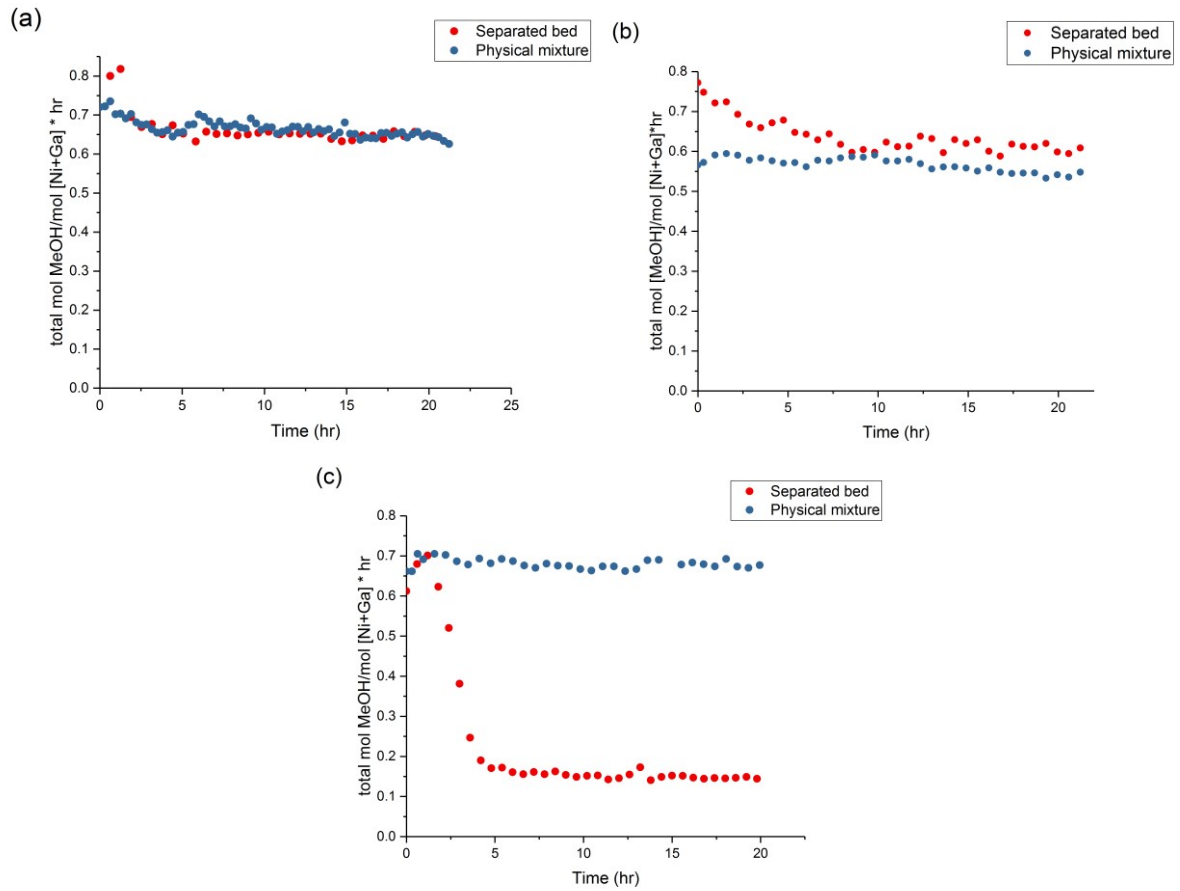


Figure 6.11, Comparison of the total MeOH activity between MSC + solid acid in separated beds and physical mixtures

(a) NiGa(a)/SiO_2 + γ-Al_2O_3 (b) NiGa(a)/SiO_2 + FER (c) NiGa(a)/SiO_2 + ZSM-5

There is always fast deactivation in the first 5 hours on stream, this is mainly due to the deactivation of the MSC by products, as discussed in the previous chapter.

γ-Al_2O_3 as the solid acid component

When γ-Al_2O_3 was used (Figure 6.11 (a)), it can be seen that both catalytic systems gave similar methanol synthesis and dehydration activity throughout the run. This suggests that the physical separation between NiGa(a)/SiO_2 and γ-Al_2O_3 does not affect the reaction rates. However, catalysts that are separated have higher methanol and DME selectivity while the physical mixture produces more CO and CH_4 (Figure 6.12). This observation suggests that the contact between NiGa(a)/SiO_2 and γ-Al_2O_3 may have caused a slight loss of active sites on the MSC that are responsible for methanol synthesis (Ga-rich sites) or altered the surface composition of the MSC. Since the difference in selectivity requires contact time and close proximity, it is likely the interaction between the two catalytic functions involve surface transport of active species. The possible causes for this will be discussed later.

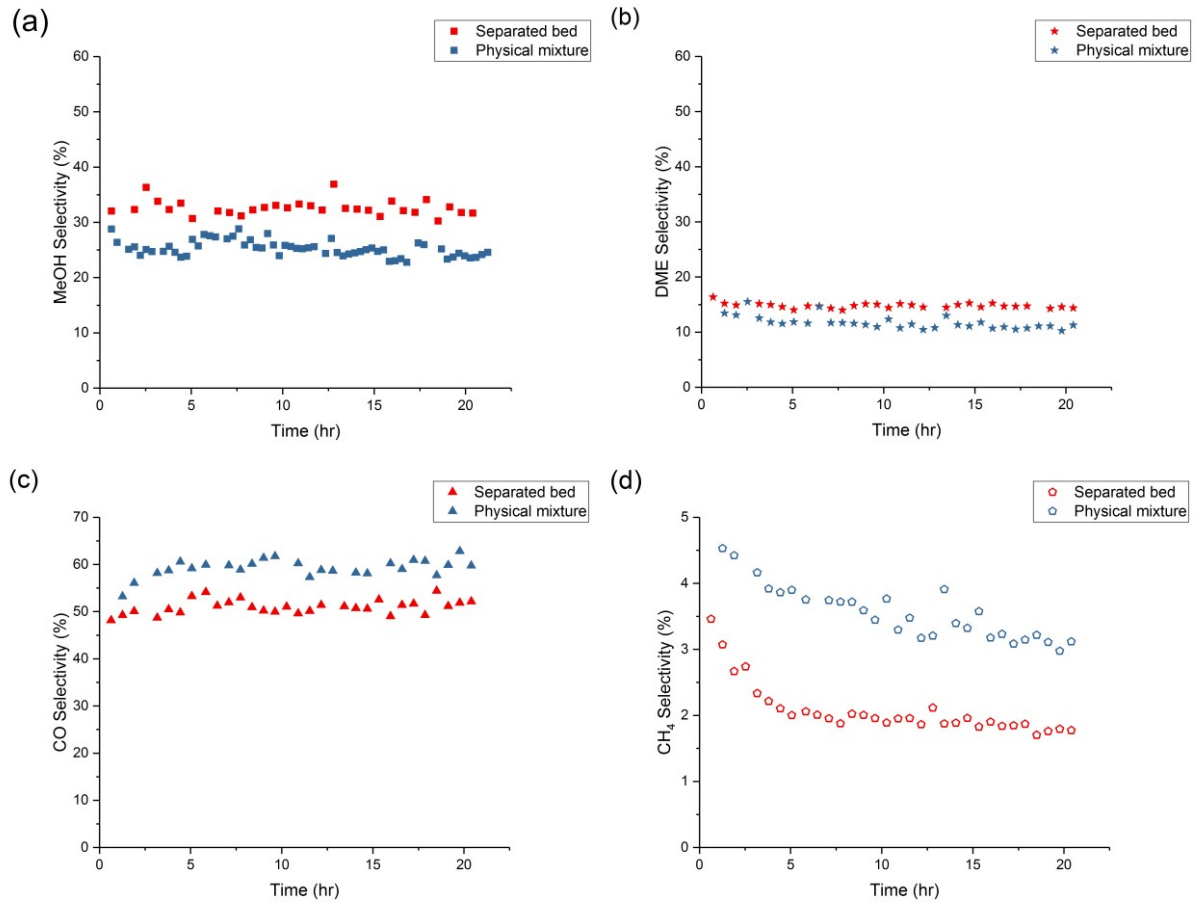


Figure 6.12, Comparison between the selectivity of NiGa(a)/SiO_2 + γ-Al_2O_3 in separated beds and physical mixture
(a) MeOH (b) DME (c) CO (d) CH_4

FER as the solid acid component

From Figure 6.11 (b), it is clear that the FER packed in separated bed had consistently higher activity (even in the initial period) compared to physical mixture throughout the entire experimental run. If the deactivation in the physical mixture is due to catalyst exposure to the reactants, the initial activity should be similar regardless of physical separation between the two catalytic functions. In addition, the absence of initial deactivation period over the physical mixture indicates that the close contact between the two catalytic functions had already caused a loss of active sites on NiGa(a)/SiO_2 even before catalysis. Therefore, it is highly likely that deactivation of the physical mixture happens in earlier stages, for example, during mixing or in situ reduction of catalyst mixtures. The dependence of reaction rate on catalyst proximity also implies that surface transport of species from one catalyst to the other [224]. This deactivation mechanism will be discussed in more detail in the next section. In contrast to γ-Al_2O_3, the methanol and DME selectivity are similar regardless of separation between the catalytic components, the results are given in Appendix C Figure C.6.

ZSM-5 as the solid acid component

As discussed in previous section, the separated ZSM-5 deactivates rapidly and produces a lot of hydrocarbons. With a physical mixture, completely different performance and selectivity were obtained (Figure 6.13). For convenience, the performance (total methanol production rate) of NiGa(a)/SiO_2 + ZSM-5 (physical mixture) is reproduced from Figure 6.11 (c) and presented in Figure 6.13 (b). The activity trend is similar to those obtained using FER or γ-Al_2O_3. This suggests that the close proximity between the two catalytic functions suppresses hydrocarbon formation on the ZSM-5 catalyst, making it as stable and selective as FER or γ-Al_2O_3. When the two catalysts are packed in physical mixture, the surface diffusion of

adsorbed water or surface hydroxyl across the contact zone might be responsible for the reduced acidity of the ZSM-5 catalyst [296, 297].

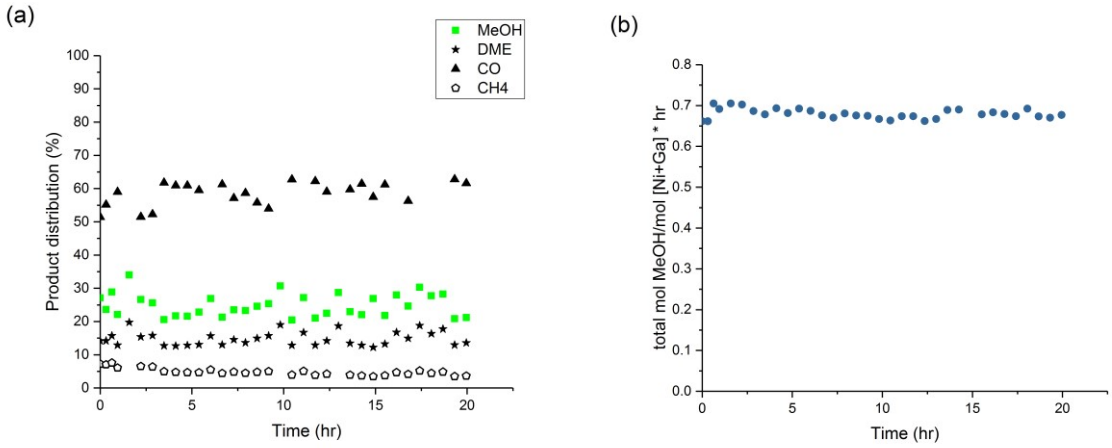


Figure 6.13, Catalytic performance NiGa(a)/SiO_2 + ZSM-5 in physical mixture (a) Product distribution (b) Total MeOH production rate Reproduced figure from Figure 6.11(c)

Metal migration in spent solid acid catalysts

To determine the cause of different catalytic performance observed, the physical mixtures were separated by manual inspection and the individual component was characterised.

Various studies have demonstrated that the close proximity of catalytic functions could result in deactivation by the transfer of active species from one catalyst component to the other [224, 225, 238] at the point of contact. Montesano [17] found that in physical mixture of Cu/ZnO/Al_2O_3 and γ-Al_2O_3, the migration of zinc-containing species to the acid catalyst is the most significant due to surface diffusion driven by the chemical potential gradient. Although the active metals in NiGa(a)/SiO_2 catalyst was expected to be more structural stable due to strong intermetallic bonding between Ni and Ga, the possibility of active-metal migration cannot be ruled out since it has been reported that gallium could de-alloy from its intermetallic state to form Ga_2O_3 [13, 133, 156]. As shown in the literature, the solid-state ion exchange of ZSM-5 with Ga_2O_3 could take place upon H_2 reduction [298, 299]. To determine if metal migration took place and was a possible cause of the dependence of activity on the catalyst proximity, the spent methanol dehydration catalyst particles were separated from the physical

mixture and analysed by ICP – OES (using HF digestion). Moreover, it was speculated that if metal transfer did occur, it might have happened even before the reaction took place. The most likely time for this to happen is during the re-activation of the physical mixture since it has been demonstrated that the metal transfer could be facilitated by a reductive environment [298, 299]. Hence, a blank ICP analysis was conducted over a mixture of NiGa(a)/SiO_2 and FER that was re-activated, cooled down and separated without being exposed to CO_2/H_2 catalysis. The results are summarised in Table 6.4.

Table 6.4, Metal content on the recovered solid acids from NiGa(a)/SiO_2 based physical mixtures

Sample	Ni (± 10 ppm)	Ga (± 1 ppm)	Ni:Ga Ratio
Mixed & reduced FER	51	24	1.78
Spent γ-Al_2O_3	26	48	0.54
Spent FER	65	30	2.17
Spent ZSM-5	67	34	1.97

Clearly, transfer of both Ni and Ga occurred in all the physical mixtures. It would appear that most of the migration took place during the re-activation stage. For spent zeolites (FER and ZSM-5), the amount of metal transfer is similar and the ratio of Ni to Ga transferred is slightly lower than the bulk value of the MSC (2.34). This is expected because at point of contact between the MSC and the solid acid, the surface of NiGa(a)/SiO_2 is enriched with gallium as shown by XPS analysis in Chapter 4 Table 4.5 and in literature [128]. However for γ-Al_2O_3, the amount of Ni found was significantly lower while more Ga appears to have migrated to γ-Al_2O_3. This could explain why the selectivity to CO and CH_4 increased in the physical mixture of NiGa(a)/SiO_2 + γ-Al_2O_3. Evidently, the metal migration rates and mechanisms for zeolites and γ-Al_2O_3 are different, perhaps not surprising since they have different surface properties, surface area, particle size, etc. Ion exchange, relevant to zeolites, has been studied for various salts and oxides under different environment. This mechanism is driven by the imbalance of

charge due to isomorphous substitution of Al^{3+} ions in the crystalline framework of zeolites. Compensation must be made by extra-framework metal cations, like those from the methanol synthesis catalyst (i.e. Cu, Zn) [17, 226, 284]. For γ-Al_2O_3 based mixtures, different mechanisms have been proposed. García-Trenco and co-workers proposed a water-facilitated migration of Al^{3+} species from solid acids [226] to the MSC, modifying the interaction between the components in the Cu/ZnO catalyst. Peng and co-workers suggested that it was the transfer of Cu and Zn to γ-Al_2O_3 that causes deactivation by reducing the number of active sites. However, Montesano [17] speculated that the close contact between the two catalytic functions provides a chemical potential sink for ZnO_x migration, hence reduces the Cu surface area. Since most of the studies on metal transfer were done on Cu based catalyst, it is difficult to determine the exact mechanism for the transfer of intermetallic compounds to the acid catalysts without more detailed research.

Further characterisation of individual components in the spent physical mixtures

Since the ICP analysis of spent materials requires at least 100 mg for analysis of elements at ppm level. The quantification of metal transfer was a priority as it was considered to be the controlling mechanism for the deactivation observed in the physical mixtures. The amount of remaining solid acid catalysts was only enough for the next important characterisation test – temperature programmed oxidation. As the previously obtained characterisation results for the separated bed study showed no obvious change in catalyst structure after catalysis, BET and XRD analyses were not carried out for the solid acid recovered from the physical mixture. This is part of the reason that the spent MSCs from the physical mixture were not characterised, another reason being the inefficient recovery of the MSC from the physical mixture (recovered MSCs were mixed with fine solid acid particles that were impossible to remove).

The coke content for physical mixtures are summarised in Table 6.5 below. The values for separated beds are included for comparison.

Table 6.5, Comparison of coke content on different catalyst arrangements (NiGa(a)/SiO_2 as the MSC)

	Catalyst separation	Methanol synthesis component (µmol/g)	Methanol dehydration component (µmol/g)	Coke selectivity (mg C/g_{MeOH})
NiGa(a)/SiO_2 + FER	Physical mixture	6.54 ± 0.06	9.9 ± 0.1	0.43 ± 0.02
	Separated bed	5.48 ± 0.05	4.59 ± 0.05	0.173 ± 0.009
NiGa(a)/SiO_2 + ZSM-5	Physical mixture	6.22 ± 0.06	2.94 ± 0.03	0.998 ± 0.005
	Separated bed	23.8 ± 0.02	48.9 ± 0.05	1.22 ± 0.06
NiGa(a)/SiO_2 + γ-Al_2O_3	Physical mixture	7.05 ± 0.07	4.07 ± 0.04	0.161 ± 0.009
	Separated bed	8.47 ± 0.08	10.3 ± 0.1	0.41 ± 0.02

As no additional formation of hydrocarbon was found over all three physical mixtures, it is unlikely that extent of coking would be different from separated beds.

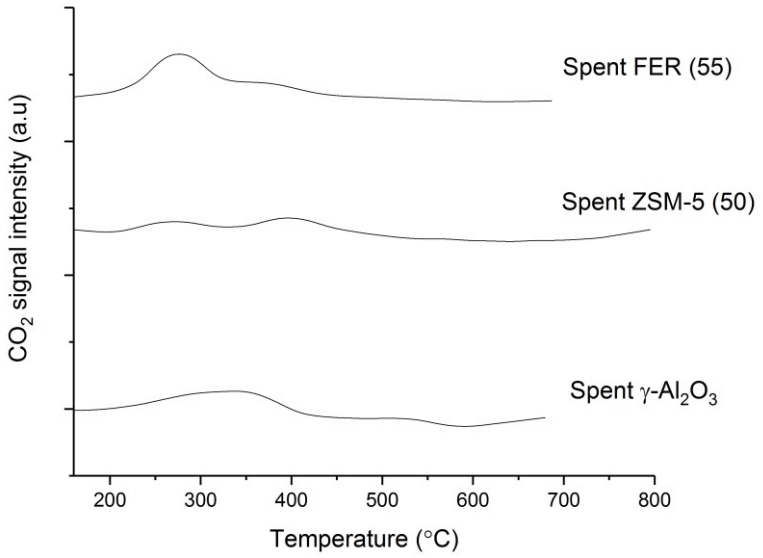


Figure 6.14, TPO profiles for spent solid acids in physical mixture

For ZSM-5, the observed stable performance over physical mixture was linked to a significantly lower amount of coke found in individual catalyst from the physical mixtures. Moreover, heavy coke was not found as the oxidation temperature was below 400 °C. This is probably due to the suppression of coking in the presence of relatively high surface water concentration when the MSC and ZSM-5 catalysts were in close contact, as discussed above. For FER based mixture (especially on FER), the amount of coke deposition is higher. This is consistent with the more pronounced deactivation and slightly higher CO production observed over the physical mixture. For both FER and γ-Al_2O_3, CO_2 evolution temperatures are similar in the case of physical mixture and separated bed, suggesting that the type of coke formed is similar regardless of physical separation.

6.3.3 $PdGa_{0.5}/SiO_2$ as the methanol synthesis component for the single-stage DME synthesis from CO_2/H_2

6.3.3.1 Performance of $PdGa_{0.5}/SiO_2$ + zeolites in separated beds

Pd-Ga based catalyst has been demonstrated to be a promising methanol synthesis catalyst due to its good activity and selectivity. Most of the previous works use Ga_2O_3 both as a support and the source of Ga (promoter) for the formation of Pd_2Ga intermetallic phase with Pd, for example, Pd/Ga_2O_3 [264] or Ga_2O_3-Pd/silica [127]. Due to the acidic nature of Ga_2O_3, it has been shown that the DME is produced as a byproduct over these Pd-Ga based catalysts along with methanol. In the work by Oyola-Rivera and co-workers [264], the DME selectivity ranges from 0 to 22% depending on the type of Ga_2O_3 support used. Attempts to increase the selectivity to DME were made by the addition of niobium oxide, which increased the acidity of Ga_2O_3 support. However, there is limited literature on the use of Pd_2Ga intermetallic based catalyst as the methanol synthesis component combined with other solid acid catalysts for the single-stage DME synthesis. In this section, the use of $PdGa_{0.5}/SiO_2$ (as prepared and tested in Chapter 5) as the MSC with FER and ZSM-5 is investigated and compared to $NiGa(a)/SiO_2$. The reactions were run under the same temperature and pressure as before (270 °C, 30 bar,

CO_2/H_2). Separated beds are used to eliminate the effect of proximity between catalytic functions.

The conversion level obtained using $PdGa_{0.5}/SiO_2$ is slightly higher (1.3%) than $NiGa(a)/SiO_2$ (0.9%) but the normalised activity of $PdGa_{0.5}/SiO_2$ is significantly higher due to low active metal content. The total MeOH production rates per mole of active metals and product distribution for FER and ZSM-5 are presented in Figure 6.15 and Figure 6.16. The initial conversion obtained over separated $PdGa_{0.5}/SiO_2$ + FER is 1.4% while the conversion level for separated $PdGa_{0.5}/SiO_2$ + ZSM-5 dropped from 1.2% to 0.4%. Nevertheless, the conversion obtained over $PdGa_{0.5}/SiO_2$ based catalysts is higher than $NiGa(a)/SiO_2$.

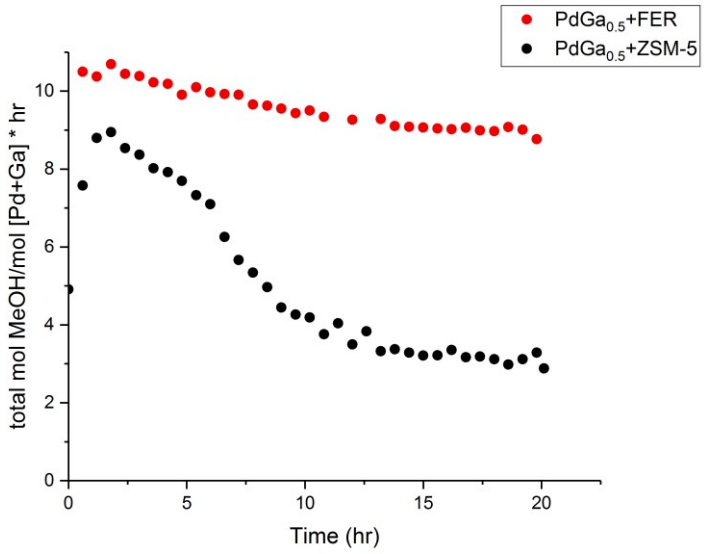


Figure 6.15, Total MeOH production rate for $PdGa_{0.5}/SiO_2$ + FER/ZSM-5 at 270 °C, 30 bar (separated bed)

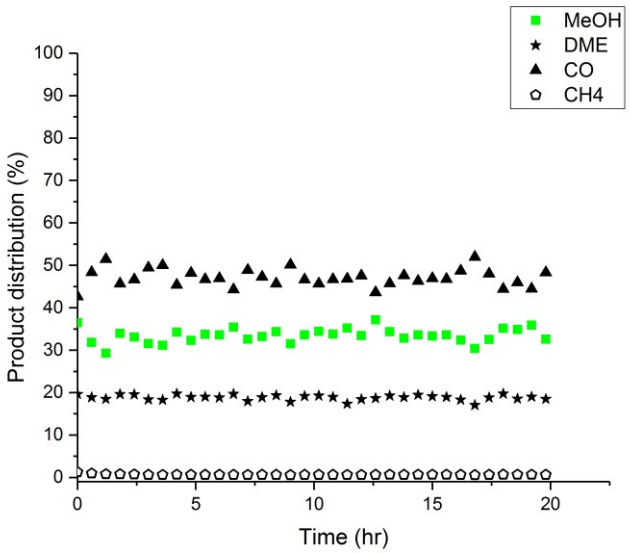


Figure 6.16, Product distribution for $PdGa_{0.5}/SiO_2$ + FER at 270 °C, 30 bar (separated bed)

In $PdGa_{0.5}/SiO_2$ + FER system, although water is known to have deleterious effect on the $PdGa_{0.5}/SiO_2$ catalyst [127], there was no obvious change in the deactivation behaviour or selectivity from methanol-only synthesis. This system showed similar trend of deactivation and product distribution as the $NiGa(a)/SiO_2$ + FER system.

Again, ZSM-5 begins to lose methanol and DME synthesis activity shortly after it was exposed to the reactants as hydrocarbons were formed. However, the rate of deactivation over $PdGa_{0.5}/SiO_2$ + ZSM-5 was found to be lower than $NiGa(a)/SiO_2$ + ZSM-5 as it took nearly 15 hours for the methanol synthesis and dehydration activity to reach a stable value. Moreover, the extent of deactivation was less severe (33% of the maximum activity remained at the end of the run). The difference in deactivation rate could be attributed to the higher total CO_2 conversion (thus higher water concentration) over $PdGa_{0.5}/SiO_2$. The hydrocarbons produced over $PdGa_{0.5}/SiO_2$ + ZSM-5 are the same as $NiGa(a)/SiO_2$ + ZSM-5, the GC profile showing the distribution of products can be found in Appendix Figure C.7.

6.3.3.2 Effect of proximity between $PdGa_{0.5}/SiO_2$ and zeolites

As discussed previously, the majority of metal transfer from $NiGa(a)/SiO_2$ occurs during the re-activation step after mixing with solid acids. Since $PdGa_{0.5}/SiO_2$ requires a lower re-

activation temperature, it is likely that the extent of metal migration in a physical mixture of $PdGa_{0.5}/SiO_2$ and solid acids will be less compared to the Ni-Ga based mixtures. Hence, the effect of proximity between $PdGa_{0.5}/SiO_2$ with FER and ZSM-5 is investigated.

Using FER as the dehydration component, the physical mixture gives slightly lower activity initially and after 10 hours on stream the effect of proximity becomes even less significant, as seen in Figure 6.17(a). Moreover, the product distribution is very similar regardless of separation (comparing Figure 6.16 and 6.17 (b)). This suggests that the $PdGa_{0.5}/SiO_2$ is more stable against deactivation by close proximity. The deactivation behaviour of both physical mixture and separated beds mainly follows that of the MSC: the activity does not stabilise in 20 hours due to continuous deactivation of the active Pd_2Ga phase by the reaction products (see Chapter 5 section 5.3.2) [127].

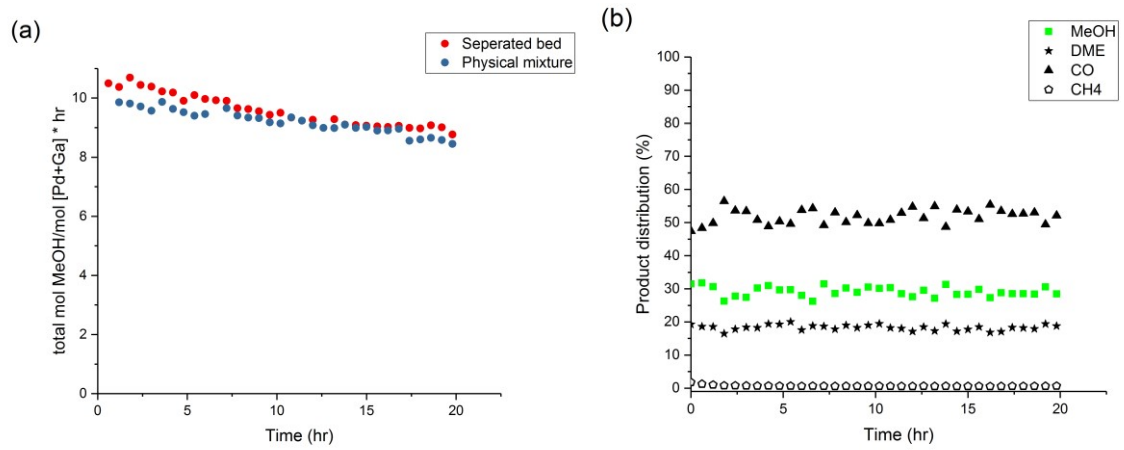


Figure 6.17, Performance comparison between separated beds and physical mixture of $PdGa_{0.5}/SiO_2$ + FER

(a) Total MeOH activity (b) Product distribution over physical mixture

Similar to Ni-Ga + ZSM-5 physical mixture, ZSM-5 used in physical mixture with $PdGa_{0.5}/SiO_2$ shows good performance and stability (Figure 6.18).

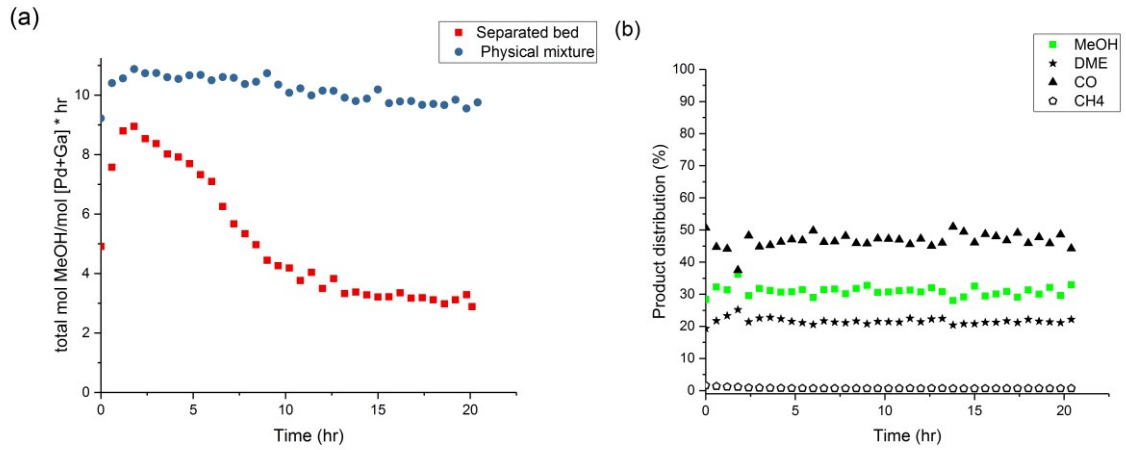


Figure 6.18, Performance comparison between separated beds and physical mixture of $PdGa_{0.5}/SiO_2$ + ZSM-5

(a) Total MeOH activity (b) Product distribution over physical mixture

Metal transfer in $PdGa_{0.5}/SiO_2$ based physical mixtures

Physical mixtures of $PdGa_{0.5}/SiO_2$ and zeolites were separated and the zeolites were analysed for the presence of MSC by ICP – OES. Results are given in Table 6.6.

Table 6.6, Metal content on the recovered zeolites from $PdGa_{0.5}/SiO_2$ based physical mixtures

Sample	Pd (ppm)	Ga (ppm)
Spent FER	< 10	< 10
Spent ZSM-5	< 10	< 10

In contrast to the $NiGa(a)/SiO_2$ based mixtures, none of the $PdGa_{0.5}/SiO_2$ based mixtures showed significant metal transfer. This is consistent with the observation that there is negligible influence of proximity on the catalytic performance of $PdGa_{0.5}/SiO_2$ based mixtures. Evidently, metal transfer from $NiGa(a)/SiO_2$ to the acid catalyst is the main cause of deactivation when the two catalysts are in close contact. The most significant difference in the two MSCs is the in situ re-activation condition required. For $NiGa(a)/SiO_2$ to recover most of its activity from N_2O passivation, a re-activation temperature of 340 °C is required. $PdGa_{0.5}/SiO_2$ only required a lower temperature of 250 °C. Therefore, the transfer of active

metals from intermetallic compound based MSC is dependent on the reduction temperature at which the physical mixture is exposed to. The higher the temperature, the more likely metals from MSC will migrate to the acid catalyst that is in close contact. It is also possible that $PdGa_{0.5}/SiO_2$ is more stable against metal migration due to the higher structural stability of the Pd_2Ga intermetallic [133].

6.3.3.3 Characterisation of coke on spent catalysts from CO_2/H_2 runs

The formation of carbonaceous species on both MSC and dehydration catalysts was quantified by TPO experiments. The results are summarised in the Table 6.7.

Table 6.7, Comparison of coke content on different catalyst arrangements

	Catalyst separation	Methanol synthesis component (µmol/g)	Methanol dehydration component (µmol/g)	Coke selectivity (mg C/g_{MeOH})
$PdGa_{0.5}/SiO_2$ + FER	Physical mixture	3.59 ± 0.04	3.07 ± 0.03	0.112 ± 0.006
	Separated bed	7.11 ± 0.07	6.04 ± 0.06	0.138 ± 0.007
$PdGa_{0.5}/SiO_2$ + ZSM-5	Physical mixture	4.07 ± 0.04	9.32 ± 0.09	0.184 ± 0.009
	Separated bed	5.41 ± 0.05	28.3 ± 0.3	0.67 ± 0.03

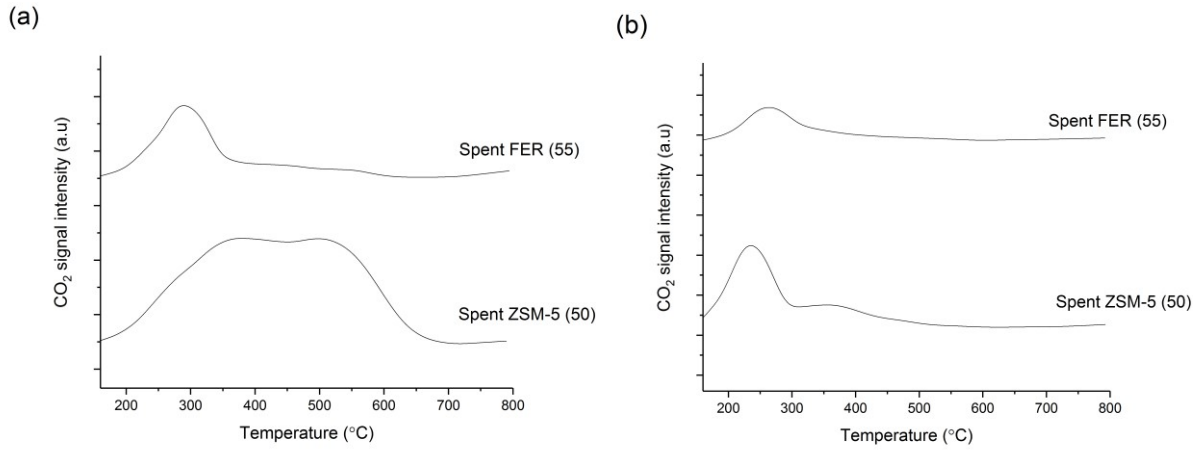


Figure 6.19, TPO profiles of spent zeolites
(a) From separated beds (b) From physical mixture

The coke content found on all catalysts is low, except over the separated ZSM-5. The results are comparable to NiGa(a)/SiO_2 + zeolites, therefore coking is also not the main cause of deactivation for these catalytic systems except for the separated ZSM-5.

6.4 Effect of CO in the PFR

6.4.1 Performance of γ-Al_2O_3 and zeolites with different MSCs

In the CSTR, the gas composition in the reactor is bound by the conversion level. As a result, catalysts are always exposed to relatively high concentration of products, which are shown to negatively impact the performance of intermetallic catalysts. In order to study the effect of CO in the feed gas in the presence of low water concentration, a tubular flow reactor (PFR) is used in which the catalysts are always exposed to gas composition similar to the feed regardless of their extent of deactivation. In the following section, the impact of CO in the feed is studied over both NiGa(a)/SiO_2 and $PdGa_{0.5}$/SiO_2 catalyst with acid catalysts in the PFR with CO/CO_2/H_2 at 270 °C, 10 bar.

Due to the detrimental effect of CO on both NiGa(a)/SiO_2 and $PdGa_{0.5}$/SiO_2 catalysts, the conversion levels from CO/CO_2/H_2 are lower than those obtained under CO_2/H_2. Again, CO produced cannot be quantified due to low conversion and sensitivity of the TCD detector, therefore in the calculations for product distribution, CO was excluded.

NiGa(a)/SiO_2 based mixtures

The results for NiGa(a)/SiO_2 based mixtures are presented in Figure 6.20.

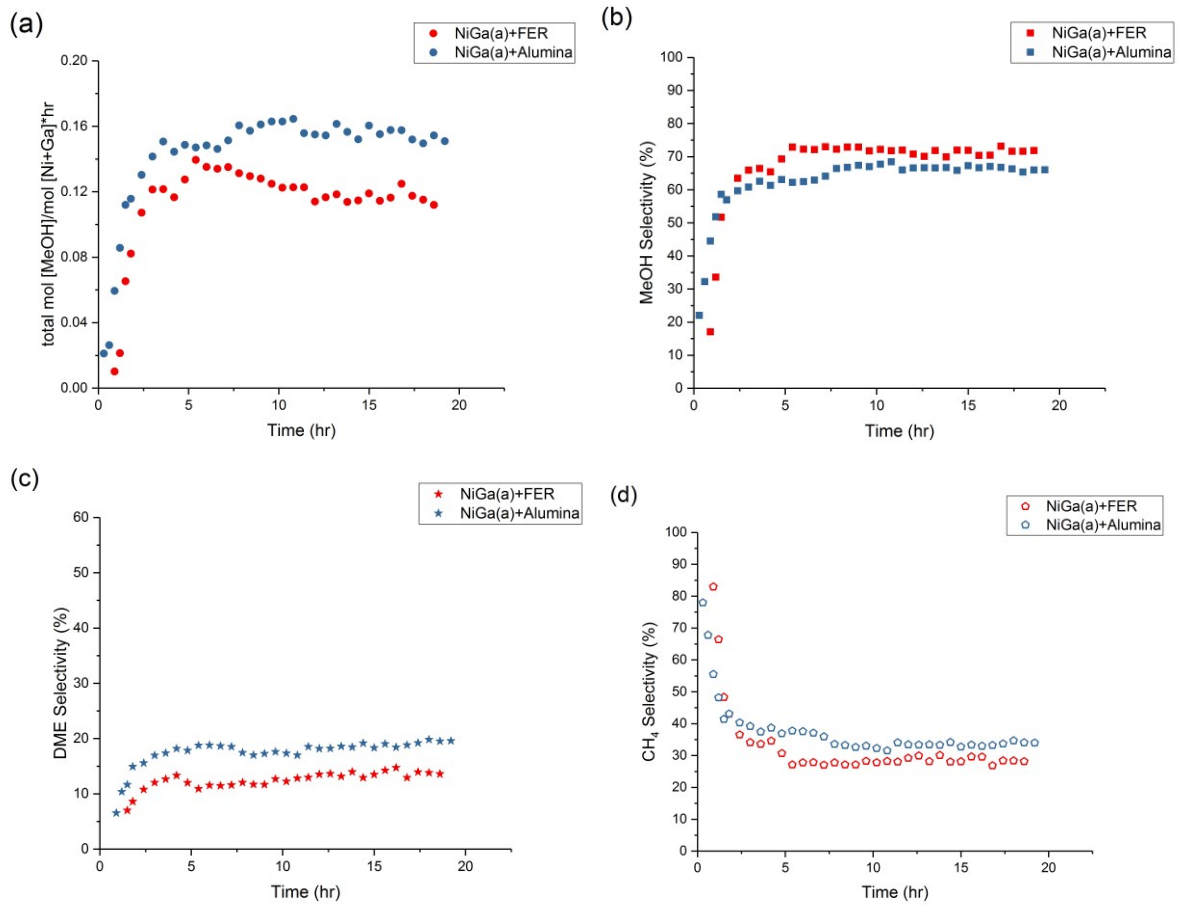


Figure 6.20, Performance of NiGa(a)/SiO_2 based physical mixtures under CO/CO_2/H_2 (a) Total MeOH production rate (b) Selectivity to MeOH (c) Selectivity to DME (d) Selectivity to CH_4

In NiGa(a)/SiO_2 based mixtures, the combined catalytic performance and stability is similar to that of NiGa(a)/SiO_2 alone under CO/CO_2/H_2. Initially methane was produced in large quantity but the production of methanol and DME gradually increased until stable methanol synthesis and dehydration activities were achieved. Only 0.74% (reactor effluent) ethane was found as the additional product other than CO, CH_4, methanol and DME over FER mixture. The absence of higher hydrocarbon is in agreement with literature, where it was speculated that the narrow channels within FER provides preferential path for the diffusion of small enough reactants and products such as methanol, DME and ethane [20, 300].

Since the water concentration in the PFR is relatively low, the mixture with γ-Al_2O_3 performs best. The activity is only restricted by the low methanol synthesis rate of the MSC under

$CO/CO_2/H_2$. As expected for γ-Al_2O_3 based mixtures, methane, CO, methanol and DME are the main products as no hydrocarbons were detected.

The product distribution over NiGa(a)/SiO_2 + ZSM-5 physical mixtures under $CO/CO_2/H_2$ is shown in Figure 6.21, obtained from the GC profile at the 20th hour.

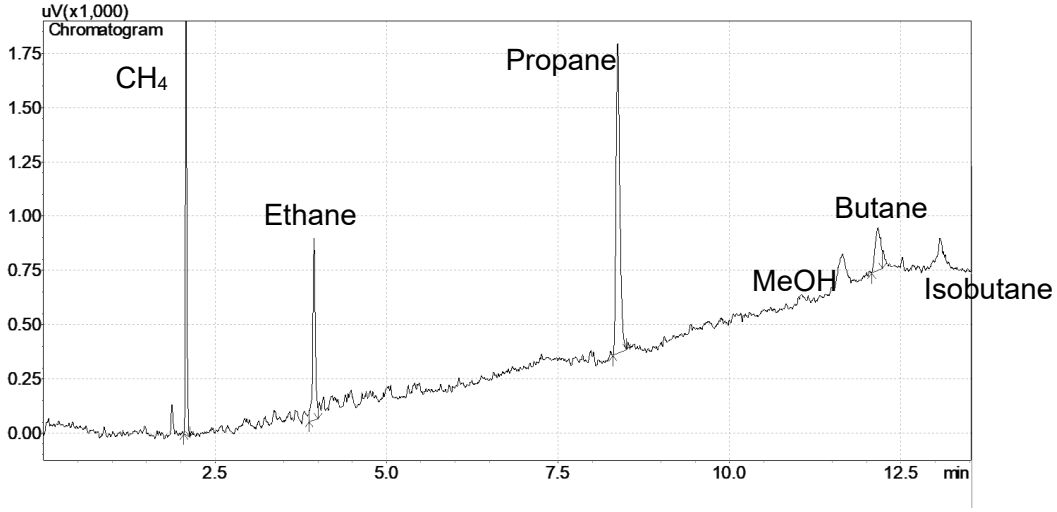


Figure 6.21, Product distribution (from GC data) over NiGa(a)/SiO_2 + ZSM-5 based physical mixtures under $CO/CO_2/H_2$

With ZSM-5, no DME production was detected (retention time at 9.7 min). Methane, ethane and several other hydrocarbons were produced. Methanol was found at trace level (0.2% of reactor effluent), suggesting that MeOH formed was immediately converted to hydrocarbons. These hydrocarbons are similar to the ones produced under CO_2/H_2 (same retention times). The formation of hydrocarbon under CO-containing syngas contradicts previous result that hydrocarbon formation is limited over physical mixture of NiGa(a)/SiO_2 (section 6.3.2.2). However, as the water content in this case is much lower, the observation of hydrocarbon activity is in agreement with previous speculation that the presence of MeOH under low water content causes ZSM-5 to produce hydrocarbons.

$PdGa_{0.5}/SiO_2$ based mixtures

Over $PdGa_{0.5}/SiO_2$ + FER (Figure 6.22), higher methanol and DME synthesis activity (compared to NiGa(a)/SiO_2 based mixtures) was obtained. Only methane, ethane, DME and methanol were found as carbon products. Over $PdGa_{0.5}/SiO_2$ + γ-Al_2O_3, methane, DME and

methanol are the only products since the acid characteristic of γ-Al_2O_3 does not promote side reactions [19]. Seeing that NiGa(a)/SiO_2 + ZSM-5 under CO/CO_2/H_2 does not produce any DME, $PdGa_{0.5}$/SiO_2 + ZSM-5 was not tested as result would be similar regardless of the type of MSC used (as shown in the runs conducted under CO_2/H_2).

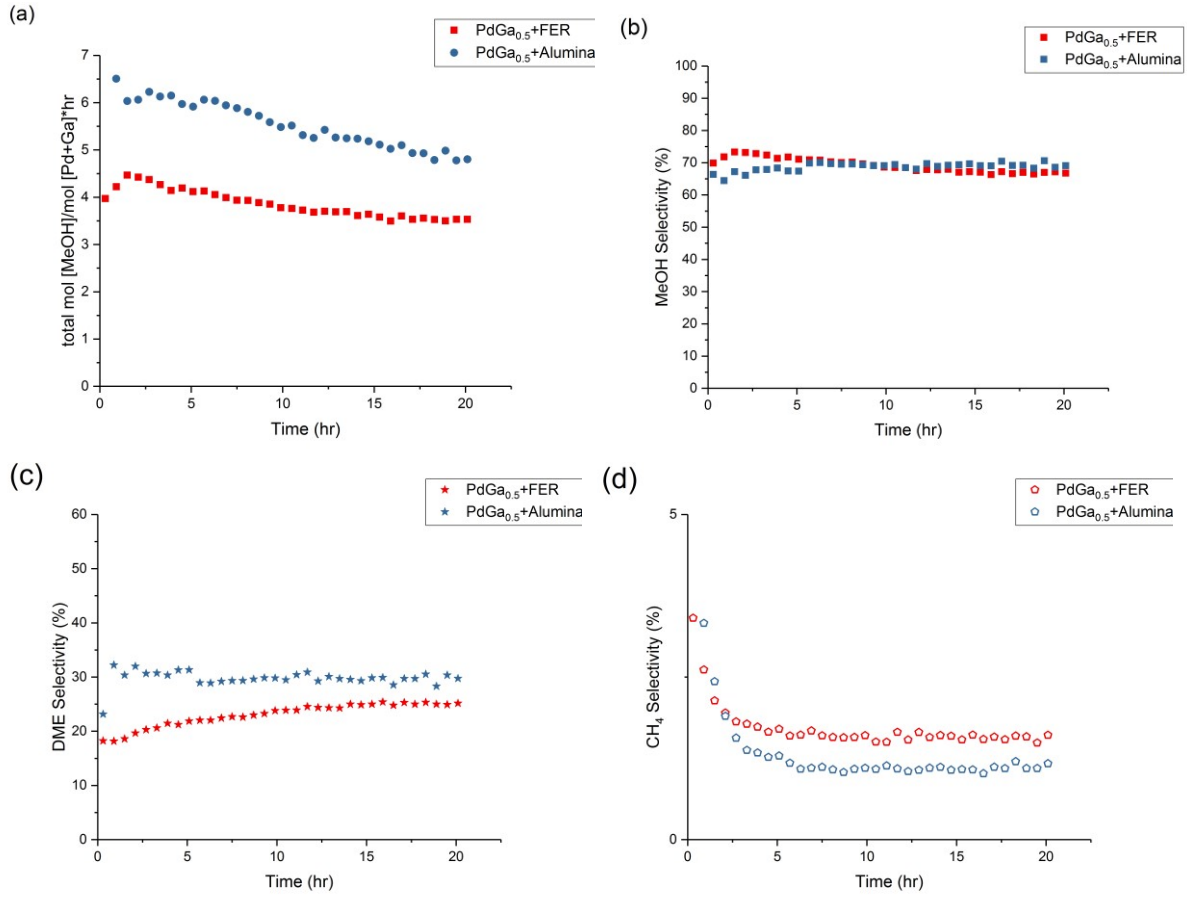


Figure 6.22, Performance of $PdGa_{0.5}$/SiO_2 based physical mixtures under CO/CO_2/H_2 (a) Total MeOH production rate (b) Selectivity to MeOH (c) Selectivity to DME (d) Selectivity to CH_4

6.4.1.1 Characterisation of coke on spent catalysts

TPO was carried out on all catalysts and it was found that the coke content was generally lower than those found under CO_2/H_2 (Table 6.8). This is expected because of the overall low conversion achieved under CO/CO_2/H_2, especially in the case of NiGa(a)/SiO_2 based mixtures. The deactivation observed is mainly due to the low activity and poor selectivity of intermetallic MSC under CO-containing feed (as discussed in Chapter 4 section 4.2.4), not due to the deposition of carbonaceous species. Although some hydrocarbons were observed

over NiGa(a)/SiO_2 + ZSM-5, coke formation was low. No heavy type of carbonaceous species was found over any solid acid catalyst under $CO/CO_2/H_2$.

Table 6.8, Coke content on catalysts run under $CO/CO_2/H_2$

MSC	Solid acid	Methanol synthesis component (μmol/g)	Methanol dehydration component (μmol/g)	Coke selectivity (mg C/g_{MeOH})
NiGa(a)/SiO_2	γ-Al_2O_3	2.81 ± 0.03	2.26 ± 0.02	0.61 ± 0.03
	FER	N/A	4.14 ± 0.04	0.69 ± 0.04
	ZSM-5	4.93 ± 0.05	2.61 ± 0.03	0.26 ± 0.01
$PdGa_{0.5}/SiO_2$	γ-Al_2O_3	9.7 ± 0.1	10.8 ± 0.1	0.48 ± 0.02
	FER	4.27 ± 0.04	2.28 ± 0.02	0.102 ± 0.005

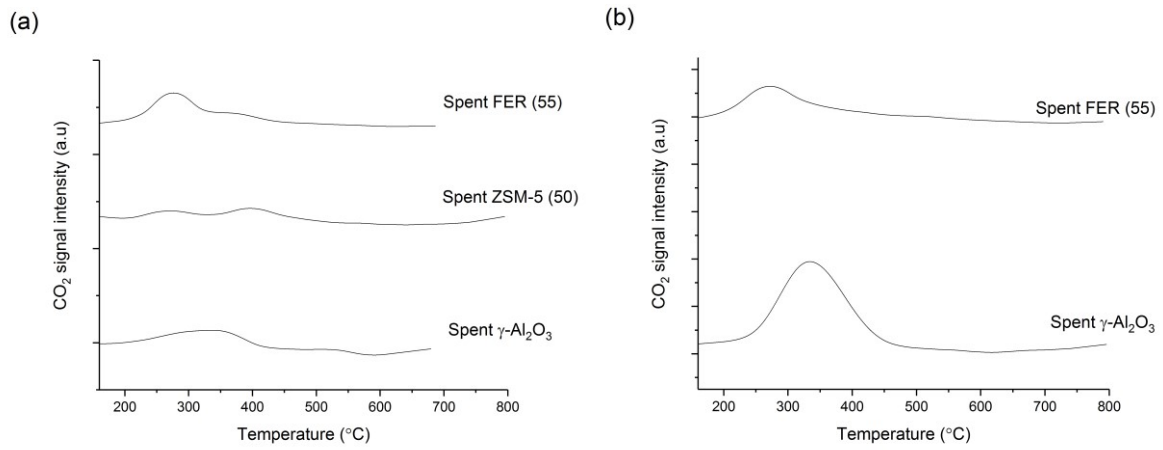


Figure 6.23, TPO profiles for spent solid acids from $CO/CO_2/H_2$ runs
(a) With NiGa(a)/SiO_2 (b) With $PdGa_{0.5}/SiO_2$

6.5 Conclusions

The suitability of using intermetallic compounds based catalysts such as NiGa(a)/SiO_2 and $PdGa_{0.5}/SiO_2$ as the methanol synthesis component in combination with a methanol dehydration catalyst for the single-stage DME synthesis is assessed. When the two catalytic functions are in separated beds, both intermetallic Ni-Ga and Pd-Ga catalysts with ferrierite and γ-alumina both gave good performance in terms of activity and selectivity to methanol and DME under CO_2/H_2. The deactivation behaviour of the combined catalysts is predominantly determined by the methanol synthesis catalyst.

The performance of ZSM-5 based catalysts greatly depend on the water concentration during CO_2/H_2 catalysis. Under low levels of water, the formation of various hydrocarbons over ZSM-5 causes the methanol and DME synthesis rates to deteriorate rapidly. As such, the build-up of carbonaceous species on the ZSM-5 also contributed to the fast deactivation of the catalysts. When the ZSM-5 catalyst is used in a physical mixture or with a methanol synthesis catalyst that has high CO_2 conversion to DME and CO, hydrocarbon formation is suppressed due to reduced acidity of ZSM-5 by water.

Close proximity was shown to have an effect on the reaction rate over NiGa(a)/SiO_2 based mixtures. Surface transfer of active metals from the methanol synthesis component to the dehydration catalyst was involved, most of which occurred during the in situ re-activation of the mixture. Insignificant effect of proximity was observed in $PdGa_{0.5}/SiO_2$ based mixtures due to negligible metal transfer. The possible loss of active sites on both catalysts due to metal migration (which appeared to be dependent on the reduction temperature) is the main cause of lower activity when the two catalytic functions are in close contact.

Under the influence of excess CO in the feed, the poor stability of the intermetallic methanol synthesis catalyst causes lower methanol synthesis activity and selectivity, which subsequently reduces the methanol dehydration activity. Owing to the topology of ferrierite, hydrocarbon formation over ferrierite based mixtures was found to be limited to trace levels of

ethane only. In contrast, DME and methanol synthesis activity over ZSM-5 based mixtures under $CO/CO_2/H_2$ are further deactivated due to hydrocarbon formation, as the intersecting channels and medium-size pores within ZSM-5 offer enough space for the formation of bulkier hydrocarbons.

Chapter 7 Conclusions

This chapter gives a summary of the work and findings presented in earlier chapters. The overall significance of the research and suggestions for future work are also briefly discussed later in the chapter.

7.1 Conclusions

This work examined the performance of Ni-Ga and Pd-Ga based intermetallic catalysts for methanol synthesis and the single-stage DME synthesis with selected zeolites at elevated pressures. Due to the harsh reduction conditions (700 °C) required for the successful formation of active Ni-Ga intermetallic phase [13, 14], currently there is no literature on the performance of Ni-Ga based catalysts under industrial conditions. Therefore, an important part of the present work was to develop a passivation technique to allow the Ni-Ga based catalysts to be transferred successfully and used in high-pressure reactors. The performance of the Ni-Ga based catalysts for CO_2 hydrogenation to methanol were investigated in a fixed bed stirred tank reactor at elevated pressures and compared to that of a commercial $Cu/ZnO/Al_2O_3$ catalyst. In addition, palladium promotion was studied to determine if the reducibility of the Ni-Ga catalysts could be improved.

For the single-stage CO_2 to DME synthesis, it was aimed to find out the suitability of using Ni-Ga and Pd-Ga catalysts as the methanol synthesis component and zeolites (ferrierite and ZSM-5) as the methanol dehydration component, with an emphasis on the deactivation behaviour and effect of proximity of the catalytic components.

Performance of Ni-Ga/SiO_2 catalysts at elevated pressures (methanol synthesis)

It was shown that using surface oxidation by N_2O, the activity of the Ni-Ga catalysts could be recovered in situ at a lower reduction temperature of 340 °C.

Despite the apparent promise of these catalysts suggested by Studt et al. [12] based on their work at atmospheric pressure, the conversion achieved by the Ni-Ga catalysts at elevated pressure was significantly lower than that of the conventional copper based catalyst. Moreover, increasing pressure did not result in significant increase in activity, suggesting that without further catalyst modification, Ni-Ga is best suited for low-pressure applications, while high-pressure operation is more suitable for Cu based catalysts or some other catalyst system. On the other hand, the methanol selectivity of the Ni-Ga catalysts is better due to the much reduced rWGS activity. It was also revealed that the reaction products, especially CO, had detrimental effect on the Ni-Ga catalysts due to the surface composition of the intermetallic phase being altered in the presence of CO. This effect was found to be reversible in the case of catalyst with higher Ni content. However, irreversible deactivation due to de-alloying of the Ni-Ga intermetallic phase was observed in the Ga-rich catalysts.

Effect of Pd promotion on Ni-Ga

Palladium was added to the Ni-Ga catalyst in the hope that Pd would act as a reduction promoter. Pd promotion did not appear to improve the formation of the Ni-Ga intermetallic phase at low temperature. However, a promotional effect in the catalytic activity was observed in the Pd promoted Ni-Ga catalyst, which is speculated to be a consequence of hydrogen spillover from the added palladium, since this phenomenon is widely reported in the literature [241, 263, 265]. The performance of the Pd promoted catalyst severely deteriorated under high level of CO, making it unsuitable for application under CO-rich conditions.

Single-stage DME synthesis

Both Ni-Ga and Pd-Ga catalysts were found to be suitable as the methanol synthesis component for the single-stage DME synthesis. For the methanol dehydration component, ferrierite and ZSM-5 were investigation since the unique unidirectional channel structure of FER has been shown to suppress hydrocarbon formation [20, 202, 284] and ZSM-5 has been reported to have stable performance under CO_2/H_2 [17]. In agreement with literature [17], FER

based catalysts gave good activity and selectivity. In contrast, the performance of Ni-Ga or Pd-Ga + ZSM-5 based catalysts greatly depended on the water concentration, which was not observed previously. Montesano et al. [17] used a much more active methanol synthesis and rWGS catalyst ($Cu/ZnO/Al_2O_3$), which gave a higher water concentration. Therefore, FER could be used with a range of methanol synthesis components to achieve good selectivity, while ZSM-5 can only be used in combination with a methanol synthesis catalyst component that has high activity for methanol synthesis/rWGS.

Despite the hope that Ni-Ga catalysts would be more structurally stable due to covalent nature of metal-metal bonds, metal transfer was still observed when the catalyst was in close contact with the solid acid catalyst, leading to a lower catalytic activity. This phenomenon was absent in the Pd-Ga based catalysts. These were reduced in situ at a lower temperature, indicating that the metal transfer between the intermetallic compounds and the solid acid catalyst might be facilitated by the high-temperature reducing conditions required for catalyst re-activation.

General comments

The findings from present work contribute towards the understanding of Ni-Ga intermetallic based catalysts as the methanol synthesis catalyst for CO_2 hydrogenation to methanol and DME. The higher sintering resistance of the Ni-Ga based catalysts in CO_2-rich environment indicates the attraction of using these catalysts for CO_2 hydrogenation with solar- or wind-generated hydrogen, which is considered to be a promising strategy to reduce industrial emissions. However, several challenges still remain to be overcome before these catalysts can be used for industrial applications. These are mainly the susceptibility to poisoning by CO (one of the reaction products), Ga segregation from the active phase under reaction conditions, and achieving a lower reduction temperature. These challenges could be addressed in future improvements in catalyst design. Based on the preliminary study of Pd promotion made here, the addition of a reduction promoter is a promising approach and could be further explored and optimised. Alternatively, other intermetallic compound based catalysts

which have a lower re-activation temperature could be explored. These would be essential for such catalysts to be used in the single-stage methanol-DME synthesis to avoid long-term deactivation by metal transfer, especially with zeolites as the solid acid component.

From the perspective of industrial process, due to the low conversion achieved with Ni-Ga in the present study, the reactor effluent would need to be recycled. However, CO would eventually build up in the recycle loop and would cause strong deactivation of these Ni-Ga intermetallic based catalysts. Therefore, without modification of the catalysts, once-through operation would be necessary, for example integrated with power generation [301]. However, such an approach is unlikely to be successful for the present Ni-Ga/SiO_2 catalysts without significant catalyst development.

7.2 Future work

The identification of methanol synthesis and dehydration catalysts that have good performance and stability will continue to be crucial for the development of CO_2 hydrogenation processes. Although the research work presented in this thesis gives valuable insight into the performance of Ni-Ga based catalysts at elevated pressure, it is clear they suffer from a range of problems. The followings are suggested for future work:

- Understanding of the changes occurring during passivation of Ni-Ga catalysts using in situ XRD/XPS
- Improving the passivation technique for various Ni:Ga ratios
- Study of the underlying mechanism for the initial deactivation observed in the Ni-Ga based catalysts
- Identification of the species present in the Pd promoted catalyst by in situ XRD/ XPS or STEM-HAADF to gain deeper understanding of the changes induced by the promoter atoms [302] and correlate the promotional effect with performance

- Investigation of other promoted catalysts in terms of promoter loading combined with testing the catalysts at high pressures
- Identification and quantification of the species that are transferred between the Ni-Ga based catalysts and solid acid catalysts and correlate them with deactivation observed when the two catalytic functions are in close proximity
- Investigating other catalysts based on intermetallic compound (such as PdZn) as the methanol synthesis component for the single-stage DME synthesis with zeolites, and evaluate the extent of metal transfer
- Carrying out techno-economic and environmental impact assessment for CO_2 hydrogenation to methanol and DME with renewable hydrogen [303] over bimetallic catalysts
- Explore the possibility of using a CO removal catalyst in the same reactor as the intermetallic compound based catalysts to improve the stability of these catalysts under CO
- Investigate the single-stage DME synthesis with in situ water removal using sorbents or hydrophilic membranes [304]
- Design the process/reactor for the single-stage DME synthesis such that low product concentration at the inlet zone to main high methanol synthesis activity
- Investigate the potential of CO_2 hydrogenation at low temperature to obtain high equilibrium methanol conversion (e.g. catalysed electrochemical CO_2 reduction [305])

References

[1] Global Economic Symposium, Proposal - The Energy Crisis and Climate Change, 2009.

[2] The end of fossil fuels, Ecotricity, 2015.

[3] I.E.A. Staff, CO2 Emissions from Fuel Combustion: 1972, Organization for Economic2008.

[4] G.A. Olah, Beyond oil and gas: the methanol economy, Angewandte Chemie International Edition, 44 (2005) 2636-2639.

[5] G.A. Olah, G.S. Prakash, Efficient and selective conversion of carbon dioxide to methanol, dimethyl ether and derived products, Google Patents, 2009.

[6] G.A. Olah, G.S. Prakash, A. Goeppert, Anthropogenic chemical carbon cycle for a sustainable future, Journal of the American Chemical Society, 133 (2011) 12881-12898.

[7] Sustainable Fuels from Renewable Energies, IASS Potsdam, 2014.

[8] J.T. Sun, I.S. Metcalfe, M. Sahibzada, Deactivation of Cu/ZnO/Al2O3 methanol synthesis catalyst by sintering, Industrial & engineering chemistry research, 38 (1999) 3868-3872.

[9] J. Skrzypek, M. Lachowska, D. Serafin, Methanol synthesis from CO2 and H2: dependence of equilibrium conversions and exit equilibrium concentrations of components on the main process variables, Chemical engineering science, 45 (1990) 89-96.

[10] M.M.-J. Li, S.C.E. Tsang, Bimetallic catalysts for green methanol production via CO 2 and renewable hydrogen: a mini-review and prospects, Catalysis Science & Technology, 8 (2018) 3450-3464.

[11] M. Armbrüster, R. Schlögl, Y. Grin, Intermetallic compounds in heterogeneous catalysis—a quickly developing field, Science and technology of advanced materials, 15 (2014) 034803.

[12] F. Studt, I. Sharafutdinov, F. Abild-Pedersen, C.F. Elkjær, J.S. Hummelshøj, S. Dahl, I. Chorkendorff, J.K. Nørskov, Discovery of a Ni-Ga catalyst for carbon dioxide reduction to methanol, Nature chemistry, 6 (2014) 320.

[13] I. Sharafutdinov, S. Dahl, I. Chorkendorff, Investigations into low pressure methanol synthesis, (2013).

[14] I. Sharafutdinov, C.F. Elkjær, H.W.P. de Carvalho, D. Gardini, G.L. Chiarello, C.D. Damsgaard, J.B. Wagner, J.-D. Grunwaldt, S. Dahl, I. Chorkendorff, Intermetallic compounds of Ni and Ga as catalysts for the synthesis of methanol, Journal of catalysis, 320 (2014) 77-88.

[15] E.S. Yoon, C. Han, A review of sustainable energy–recent development and future prospects of dimethyl ether (DME), Computer aided chemical engineering, Elsevier2009, pp. 169-175.

[16] Z. Azizi, M. Rezaeimanesh, T. Tohidian, M.R. Rahimpour, Dimethyl ether: A review of technologies and production challenges, Chemical Engineering and Processing: Process Intensification, 82 (2014) 150-172.

[17] R. Montesano Lopez, Selectivity and deactivation in the single-stage synthesis of dimethyl ether from CO2/CO/H2, (2014).

[18] M.C. Alain Goeppert, John-Paul Jones, G. K. Surya Prakash, George A. Olah, Recycling of carbon dioxide to methanol and derived products – closing the loop, Chemical Society, (2014) 7995-8048.

[19] E. Catizzone, G. Bonura, M. Migliori, F. Frusteri, G. Giordano, CO2 recycling to dimethyl ether: State-of-the-art and perspectives, Molecules, 23 (2017) 31.

[20] R. Montesano, A. Narvaez, D. Chadwick, Shape-selectivity effects in syngas-to-dimethyl ether conversion over Cu/ZnO/Al2O3 and zeolite mixtures: Carbon deposition and by-product formation, Applied Catalysis A: General, 482 (2014) 69-77.

[21] E. Ortelli, J. Wambach, A. Wokaun, Methanol synthesis reactions over a CuZr based catalyst investigated using periodic variations of reactant concentrations, Applied Catalysis A: General, 216 (2001) 227-241.

[22] S. Saeidi, N.A.S. Amin, M.R. Rahimpour, Hydrogenation of CO2 to value-added products—A review and potential future developments, Journal of CO2 Utilization, 5 (2014) 66-81.

[23] I. Ganesh, Conversion of carbon dioxide into methanol–a potential liquid fuel: Fundamental challenges and opportunities (a review), Renewable and Sustainable Energy Reviews, 31 (2014) 221-257.

[24] M. Aresta, A. Dibenedetto, E. Quaranta, State of the art and perspectives in catalytic processes for CO2 conversion into chemicals and fuels: The distinctive contribution of chemical catalysis and biotechnology, Journal of catalysis, 343 (2016) 2-45.

[25] F.D. Meylan, V. Moreau, S. Erkman, CO2 utilization in the perspective of industrial ecology, an overview, Journal of CO2 Utilization, 12 (2015) 101-108.

[26] R. Schlögl, C. Abanades, M. Aresta, E.A. Blekkan, T. Cantat, G. Centi, N. Duic, A. El Khamlichi, G. Hutchings, M. Mazzotti, Novel carbon capture and utilisation technologies, (2018).

[27] I. Ganesh, Conversion of carbon dioxide into methanol – a potential liquid fuel: Fundamental challenges and opportunities (a review), Renewable and Sustainable Energy Reviews, 31 (2014) 221-257.

[28] B. Metz, O. Davidson, H. De Coninck, M. Loos, L. Meyer, IPCC special report on carbon dioxide capture and storage, Intergovernmental Panel on Climate Change, Geneva (Switzerland). Working …, 2005.

[29] K.M.K. Yu, I. Curcic, J. Gabriel, S.C.E. Tsang, Recent advances in CO2 capture and utilization, ChemSusChem: Chemistry & Sustainability Energy & Materials, 1 (2008) 893-899.

[30] M. Songolzadeh, M. Soleimani, M. Takht Ravanchi, R. Songolzadeh, Carbon dioxide separation from flue gases: a technological review emphasizing reduction in greenhouse gas emissions, The Scientific World Journal, 2014 (2014).

[31] A. Álvarez, A. Bansode, A. Urakawa, A.V. Bavykina, T.A. Wezendonk, M. Makkee, J. Gascon, F. Kapteijn, Challenges in the greener production of formates/formic acid, methanol, and DME by heterogeneously catalyzed CO2 hydrogenation processes, Chemical reviews, 117 (2017) 9804-9838.

[32] Y. Wang, L. Zhao, A. Otto, M. Robinius, D. Stolten, A review of post-combustion CO2 capture technologies from coal-fired power plants, Energy Procedia, 114 (2017) 650-665.

[33] S. Chu, Carbon capture and sequestration, American Association for the Advancement of Science, 2009.

[34] E.D. Bates, R.D. Mayton, I. Ntai, J.H. Davis, CO2 capture by a task-specific ionic liquid, Journal of the American Chemical Society, 124 (2002) 926-927.

[35] J. Merel, M. Clausse, F. Meunier, Experimental investigation on CO2 post− combustion capture by indirect thermal swing adsorption using 13X and 5A zeolites, Industrial & Engineering Chemistry Research, 47 (2008) 209-215.

[36] C. Lu, H. Bai, B. Wu, F. Su, J.F. Hwang, Comparative study of CO2 capture by carbon nanotubes, activated carbons, and zeolites, Energy & Fuels, 22 (2008) 3050-3056.

[37] S. Gadipelli, Z.X. Guo, Graphene-based materials: Synthesis and gas sorption, storage and separation, Progress in Materials Science, 69 (2015) 1-60.

[38] R. Khalilpour, K. Mumford, H. Zhai, A. Abbas, G. Stevens, E.S. Rubin, Membrane-based carbon capture from flue gas: a review, Journal of Cleaner Production, 103 (2015) 286-300.

[39] J.D. Holladay, J. Hu, D.L. King, Y. Wang, An overview of hydrogen production technologies, Catalysis today, 139 (2009) 244-260.

[40] C.M. Kalamaras, A.M. Efstathiou, Hydrogen production technologies: current state and future developments, Conference papers in science, Hindawi, 2013.

[41] S.E. Hosseini, M.A. Wahid, Hydrogen production from renewable and sustainable energy resources: promising green energy carrier for clean development, Renewable and Sustainable Energy Reviews, 57 (2016) 850-866.

[42] K. Zeng, D. Zhang, Recent progress in alkaline water electrolysis for hydrogen production and applications, Progress in Energy and Combustion Science, 36 (2010) 307-326.

[43] X. Chen, S. Shen, L. Guo, S.S. Mao, Semiconductor-based photocatalytic hydrogen generation, Chemical reviews, 110 (2010) 6503-6570.

[44] H. Ahmad, S. Kamarudin, L. Minggu, M. Kassim, Hydrogen from photo-catalytic water splitting process: A review, Renewable and Sustainable Energy Reviews, 43 (2015) 599-610.

[45] E.P. Melián, O.G. Díaz, A.O. Méndez, C.R. López, M.N. Suárez, J.D. Rodríguez, J. Navío, D.F. Hevia, J.P. Peña, Efficient and affordable hydrogen production by water photo-splitting using TiO2-based photocatalysts, International Journal of Hydrogen Energy, 38 (2013) 2144-2155.

[46] K. Lalitha, J.K. Reddy, M.V.P. Sharma, V.D. Kumari, M. Subrahmanyam, Continuous hydrogen production activity over finely dispersed Ag2O/TiO2 catalysts from methanol: water mixtures under solar irradiation: a structure–activity correlation, International Journal of hydrogen energy, 35 (2010) 3991-4001.

[47] N.-L. Wu, M.-S. Lee, Enhanced TiO2 photocatalysis by Cu in hydrogen production from aqueous methanol solution, International Journal of Hydrogen Energy, 29 (2004) 1601-1605.

[48] H. Park, Y. Park, W. Kim, W. Choi, Surface modification of TiO2 photocatalyst for environmental applications, Journal of Photochemistry and Photobiology C: Photochemistry Reviews, 15 (2013) 1-20.

[49] P. Serp, J.L. Figueiredo, Carbon materials for catalysis, John Wiley & Sons2009.

[50] X. Jiang, J. Nisar, B. Pathak, J. Zhao, R. Ahuja, Graphene oxide as a chemically tunable 2-D material for visible-light photocatalyst applications, Journal of catalysis, 299 (2013) 204-209.

[51] S.N. Reddy, S. Nanda, A.K. Dalai, J.A. Kozinski, Supercritical water gasification of biomass for hydrogen production, International Journal of Hydrogen Energy, 39 (2014) 6912-6926.

[52] R.D. Cortright, R. Davda, J.A. Dumesic, Hydrogen from catalytic reforming of biomass-derived hydrocarbons in liquid water, Materials For Sustainable Energy: A Collection of Peer-Reviewed Research and Review Articles from Nature Publishing Group, World Scientific2011, pp. 289-292.

[53] M.V. Twigg, Catalyst handbook, Routledge2018.

[54] J.S. J. Skrzypek, S. Ledakowicz, Methanol synthesis, Polish Scientific Publishers1994.

[55] F.S.S. V.D. Kuznetzov, J.V. Bolysheva and M.I. Temkin, Equilibrium of Methanol Synthesis, Theoretical Foundations of Chemical Engineering, (1977) 866-871.

[56] P.J.J.M.S. G.H. Graaf, E.J. Stamhuis, G.E.H. Joosten, Chemical Equilibria in Methanol Synthesis, Chemical Engineering Science, (1986) 2883-2890.

[57] L. Wade, R. Gengelbach, J. Trumbley, W. Hallbauer, Methanol, Kirk-Othmer Encyclopedia of Chemical Technology, (1981) 16.

[58] L. Bissett, EQUILIBRIUM-CONSTANTS FOR SHIFT REACTIONS, MCGRAW HILL INC 1221 AVENUE OF THE AMERICAS, NEW YORK, NY 10020, 1977, pp. 155-156.

[59] M.L. Jerzy Skrzypek, Miroslaw Grzesik, Jerzy Sloczynski, Pawel Nowak, Thermodynamics and kinetics of low pressure methanol synthesis, The Chemical Engineering Journal, (1995) 101-108.

[60] H. Arakawa, Research and development on new synthetic routes for basic chemicals by catalytic hydrogenation of CO2, Studies in surface science and catalysis, Elsevier1998, pp. 19-30.

[61] M. Mikkelsen, M. Jørgensen, F.C. Krebs, The teraton challenge. A review of fixation and transformation of carbon dioxide, Energy & Environmental Science, 3 (2010) 43-81.

[62] K.-D.J. Oh-Shim Joo, Il Moon, Alexander Ya. Rozovskii, Galina I. Lin, Sung-Hwan Han, Sung-Jin Uhm, Carbon Dioxide Hydrogenation To Form Methanol via a Reverse-Water-Gas-Shift Reaction (the CAMERE Process), Industrial & Engineering Chemistry Research (1999) 1808-1812.

[63] V.C. K. Klier, R. G. Herman and G. W. Simmons, Catalytic Synthesis of Methanol fi-om CO/H2:4 the Effects of Carbon Dioxide, Journal of Catalysis, (1982) 343.

[64] A.Y. Rozovskii, Y.B. Kagan, G. Lin, E. Slivinskii, S. Loktev, L. Liberov, A. Bashkirov, Mechanism of methanol synthesis from carbon dioxide and hydrogen. II. Selection of the reaction mechanism, Kinet. Catal.(USSR)(Engl. Transl.);(United States), 17 (1977).

[65] P.J.D. G.C. Chinchen, D.G. Parker, M.S. Spencer, D.A. Whan, Mehanism of methanol synthesis from CO2/CO/H2 mixtures over copper/zinc oxide/alumina catalysts: use of 14C-labelled reactants, Applied Catalysis, (1987) 333-338.

[66] C.A.M. Y. Yang, D.H. Mei, C.H.F. Peden, C.T. Campbell, Mechanistic studies of methanol synthesis over Cu from CO/CO2/H2/H2O mixtures: The source of C in methanol and the role of water, Journal of Catalysis, (2013) 10-17.

[67] K.H.L. J.S. Lee, S.Y. Lee, Y.G. Kim, A Comparative Study of Methanol Synthesis from CO2/H2 and CO/H2 over a Cu/ZnO/Al2O3 Catalyst, Journal of Catalysis (1993) 414-424.

[68] D.W. G. Liu, M. Garland, H. H. Kung, The Role of CO2 in Methanol Synthesis on Cu-Zn Oxide: An Isotope Labeling Study, Catalysis, (1985) 251-260.

[69] S. Lee, Methanol synthesis technology, CRC Press1989.

[70] G. Wang, Y. Morikawa, T. Matsumoto, J. Nakamura, Why is formate synthesis insensitive to copper surface structures?, The Journal of Physical Chemistry B, 110 (2006) 9-11.

[71] T.S.B.T. Yeonwoo Kim, Sena Yang, Sehun Kim, and Hangil Lee, Mechanism of the Surface Hydrogen Induced Conversion of CO2 to Methanol at Cu(111) Step Sites, ACS Catalysis, (2016) 1037-1044.

[72] M.M. L. C. Grabow, Mechanism of Methanol Synthesis on Cu through CO2 and CO hydrogenation, ACS Catalysis, (2011) 365-384.

[73] C.A.M. Yong Yang, R.S. Disselkamp, Ja-Hun Kwak, C. H. F. Peden, C. T. Campbell, (Non)formation of Methanol by Direct Hydrogenation of Formate on Copper Catalysts, Physical Chemistry, (2010) 17205-17211.

[74] D.M. Yong Yang, Charles H. F. Peden, Charles T. Campbell, Charles A. Mims, Surface-Bound Intermediates in Low-Temperature Methanol Synthesis on Copper: Participants and Spectators, ACS Catalysis, (2015) 7328-7337.

[75] M.M.K. V. E. Leonov, E. N. Tsybina, G. S. Petrischeva, Kinetics and Catalysis, (1973) 848.

[76] K. Klier, Methanol Synthesis, Advances in Catalysis, (1982) 243-313.

[77] P.F. Plerlulgl Villa, Guldo Buzzi-Ferrarls, Guldo Garone, Halo Paoquon, Synthesis of Aicohots from Carbon Oxides and Hydrogen. 1. Kinetics of the Low-Pressure Methanol Synthesis, Industrial & Engineering Chemistry Process, (1985) 12-19.

[78] E.J.S. G. H. Graaf, A. A. C. M. Beenackers, Kinetics of Low-Pressure Methanol Synthesis, Chemical Engineering Science, (1988) 3185-3195.

[79] G.F.F. K. M. Vanden Bussche, A Steady-State Kinetic Model for Methanol Synthesis and the Water Gas Shift Reaction on a Commercial Cu/ZnO/Al2O3 Catalyst, Journal of Catalysis, (1996) 1-10.

[80] D. Mignard, C. Pritchard, On the use of electrolytic hydrogen from variable renewable energies for the enhanced conversion of biomass to fuels, Chemical Engineering Research and Design, 86 (2008) 473-487.

[81] A. Bernardi, L. Gomoescu, J. Wang, C.C. Pantelides, D. Chadwick, B. Chachuat, Kinetic Model Discrimination for Methanol and DME Synthesis using Bayesian Estimation, IFAC-PapersOnLine, 52 (2019) 335-340.

[82] Y. Choi, K. Futagami, T. Fujitani, J. Nakamura, The difference in the active sites for CO2 and CO hydrogenations on Cu/ZnO-based methanol synthesis catalysts, Catalysis letters, 73 (2001) 27-31.

[83] N. Park, M.-J. Park, K.-S. Ha, Y.-J. Lee, K.-W. Jun, Modeling and analysis of a methanol synthesis process using a mixed reforming reactor: Perspective on methanol production and CO2 utilization, Fuel, 129 (2014) 163-172.

[84] N. Park, M.-J. Park, Y.-J. Lee, K.-S. Ha, K.-W. Jun, Kinetic modeling of methanol synthesis over commercial catalysts based on three-site adsorption, Fuel Processing Technology, 125 (2014) 139-147.

[85] C. Seidel, A. Jörke, B. Vollbrecht, A. Seidel-Morgenstern, A. Kienle, Kinetic modeling of methanol synthesis from renewable resources, Chemical Engineering Science, 175 (2018) 130-138.

[86] C.N. Satterfield, Heterogeneous catalysis in industrial practice. 2nd edition, New York, NY (United States); McGraw Hill Book Co.; None1991.

[87] C. Lormand, Industrial Production of Synthetic Methanol, Industrial & Engineering Chemistry, 17 (1925) 430-432.

[88] J.W.L. Sittichai Natesakhawat, John P. Baltrus, Paul R. Ohodnicki, Jr, Bret H. Howard, Xingyi Deng, Christopher Matranga, Active Sites and Structure−Activity Relationships of Copper-Based Catalysts for Carbon Dioxide Hydrogenation to Methanol, ACS Catalysis, (2012) 1667-1676.

[89] F.S. Malte Behrens, Igor Kasatkin, Stefanie Kuhl, Michael Havecker, Frank Abild-Pedersen, Stefan Zender, Frank Girgdies, Patrick Kurr, Michael Tovar, Richard W. Fischer, Jens K. Nørskov, R. Schlög, Methanol synthesis over Cu/ZnO/Al2O3: The active sites in industrial catalysis.

[90] I.N. T. Fujitani, T. Watanabe, T. Uchijima, J. Nakamura, Methanol synthesis by the hydrogenation of CO2 over Zn-deposited Cu(111) and Cu(110) surfaces, Catalysis Letters, (1995) 297-302.

[91] R.J.B. Zhenming Hu, Structure sensitivity and cluster size convergence for formate adsorption on copper surfaces: A DFT cluster model study, The Journal of Chemical Physics, (2000) 9562-9568.

[92] K.C.W. G.C. Chinchen, D.A. Whan, THE ACTIVITY AND STATE OF THE COPPER SURFACE IN METHANOL SYNTHESIS CATALYSTS, Applied catalysis, (1986) 101-107.

[93] M.S. Spencer, The role of zinc oxide in Cu/ZnO catalysts for methanol synthesis and the water–gas shift reaction, Topics in Catalysis, (1999) 259-266.

[94] S. Kattel, P.J. Ramírez, J.G. Chen, J.A. Rodriguez, P. Liu, Active sites for CO2 hydrogenation to methanol on Cu/ZnO catalysts, Science, 355 (2017) 1296-1299.

[95] M. Behrens, F. Studt, I. Kasatkin, S. Kühl, M. Hävecker, F. Abild-Pedersen, S. Zander, F. Girgsdies, P. Kurr, B.-L. Kniep, The active site of methanol synthesis over Cu/ZnO/Al2O3 industrial catalysts, Science, 336 (2012) 893-897.

[96] Y. Kanai, T. Watanabe, T. Fujitani, T. Uchijima, J. Nakamura, The synergy between Cu and ZnO in methanol synthesis catalysts, Catalysis Letters, 38 (1996) 157-163.

[97] R. Burch, R.J. Chappell, S.E. Golunski, Synergy between copper and zinc oxide during methanol synthesis. Transfer of activating species, Journal of the Chemical Society, Faraday Transactions 1: Physical Chemistry in Condensed Phases, 85 (1989) 3569-3578.

[98] R. Burch, R. Chappell, S. Golunski, Synergy at a distance in the synthesis of methanol over copper catalysts, Catalysis letters, 1 (1988) 439-443.

[99] R. Burch, S.E. Golunski, M.S. Spencer, The role of hydrogen in methanol synthesis over copper catalysts, Catalysis Letters, 5 (1990) 55-60.

[100] R. Burch, R. Chappell, Support and additive effects in the synthesis of methanol over copper catalysts, Applied catalysis, 45 (1988) 131-150.

[101] I.N. J. Nakamura, T. Uchijima, Y. Kanai, T. Watanabe, M. Saito and T. Fujitani, Methanol synthesis over a Zn-deposited copper model catalyst, Catalysis Letters, (1995) 325-331.

[102] G.Q.L. Xin-Mei Liu, Zi-Feng Yan, Jorge Beltramini, Recent Advances in Catalysts for Methanol Synthesis via Hydrogenation of CO and CO2, Industrial & Engineering Chemistry Research, (2003) 6518-6530.

[103] X. Zhai, J. Shamoto, H. Xie, Y. Tan, Y. Han, N. Tsubaki, Study on the deactivation phenomena of Cu-based catalyst for methanol synthesis in slurry phase, Fuel, 87 (2008) 430-434.

[104] C.T. Campbell, B.E. Koel, H2S/Cu (111): A model study of sulfur poisoning of water-gas shift catalysts, Surface science, 183 (1987) 100-112.

[105] P.R.O.J. Sittichai Natesakhawata, Bret H. Howarda, Jonathan W. Lekse, John P. Baltrusa, Christopher Matranga, Adsorption and Deactivation Characteristics of Cu/ZnO-Based Catalysts for Methanol Synthesis from Carbon Dioxide, Topics in Catalysis, (2013).

[106] I.S.M. James T. Sun, Mortaza Sahibzada, Deactivation of Cu/ZnO/Al2O3 Methanol Synthesis Catalyst by Sintering, Industrial and Engineering Chemistry Research, (1999) 3868-3872.

[107] M.S.S. Martyn V. Twigg, Deactivation of Copper Metal Catalysts for Methanol Decomposition, Methanol Steam Reforming and Methanol Synthesis, Topics in Catalysis, (2003) 191-203.

[108] T. Lunkenbein, F. Girgsdies, T. Kandemir, N. Thomas, M. Behrens, R. Schlögl, E. Frei, Bridging the time gap: a copper/zinc oxide/aluminum oxide catalyst for methanol synthesis studied under industrially relevant conditions and time scales, Angewandte Chemie International Edition, 55 (2016) 12708-12712.

[109] T. Van Herwijnen, W. De Jong, Brass formation in a copper/zinc oxide CO shift catalyst, Journal of Catalysis, 34 (1974) 209-214.

[110] K.-D. Jung, O.-S. Joo, S.-H. Han, Structural change of Cu/ZnO by reduction of ZnO in Cu/ZnO with methanol, Catalysis letters, 68 (2000) 49.

[111] M. Spencer, α-Brass formation in copper/zinc oxide catalysts: I. Bulk equilibrium concentrations of zinc under methanol synthesis and water-gas shift reaction conditions, Surface science, 192 (1987) 323-328.

[112] J. Wu, M. Saito, M. Takeuchi, T. Watanabe, The stability of Cu/ZnO-based catalysts in methanol synthesis from a CO2-rich feed and from a CO-rich feed, Applied Catalysis A: General, 218 (2001) 235-240.

[113] B. Liang, J. Ma, X. Su, C. Yang, H. Duan, H. Zhou, S. Deng, L. Li, Y. Huang, Investigation on Deactivation of Cu/ZnO/Al2O3 Catalyst for CO2 Hydrogenation to Methanol, Industrial & Engineering Chemistry Research, (2019).

[114] D.C. M. Sahibzada, I.S. Metcalfe, Methanol synthesis from CO2/H2 over Pd-promoted Cu/ZnO/Al2O3 catalysts: Kinetics and deactivation, Studies in Surface Science and Catalysis, (1997) 29-34.

[115] I. Melian-Cabrera, M.L. Granados, J. Fierro, Pd-modified Cu–Zn catalysts for methanol synthesis from CO2/H2 mixtures: catalytic structures and performance, Journal of Catalysis, 210 (2002) 285-294.

[116] C. Yang, Z. Ma, N. Zhao, W. Wei, T. Hu, Y. Sun, Methanol synthesis from CO2-rich syngas over a ZrO2 doped CuZnO catalyst, Catalysis Today, 115 (2006) 222-227.

[117] M. Lachowska, J. Skrzypek, Methanol synthesis from carbon dioxide and hydrogen over Mn-promoted copper/zinc/zirconia catalysts, Reaction kinetics and catalysis letters, 83 (2004) 269-273.

[118] X. Guo, D. Mao, G. Lu, S. Wang, G. Wu, CO2 hydrogenation to methanol over Cu/ZnO/ZrO2 catalysts prepared via a route of solid-state reaction, Catalysis communications, 12 (2011) 1095-1098.

[119] X. Guo, D. Mao, S. Wang, G. Wu, G. Lu, Combustion synthesis of CuO–ZnO–ZrO2 catalysts for the hydrogenation of carbon dioxide to methanol, Catalysis Communications, 10 (2009) 1661-1664.

[120] F. Arena, K. Barbera, G. Italiano, G. Bonura, L. Spadaro, F. Frusteri, Synthesis, characterization and activity pattern of Cu–ZnO/ZrO2 catalysts in the hydrogenation of carbon dioxide to methanol, Journal of Catalysis, 249 (2007) 185-194.

[121] M. Saito, K. Murata, Development of high performance Cu/ZnO-based catalysts for methanol synthesis and the water-gas shift reaction, Catalysis Surveys from Asia, 8 (2004) 285-294.

[122] J.B. Wang, H.-K. Lee, T.-J. Huang, Synergistic catalysis of carbon dioxide hydrogenation into methanol by yttria-doped ceria/γ-alumina-supported copper oxide catalysts: effect of support and dopant, Catalysis letters, 83 (2002) 79-86.

[123] Y. Zhang, J. Fei, Y. Yu, X. Zheng, Study of CO2 Hydrogenation to methanol over Cu-V/γ-Al2O3 catalyst, Journal of natural gas chemistry, 16 (2007) 12-15.

[124] O. Martin, A.J. Martín, C. Mondelli, S. Mitchell, T.F. Segawa, R. Hauert, C. Drouilly, D. Curulla-Ferré, J. Pérez-Ramírez, Indium oxide as a superior catalyst for methanol synthesis by CO2 hydrogenation, Angewandte Chemie International Edition, 55 (2016) 6261-6265.

[125] J. Ma, N. Sun, X. Zhang, N. Zhao, F. Xiao, W. Wei, Y. Sun, A short review of catalysis for CO2 conversion, Catalysis Today, 148 (2009) 221-231.

[126] L. Jia, J. Gao, W. Fang, Q. Li, Carbon dioxide hydrogenation to methanol over the pre-reduced LaCr0. 5Cu0. 5O3 catalyst, Catalysis Communications, 10 (2009) 2000-2003.

[127] D.L. Chiavassa, J. Barrandeguy, A.L. Bonivardi, M.A. Baltanás, Methanol synthesis from CO2/H2 using Ga2O3–Pd/silica catalysts: Impact of reaction products, Catalysis Today, 133 (2008) 780-786.

[128] M. Wencka, J. Kovač, V.D.B.C. Dasireddy, B. Likozar, A. Jelen, S. Vrtnik, P. Gille, H.J. Kim, J. Dolinšek, The effect of surface oxidation on the catalytic properties of Ga3Ni2 intermetallic compound for carbon dioxide reduction, Journal of Analytical Science and Technology, 9 (2018) 12.

[129] N. Iwasa, S. Masuda, N. Ogawa, N. Takezawa, Steam reforming of methanol over Pd/ZnO: effect of the formation of PdZn alloys upon the reaction, Applied Catalysis A: General, 125 (1995) 145-157.

[130] S.E. Collins, J.J. Delgado, C. Mira, J.J. Calvino, S. Bernal, D.L. Chiavassa, M.A. Baltanás, A.L. Bonivardi, The role of Pd–Ga bimetallic particles in the bifunctional mechanism of selective methanol synthesis via CO2 hydrogenation on a Pd/Ga2O3 catalyst, Journal of Catalysis, 292 (2012) 90-98.

[131] T. Fujitani, M. Saito, Y. Kanai, T. Watanabe, J. Nakamura, T. Uchijima, Development of an active Ga2O3 supported palladium catalyst for the synthesis of methanol from carbon dioxide and hydrogen, Applied Catalysis A: General, 125 (1995) L199-L202.

[132] X. Zhou, J. Qu, F. Xu, J. Hu, J.S. Foord, Z. Zeng, X. Hong, S.C.E. Tsang, Shape selective plate-form Ga2O3 with strong metal–support interaction to overlying Pd for hydrogenation of CO2 to CH3OH, Chemical Communications, 49 (2013) 1747-1749.

[133] L. Li, B. Zhang, E. Kunkes, K. Föttinger, M. Armbrüster, D.S. Su, W. Wei, R. Schlögl, M. Behrens, Ga-Pd/Ga_2O_3 Catalysts: The Role of Gallia Polymorphs, Intermetallic Compounds, and Pretreatment Conditions on Selectivity and Stability in Different Reactions, ChemCatChem, 4 (2012) 1764-1775.

[134] E.M. Fiordaliso, I. Sharafutdinov, H.W. Carvalho, J.-D. Grunwaldt, T.W. Hansen, I. Chorkendorff, J.B. Wagner, C.D. Damsgaard, Intermetallic GaPd2 nanoparticles on SiO2 for low-pressure CO2 hydrogenation to methanol: Catalytic performance and in situ characterization, ACS Catalysis, 5 (2015) 5827-5836.

[135] A. Ota, E.L. Kunkes, I. Kasatkin, E. Groppo, D. Ferri, B. Poceiro, R.M.N. Yerga, M. Behrens, Comparative study of hydrotalcite-derived supported Pd2Ga and PdZn intermetallic nanoparticles as methanol synthesis and methanol steam reforming catalysts, Journal of catalysis, 293 (2012) 27-38.

[136] X.-L. Liang, X. Dong, G.-D. Lin, H.-B. Zhang, Carbon nanotube-supported Pd–ZnO catalyst for hydrogenation of CO2 to methanol, Applied Catalysis B: Environmental, 88 (2009) 315-322.

[137] H. Bahruji, M. Bowker, W. Jones, J. Hayward, J. Ruiz Esquius, D.J. Morgan, G.J. Hutchings, PdZn catalysts for CO2 hydrogenation to methanol using chemical vapour impregnation (CVI), Faraday Discussions, 197 (2017) 309-324.

[138] X. Jiang, N. Koizumi, X. Guo, C. Song, Bimetallic Pd–Cu catalysts for selective CO2 hydrogenation to methanol, Applied Catalysis B: Environmental, 170 (2015) 173-185.

[139] H. Kusama, K. Okabe, K. Sayama, H. Arakawa, Alcohol synthesis by catalytic hydrogenation of CO2 over Rh–Co/SiO2, Applied organometallic chemistry, 14 (2000) 836-840.

[140] C. Shao, L. Fan, K. Fujimoto, Y. Iwasawa, Selective methanol synthesis from CO2/H2 on new SiO2-supported PtW and PtCr bimetallic catalysts, Applied Catalysis A: General, 128 (1995) L1-L6.

[141] J. Strunk, K. Kaehler, X. Xia, M. Comotti, F. Schueth, T. Reinecke, M. Muhler, Au/ZnO as catalyst for methanol synthesis: The role of oxygen vacancies, Applied Catalysis A: General, 359 (2009) 121-128.

[142] R. Ferrando, J. Jellinek, R.L. Johnston, Nanoalloys: from theory to applications of alloy clusters and nanoparticles, Chemical reviews, 108 (2008) 845-910.

[143] G. Guisbiers, S. Khanal, F. Ruiz-Zepeda, J.R. de la Puente, M. José-Yacaman, Cu–Ni nano-alloy: mixed, core–shell or Janus nano-particle?, Nanoscale, 6 (2014) 14630-14635.

[144] B. Hammer, J. Nørskov, Electronic factors determining the reactivity of metal surfaces, Surface Science, 343 (1995) 211-220.

[145] B. Hammer, J.K. Nørskov, Theoretical surface science and catalysis—calculations and concepts, Advances in catalysis, Elsevier2000, pp. 71-129.

[146] P. Liu, J.K. Nørskov, Ligand and ensemble effects in adsorption on alloy surfaces, Physical Chemistry Chemical Physics, 3 (2001) 3814-3818.

[147] J. Kitchin, J.K. Nørskov, M. Barteau, J. Chen, Modification of the surface electronic and chemical properties of Pt (111) by subsurface 3d transition metals, The Journal of chemical physics, 120 (2004) 10240-10246.

[148] M. Mavrikakis, B. Hammer, J.K. Nørskov, Effect of strain on the reactivity of metal surfaces, Physical Review Letters, 81 (1998) 2819.

[149] H. Kusama, K. Okabe, K. Sayama, H. Arakawa, Ethanol synthesis by catalytic hydrogenation of CO2 over Rh□ FeSiO2 catalysts, Energy, 22 (1997) 343-348.

[150] F. Liao, X.-P. Wu, J. Zheng, M.M.-J. Li, A. Kroner, Z. Zeng, X. Hong, Y. Yuan, X.-Q. Gong, S.C.E. Tsang, A promising low pressure methanol synthesis route from CO 2 hydrogenation over Pd@ Zn core–shell catalysts, Green Chemistry, 19 (2017) 270-280.

[151] A.L. Bonivardi, D.L. Chiavassa, C.A. Querini, M.A. Baltanas, Enhancement of the catalytic performance to methanol synthesis from CO2/H2 by gallium addition to palladium/silica catalysts, Studies in Surface Science and Catalysis, Elsevier2000, pp. 3747-3752.

[152] K. Kovnir, M. Armbrüster, D. Teschner, T. Venkov, F.C. Jentoft, A. Knop-Gericke, Y. Grin, R. Schlögl, A new approach to well-defined, stable and site-isolated catalysts, Science and Technology of Advanced Materials, 8 (2007) 420.

[153] M. Friedrich, D. Teschner, A. Knop-Gericke, M. Armbrüster, Surface and subsurface dynamics of the intermetallic compound ZnNi in methanol steam reforming, The Journal of Physical Chemistry C, 116 (2012) 14930-14935.

[154] A. Haghofer, K. Föttinger, F. Girgsdies, D. Teschner, A. Knop-Gericke, R. Schlögl, G. Rupprechter, In situ study of the formation and stability of supported Pd2Ga methanol steam reforming catalysts, Journal of catalysis, 286 (2012) 13-21.

[155] A. Ota, J. Kröhnert, G. Weinberg, I. Kasatkin, E.L. Kunkes, D. Ferri, F. Girgsdies, N. Hamilton, M. Armbrüster, R. Schlögl, Dynamic surface processes of nanostructured Pd2Ga catalysts derived from hydrotalcite-like precursors, ACS Catalysis, 4 (2014) 2048-2059.

[156] A.s. García-Trenco, E.R. White, A. Regoutz, D.J. Payne, M.S. Shaffer, C.K. Williams, Pd2Ga-based colloids as highly active catalysts for the hydrogenation of CO2 to methanol, Acs Catalysis, 7 (2017) 1186-1196.

[157] J. Edvardsson, P. Rautanen, A. Littorin, M. Larsson, Deactivation and coke formation on palladium and platinum catalysts in vegetable oil hydrogenation, Journal of the American Oil Chemists' Society, 78 (2001) 319-327.

[158] C. Arcoumanis, C. Bae, R. Crookes, E. Kinoshita, The potential of di-methyl ether (DME) as an alternative fuel for compression-ignition engines: A review, Fuel, 87 (2008) 1014-1030.

[159] S. Lee, Dimethyl Ether Synthesis and Conversion to Value-Added Chemicals.

[160] C.-S.T. Chih-Hung Huang, A Review: CO2 Utilization, Aerosol and Air Quality Research, (2014) 480-499.

[161] V.E. Ivanova S, Louis B, Libs S, Ledoux MJ, Rigolet S, Marichal C, Pham C, Luck F, Pham-Huu C, Efficient synthesis of dimethyl ether over HZSM-5 supported on medium-surface-area beta-SiC foam, ChemSusChem, (2008) 851-857.

[162] H.-S.L. Ki-Won Jun, Hyun-Seog Roh, Sang- Eon Park, Catalytic Dehydration of Methanol to Dimethyl Ether (DME) Over Solid-Acid Catalysts, Bulletin of the Korean Chemical Society (2002) 803-806.

[163] M.K. N. Khandan, M. Aghaziarati, Dehydration of Methanol to Dimethyl Ether Employing Modified H-ZSM-5 Catalysts, Iranian Journal of Chemical Engineering, (2009) 3-11.

[164] W. Alharbi, E.F. Kozhevnikova, I.V. Kozhevnikov, Dehydration of methanol to dimethyl ether over heteropoly acid catalysts: the relationship between reaction rate and catalyst acid strength, ACS Catalysis, 5 (2015) 7186-7193.

[165] A. Ciftci, N.A. Sezgi, T. Dogu, Nafion-incorporated silicate structured nanocomposite mesoporous catalysts for dimethyl ether synthesis, Industrial & Engineering Chemistry Research, 49 (2010) 6753-6762.

[166] D. Varışlı, T. Doğu, Production of clean transportation fuel dimethylether by dehydration of methanol over nafion catalyst, Gazi University Journal of Science, 21 (2008) 37-41.

[167] R.A.v.S. Solange R. Blaszkowski, Theoretical Study of the Mechanism of Surface Methoxy and Dimethyl Ether Formation from Methanol Catalyzed by Zeolitic Protons, The Journal of Physical Chemistry, (1997) 2292-2305.

[168] A.J. Louise Samain, Mattias Edén, Danielle M. Laddc, Dong-Kyun Seo, F. Javier Garcia-Garcia, Ulrich Häussermann, Structural analysis of highly porous γ-Al2O3, Journal of Solid State Chemistry, (2014) 1-8.

[169] K.M.D. James J. Spivey, Catalysis, Royal Society of Chemistry2011.

[170] J.B. Peri, A Model for the Surface of gamma-Alumina, The Journal of Physical Chemistry, (1964) 220-230.

[171] R.P.M. Rinaldo S.Schiffimo, A Mechanistic Study of the Methanol Dehydration Reaction on γ-Alumina Catalyst, The Journal of Physical Chemistry, (1993) 6425-6435.

[172] J.K. Thomas, Physical Aspects of Photochemistry and Radiation Chemistry of Molecules Adsorbed on SiO2, gamma-Al2O3, Zeolites and Clays, Chemical Reviews, (1993) 301-320.

[173] P.R. H. Knözinger, Catalytic Aluminas: Surface Models and Characterization of Surface Sites, Catalysis Reviews: Science and Engineering, (1978) 31-70.

[174] G.M. Claudio Morterra, A case study: surface chemistry and surface structure of catalytic aluminas, as studied by vibrational spectroscopy of adsorbed species, Catalysis Today, (1996) 497-532.

[175] M. Xu, J.H. Lunsford, D.W. Goodman, A. Bhattacharyya, Synthesis of dimethyl ether (DME) from methanol over solid-acid catalysts, Applied Catalysis A: General, 149 (1997) 289-301.

[176] F. Raoof, M. Taghizadeh, A. Eliassi, F. Yaripour, Effects of temperature and feed composition on catalytic dehydration of methanol to dimethyl ether over γ-alumina, Fuel, 87 (2008) 2967-2971.

[177] K. Larmier, A. Nicolle, C. Chizallet, N. Cadran, S. Maury, A.-F. Lamic-Humblot, E. Marceau, H.l.n. Lauron-Pernot, Influence of coadsorbed water and alcohol molecules on isopropyl alcohol dehydration on γ-alumina: multiscale modeling of experimental kinetic profiles, ACS Catalysis, 6 (2016) 1905-1920.

[178] J. Boon, J. van Kampen, R. Hoogendoorn, S. Tanase, F.P. van Berkel, M. van Sint Annaland, Reversible deactivation of γ-alumina by steam in the gas-phase dehydration of methanol to dimethyl ether, Catalysis Communications, 119 (2019) 22-27.

[179] D. Liu, C. Yao, J. Zhang, D. Fang, D. Chen, Catalytic dehydration of methanol to dimethyl ether over modified γ-Al2O3 catalyst, Fuel, 90 (2011) 1738-1742.

[180] A. Khaleel, Titanium-doped alumina for catalytic dehydration of methanol to dimethyl ether at relatively low temperatures, Fuel, 90 (2011) 2422-2427.

[181] M. Mollavali, F. Yaripour, S. Mohammadi-Jam, H. Atashi, Relationship between surface acidity and activity of solid-acid catalysts in vapour phase dehydration of methanol, Fuel Processing Technology, 90 (2009) 1093-1098.

[182] J. Xia, D. Mao, B. Zhang, Q. Chen, Y. Zhang, Y. Tang, Catalytic properties of fluorinated alumina for the production of dimethyl ether, Catalysis Communications, 7 (2006) 362-366.

[183] F. Yaripour, Z. Shariatinia, S. Sahebdelfar, A. Irandoukht, The effects of synthesis operation conditions on the properties of modified γ-alumina nanocatalysts in methanol dehydration to dimethyl ether using factorial experimental design, Fuel, 139 (2015) 40-50.

[184] M.C.P. Rajiv Shah, J. D. Gale, Acid-Base Catalysis in Zeolites from First Principles, International Journal of Quantum Chemistry, (1997) 393-398.

[185] G.B. H.G. Karge, H.K. Beyer and G. Onyestyak, Proceedings of the 9th Interna- tional Congress on Catalysis, Ottawa, 1988, pp. 396-403.

[186] J.W.a.M. Hunger, ACID AND BASE CATALYSIS ON ZEOLITES, 2007, pp. 787-835.

[187] A.W. Wang, MOLECULAR SIEVES AS CATALYSTS FOR METHANOL DEHYDRATION IN THE LPDMEtm PROCESS, National Energy Technology Laboratory, Pittsburgh, PA, and Morgantown, WV (US), US, 2002.

[188] F.R. Ali A. Rownaghi, Matteo Stante, Jonas Hedlund, Selective dehydration of methanol to dimethyl ether on ZSM-5 nanocrystals, Applied Catalysis B: Environmental, (2012) 56-61.

[189] F.Y. Samaneh Hassanpour, Majid Taghizadeh, Performance of modified H-ZSM-5 zeolite for dehydration of methanol to dimethyl ether, Fuel Processing Technology, (2010) 1212-1221.

[190] E. Catizzone, A. Aloise, M. Migliori, G. Giordano, Dimethyl ether synthesis via methanol dehydration: Effect of zeolite structure, Applied Catalysis A: General, 502 (2015) 215-220.

[191] J. Flores, D. Peixoto, L. Appel, R. De Avillez, M.P. da Silva, The influence of different methanol synthesis catalysts on direct synthesis of DME from syngas, Catalysis today, 172 (2011) 218-225.

[192] Q. Xie, P. Chen, P. Peng, S. Liu, P. Peng, B. Zhang, Y. Cheng, Y. Wan, Y. Liu, R. Ruan, Single-step synthesis of DME from syngas on CuZnAl–zeolite bifunctional catalysts: the influence of zeolite type, RSC Advances, 5 (2015) 26301-26307.

[193] J.F. Haw, W. Song, D.M. Marcus, J.B. Nicholas, The mechanism of methanol to hydrocarbon catalysis, Accounts of chemical research, 36 (2003) 317-326.

[194] U. Olsbye, S. Svelle, M. Bjørgen, P. Beato, T.V. Janssens, F. Joensen, S. Bordiga, K.P. Lillerud, Conversion of methanol to hydrocarbons: how zeolite cavity and pore size controls product selectivity, Angewandte Chemie International Edition, 51 (2012) 5810-5831.

[195] S. Svelle, F. Joensen, J. Nerlov, U. Olsbye, K.-P. Lillerud, S. Kolboe, M. Bjørgen, Conversion of methanol into hydrocarbons over zeolite H-ZSM-5: Ethene formation is mechanistically separated from the formation of higher alkenes, journal of the American Chemical Society, 128 (2006) 14770-14771.

[196] D.M. Bibby, R.F. Howe, G.D. McLellan, Coke formation in high-silica zeolites, Applied Catalysis A: General, 93 (1992) 1-34.

[197] P.L. Benito, A.G. Gayubo, A.T. Aguayo, M. Olazar, J. Bilbao, Deposition and characteristics of coke over a H-ZSM5 zeolite-based catalyst in the MTG process, Industrial & engineering chemistry research, 35 (1996) 3991-3998.

[198] M. Bjørgen, S. Svelle, F. Joensen, J. Nerlov, S. Kolboe, F. Bonino, L. Palumbo, S. Bordiga, U. Olsbye, Conversion of methanol to hydrocarbons over zeolite H-ZSM-5: On the origin of the olefinic species, Journal of Catalysis, 249 (2007) 195-207.

[199] J. Kim, M. Choi, R. Ryoo, Effect of mesoporosity against the deactivation of MFI zeolite catalyst during the methanol-to-hydrocarbon conversion process, Journal of Catalysis, 269 (2010) 219-228.

[200] E. Catizzone, A. Aloise, M. Migliori, G. Giordano, From 1-D to 3-D zeolite structures: Performance assessment in catalysis of vapour-phase methanol dehydration to DME, Microporous and Mesoporous Materials, 243 (2017) 102-111.

[201] S.-C. Baek, Y.-J. Lee, K.-W. Jun, S.B. Hong, Influence of catalytic functionalities of zeolites on product selectivities in methanol conversion, Energy & Fuels, 23 (2009) 593-598.

[202] E. Catizzone, A. Aloise, M. Migliori, G. Giordano, The effect of FER zeolite acid sites in methanol-to-dimethyl-ether catalytic dehydration, Journal of energy chemistry, 26 (2017) 406-415.

[203] Q. Tang, H. Xu, Y. Zheng, J. Wang, H. Li, J. Zhang, Catalytic dehydration of methanol to dimethyl ether over micro–mesoporous ZSM-5/MCM-41 composite molecular sieves, Applied Catalysis A: General, 413 (2012) 36-42.

[204] M. Rutkowska, D. Macina, Z. Piwowarska, M. Gajewska, U. Diaz, L. Chmielarz, Hierarchically structured ZSM-5 obtained by optimized mesotemplate-free method as active catalyst for methanol to DME conversion, Catalysis Science & Technology, 6 (2016) 4849-4862.

[205] S.D. Kim, S.C. Baek, Y.-J. Lee, K.-W. Jun, M.J. Kim, I.S. Yoo, Effect of γ-alumina content on catalytic performance of modified ZSM-5 for dehydration of crude methanol to dimethyl ether, Applied Catalysis A: General, 309 (2006) 139-143.

[206] S. Hassanpour, F. Yaripour, M. Taghizadeh, Performance of modified H-ZSM-5 zeolite for dehydration of methanol to dimethyl ether, Fuel Processing Technology, 91 (2010) 1212-1221.

[207] N. Khandan, M. KAZEMEYNI, M. Aghaziarati, Dehydration of methanol to dimethyl ether employing modified H-ZSM-5 catalysts, (2009).

[208] S. Hassanpour, M. Taghizadeh, F. Yaripour, Preparation, characterization, and activity evaluation of H-ZSM-5 catalysts in vapor-phase methanol dehydration to dimethyl ether, Industrial & Engineering Chemistry Research, 49 (2010) 4063-4069.

[209] T. Armaroli, L. Simon, M. Digne, T. Montanari, M. Bevilacqua, V. Valtchev, J. Patarin, G. Busca, Effects of crystal size and Si/Al ratio on the surface properties of H-ZSM-5 zeolites, Applied Catalysis A: General, 306 (2006) 78-84.

[210] C.N. Jean Bandiera, Kinetics of methanol dehydration on dealuminated H-mordenite: Model with acid and basic active centres, Applied Catalysis, (1991) 139-148.

[211] J.J. Spivey, REVIEW: DEHYDRATION CATALYSTS FOR THE METHANOL/DIMETHYL ETHER REACTION, Chemical Engineering Communications, (1991) 123-142.

[212] L. Kubelková, J. Nováková, K. Nedomová, Reactivity of surface species on zeolites in methanol conversion, Journal of catalysis, 124 (1990) 441-450.

[213] R.A.v.S. Solange R. Blaszkowski, The Mechanism of Dimethyl Ether Formation from Methanol Catalyzed by Zeolitic Protons, The Journal of American Chemical Society, (1996) 5152-5153.

[214] Y.J. Wei Wang, Michael Hunger, Mechanistic investigations of the methanol-to-olefin (MTO) process on acidic zeolite catalysts by in situ solid-state NMR spectroscopy, Catalysis Today, (2006) 102-114.

[215] T.T. Nobuo Tajima, Fuminori Toyama , and Kimihiko Hirao, A New Mechanism for the First Carbon−Carbon Bond Formation in the MTG Process: A Theoretical Study, The Journal of American Chemical Society, (1998) 8222-8229.

[216] T.M. Yoshi Ono, Mechanism of Methanol Conversion into Hydrocarbons over ZSM-5 Zeolite, Journal of the Chemical Society, Faraday Transactions, (1981) 2209-2221.

[217] J.L. Gorazd Bercic, Intrinsic and Global Reaction Rate of Methanol Dehydration over gamma-Al2O3 Pellets, Industrial & Engineering Chemistry Research, (1992) 1035-1040.

[218] L.N.J. B.C Gates, Lungmuir-HinshelwoodKineticsofthe Dehydration of Methanol Catalyzed by Cation Exchange Resin, AIChE J, (1971) 981-983.

[219] K.L. Ng, D. Chadwick, B. Toseland, Kinetics and modelling of dimethyl ether synthesis from synthesis gas, Chemical Engineering Science, 54 (1999) 3587-3592.

[220] B.W.D. Xiang-Dong Peng, Tsun-Chiu Robert Tsao, Bharat Lajjaram Bhatt, Separation process for one-step production of dimethyl ether from synthesis gas US, 2002.

[221] M.J.P. Ji-Hyun Kim, Sun Jin Kim, Oh-Shim Joo, Kwang-Deog Jung, DME synthesis from synthesis gas on the admixed catalysts of Cu/ZnO/Al2O3 and ZSM-5, Applied Catalysis A: General, (2004) 37-41.

[222] F. Ramos, A.D. de Farias, L.E.P. Borges, J. Monteiro, M.A. Fraga, E.F. Sousa-Aguiar, L.G. Appel, Role of dehydration catalyst acid properties on one-step DME synthesis over physical mixtures, Catalysis Today, 101 (2005) 39-44.

[223] S.P. Naik, T. Ryu, V. Bui, J.D. Miller, N.B. Drinnan, W. Zmierczak, Synthesis of DME from CO2/H2 gas mixture, Chemical engineering journal, 167 (2011) 362-368.

[224] X. Peng, B. Toseland, R. Underwood, A novel mechanism of catalyst deactivation in liquid phase synthesis gas-to-DME reactions, Studies in surface science and catalysis, Elsevier1997, pp. 175-182.

[225] V. Ordomsky, M. Cai, V. Sushkevich, S. Moldovan, O. Ersen, C. Lancelot, V. Valtchev, A. Khodakov, The role of external acid sites of ZSM-5 in deactivation of hybrid CuZnAl/ZSM-5 catalyst for direct dimethyl ether synthesis from syngas, Applied Catalysis A: General, 486 (2014) 266-275.

[226] A. García-Trenco, A. Martínez, The influence of zeolite surface-aluminum species on the deactivation of CuZnAl/zeolite hybrid catalysts for the direct DME synthesis, Catalysis Today, 227 (2014) 144-153.

[227] F. Frusteri, M. Migliori, C. Cannilla, L. Frusteri, E. Catizzone, A. Aloise, G. Giordano, G. Bonura, Direct CO2-to-DME hydrogenation reaction: New evidences of a superior behaviour of FER-based hybrid systems to obtain high DME yield, Journal of CO2 Utilization, 18 (2017) 353-361.

[228] S. Allahyari, M. Haghighi, A. Ebadi, S. Hosseinzadeh, Effect of irradiation power and time on ultrasound assisted co-precipitation of nanostructured CuO–ZnO–Al2O3 over HZSM-5 used for direct conversion of syngas to DME as a green fuel, Energy conversion and management, 83 (2014) 212-222.

[229] F. Frusteri, G. Bonura, C. Cannilla, G.D. Ferrante, A. Aloise, E. Catizzone, M. Migliori, G. Giordano, Stepwise tuning of metal-oxide and acid sites of CuZnZr-MFI hybrid catalysts

for the direct DME synthesis by CO2 hydrogenation, Applied Catalysis B: Environmental, 176 (2015) 522-531.

[230] G. Bonura, F. Frusteri, C. Cannilla, G.D. Ferrante, A. Aloise, E. Catizzone, M. Migliori, G. Giordano, Catalytic features of CuZnZr–zeolite hybrid systems for the direct CO2-to-DME hydrogenation reaction, Catalysis Today, 277 (2016) 48-54.

[231] A. Bansode, A. Urakawa, Towards full one-pass conversion of carbon dioxide to methanol and methanol-derived products, Journal of catalysis, 309 (2014) 66-70.

[232] J.W. Bae, S.-H. Kang, Y.-J. Lee, K.-W. Jun, Effect of precipitants during the preparation of Cu-ZnO-Al2O3/Zr-ferrierite catalyst on the DME synthesis from syngas, Journal of Industrial and Engineering Chemistry, 15 (2009) 566-572.

[233] Q. Ge, Y. Huang, F. Qiu, S. Li, Bifunctional catalysts for conversion of synthesis gas to dimethyl ether, Applied Catalysis A: General, 167 (1998) 23-30.

[234] S. Ren, S. Li, N. Klinghoffer, M. Yu, X. Liang, Effects of mixing methods of bifunctional catalysts on catalyst stability of DME synthesis via CO2 hydrogenation, Carbon Resources Conversion, (2019).

[235] P.S. Prasad, J.W. Bae, S.-H. Kang, Y.-J. Lee, K.-W. Jun, Single-step synthesis of DME from syngas on Cu–ZnO–Al2O3/zeolite bifunctional catalysts: The superiority of ferrierite over the other zeolites, Fuel Processing Technology, 89 (2008) 1281-1286.

[236] K. Sun, W. Lu, M. Wang, X. Xu, Low-temperature synthesis of DME from CO2/H2 over Pd-modified CuO–ZnO–Al2O3–ZrO2/HZSM-5 catalysts, Catalysis Communications, 5 (2004) 367-370.

[237] K. Sun, W. Lu, F. Qiu, S. Liu, X. Xu, Direct synthesis of DME over bifunctional catalyst: surface properties and catalytic performance, Applied Catalysis A: General, 252 (2003) 243-249.

[238] A. García-Trenco, A. Vidal-Moya, A. Martínez, Study of the interaction between components in hybrid CuZnAl/HZSM-5 catalysts and its impact in the syngas-to-DME reaction, Catalysis today, 179 (2012) 43-51.

[239] M. Stiefel, R. Ahmad, U. Arnold, M. Döring, Direct synthesis of dimethyl ether from carbon-monoxide-rich synthesis gas: Influence of dehydration catalysts and operating conditions, Fuel Processing Technology, 92 (2011) 1466-1474.

[240] X. Ning, Z. An, J. He, Remarkably efficient CoGa catalyst with uniformly dispersed and trapped structure for ethanol and higher alcohol synthesis from syngas, Journal of catalysis, 340 (2016) 236-247.

[241] M. Sahibzada, D. Chadwick, I. Metcalfe, Hydrogenation of carbon dioxide to methanol over palladium-promoted Cu/ZnO/Al_2O_3 catalysts, Catalysis today, 29 (1996) 367-372.

[242] D.L. Chiavassa, S.E. Collins, A.L. Bonivardi, M.A. Baltanás, Methanol synthesis from CO2/H2 using Ga2O3–Pd/silica catalysts: Kinetic modeling, Chemical Engineering Journal, 150 (2009) 204-212.

[243] M.A. Vannice, W.H. Joyce, Kinetics of catalytic reactions, Springer2005.

[244] G. Graaf, P. Sijtsema, E. Stamhuis, G. Joosten, Chemical equilibria in methanol synthesis, Chemical Engineering Science, 41 (1986) 2883-2890.

[245] S.G. Jadhav, P.D. Vaidya, B.M. Bhanage, J.B. Joshi, Catalytic carbon dioxide hydrogenation to methanol: A review of recent studies, Chemical Engineering Research and Design, 92 (2014) 2557-2567.

[246] S. Sato, R. Takahashi, T. Sodesawa, K.-i. Yuma, Y. Obata, Distinction between surface and bulk oxidation of Cu through N2O decomposition, Journal of Catalysis, 196 (2000) 195-199.

[247] M. Luys, P. Van Oeffelt, W. Brouwer, A. Pijpers, J. Sscholten, Surface and sub-surface oxidation of copper and supported copper catalysts by nitrous oxide, Applied catalysis, 46 (1989) 161-173.

[248] J. Scholten, J. Konvalinka, Reaction of nitrous oxide with copper surfaces. Application to the determination of free-copper surface areas, Transactions of the Faraday Society, 65 (1969) 2465-2473.

[249] D.J. Heldebrant, H.N. Witt, S.M. Walsh, T. Ellis, J. Rauscher, P.G. Jessop, Liquid polymers as solvents for catalytic reductions, Green Chemistry, 8 (2006) 807-815.

[250] R. Knapp, A. Jentys, J.A. Lercher, Impact of supported ionic liquids on supported Pt catalysts, Green Chemistry, 11 (2009) 656-661.

[251] D.H.H. Von, J. Margarete, Method of preserving the catalytic activity of sensitive catalysts, Google Patents, 1968.

[252] G.A. Mills, F.W. Steffgen, Catalytic methanation, Catalysis Reviews, 8 (1974) 159-210.

[253] P. Sabatier, J. Senderens, Hydrogenation of CO over nickel to produce methane, J. Soc. Chim. Ind, 21 (1902) 504-506.

[254] M. Araki, V. Ponec, Methanation of carbon monoxide on nickel and nickel-copper alloys, Journal of Catalysis, 44 (1976) 439-448.

[255] D.A. Torelli, S.A. Francis, J.C. Crompton, A. Javier, J.R. Thompson, B.S. Brunschwig, M.P. Soriaga, N.S. Lewis, Nickel–gallium-catalyzed electrochemical reduction of CO2 to highly reduced products at low overpotentials, Acs Catalysis, 6 (2016) 2100-2104.

[256] F. Yaripour, F. Baghaei, I. Schmidt, J. Perregaard, Catalytic dehydration of methanol to dimethyl ether (DME) over solid-acid catalysts, Catalysis Communications, 6 (2005) 147-152.

[257] R. Sahki, O. Benlounes, O. Chérifi, R. Thouvenot, M.M. Bettahar, S. Hocine, Effect of pressure on the mechanisms of the CO 2/H 2 reaction on a CO-precipitated CuO/ZnO/Al 2 O 3 catalyst, Reaction Kinetics, Mechanisms and Catalysis, 103 (2011) 391-403.

[258] J. Skrzypek, M. Lachowska, M. Grzesik, J. Słoczyński, P. Nowak, Thermodynamics and kinetics of low pressure methanol synthesis, The Chemical Engineering Journal and the Biochemical Engineering Journal, 58 (1995) 101-108.

[259] M. Sahibzada, D. Chadwick, I. Metcalfe, Hydrogenation of carbon dioxide to methanol over palladium-promoted Cu/ZnO/A12O3 catalysts, Catalysis today, 29 (1996) 367-372.

[260] G. Jacobs, T.K. Das, Y. Zhang, J. Li, G. Racoillet, B.H. Davis, Fischer–Tropsch synthesis: support, loading, and promoter effects on the reducibility of cobalt catalysts, Applied Catalysis A: General, 233 (2002) 263-281.

[261] N. Lohitharn, J.G. Goodwin Jr, E. Lotero, Fe-based Fischer–Tropsch synthesis catalysts containing carbide-forming transition metal promoters, Journal of Catalysis, 255 (2008) 104-113.

[262] K. Fujimoto, Y. Yu, Spillover effect on the stabilization of Cu-Zn catalyst for CO2 hydrogenation to methanol, Studies in Surface Science and Catalysis, Elsevier1993, pp. 393-396.

[263] S.E. Collins, D.L. Chiavassa, A.L. Bonivardi, M.A. Baltanás, Hydrogen Spillover in Ga2O3–Pd/SiO2 Catalysts for Methanol Synthesis from CO2/H2, Catalysis Letters, 103 (2005) 83-88.

[264] O. Oyola-Rivera, M.A. Baltanás, N. Cardona-Martínez, CO2 hydrogenation to methanol and dimethyl ether by Pd–Pd2Ga catalysts supported over Ga2O3 polymorphs, Journal of CO2 Utilization, 9 (2015) 8-15.

[265] R. Sasikala, S. Kulshreshtha, Temperature programmed reduction studies of spillover effect in Pd impregnated metal oxide catalysts, Journal of thermal analysis and calorimetry, 78 (2004) 723-729.

[266] S. Penner, B. Jenewein, K. Hayek, Pd–Al interaction at elevated temperatures: a TEM and SAED study, Catalysis Letters, 113 (2007) 65-72.

[267] M. Armbrüster, G. Wowsnick, M. Friedrich, M. Heggen, R. Cardoso-Gil, Synthesis and catalytic properties of nanoparticulate intermetallic Ga–Pd compounds, Journal of the American Chemical Society, 133 (2011) 9112-9118.

[268] I. Locka, S. Lockb, N. Dai-viet, B. Abdullah, Influence of palladium on Ni-based catalyst for hydrogen production via thermo-catalytic methane decomposition, Chem Eng, 57 (2017).

[269] A. Berenblyum, H.A. Al-Wadhaf, E. Katsman, V. Flid, Kinetics and mechanism of palladium (II) acetate reduction by hydrogen on the surface of a carbon support, Kinetics and Catalysis, 52 (2011) 296-304.

[270] L. Li, W. Wei, M. Behrens, Synthesis and characterization of α-, β-, and γ-Ga2O3 prepared from aqueous solutions by controlled precipitation, Solid State Sciences, 14 (2012) 971-981.

[271] N. Iwasa, T. Mayanagi, N. Ogawa, K. Sakata, N. Takezawa, New catalytic functions of Pd–Zn, Pd–Ga, Pd–In, Pt–Zn, Pt–Ga and Pt–In alloys in the conversions of methanol, Catalysis Letters, 54 (1998) 119-123.

[272] F. Roessner, U. Roland, T. Braunschweig, Investigations on hydrogen spillover. Part 2.—Hydrocarbon conversion on bifunctional catalysts, Journal of the Chemical Society, Faraday Transactions, 91 (1995) 1539-1545.

[273] A.D. Lueking, R.T. Yang, Hydrogen spillover to enhance hydrogen storage—study of the effect of carbon physicochemical properties, Applied Catalysis A: General, 265 (2004) 259-268.

[274] A.J. Robell, E. Ballou, M. Boudart, Surface diffusion of hydrogen on carbon, The Journal of Physical Chemistry, 68 (1964) 2748-2753.

[275] H. Zhu, Z. Qin, W. Shan, W. Shen, J. Wang, Pd/CeO2–TiO2 catalyst for CO oxidation at low temperature: a TPR study with H2 and CO as reducing agents, Journal of Catalysis, 225 (2004) 267-277.

[276] P. Albers, J. Pietsch, S.F. Parker, Poisoning and deactivation of palladium catalysts, Journal of molecular catalysis A: Chemical, 173 (2001) 275-286.

[277] M. Argyle, C. Bartholomew, Heterogeneous catalyst deactivation and regeneration: a review, Catalysts, 5 (2015) 145-269.

[278] M.M. Nair, S. Kaliaguine, Structured catalysts for dry reforming of methane, New Journal of Chemistry, 40 (2016) 4049-4060.

[279] C. Montero, A. Ochoa, P. Castaño, J. Bilbao, A.G. Gayubo, Monitoring Ni0 and coke evolution during the deactivation of a Ni/La2O3–αAl2O3 catalyst in ethanol steam reforming in a fluidized bed, Journal of Catalysis, 331 (2015) 181-192.

[280] T. Kumari, R. Gopal, A. Goyal, J. Joshi, Sol–Gel Synthesis of Pd@ PdO Core–Shell Nanoparticles and Effect of Precursor Chemistry on Their Structural and Optical Properties, Journal of Inorganic and Organometallic Polymers and Materials, 29 (2019) 316-325.

[281] A. Ota, M. Armbrüster, M. Behrens, D. Rosenthal, M. Friedrich, I. Kasatkin, F. Girgsdies, W. Zhang, R. Wagner, R. Schlögl, Intermetallic compound Pd2Ga as a selective catalyst for the semi-hydrogenation of acetylene: from model to high performance systems, The Journal of Physical Chemistry C, 115 (2010) 1368-1374.

[282] W.A. Brantley, Z. Cai, D.W. Foreman, J.C. Mitchell, E. Papazoglou, A.B. Carr, X-ray diffraction studies of as-cast high-palladium alloys, Dental Materials, 11 (1995) 154-160.

[283] A. Borodziński, G.C. Bond, Selective hydrogenation of ethyne in ethene-rich streams on palladium catalysts. Part 1. Effect of changes to the catalyst during reaction, Catalysis Reviews, 48 (2006) 91-144.

[284] A. García-Trenco, S. Valencia, A. Martínez, The impact of zeolite pore structure on the catalytic behavior of CuZnAl/zeolite hybrid catalysts for the direct DME synthesis, Applied Catalysis A: General, 468 (2013) 102-111.

[285] J.-H. Kim, M.J. Park, S.J. Kim, O.-S. Joo, K.-D. Jung, DME synthesis from synthesis gas on the admixed catalysts of Cu/ZnO/Al2O3 and ZSM-5, Applied Catalysis A: General, 264 (2004) 37-41.

[286] L. Wang, Y. Qi, Y. Wei, D. Fang, S. Meng, Z. Liu, Research on the acidity of the double-function catalyst for DME synthesis from syngas, Catalysis Letters, 106 (2006) 61-66.

[287] Y. Rozita, R. Brydson, A. Scott, An investigation of commercial gamma-Al2O3 nanoparticles, Journal of Physics: Conference Series, IOP Publishing, 2010, pp. 012096.

[288] F. Lónyi, J. Valyon, On the interpretation of the NH3-TPD patterns of H-ZSM-5 and H-mordenite, Microporous and Mesoporous Materials, 47 (2001) 293-301.

[289] N. Katada, H. Igi, J.-H. Kim, M. Niwa, Determination of the acidic properties of zeolite by theoretical analysis of temperature-programmed desorption of ammonia based on adsorption equilibrium, The Journal of Physical Chemistry B, 101 (1997) 5969-5977.

[290] X. Peng, B. Toseland, P. Tijm, Kinetic understanding of the chemical synergy under LPDMETM conditions—once-through applications, Chemical Engineering Science, 54 (1999) 2787-2792.

[291] G. Jia, Y. Tan, Y. Han, A comparative study on the thermodynamics of dimethyl ether synthesis from CO hydrogenation and CO2 hydrogenation, Industrial & engineering chemistry research, 45 (2006) 1152-1159.

[292] G.J. Hutchings, R. Hunter, Hydrocarbon formation from methanol and dimethyl ether: a review of the experimental observations concerning the mechanism of formation of the primary products, Catalysis today, 6 (1990) 279-306.

[293] J. Erena, R. Garoña, J.M. Arandes, A.T. Aguayo, J. Bilbao, Effect of operating conditions on the synthesis of dimethyl ether over a CuO-ZnO-Al2O3/NaHZSM-5 bifunctional catalyst, Catalysis today, 107 (2005) 467-473.

[294] X.-M. Liu, G. Lu, Z.-F. Yan, J. Beltramini, Recent advances in catalysts for methanol synthesis via hydrogenation of CO and CO2, Industrial & engineering chemistry research, 42 (2003) 6518-6530.

[295] U. Olsbye, M. Bjørgen, S. Svelle, K.-P. Lillerud, S. Kolboe, Mechanistic insight into the methanol-to-hydrocarbons reaction, catalysis Today, 106 (2005) 108-111.

[296] D. Wang, O. Dewaele, A.M. De Groote, G.F. Froment, Reaction mechanism and role of the support in the partial oxidation of methane on Rh/Al2O3, Journal of Catalysis, 159 (1996) 418-426.

[297] R. Montesano, D. Chadwick, Combined methanol and dimethyl ether synthesis from CO/H2: Phosphorus mediated deactivation, Catalysis Communications, 29 (2012) 137-140.

[298] G.L. Price, V. Kanazirev, Ga2O3/HZSM-5 propane aromatization catalysts: Formation of active centers via solid-state reaction, Journal of Catalysis, 126 (1990) 267-278.

[299] G.L. Price, V.I. Kanazirev, K.M. Dooley, Characterization of [Ga] MFI via thermal analysis, Zeolites, 15 (1995) 725-731.

[300] C.E. Gounaris, C.A. Floudas, J. Wei, Rational design of shape selective separation and catalysis—I: Concepts and analysis, Chemical engineering science, 61 (2006) 7933-7948.

[301] A. Narvaez, D. Chadwick, L. Kershenbaum, Small-medium scale polygeneration systems: Methanol and power production, Applied energy, 113 (2014) 1109-1117.

[302] F. Besenbacher, M. Brorson, B.S. Clausen, S. Helveg, B. Hinnemann, J. Kibsgaard, J.V. Lauritsen, P.G. Moses, J.K. Nørskov, H. Topsøe, Recent STM, DFT and HAADF-STEM studies of sulfide-based hydrotreating catalysts: Insight into mechanistic, structural and particle size effects, Catalysis Today, 130 (2008) 86-96.

[303] M. Matzen, Y. Demirel, Methanol and dimethyl ether from renewable hydrogen and carbon dioxide: Alternative fuels production and life-cycle assessment, Journal of cleaner production, 139 (2016) 1068-1077.

[304] H.-J. Kim, H. Jung, K.-Y. Lee, Effect of water on liquid phase DME synthesis from syngas over hybrid catalysts composed of Cu/ZnO/Al 2 O 3 and γ-Al 2 O 3, Korean Journal of Chemical Engineering, 18 (2001) 838-841.

[305] D.T. Whipple, P.J. Kenis, Prospects of CO2 utilization via direct heterogeneous electrochemical reduction, The Journal of Physical Chemistry Letters, 1 (2010) 3451-3458.

Appendix A Experimental Procedures

Section 3.1.1

Calculation of recycle ratio

The height of gas pumped by the impeller is calculated by:

$$\Delta h = 1.1\left(\frac{impeller\ speed}{1000}\right)^2$$

The velocity head generated by the impeller was considered to be equal to the pressure head resulted from the packed bed [17].

The pressure drop through the packed bed was determined using the following equation by Leva [17] (modified):

$$\Delta h = \frac{\Delta p}{\rho g} = \left[\frac{4f(1-\varepsilon)^{3-n}}{\varphi^{3-n}\varepsilon^n}\right]\left(\frac{L}{d_p}\right)\left(\frac{v^2}{2g}\right)$$

Where the height of the bed, L, is 0.4 cm, the void fraction of the bed, ε, is assumed to be 0.4 with a shape factor φ equal to 1 (for spherical particles). The friction factor, f, and the exponent, n, are set to 1 (turbulent flow) [17].

Problem with the design of CSTR

With frequent use of the CSTR, the bearing inside the catalyst basket eventually wore out and the impeller was gradually bent. This caused the catalyst basket to move around at high speed, which eventually damaged the inert reactor surface (Figure A.1). During this period, unusual high methane production was observed over NiGa(a)/SiO_2 under typical reaction conditions (245 °C, 10 bar, CO_2/H_2).



Figure A.1, Damaged reactor vessel (inside)

A series of blank experiments was carried out to find the source of methane production. It was found that when the catalyst basket was rattling inside the reactor, the methanation reaction took place even in the absence of any catalyst (Figure A.2).

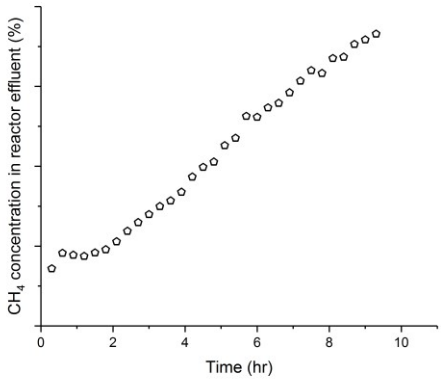


Figure A.2, CH_4 concentration over time in a blank experiment (conditions: 245 °C, 10 bar, CO_2/H_2)

In the presence of the NiGa(a)/SiO_2 catalyst, methanation reaction became the dominant reaction over time and methanol synthesis deteriorated (Figure A.3). It was speculated that the metals underneath the reactor surface was exposed by the scratching effect of rattling basket, which then catalysed methanation reaction. Clearly, in the CO_2 hydrogenation reaction over NiGa(a)/SiO_2 when the reactor was damaged, the additional CH_4 produced by the reactor surface also deactivated NiGa(a)/SiO_2 catalyst. Therefore, to ensure inertness of the reaction environment, the bearing within the basket was replaced, impeller was secured and a Teflon disc was placed between the basket and reactor bottom to prevent scratching.

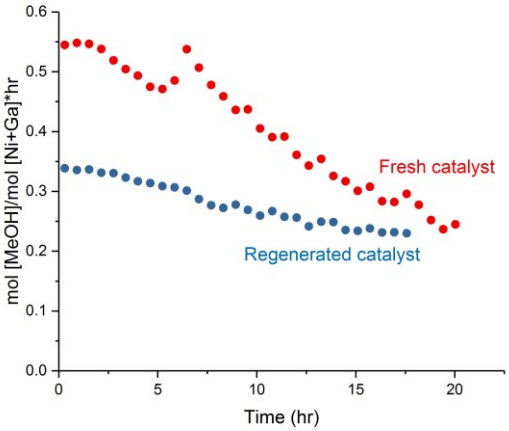


Figure A.3, MeOH production rate measured in the damaged reactor (conditions: 245 °C, 10 bar, CO_2/H_2)

Section 3.2.1.1 – Effect of reduction conditions

Owing to the large CSTR volume (300 mL), it was necessary to load more catalyst into the reactor to obtain a more accurate measure of the catalytic activity. However, the quartz tube used in the TPR was only able to produce around 150mg reduced and passivated catalyst. A half-inch wide stainless steel tube was used initially. The feed gas flowrate and heating rate and the furnace temperature were varied to obtain the required reduction temperature inside the reactor. It was found that a heating rate of 7 °C/min and gas flowrate of 350 mL/min and a furnace temperature setting of 710 °C gave the most suitable reduction conditions. Therefore, a trial reduction of NiGa(a)/SiO_2 precursor was carried out with this combination of settings and the catalysts were passivated using the method described in Chapter 4. In order to determine if the correct material was obtained, the resulting catalyst was characterised by XRD and compared to earlier catalyst that was reduced in the quartz tube.

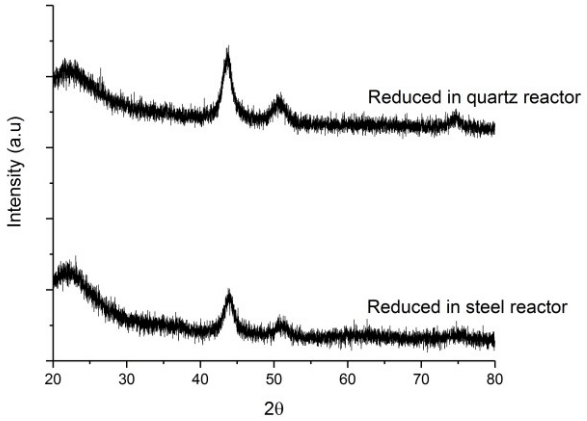


Figure A.4, XRD pattern for catalysts reduced in different reactors

Although the peak position of the major peaks is the same in both catalysts, the peak intensities are low in the steel tube-reduced sample. Since no other crystalline species are found in the sample, the difference in the diffraction patterns could be due to the incomplete formation of Ni-Ga alloy. In order to compare the catalytic performance of both samples, after the catalyst was re-activated in the CSTR, runs with CO_2/H_2 was conducted at 245 °C, 10 bar and 110 mL/min. Results are given in Table A.1.

Table A.1, Catalytic performance of NiGa(a)/SiO_2 catalyst reduced in different reactors

Reactor material	Furnace temperature/actual temperature (°C)	Methanol production rate (mol MeOH/mol [Ni+Ga]*hr)	MeOH:CH_4 ratio	Selectivity to CO (%)
Stainless steel	710/699	0.36	6.12	35
Quartz	710/698	0.53	105	26

As expected, poor methanol synthesis activity and selectivity was observed in the catalyst reduced in the steel tube. The high methane production suggests that the alloying between Ni and Ga is incomplete, making the catalyst to behave as metallic nickel. The catalyst reduced in quartz tube was significantly more active and selective towards methanol synthesis, which

is due to more successful formation of active alloy phase as shown in the diffraction pattern. These results imply that the material of the reactor can affect the formation of the Ni-Ga intermetallic phase. While quart is considered to be inert material, steel usually contains other elements, it is possible that foreign metals interacted with Ni and Ga at high temperature and impeded the formation of Ni-Ga alloy. So far, published work on the Ni-Ga catalysts were conducted in quartz reactors under atmospheric pressure, therefore the influence of reactor composition on the Ni-Ga catalysts has not been reported. However, similar phenomenon was also observed by I. Sharafutdinov, who examined different types of support for the Ni-Ga based catalysts [13]. It was speculated that the poor catalytic activity of Ni-Ga supported on support other than SiO_2 could be due to incomplete formation of Ni-Ga alloy. Regrettably, the author did not carry out further investigation to elucidate the cause.

From this investigation, it can be said that the material of the reduction equipment is essential for the Ni-Ga intermetallic phase to be formed correctly. Therefore, a quartz tube with larger volume was designed and used to carry out all subsequent catalyst reduction.

Section 3.2.2 – Mass transfer effect (internal mass transfer limitation)

Table A.2, Effect of particle size on the methanol synthesis and dehydration rates over physical mixtures of HiFuel R120 and γ-Al_2O_3 in an internal recycle Berty reactor* (results reproduced from R. Montesano's work [17])

Methanol synthesis catalyst			
Particle size (μm)	4125	250 – 500	106 – 250
mmol [MeOH]/g*hr	14.9	17.1	17.0
$N_{W\text{-}P}$	0.108	0.002	0.0004
Methanol dehydration catalyst			

Particle size (μm)	3000	250 – 500	106 – 250
mmol [DME]/g*hr	3.5	4.2	4.3
$N_{W\text{-}P}$	1.006	0.033	0.0086

*conditions: 260 °C, 50 bar, 24.7%CO_2/1.2%Ar/H_2, 1500 rpm

Section 3.2.4 – Product analysis (response factors by GC calibration)

Table A.3, Response factor for each substance detected in the GC

	Response factor	
	RF_{FID} ($\times 10^5$)	RF_{TCD} ($\times 10^4$)
CH_4	5.82	-
Methanol	4.24	-
DME	8.10	-
Ar	-	5.28
CO	-	4.99
CO_2	-	6.11

Error analysis

The standard deviation of the response factor for each substance in Table A.3 was calculated using the following equation:

$$\sigma_{RF}{}^2 = \frac{RF^2}{n} - \overline{RF}^2$$

where σ_{RF} is the standard deviation and n is the total number of response factors (number of calibrations done) and $\overline{RF}$ is the average response factor.

Error in the calculated variables was estimated using:

$$\Delta a = a \times \sum \left(\frac{\Delta b}{b}\right)$$

where Δ refers to the error in the variable, a is the conversion/MeOH rate/selectivity and b is the variable(s) used for the calculation of a.

Section 3.3 Thermodynamic analysis of methanol synthesis process

Table A.4, Values of $\Delta H_{r,i}^{\ominus}$ and $\Delta G_{i,298K}^{\circ}$ used in the calculation are taken from the book by M. V. Twigg [53]

Reaction	$\Delta H_r^{\ominus}$ (kJ/mol)	ΔG_{298K}° (kJ/mol)
$CO + 2H_2 \rightarrow CH_3OH$	-91	-25.31
$CO_2 + 3H_2 \rightarrow CH_3OH + H_2O$	-49.5	3.3
$CO + H_2O \rightarrow CO_2 + H_2$	-41.2	-28.6

Appendix B CO_2 Hydrogenation to Methanol over Ni-Ga Based Catalyst at Elevated Pressures

Section 4.2.2.2 – Protection by liquid

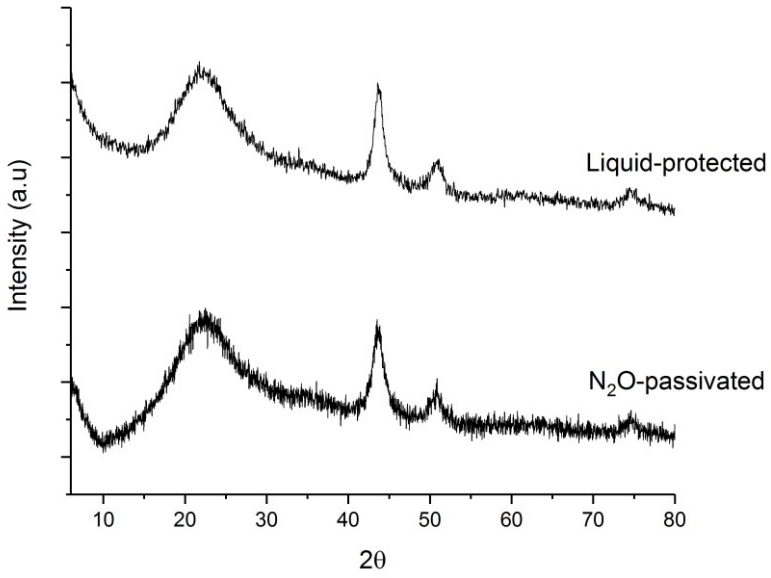


Figure B.1, Diffration patterns for the Ni-Ga catalysts using different passivation technique

Section 4.2.2.3 – Characterisation of Cu/ZnO/Al₂O₃ catalyst

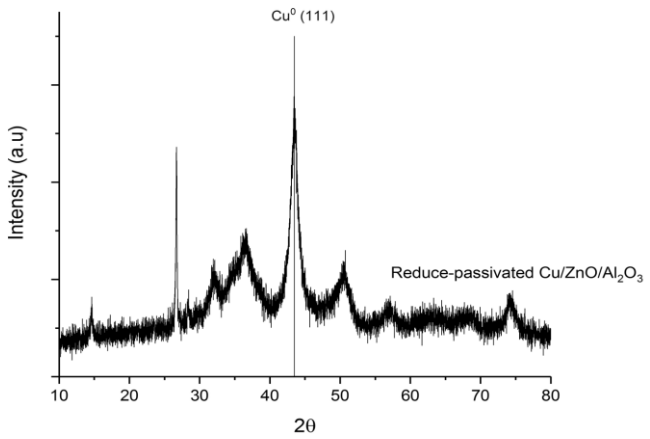


Figure B.2, Diffraction pattern of reduced-passivated $Cu/ZnO/Al_2O_3$ catalyst

Table B.1, Chemical and textural properties of $Cu/ZnO/Al_2O_3$ catalyst

	Graphite free composition* (wt%)			BET surface area (± 1 m^2/g)
	CuO	ZnO	Al_2O_3	
Nominal	50.5	30.8	18.7	72
Calculated from ICP-OES result	49.3	29.4	16.9	

*results reproduced from R. Montesano's work [17]

Section 4.2.3.2

Isotherms of Ni-Ga based catalysts

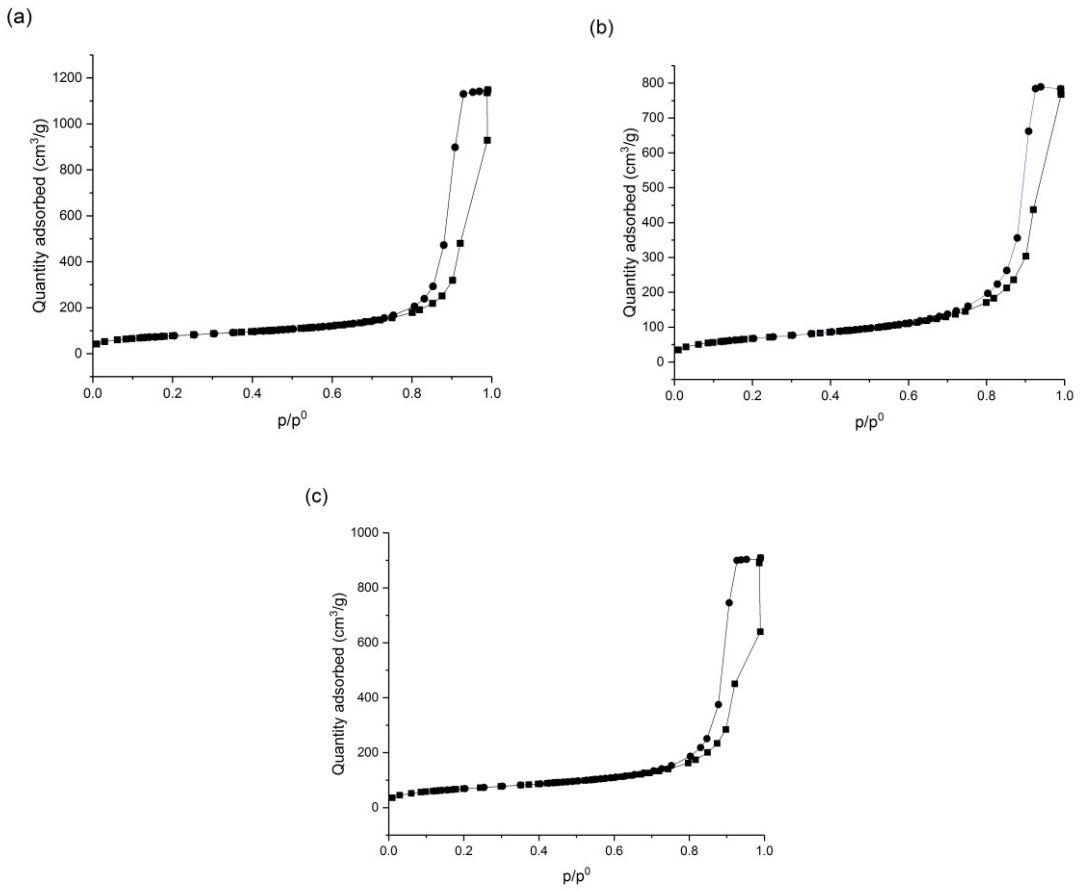


Figure B.3, Isotherms (a) SiO_2 (b) NiGa(b)/SiO_2 (c) NiGa(a)/SiO_2

XPS spectra of Ga 3d

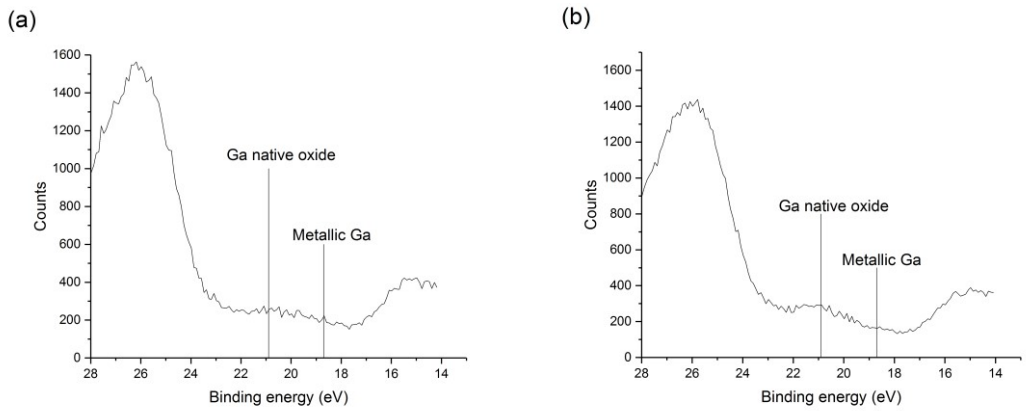
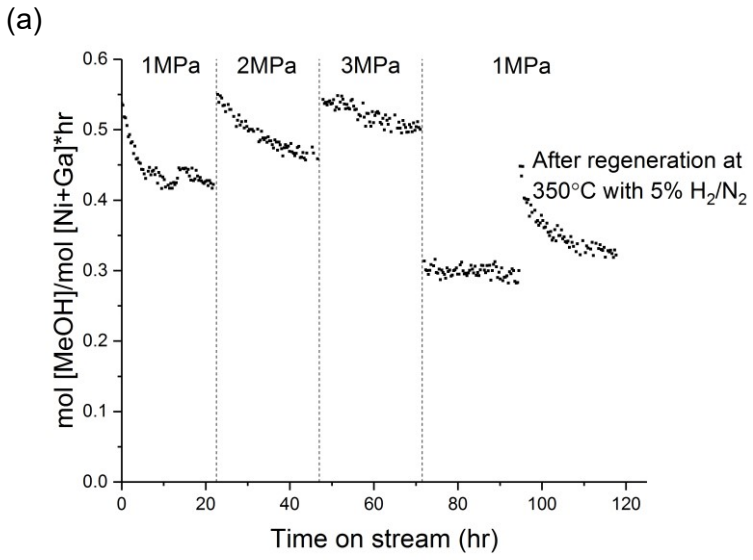


Figure B.4, XPS spectra of Ga 3d (a) NiGa(a)/SiO_2 (b) NiGa(b)/SiO_2

Section 4.2.3 – (additional work) – Long term stability of Ni-Ga catalyst (pressure cycle)

Previously the NiGa(a)/SiO_2 catalyst was found to show only initial deactivation in the 20-hour experiment. In order to study the long-term stability of the NiGa(a)/SiO_2 catalyst and compare to that of the conventional Cu/ZnO/Al_2O_3 catalyst, an 80-hour pressure cycle experiment was conducted over each catalyst. Each experiment consisted of four consecutive 20-hour runs at 10, 20, 30 and 10 bar (245 °C). NiGa(a)/SiO_2 catalyst was regenerated at 350 °C for 2 hours at the end of the pressure cycle and the activity was measured again at 10 bar. The measured conversion and selectivity of both catalysts can be found in Figure B.5.



(b)

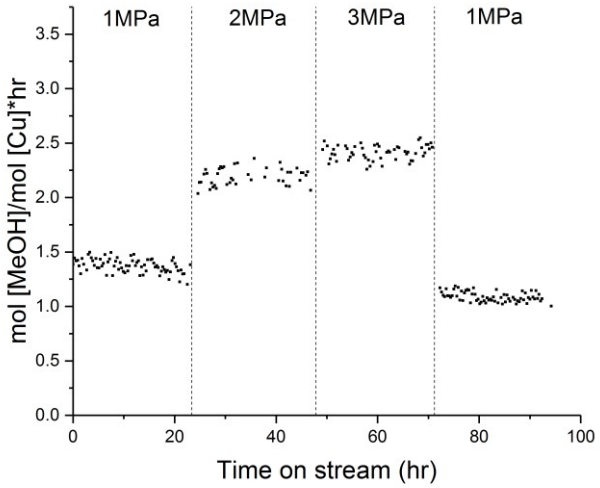


Figure B.5, Catalytic performance (MeOH production rate) in pressure cycle experiment

(a) NiGa(a)/SiO_2 (b) Cu/ZnO/Al_2O_3

As discussed in Chapter 4, the measured methanol synthesis rate over NiGa(a)/SiO_2 catalyst was always lower compared to Cu catalyst, the difference in activity became more significant as reaction pressure increased from 10 bar to 30 bar due to the difference in pressure dependence of the two catalysts.

For NiGa(a)/SiO_2 catalyst, as the pressure decreased from 30 bar back to 10 bar, the activity was clearly lower compared to the results obtained in the initial 10 bar reaction. In fact, the activity now was only 68% of the steady state value measured in the initial 10 bar run. Even after the catalyst regeneration, the highest activity at the same pressure (10 bar) was 83% of the maximum value for the fresh catalyst. This indicates that the catalyst experienced deactivation throughout the pressure cycle and some deactivation was irreversible.

Cu/ZnO/Al_2O_3 deactivated more gradually throughout the experiment. The methanol selectivity increased with pressure as expected. When the pressure was returned to 10 bar, the activity dropped to 75% of the initial value. This is due to the gradual agglomeration of Cu particles in the presence of water as well as the deposition of coke, as discussed in Chapter 4.

The selectivity of both catalysts throughout the pressure cycle is shown in Figure B.6.

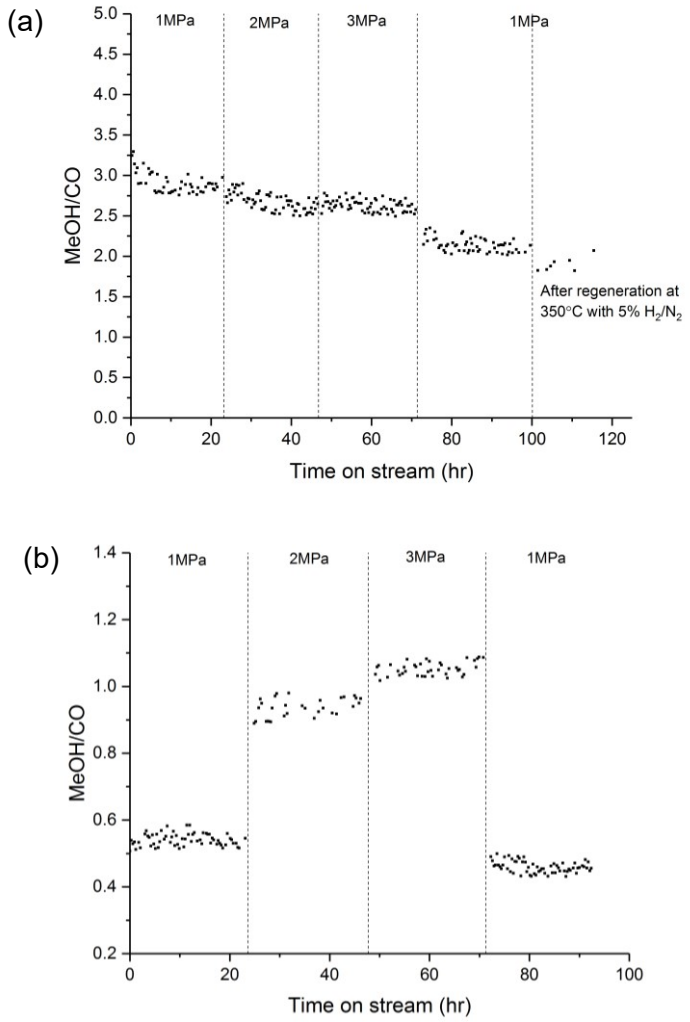


Figure B.6, Selectivity for both catalysts in pressure cycle

(a) NiGa(a)/SiO_2 (b) Cu/ZnO/Al_2O_3

For both catalysts, the reactions with CO_2/H_2 produced only CH_4, CO, MeOH as C-containing products, no hydrocarbons were detected. In the case of NiGa(a)/SiO_2, the selectivity to methanol gradually declined as CO and methane production increased. Once the pressure was returned to 10 bar, the methane level becomes negligible again but CO level was increased further. After the regeneration treatment, selectivity was not restored.

The facts that both the MeOH activity and selectivity dropped throughout the experiment and the regeneration process did not have significant effect suggest that the catalyst suffered

irreversible deactivation. As discussed in Chapter 4, the Ga-containing intermetallic compounds are prone to the decomposition of active phase and Ga segregation [13, 133, 156]. Although NiGa(a)/SiO_2 has intermediate Ga content (5.11 wt%), de-alloy of the Ni-Ga phase to more Ni-rich phase could still occur, which is evidenced by the increase in CO and methane production throughout the experiment. However, the change in intermetallic phase in the case of NiGa(a)/SiO_2 catalyst is difficult to detect (no change in the diffraction pattern was observed).

As expected, Cu/ZnO/Al_2O_3 is a good rWGS catalyst under low-pressure CO_2/H_2. CO is the main product, which accounts for 66%, methanol 34% and no methane was detected. At higher pressure (e.g. 30 bar), selectivity to methanol increased to 51%. Returning the pressure to 10 bar the selectivity to methanol decreased to 30% due to the deactivation of Cu catalyst during the prolonged exposure to high water level.

Section 4.2.3.3 – (additional work) – Methanol synthesis at elevated pressures in the PFR

In addition to the CSTR, a tubular packed bed flow reactor was also used to test catalytic performance. As discussed in Chapter 4 section 4.2.3.1, due to the nature of the CSTR, it is often difficult to achieve intermediate or high conversion. In the PFR, high conversion per unit mass can be more easily obtained. This is particularly useful for the Ni-Ga based catalysts that deactivates significantly in the presence of reaction products. In this section, only NiGa(a)/SiO_2 was studied as it was shown to be more stable against de-alloying than NiGa(b)/SiO_2.

Methanol synthesis with CO_2/H_2 (PFR)

Experiment was carried out in the PFR at 245 °C at 10 bar with 110 mL/min STP CO_2/H_2. The same mass (0.3 g) of NiGa(a)/SiO_2 was used to measure its catalytic performance. The measured activity and selectivity are presented in Figure B.7.

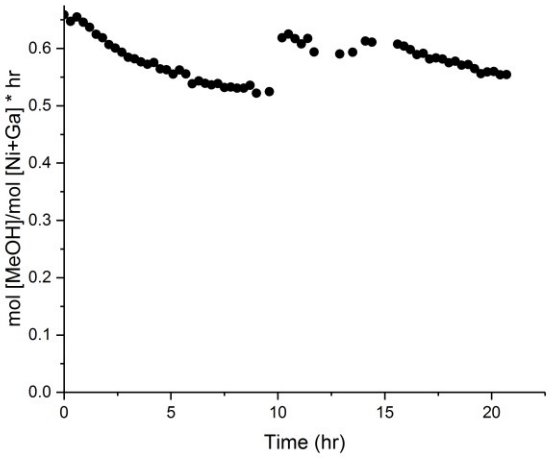


Figure B.7, Catalytic performance (MeOH production rate) over NiGa(a)/SiO_2 in the PFR

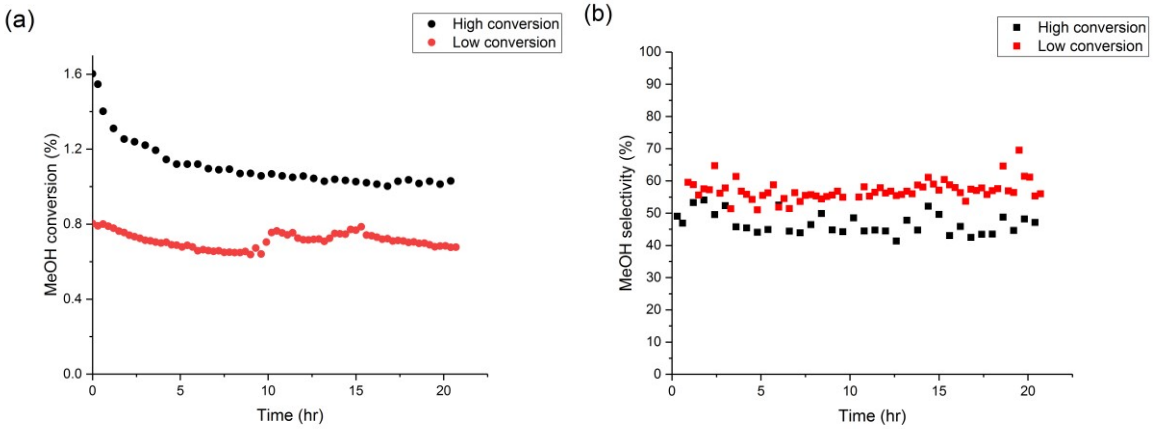
The deactivation behaviour in the PFR is similar to that in the CSTR (both at a rate of 20% drop in the first 10 hours on stream). During the PFR experiment, the rig was required to shut down overnight after 10 hours on stream and the experiment was resumed the next day. To shutdown, the reactor was flushed with nitrogen for a period of time and the reactor was pressurised with pure N_2 overnight. Therefore there was a sudden increase in activity at 10^{th} hour due to the removal of adsorbed molecules such as CO, which is proven to cause a loss of activity. The maximum initial activity on the second day is about 95% of the maximum initial activity on the first day, suggesting that the removal of adsorbed substances alone did not completely regenerate the catalyst. This result again shows that the catalyst mainly deactivates by the reversible adsorption of CO and maybe water. Therefore, regeneration with H_2 not only re-exposes the active sites by desorption but also reconstructs the catalyst structure and/or removes coke deposition [12].

In the PFR reaction, methanol, CO and methane accounts for 56%, 43% and 1% of the total water-free products. Slightly lower MeOH selectivity supports the postulation in the literature that there exists Ni-rich sites which are responsible for methanation and rWGS reactions until they are self-poisoned by CO [12].

Effect of catalyst mass on the catalytic performance (PFR)

Due to the unsuccessful attempt to increase the conversion in the CSTR (Chapter 4 section 4.2.3.2), mass of catalyst was doubled and the flowrate was reduced to 40 mL/min STP (GHSV 1280 h^{-1}) in order to achieve an even higher conversion. The MeOH conversion is shown in Figure B.8 (a). Although the conversion has increased to a maximum of 1.6% which is close to the thermodynamic equilibrium value of 1.9% at 10 bar, the production rate of methanol per unit amount of active metals is actually lower than that obtained at low conversions (0.40 versus 0.55 mol [MeOH]/[mol [Ni+Ga]*hr respectively at steady state). In addition, the rate of deactivation is much faster at high conversion during the first 5 hours on stream (Figure B.9). At the end of the experiment, the catalyst only has 63% of the original activity whereas at low conversion, nearly 80% of the initial activity remains.

At high conversion, selectivity to methanol is lower due to more rWGS and methanation activity. DME is also found to be present at a level of 2% as a result of methanol dehydration on the acid sites of gallium oxide [175, 256]. These results again confirm that the Ni-Ga/SiO_2 catalysts are not suitable for high-conversion applications due to strong deactivation.



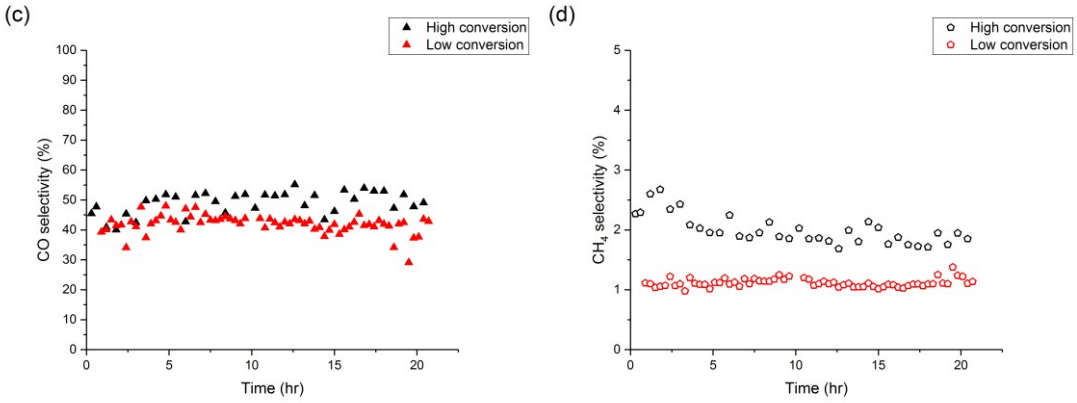


Figure B.8, Catalytic performance of NiGa(a)/SiO_2 at high conversion

(a) MeOH conversion (b) MeOH selectivity (c) CO selectivity (d) CH_4 selectivity

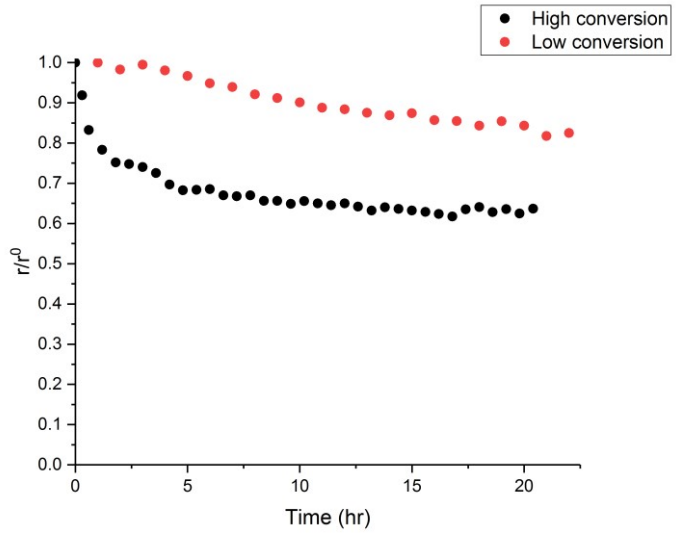


Figure B.9, Normalised MeOH activity at high and low conversions

Section 4.2.3.4 – Characterisation of spent $Cu/ZnO/Al_2O_3$

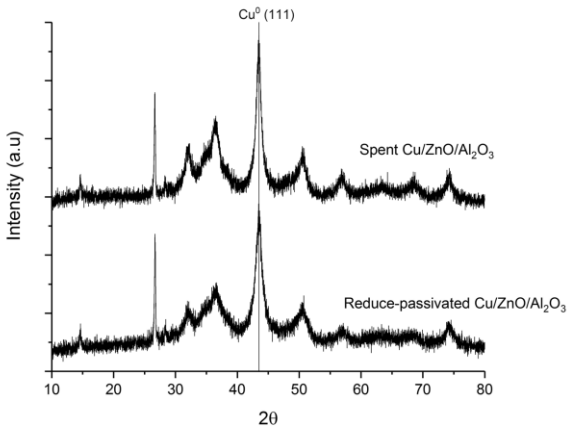


Figure B.10, XRD pattern of spent $Cu/ZnO/Al_2O_3$

Section 4.2.3.4 – Determination of desorption of CO_2 in TPO experiments

The TPO profile of the Ni-Ga based catalysts (Figure 4.16) showed a low-temperature CO_2 evolution peak as well a high-temperature one. To confirm whether both peaks come from coke oxidation, a TPO was carried out with a freshly passivated and re-activated NiGa(a)/SiO_2 sample that was exposed to CO_2/H_2 at room temperature. It was found that the peak at 260 °C comes from CO_2 adsorption when the catalyst was exposed to the reaction gas. This peak is equivalent to 1.5 µmol CO_2 per gram being adsorbed by the fresh catalyst, which is small compared to the peaks observed in the spent catalysts.

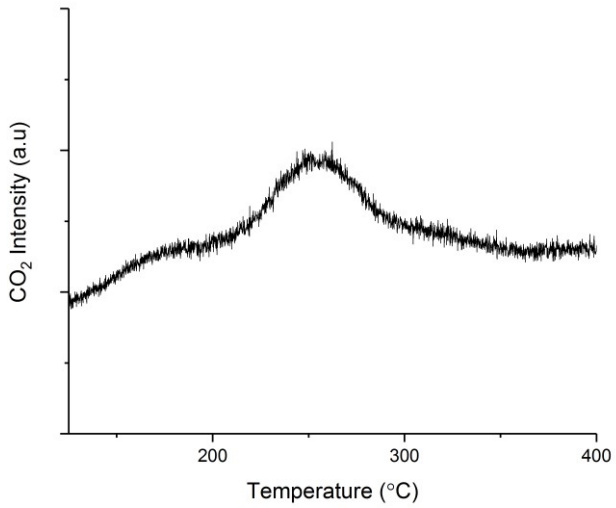


Figure B.11, TPO profile of catalyst exposed to CO_2/H_2 gas mixture without catalysis

Appendix C Single-stage DME Synthesis over Intermetallic Catalysts and Solid Acids under CO_2/H_2

Section 6.2 – Characterisation of zeolites

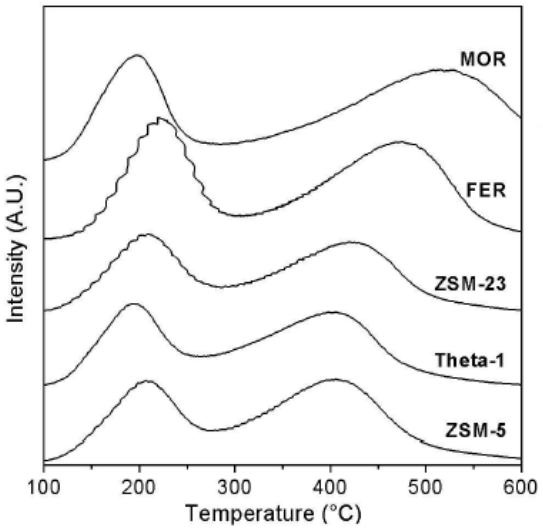


Figure C.1, NH_3-TPD profiles of fresh zeolites. Adsorption at 110 °C, heating rate 10 °C/min. Figure taken from the work by R. Montesano [17]

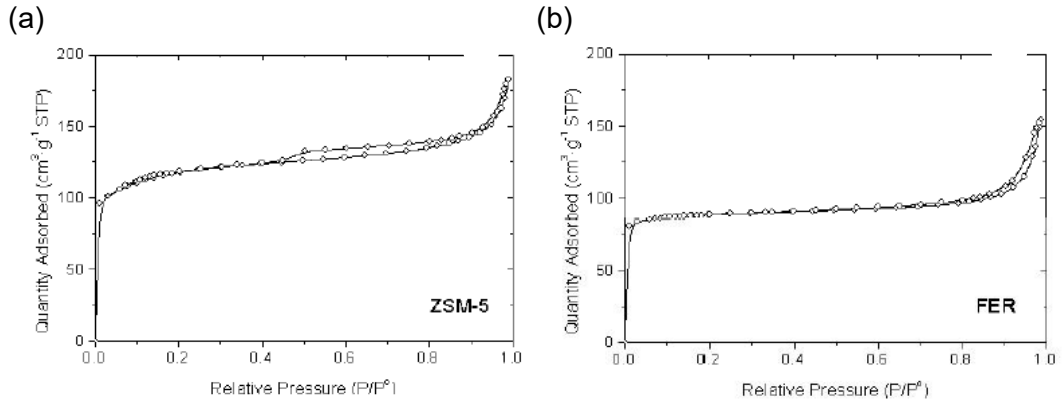


Figure C.2, N_2 adsorption and desorption isotherm at 77 K

(a) ZSM-5 (b) FER (Figure taken from the work by R. Montesano [17])

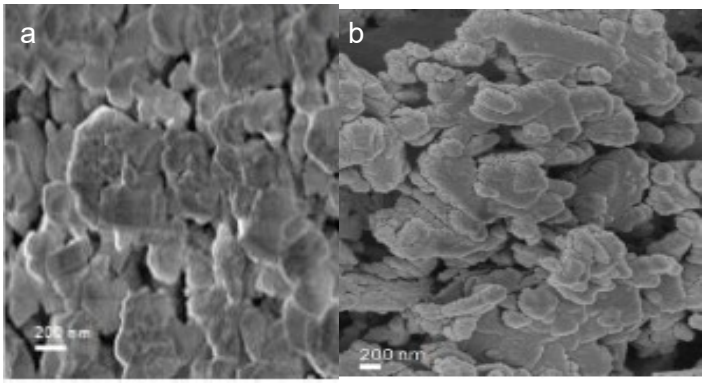


Figure C.3, SEM images of (a) ZSM-5 (b) FER (Figure taken from the work by R. Montesano [17])

Section 6.3 – Confirmation of methanol and DME production in the GC trace

To confirm the products obtained over Ni-Ga/SiO_2 + solid acid (excluding ZSM-5) catalyst are indeed methanol and DME, the GC trace from the run over Cu/ZnO/Al_2O_3 + γ-Al_2O_3 is given as a reference.

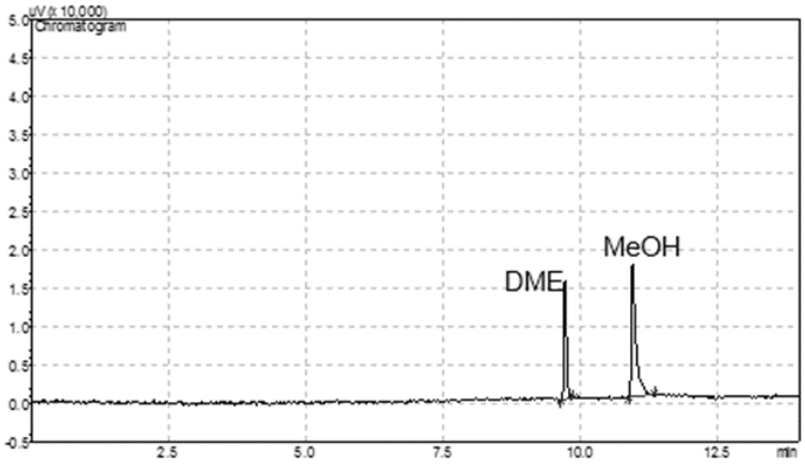


Figure C.4, GC trace from Cu/ZnO/Al_2O_3 + γ-Al_2O_3 experiment

Section 6.3.1.1 – Selectivity over NiGa(a)/SiO_2 + γ-Al_2O_3 (separated bed)

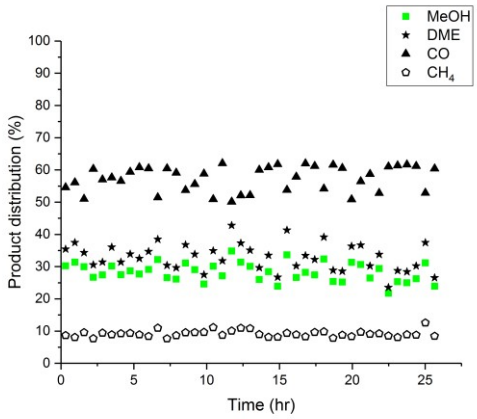


Figure C.5, Product distribution over NiGa(a)/SiO_2 + γ-Al_2O_3 in separated beds at 245 °C, 10 bar

Section 6.3.1.4 Effect of proximity on the selectivity over NiGa(a)/SiO_2 + FER

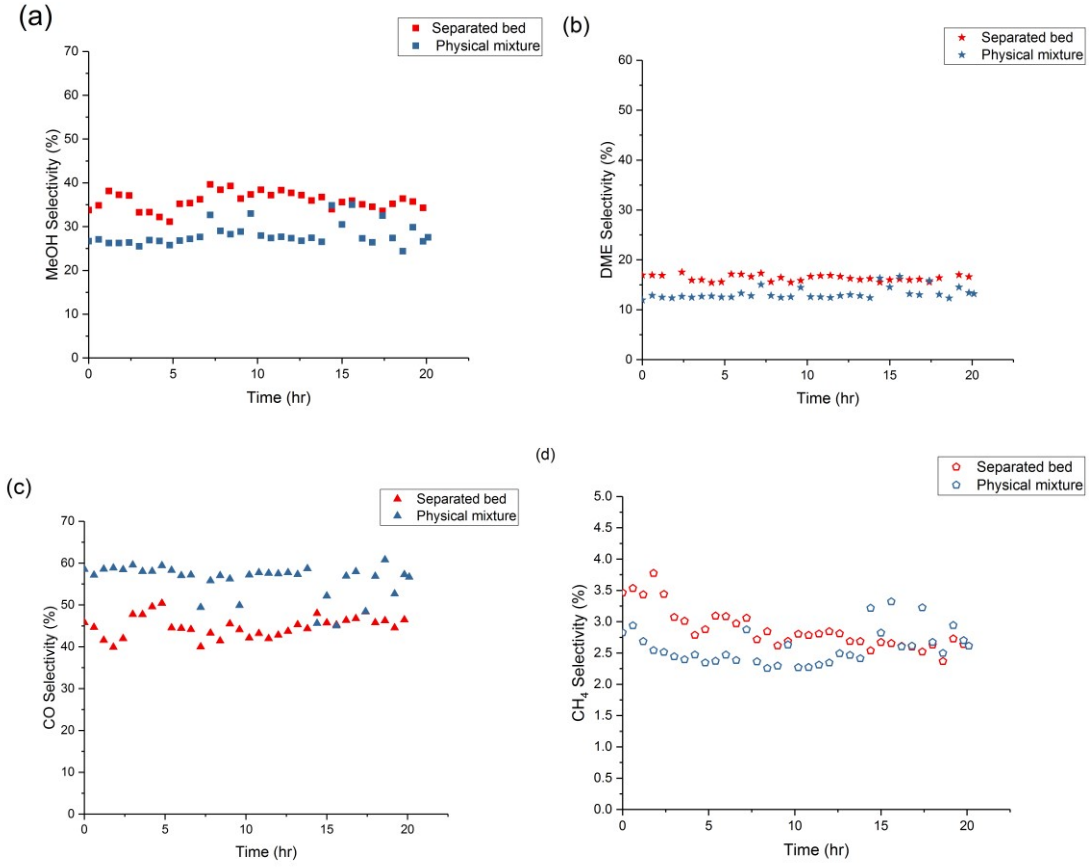


Figure C.6, Selectivity of NiGa(a)/SiO_2 + FER in physical mixtures and separated bed at 270 °C, 30 bar

(a) MeOH (b) DME (c) CO (d) CH_4

Section 6.3.2.1 – Selectivity of $PdGa_{0.5}/SiO_2$ + ZSM-5 (separated bed)

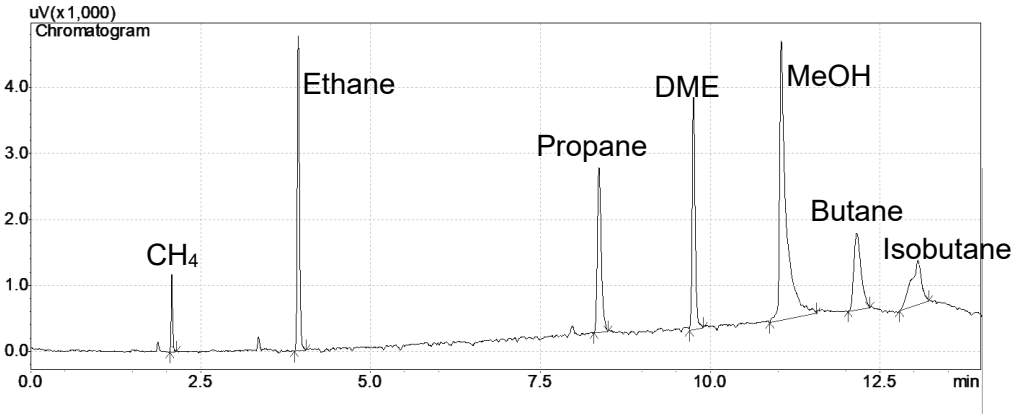


Figure C.7, GC trace given by the reaction over $PdGa_{0.5}/SiO_2$ + ZSM-5 in separated bed at 270 °C, 30 bar